Modelling and Control of Micro Environmental Systems

Philip Alexander Leigh
B.Sc. (Hons.)

A thesis submitted to the
University of Lancaster for the
Degree of Doctor of Philosophy

September 2002

Environmental Science Division
Institute of Environmental
and Biological Sciences,
University of Lancaster,
United Kingdom

"IT IS A CAPITAL MISTAKE TO THEORISE BEFORE ONE HAS DATA. INSENSIBLY ONE BEGINS TO TWIST FACTS TO SUIT THEORIES, INSTEAD OF THEORIES TO SUIT FACTS."

Sherlock Holmes in Scandal in Bohemia

DECLARATION

I declare that this thesis consists of original work undertaken solely by myself at Lancaster University between 1998 and 2002; where work by other authors is referred to, it has been properly referenced.

25th September 2002

Abstract

This thesis investigates the potential for improving the control of the microclimate within agricultural buildings, by experimenting with the application of proven and advanced control algorithms used in other fields. The Proportional-Integral-Plus (PIP) control system design methodology has been applied to two micro-environmental chambers. The PIP control design has been extended with a number of procedures that linearize a normally non-linear system. These procedures may be applied at either the design stage or implemented as extra elements to the actual controller. Taking the process a stage further, a full adaptive PIP control design has been implemented on the Leuven chamber. Additionally, a unique fan/valve controller was designed and implemented on the (Leuven) ventilation chamber with considerable success.

The primary aim of this research has been to further develop an automatic forced ventilation control system suitable for imperfectly mixed air spaces within agricultural buildings.

The final contribution of this research has been the Lancaster micro-environmental chamber. This was designed, built and instrumented in Lancaster. Previously no similar facility existed at Lancaster and the chamber is now an integrated high quality adaptable research test chamber for carrying out a vast array of experimental work in modelling and control with the capacity to test theories in a real scale building structure. The facility has also been used as a teaching aid for control courses in both Engineering and Environmental Science at Lancaster, and will continue to be used for teaching.

Acknowledgements

Firstly I would like to say a big thank you to Peter Young and Arun Chotai, my supervisors without their unstinting support and encouragement I would never have reached the finishing line. I am also grateful for the support of my colleagues past and present from the Systems and Control Group; their input and discussions have been a great help in keeping me sane. Thanks to Laura, Andy, Paul, Jamie, Wlodek, Martin, Periklis, and Farideh; also thanks to Renata Romanowicz and Rick Gould for reading the early chapters. Special thanks go to Paul McKenna for reading the whole thesis and suggesting improvements. Also thanks to Trevor Page for helping to keep things in perspective.

This research has been carried out under collaboration between Lancaster University and the Laboratory for Agricultural Buildings Research, Katholieke Universiteit, Leuven, Belgium. I am eternally grateful for their help and use of their excellent facilities. Special thanks to Erik Vranken and Karl Janssens; also to Jean-Marie Aerts and Andres Van Brecht. Additional thanks go to Fancom from the Netherlands for supporting the research at Leuven.

I am indebted to Geoff Johnson, technician in the Environmental Science Dept. Without our fruitful discussions on chamber design and his kind permission for free run of the workshop, my task would have been that much more difficult. Also, thanks to Andy Jarvis for initial discussions on chamber design. I am also very grateful to the Engineering Department at Lancaster for allowing me to build and house the micro environmental chamber within their department. Thanks especially to Mark Salisbury and Jim Newton, for invaluable help and suggestions with the chamber.

Also I would like to say thanks to North Yorkshire Fire and Rescue Service, especially Geoff and the lads at Bentham Fire Station for supporting me through my student years. Time spent on the fire ground was a great contrast to hours spent in front of the computer. Additionally, I am indebted to my ex-colleagues in the Electrical industry, which I left to pursue a new career path. Skills learnt during 20

years proved invaluable; especially when designing and constructing the Lancaster chamber.

While thanking people supporting me I can't finish without mentioning my many friends and colleagues in the cycling world. Without my bike to turn to and the experience of many years of suffering and grovelling up hill-down dale over hundreds of thousands of miles I am sure I would never have completed this thesis. Special thanks go to Smithy (World Champ), Hunting Dog (Mick) and the crew from Down Under; Tony, Dermot and everyone associated with Irish Cycling; Tim S., Martin, Tim G., Ozzy, Cozy, Gethin, Charlie, 'J' and all my UK teammates past and present, all to numerous to mention, including the strongest man in the world (age related)! In fact everyone from Colombia to New Zealand I have met in the cycling fraternity, you have all played your part in shaping someone who at the advanced age of 30 something took on a project far outside his "comfort zone".

Thanks to my family, Mum and Dad, plus siblings Adrian, Helen and Debbie your words of encouragement have been a great source of help and inspiration. Finally, last and far from least, on a personal note I would like to say an enormous thankyou to my partner Janette who has supported me unstinting for the last 8 years while I have been a student. Undoubtedly without her love and support I would still be "wiring houses". Thank you Janette, it is time to reclaim our lives! And, Josie thanks a million for your love and encouragement.

And lastly, I would like to thank the BBSRC for funding this research through a BBSRC research studentship.

Phil Leigh

Lancaster

September 2002

Table of contents

****

List of figures

CHAPTER 1

CHAPTER 2

CHAPTER 3

CHAPTER 4

CHAPTER 5

CHAPTER 6

CHAPTER 7

CHAPTER 8

APPENDIX 2

APPENDIX 3

APPENDIX 4

List of tables

APPENDIX 3

Chapter 1

INTRODUCTION

Climate control within agricultural buildings is of great significance, both economically and in terms of animal welfare; presently, ~15% of domestic animal production costs are attributed to microclimate control (Vranken, 1999). It has been shown that domestic animals, such as pigs or cattle, inhabiting a microenvironment that is cooler than ideal, use extra energy to maintain their body heat; or where

conditions are too warm weight loss occurs, (e.g. Geers *et al.*, (1989); Nienaber *et al.*, (1993)). Also, White *et al.*, (1983) found a correlation between air movement and the dispersion of germs in and around livestock buildings; and Zuidhof *et al.*, (1993) showed how ventilation rate and animal occupancy adversely affect the health and growth of turkeys.

This thesis investigates the potential for improving the control of ventilation and microclimate in agricultural buildings using a data-based modelling approach (Young *et al.*, 1996); and the models so identified are then used as a basis for Proportional Integral Plus (PIP) control design within the True Digital Control (TDC) framework of Young *et al.*, 1987, 1988; Chotai *et al.*, 1991 and more recently Taylor *et al.*, 1996, 2000. Here, the problem to be addressed is the modelling and control of the microclimate within agricultural animal housing; or more specifically the control of airflow rate, temperature and humidity in the region where the animals live and breathe.

During the research, a series of control system designs were formulated and implemented on two instrumented micro environmental chambers, beginning with a fixed gain controller. Then a number of more sophisticated controllers were designed and investigated: a switched gain control design, followed by a three operating point controller, scheduled control and finally adaptive control. Additionally, a unique fan/valve control design was implemented: this design gives greater stability at low airflow rates and consumes less power than the conventional fan only ventilation rate control system. The micro environmental chambers are briefly described below and in detail in chapters three, four and appendix 3:

i) The first chamber is a 2.8m x 2.8m x 2.8m cube with an axial fan housed at each end. It was designed in order to carry out single-input single-output (SISO) modelling and control of the ventilation rate produced by a propeller fan. A full description of this chamber is given in chapter three. This chamber was designed and constructed at the Katholieke Universiteit in Leuven, Belgium.

ii) The second chamber (2m x 2m x 1m) was designed, constructed and instrumented by the author in Lancaster as part of his research programme. It is similarly instrumented to the Leuven chamber but the addition of another controllable input, namely a heat source at the air inlet, allows for the investigation of multi-input multi-output (MIMO) control systems. Chapter four and appendix three describe the design, construction and implementation of this chamber.

This introductory chapter presents an overview of the micro-climate modelling and control problem, reviews the recent literature on the subject, and outlines the rest of the study.

1.1 IMPORTANCE OF MICROCLIMATE IN ANIMAL HOUSING

It is important. at this early stage in the thesis, to establish definitions for ventilation rate, ventilation pattern, indoor climate, microclimate and temperature distribution. The following descriptions apply throughout this thesis:

i) *Ventilation rate*: the volumetric rate of the air passing a given point, usually at the inlet or outlet. Measured in m^3/s or m^3/hr(Guss *et al.*, 1973; Gunn *et al.*, 1991).

ii) *Ventilation pattern*: the observed and/or measured airflow distribution in a given 3D space (White *et al.*, 1983, Gloster *et al.*, 1984).

iii) *Indoor climate*: the climate (temperature, humidity, airspeed etc.) wholly within a building structure, excluding the surrounding airspace, e.g. the climate within pig or broiler houses. (Webster, 1985; Julian, 1993).

iv) *Micro-climate*: the measure of climatic conditions within or around a specified place or region, e.g. the micro-climate directly around an animal within a livestock building. (e.g. Carpenter, 1986; Attwood *et al.*, 1987).

v) *Temperature distribution*: the 3D temperature distribution within animal housing, e.g. temperature profiles from floor to ceiling and left to right. (Nienaber *et al.*, 1993; Ogilvie, 1993).

Ventilation rate has been shown to be the single most significant influence on the quality of the physical micro-environment surrounding animals or plants within the majority of agricultural buildings (livestock housing, glasshouses, storage warehouses: see Carpenter, (1974), Randall, (1975, 1981), Boon (1978), Timmons (1980), Barber (1981) and Hebner *et al.*, (1996)). Bruce and Clarke, (1979) showed that the heat production of an animal is affected by many environmental parameters, of which the most important ones (temperature, humidity and air speed around the animal) are determined by the applied ventilation strategy. Consequently, the ventilation system plays an important role in controlling animal heat production (Monteith and Mount, 1973; Curtis, 1983). For example, in the case of livestock housing lacking a uniform

air distribution within the building enclosure, the animal comfort and welfare – and therefore productivity - are drastically reduced due to high-density occupation; especially in the cases of poultry, pigs and cattle, where a large amount of moisture, heat and internal gasses (e.g. methane (CH_4) and ammonia (NH_3)) are produced.

1.1.1 IMPERFECT MIXING

It has been demonstrated in numerous studies that imperfect mixing is present in many agricultural buildings due to internal pressure disturbances caused by variations in external wind speed and direction: Price *et al.*, (1999); Price, (1999); De Moor and Berckmans, (1993); Barber and Ogilvie, (1982); and Harral and Boon, (1997). A number of researchers including Randall, 1975; Boon, 1978 and Berckmans, 1986, recognised that a specific airflow pattern within a building can ensure an optimum microclimate at animal level; thus linking airflow input to optimum microclimate where it is needed. Berckmans *et al.*, (1988) and Vranken *et al.*, (1992) have found, from field studies on data collected from around 100 commercial pig houses in Belgium (1985-1992), that the lack of effective ventilation control is a major cause of production losses and ventilation-related health problems in modern livestock buildings.

This concern about poor ventilation has been the motivation for recent interest in the design of ventilation control systems, as described by Gates *et al.*, (2001) and Sigrimis *et al.*, (2000). Additionally, Zhang and Barber (1995) evaluated strategies for both heating and ventilation control in livestock buildings; while Parent *et al.*, (1998) showed that without optimal ventilation and airflow control, buildings with human occupancy show high levels of CO_2 and other contaminants. A study by Smith *et al.*,

(1996) showed that pigs given the choice of moving freely between fresh air and ammoniated air (~100 ppm ammonia) in a two-sided preference chamber, demonstrated a definite aversion to the ammoniated side. This links closely to research by Robertson *et al.*, (1990); where a strong correlation was found between ammonia exposure and the incidence and severity of common endemic respiratory disease in pigs. It is evident from this literature that a prior condition for controlling imperfectly mixed fluids is that the ventilation rate can be controlled accurately. This problem is addressed in the research conducted on the first chamber, as described in chapter three.

The concept of a Control Volume (CV), representing the imperfectly mixed airspace within a ventilated building structure, was first proposed by Barber and Ogilvie (1982). Since then, further studies by Berckmans *et al.*, (1992) and Daskalov (1997) have utilised the CV concept. In the former, variations of the ventilation rate and heat supply are related to the non-linear dynamic response of the imperfectly mixed 3D airspace; while the latter uses discrete–time 'black box' transfer function models to identify measured temperature and humidity variations within naturally ventilated pig housing. Young and Lees (1993), have also suggested that mass and energy transfer in fluid flow systems is often dominated by imperfect mixing. This has led to the development of a new data-based, Active Mixing Volume (AMV) model of imperfect mixing, which often describes experimental data much better than conventional mass and energy transport models. This AMV theory is a wider application of the Aggregated Dead Zone (ADZ) model for pollutant transport in rivers, which has proved successful in numerous practical applications, e.g. Young *et al.*, (1988); Beven *et al.*, (1990); Wallis *et al.*, (1989).

Bearing in mind the imperfect mixing scenario outlined above, the objective of the present modelling and control investigation is to design and implement a control system that not only regulates the ventilation rate through the test chamber, but is also flexible enough to introduce differing levels of sophistication, such as temperature control. The objective here is twofold: first, to ensure the comfort and well being of the animals; and second, to limit the cost to the farmer. For example, it has been shown that pigs that are kept in a draft use extra energy in order to keep warm and, consequently, consume more food; while pigs that are too warm do not eat and fail to reach their optimum weight (Nienaber *et al.*, 1993). Also pigs housed in either of these conditions are not in as good health as pigs kept in optimum micro-climatic conditions (e.g. Smith *et al.*, 1996 and Robertson *et al.*, 1998).

In order to maintain the well-mixed zone within the Leuven ventilation chamber, the voltage to the control fan has to be adjusted for any deviation from the desired airflow rate. In order to achieve more sophisticated MIMO control, additional inputs, such as temperature measurements, allow for further refinement and tighter control of thermal ranges in the living areas of the animals. In addition to controlling the microclimate of the well-mixed zone, it has also been shown that this optimised microclimate can be moved around the chamber to regions that are identified as imperfectly mixed from ventilation, heat and smoke (visualisation) experiments. This has been carried out by the use of an air direction deflector on the inlet to the chamber, (McKenna *et al.*, 2002; Young *et al.*, 2002).

A search through the literature shows a proliferation of reports from laboratory experiments that highlight how physical micro-environmental conditions, such as airflow, temperature, humidity and gas concentrations, influence the behaviour of living organisms, (e.g. see Vranken, 1999 and the references therein). Gunn and Wilson (1991) show how high animal occupancy and insufficient ventilation are correlated to respiratory diseases in cattle. Furthermore, metabolic diseases, such as ascites and sudden death syndrome in broiler chickens, are not only caused by genotype or dietary composition. They are also induced by deviation from optimal environmental conditions, such as too low temperature and improper ventilation (Julian, 1993). Low airflow levels result not only in hypoxemia (lack of oxygen in the blood) and hypoxia (absence of oxygen supply to the tissues of a vital organ) but also cause elevated ammonia concentrations in the surrounding air. And all of these factors predispose for the development of ascites. Geers, *et al.*, (1989) found that a higher mortality rate was discovered in fattening pigs exposed to high temperature fluctuations and very high temperatures; while at low temperatures, a higher incidence of coughing occurs. Carcass quality can also be affected by physical micro-environmental conditions: for example, the lean meat to fat ratio of chickens is found to be closely correlated to the environmental temperature and lighting levels during the fattening period (Howlider and Rose, 1987; Buyse *et al.*, 1996).

Apart from the effect on the internal microenvironment, overcrowding within livestock housing can lead to unacceptable ammonia emissions being discharged to the atmosphere (Demmers *et al.*, 1999; Sutton *et al.*, 1995). The resulting ammonia deposition is known to cause damage to sensitive ecosystems (Wilson and Pitcairn, 1988; van Breemen *et al.*, 1982). Furthermore, Aarninck *et al.*, 1993; Berckmans *et*

al., 1994 and Hartung *et al.*, 1994 found a relationship between the ammonia emission rate and ventilation related parameters such as the ventilation rate, the inside temperature and the airflow pattern. Consequently, an improved control of the ventilation rate can have a significant impact on the ammonia emission reduction from livestock buildings.

Additionally, it has been shown that the energy efficiency of homeothermic animals is closely linked to their heat production. For example, pigs use around 70% of their energy intake (consumed as feed) to compensate for their heat losses. Thus, by controlling the ambient microenvironment, these losses can be minimised in order to optimise the energetic efficiency of the animal in question (Mount, 1968; Monteith and Mount, 1974; Verstegen *et al.*, 1978). The fundamental environmental parameters that affect the heat production of an animal are the ambient temperature, humidity and airflow/speed. These parameters are largely determined by the ventilation strategy utilised (Bruce and Clarke, 1979). Consequently, as Curtis (1983) and Monteith and Mount (1974) point out, the ventilation system plays an important role in controlling animal heat production. Finally, it is worth noting that not all livestock buildings require warm, non-fluctuating temperatures. In the case of sheep and goats, which mainly live outdoors, naturally ventilated cold housing is adequate, providing it is draft free in pen and resting areas, with sufficient air exchanges to remove moisture, gases and airborne disease organisms from the building. It is in this case where site location, building orientation and principles of ventilation design are important (Collins, 1990).

From the above findings it may be concluded that the possible benefits of more efficient microclimate control systems, along with the use of improved building materials or ammonia reduction techniques for livestock buildings, will only be fully realised if the ventilation rate can be controlled in a more efficient way.

1.2 REVIEW OF VENTILATION AND HEATING CONTROL IN AGRICULTURAL BUILDINGS

Presently, the most common type of controller used in agricultural animal housing and greenhouse control are derived from the Proportional (P), Proportional-Integral (PI) or Proportional-Integral-Derivative (PID) algorithms (Kreider and Rabl, 1996). The aforementioned controllers are generally manually tuned, which can often lead to instability due to poor tuning of the control gains and/or lack of anti wind up mechanisms. Ziegler and Nichols, (1942) proposed empirical methods of tuning the PID coefficients by creating a set of 'tuning rules' that translate the parameters of the model into 'gain' values for P, I and D parts, resulting in a generally acceptable tracking of set-point performance. However, different PID controllers use different algorithms, and each must be tuned according to the appropriate set of rules. These tuning rules can be rather subjective and also change when the derivative or the integral action is disabled. Further deficiencies associated with P, PI and PID controllers include: lack of set-point tracking caused by type zero behaviour of simple proportional control; and hunting because pure time delays are present in the system.

Some P, PI and PID controllers incorporate the Smith Predictor (Smith, (1957)) to alleviate the problems of pure time delays (e.g. Sigrimis *et al.*, 1999a). The Smith Predictor also allows higher controller gains for time delay systems (and therefore faster responses) without the system becoming unstable, but then the closed loop

system can become more sensitive to modelling errors. Davis and Hooper (1991), Chotai *et al.*, (1991a); (1991b), Young *et al.*, (1993), (1994), Young and Lees, (1995), Lees *et al.*, (1995), Lees, (1996) and Norris *et al.*, (1996), have all used variations on PI and PID for glasshouse heating and climate control; while Davies (1984), has also applied adaptive control to regulate heating in a greenhouse by adjusting the ventilator angle. A PI controller based on H∞ control system design methods has been proposed for greenhouse temperature control by Sigrimis *et al.*, (1999b) and Sigrimis *et al.* (2000). With the aid of a simulation model, this has been shown to handle large changes in model parameters and set-point changes.

Fuzzy logic controllers have been used for both livestock housing and greenhouse control. Gates *et al.*, (2001) and Sigrimis *et al.*, (2000) show that conventional staged ventilation systems can be replaced by a fuzzy inference technique. Comparisons between the two methods are made and results indicate enhanced controller flexibility with the fuzzy method. Seginer and Sher (1992) and Seginer, (1997) utilise artificial Neural Networks (NN) for micro-environmental control. They show that NNs adapt well to non-linear data and that they can be useful in control system design because they may be taught a variety of control rules that can mimic (for example) a model-based optimal feed-forward controller. However, the main disadvantage with NNs is their proper training requires large multi-dimensional data sets to reduce the risk of poor performance due to extrapolation errors. Further glasshouse temperature control with NNs has been carried out with the Radial Basis Function Network (RBFN) application of Ferreira *et al.*, (2000). Here, the RBFN is chosen due to its structural simplicity, with the RBFN consisting of three fully connected layers. The first is the input layer connecting the source codes to the hidden middle layer of the network,

which is composed of a certain number of units, called neurons. The outputs of this hidden layer are then linearly combined by a set of parameters to produce the overall network response in the output layer. Again, as observed with the NN methods of Seginer, (1997), due to the time variability of the process, training methods with on-line adaptation are required and the system can be computationally demanding. However, despite promising initial results, the authors concede further work still has to be done on integrating an RBFN air temperature model into a robust predictive digital control scheme.

1.3 MAINTAINING THE MICROENVIRONMENT IN LIVESTOCK HOUSING

In order to supply and control an optimum microclimate in agricultural livestock buildings, as described in the previous sections, the following points are general requirements that need to be taken into consideration when designing a climate control system:

i) Temperature is maintained by adjusting the ventilation rate; i.e. by varying the speed of the inlet/outlet fan.

ii) Optimum ventilation rate depends on a balance between the following parameters:

   a) Inlet air temperature.
   b) Moisture content.
   c) Gas levels (e.g. CO_2; CH_4; NH_3).
   d) Sensible and latent heat given off by livestock.
   e) Heat supplied by the internal heating system.
   f) Conduction losses through the building structure.

iii) For any agricultural building, the external diurnal temperature variation can be up to 20°C.

iv) The sensible heat given off from livestock is dependent mainly on their weight and food consumption.

v) Normal range of air speeds at animal height is 0.15-2.00 m/s, the slower speed indicating convection currents.

A temperature of about 15-20°C is not only an optimum temperature range for animals to live in, but is also suitable for carrying out microclimate experiments: see Boon (1978). In order to maintain this temperature range in animal housing, the ventilation rate has to be controlled carefully. Normally, it has to be either high during the summer period, when the outside temperature is often greater than 20°C; and low during cool, winter periods when pre-heated air may have to be added. A high ventilation rate ensures that the animals do not suffer undue heat related stress. However, there is a cooling effect due to the high air speeds over the livestock. Thus, a compromise may have to be reached where thermal comfort is weighted against the possible discomfort of living within a draft. If the animal housing is situated in a hot climate where 20°C is regularly exceeded, then extra ventilation systems may have to be installed or some other form of pre-cooling the airflow at the inlet employed. A series of ventilators operating at a lower airflow rate can have the same overall effect as one working at maximum capacity, but the resulting cooling effect is similar with less discomfort to the stock. Furthermore, Moss (1998) summarises many of the factors that influence the natural rate of ventilation in a building; factors that must be taken into consideration when designing and implementing any advanced control system:

i) Wind speed and direction, influenced by geographical location, with respect to the orientation of the building

ii) Height of the building

iii) Buoyancy forces or stack effect which induces natural draught within the building and depends on the difference between indoor and outdoor temperature

iv) Indoor and outdoor temperature

v) Shape and location of the building with respect to buildings in the vicinity

vi) Wind breaks, both natural and artificial

vii) How effectively the building is sealed

1.3.1 NATURAL VENTILATION

Air passes through an opening due to pressure differences on either side, which are induced by two main forces: wind forces (wind effect) and temperature or buoyancy forces (chimney or stack effect). The wind effect is generally split into two components: a steady effect and a turbulent effect. In the steady state case, the wind blowing over and around a building produces a wind field, which generates different pressures at different locations. This results in a pressure distribution over and around the building. In the case of a turbulent wind, the wind is not a static quantity, but varies continuously, resulting in pressure fluctuations over and around the building. In general, air movements around a building produce both positive (+ve) and negative (-ve) pressure zones: the +ve pressure is found at the end where the wind originates (stoss side), while the other end, (lee side) is –ve (figure 1.1). Thus the prevailing wind direction should be considered when siting specific buildings such as livestock housing (Moss, 1998).

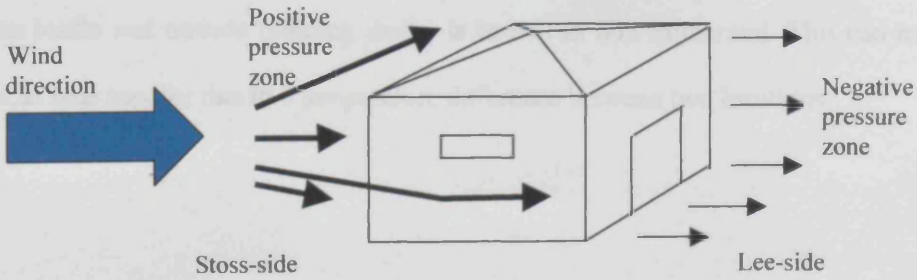

Figure 1.1: Schematic of building in relation to 'lee' and 'stoss' side winds.

The factors, which influence the effects of wind, are:

i) Building shape, size and orientation
ii) Location of the building with respect to other properties, including their shapes
iii) Natural and artificial wind breaks
iv) Type of terrain
v) Wind speed and direction
vi) Height above sea level

The stack effect is caused by differences in temperatures between both the inside and outside of a building and inlet and outlet openings. The greater the differences, the greater the potential for outdoor air to enter a building, so forcing the warm air from the inside to the outside. This effect is most noticeable in winter, especially for buildings that are heated.

1.3.2 NON-ISOTHERMAL CONDITIONS

It is often the case that temperature gradients exist between the outside and inside of buildings. These temperature gradients are strongly linked to temperature differences between the inside and outside of the building shell, and thus alter with the changing seasons. The largest gradients being present in winter on cold, frosty days when the temperature outside may be below freezing, while inside, the temperature may be controlled by a heating system which may keep the temperature up to 20°C higher. In summer, the temperature gradient will not be as great as in winter because the outside air temperature is often similar to inside. This condition (i.e. changes in temperature between inside and outside building shells) is known as non-isothermal. This can be defined as heat transfer due to a temperature difference between two locations.

1.3.3 VENTILATION SYSTEMS

One key question is the extent to which a ventilation system contributes to the control of the microenvironment within animal housing? ASHRAE (1997) defines ventilation as "the intentional introduction of air from the outside into the building structure". The block diagram in figure 1.2 outlines the different components of a typical ventilation system in a livestock building.

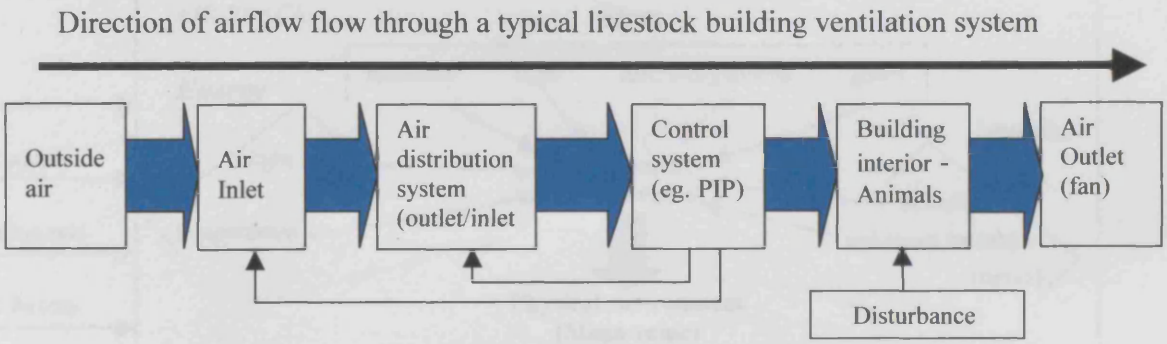

Figure 1.2: Block diagram of a typical ventilation system in a livestock building.

The influence of the above (figure 1.2) ventilation system on the heat exchange and thermal comfort of an animal is very complex, with multiple interactions existing between the micro-environmental conditions and factors such as building structure, nutrition, diseases etc. Subsequently, there are many micro-environmental variables that can be modified by a ventilation system (figure 1.3), each of them affecting the microenvironment around the animal (Carpenter, 1973; Albright, 1990; Randall and Boon, 1994).

Figure 1.3 shows the physical micro-environmental parameters likely to occur within a livestock building. As discussed earlier, each of these physical parameters is rarely uniform within the building. Consequently, they yield gradients of temperature, gas

concentrations and humidity (Barber and Ogilvie, 1982; Berckmans, 1986; De Moor and Berckmans, 1993; and Harral and Boon, 1997; Price, 1999). As a result, the physical conditions in the animal occupied zone(s) (microenvironment) can differ from the mean physical environment (T_i, X_i, G_i,) which is measured at the position of the control system sensors (figures 1.3 and 1.4).

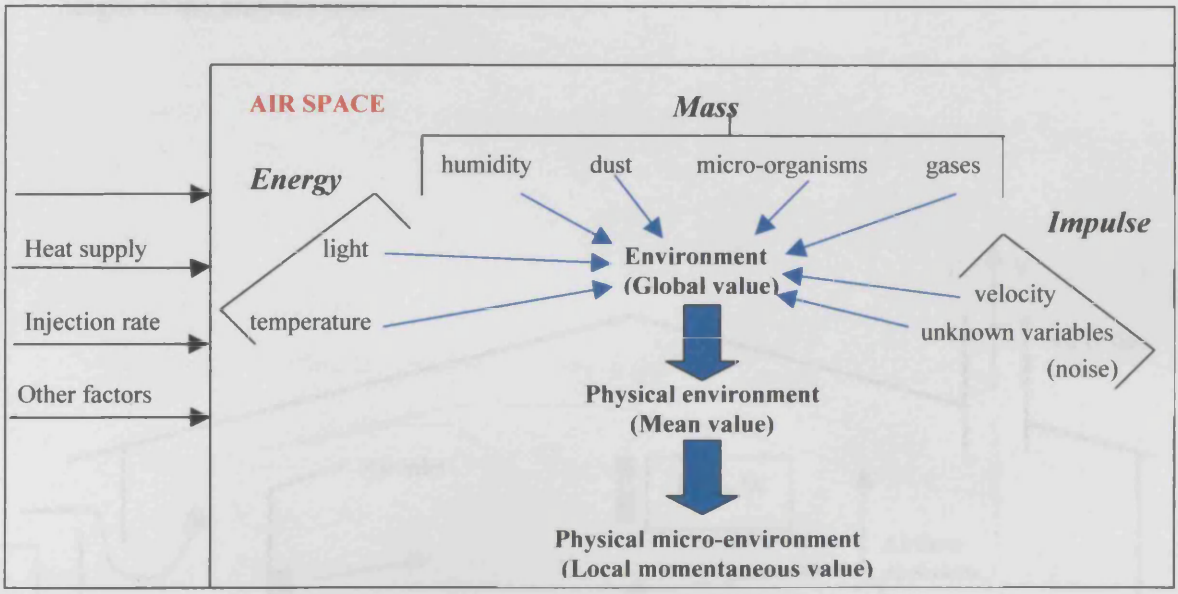

Figure 1.3: Factors influencing the microenvironment in a livestock building (after Berckmans, 1986).

In order to eradicate any imperfect mixing in the micro-environmental zone (figure 1.3) occupied by animals, the ventilation control system has to control

i) the amount of fresh air through the building envelope and the internal heat supply, i.e. control of the *global* ventilation rate;

ii) the internal distribution and mixing rate, i.e. the airflow pattern in *local* regions (Randall, 1975, 1981; Boon, 1978; Barber and Ogilvie, 1982; Berckmans, 1986).

Thus, the airflow pattern determines how much the global ventilation rate and the heat supply from the heating element truly affect the local micro-environmental conditions within the animal occupied zone (figure 1.4). This is the key objective of the modelling and control system design procedures described in the following chapters. Figure 1.5 below is a block diagram example of a global process model integrating the many parameters involved in achieving local micro-environmental control at the height of the animals nose.

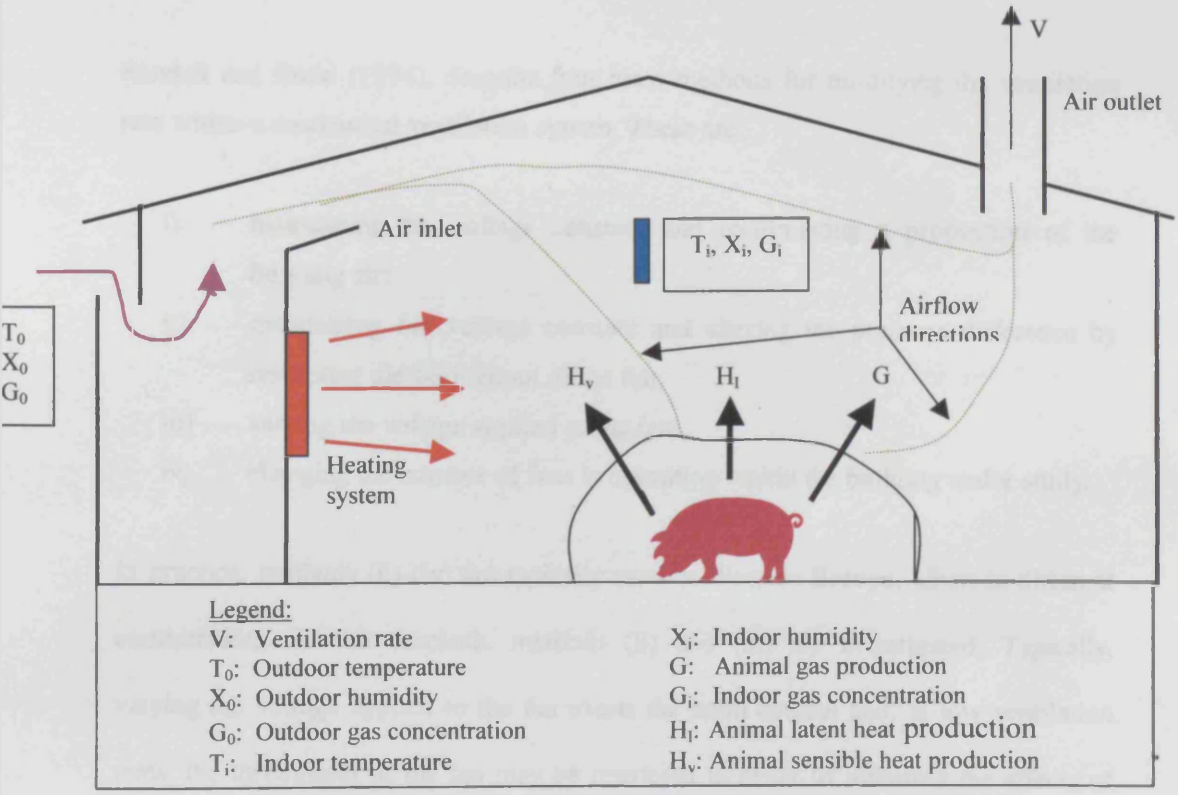

Figure 1.4: Representations of the physical microenvironment within a ventilated space and the influence of the airflow pattern (Adapted from Berckmans, 1986).

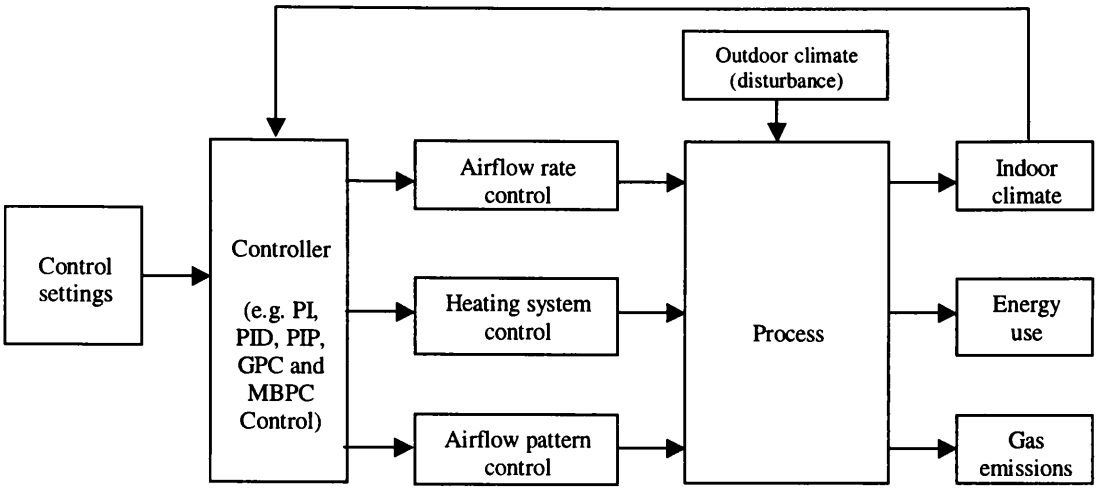

Figure 1.5: Global model structure for optimum physical microenvironment within animal housing (Vranken, 1999).

Randall and Boon (1994), describe four main methods for modifying the ventilation rate within a mechanical ventilation system. These are:

i) maintaining fan voltage constant and recirculating a proportion of the building air;
ii) maintaining fan voltage constant and altering the pressure difference by restricting the throughput of the fan;
iii) varying the voltage applied to the fan;
iv) changing the number of fans in operation within the building under study.

In practice, methods (ii)-(iv) are typically used in Western Europe, albeit in different combinations. In this research, methods (ii) and (iii) are investigated. Typically, varying the voltage applied to the fan exerts the main control and, at low ventilation rates, the throughput of the fan may be restricted in order to minimise the effects of thermal buoyancy and wind disturbance effects (Vranken, 1999).

1.3.4 LIVESTOCK BUILDING DYNAMICS

A nonlinear dynamic relationship exists between the *input* voltage to the control fan and the *output* measured ventilation rate. The nature of this relationship depends on the static pressure over the system and whether any disturbance is classed as a 'windward' or 'leeward' side disturbance. When the disturbance is windward, the absolute maximum ventilation rate the fan will reach is higher than the 'calm' (normal) maximum. Conversely, when the disturbance is 'leeward', the measured maximum airflow rate will be correspondingly lower depending on the magnitude of the leeward disturbance. Additionally, the chamber dynamics also change if either the inlet or outlet size or shapes are altered.

1.4 VENTILATION RATE – A NON-LINEAR SYSTEM

One aspect of the nonlinearity in the ventilation system can be visualised when the airflow rate is plotted against an increasing input voltage. This results in an 'S' shape or sigmoidal response curve from low to high ventilation rates and increasing internal static pressure (figures 1.6 and 1.7). This 'S' curve is a result of:

i) fan characteristics, and;

ii) a working curve as a function of static pressure.

However, at some points along the 'S' curve there are linear sections, which allow the system to be linearised and controlled as a linear or piece-wise linear system. This makes it possible to model and control the chamber without resorting to the full complexity of non-linear models and control system design methods. In this regard,

alternative piece-wise linear and adaptive control system design procedures have been developed as a major aspect of the present research project (see Chapter 5-7). These include:

i) switched gain control, where the system is programmed to automatically switch between a set of pre-determined gains for different points on the 'S' curve;

ii) a "three operating point" controller, where three model and control system designs are established for "low", "medium" and "high" ventilation rates on the 'S' curve;

iii) a "scheduled gain" control design, where model parameters are derived from a look-up table and control gains are calculated and implemented online;

iv) an "adaptive control" system design, where the model parameters are estimated recursively (see e.g. Young, 1984) and the control gains are then updated continuously, online, based on these estimates.

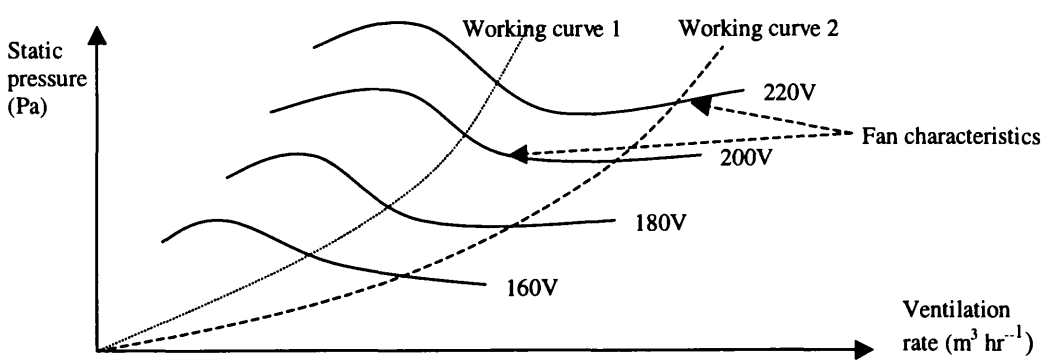

Figure 1.6: Plot to show the characteristics that shape the 'S' curve.

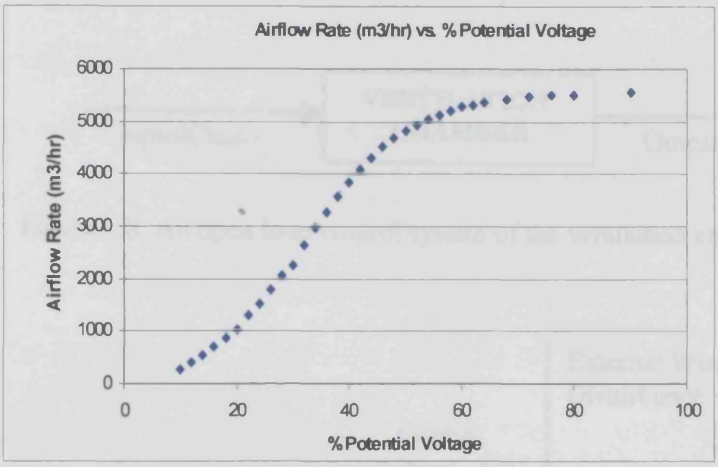

Figure 1.7: 'S' Curve response of airflow rate against voltage applied to the control fan for the Leuven ventilation chamber.

All four of these approaches are described fully in chapters 5-7, where their implementation on the Leuven ventilation chamber is also discussed. In addition, recent research in Lancaster has led to the development of a related multivariable controller that has been implemented on the Lancaster ventilation chamber.

1.5 CONTROL SYSTEM DESIGN

A control system can be defined as *altering the normal dynamic behaviour of a physical system such that it behaves in some desired way.* When designing a control system, four major objectives must be considered:

i) the closed loop control system should be *stable*;

ii) the controller should ensure that the output adequately *tracks* any applied command (desired) signal;

iii) the *transient* behaviour to the steady state should match as closely as possible the objectives of the control system design (e.g. desired transient behaviour with minimum energy consumption or even multiple objectives)

iv) the system should *reject* disturbances.

Figure 1.8: An open loop control system of the ventilation chamber.

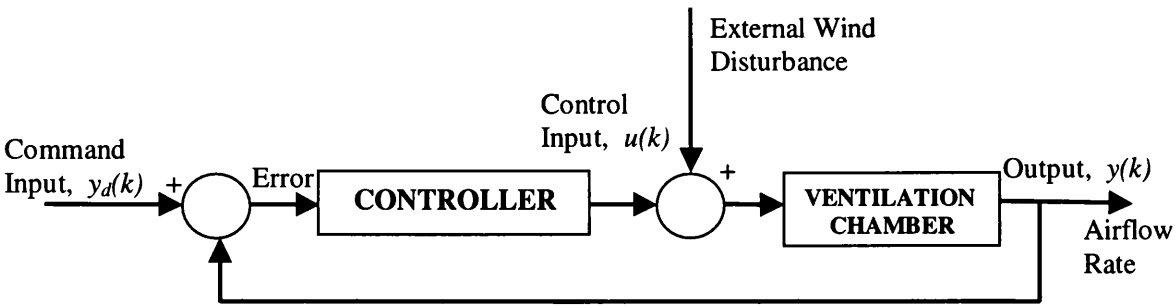

Figure 1.9: A closed loop control system of the ventilation chamber.

Sometimes, these four objectives may be achieved by "open-loop control"; i.e. by simply adjusting the *cause* and *effect* of the open loop system (figure 1.8). However, as control system science has shown, such objectives are better achieved by using a feedback controller of some sort, as illustrated in figure 1.9.

1.5.1 CONTROL SYSTEM HISTORY

Feedback control systems pre-date humanity because biological control systems evolved naturally in the earliest inhabitants of this planet (Nise, 2000). However, human beings were the first to evolve artificial automatic control systems as part of their growing interest in the development of technology that improved their life and satisfied their creative instincts. For example, a very early control system designed by man was the water clock invented by Ktesibios in ancient Greece around 300 B.C. Here, a float valve was employed similar to that used in flushed toilets today to

maintain a constant flow rate. Much later in 1745, Edmund Lee designed a speed controller for a windmill by varying the pitch of the blades against the current wind speed. Also in the same century, James Watt invented the flyball speed governor to control the speed of steam engines (Franklin *et al.*, 1991).

It was in the latter half of the 19th century that control systems theory began to emerge. In 1868 James Clerk Maxwell published the stability criterion for a third-order system based on the coefficients of the differential equation. Edward John Routh extended this in 1874 to fifth-order systems; and by 1877 this became known as the Routh-Hurwitz criterion for stability that is still in use today. This work was further extended in 1892 by Lyapunov to include non-linear systems with his thesis entitled "The General Problem of Stability in Motion".

By the twentieth century, control system design incorporated a variety of mathematical and graphical methods. These include the Nyquist diagram (1932), Bode plot (1945) and Nichols chart (1949). It was around this time that feedback control became commonplace in industrial processes and the Proportional-Integral-Derivative (PID) controller became the standard control algorithm. Callender *et al.*, (1936) introduced the PID control algorithm; and by 1942 Zieger and Nichols had proposed an empirical method of tuning the PID coefficients. Then, while working on the control and guidance of aircraft in the late 1940's, W.R. Evans developed the "Root Locus" method for evaluating how the variation of the feedback control gain affects closed loop behaviour of the system. Evans developed a set of rules for graphically following the position of the roots of the characteristic equation as a control parameter is modified. Such roots, or "closed loop poles", define the stability and transient behaviour of the system under study.

All the techniques described above still have their place today and are commonly referred to as belonging to the genre of classic control. However, it was with the advent of digital computers in the 1960's that complex calculations could be made that opened up the possibility of more sophisticated approaches to control system design. This opened up a whole new field of control possibilities within the control-engineering world, many of them associated with the concept of state space control, as evolved by Rudolf Kalman and others in the nineteen sixties. This led on to control system design methods such as Direct Digital Control (DDC), robust H_∞ control, risk averse Linear Exponential of Quadratic Gaussian (LEQG) control and adaptive control, many of which have their roots in state space concepts and methods. Additional, more recent approaches include, rule based, fuzzy logic, and neural network control systems.

In general, the state space approach to control system design is termed "modern control" and it has had an enormous influence on control system design since the nineteen sixties. Most importantly in the present context, it has stimulated the idea of True Digital Control (TDC) and the state space concepts underlying Proportional-Integral-Plus (PIP) control system design, as used in this thesis.

1.6 OVERVIEW OF THESIS

This rest of this thesis is composed of the following eight chapters:

1. **Chapter 2** outlines open-loop experimental methods and introduces the simplified refined instrumental variable (SRIV) method of model identification and estimation. Additionally, an example of Computational Fluid Dynamic (CFD) modelling, using the PHOENICS CFD software, is presented for a chamber with

similar dimensions to the ones used in this thesis. This chapter also describes the design of the Proportional Integral Plus (PIP) controller for single-input, single output (SISO) applications.

2. **Chapter 3** describes the Leuven (Belgium) test chamber and ventilation test rig used during this research; and outlines their construction, instrumentation and dynamics, along with the software used for real-time interfacing.

3. **Chapter 4** describes in detail the design, construction and instrumentation of the controlled environment chamber in Lancaster. Additionally, smoke visualisation experiments are carried out with different heating and airflow scenarios

4. **Chapter 5** describes the design, simulation and implementation of a fixed gain Proportional-Integral-Plus (PIP) controller on the Leuven chamber. The PIP approach is also compared with the alternative Proportional-Integral-Derivative (PID) control method.

5. **Chapter 6** further expands the control methodology by introducing more sophisticated controllers. This "scheduled gain" controller compensates for the nonlinearity in the system through the use of a look-up table of model parameter values over the whole operational range of the ventilation system, and the associated modification of the control system gains. The controllers are designed, simulated and finally implemented in the ventilation chambers in Leuven and Lancaster. At the end of this chapter, an adaptive control design is also implemented. Here, the aim is to design a 'plug and play' controller, which

eliminates the requirement for time consuming modelling and control design prior to implementation. It is a fully automated control design that can adapt to such changes.

6. A novel axial fan and throttling valve control system design is described in **chapter 7**, where the combined use of these two variables allows for excellent control of ventilation rates at low airflow levels with minimum power consumption. A comparison is made with a commercial controller. The final part of this chapter presents the design and implementation of a throttling valve-only controller under specific climatic conditions.

7. **Chapter 8** introduces and implements a multiple-input, multiple-output MIMO control design on the Lancaster controlled environment chamber. Here, the extra control input is heat and the additional measured output variable is temperature. A heating element is placed on the inlet and a series of thermocouples in a 3D array provide the temperature measurements. At the end of this chapter a section on bio-response control is introduced, where initial experiments with a subject inside the Lancaster chamber have been carried out.

8. Suggestions for further work, such as the air direction deflector and implementation of different control designs in an actual livestock building, along with overall conclusions, are presented in the final **Chapter 9**.

Appendix 1 lists the common acronyms and mathematical notation used throughout the text of this thesis. **Appendix 2** outlines the PHOENICS CFD program; while

Appendix 3 describes in detail the data acquisition methods used in the Lancaster controlled environment chamber, as well as the software for real-time interfacing between hardware devices, such as thermocouples and ventilators. **Appendix 4** shows further smoke experiment plots from chapter 4. **Appendix 5** describes different materials that may be utilised in different thermocouples applications. Finally, **Appendix 6** lists the publications arising from this research.

Chapter 2

SYSTEM IDENTIFICATION AND PIP CONTROL

2.1 MODELLING VENTILATED AIRSPACES

Prediction by a dynamical model is important in control-system design and the incorporation of anything more ambitious than the traditional trial and error tuned two-term controller in a control design requires a model to represent the system (Richards, 1979). In order to develop a model for use in control purposes, it is essential to determine what the control aim is. As highlighted in chapter one, there are

two basic requirements of the ventilation system, 1. Control of the global airflow rate, and 2. Efficient control over the airflow pattern at the local (animal) zone. Thus, a mathematical model, which can predict the behaviour of the dynamic airflow pattern over a range of ventilation rates, is an essential step in the design of an optimal controller for this system. It is neither practical nor conceivable to consider investigating the response of the system to all possible types of input function; thus, in general only specific types of inputs are utilised (figure 2.1). Schwarzenbach and Gill (1992), suggest three main types of forcing functions which may be applied to a system under study, in order to ensure as 'true' a representation of the system as possible is obtained. These are:

i) Transient disturbance signals, e.g. step changes of magnitude, ramp changes and
impulse changes.

ii) Sinusoidal signals with differing frequencies, or swept sinusoids.

iii) Statistical signals with random characteristics, e.g. Pseudo Random Binary Signals (PRBS).

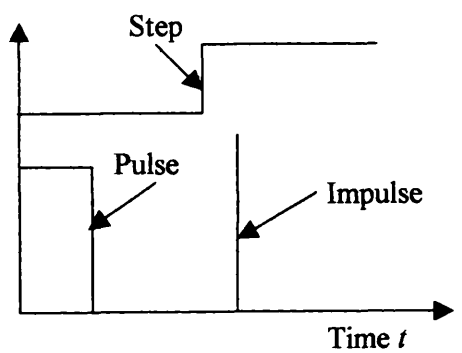

Figure 2.1: Basic system forcing functions (examples of type 1).

Input forcing functions one and two are deterministic in nature, and due to the straightforward facilitation of signal generation and the ensuing analysis these are prevalent in model identification. Additionally, they generally afford a physical comprehension of the system response (Schwarzenbach and Gill (1992). However, for stochastic or time varying systems and measurement noise, it may be necessary to use a statistical forcing function, such as PRBS. This is to obviate the risk of the output response being saturated by the noise signal due to the input perturbation signal being too low. If left, this may result in additional non-linear characteristics being added to the final model. With a PRBS, small deviations from the operating point can be attained and the noise effects can be attenuated by collecting data over a longer time period (figure 2.2).

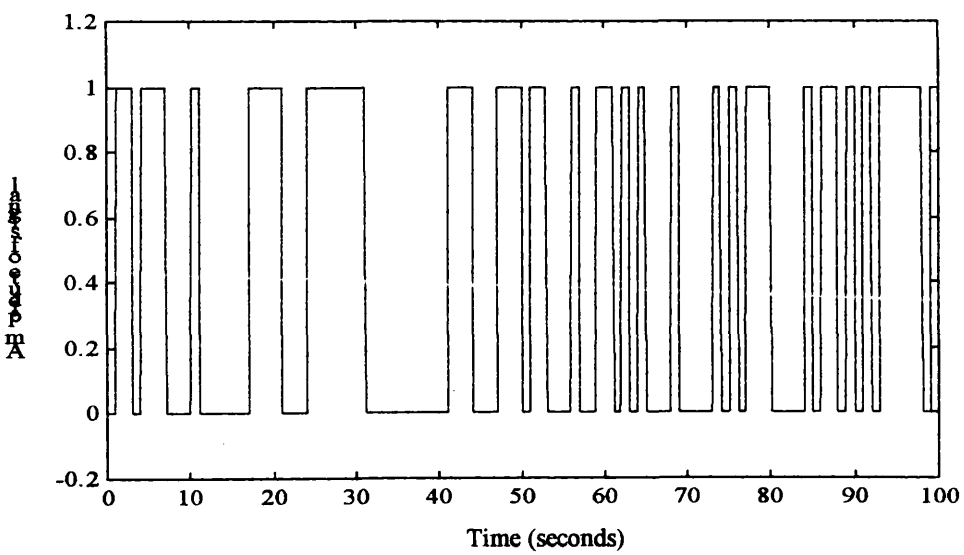

Figure 2.2: An example PRBS signal (type 3 forcing function).

2.1.1 NUMERICAL PHYSICALLY BASED MECHANISTIC MODELS

There has been a shift in recent times to modelling fluid flow problems via numerical models. Further investigation shows these mathematically, physically based (or

mechanistic) models are generally based on the continuity and conservation laws for momentum, enthalpy and mass flow, and are discretised in both time and space using partial differential equations (e.g. Navier Stokes equations) (Mistriotis *et al.*, (1997). It has been found that when these numerical (e.g. computational fluid dynamics (CFD)) models are applied to the problem of controlling ventilation rate and airflow patterns in an imperfectly mixed airspace they can be limited due to their exceptional complexity, requirement for an extensive data set for validation and general ability to generate only steady state simulations (De Moor and Berckmans, 1993; Jouini *et al.*, 1994; Daskalov, 1997; Leigh, 1999). Due to their (often) exceptional complexity (as perceived by the modeller) and over-parameterisation, these deterministic models require a number of assumptions to be made if they are to be used in digital control design. CFD simulation modelling has been attempted for the chambers under study, but validation has proved difficult (Leigh, 1999).

CFD has the advantage of allowing the 3D airspace to be modelled and visualised, but it is not easy to define parameters such as the boundary conditions Mistriotis *et al.*, (1997). One of the problems associated with CFD is the airflow in non-isothermal conditions, that is, there are changes in temperature between the incoming air and the test chamber air, which is invariably warmer. This also occurs in nature and is described in chapter 1. This introduces additional complexity to the concept of using the CFD analysis if these temperature gradients are to be accounted for. Additionally, CFD is not in an easily usable form for the present control system design context. Consequently, the Data-Based (DB) Transfer Function (TF) modelling approach outlined in the next section provides a more straightforward solution. An outline of the CFD modelling utilising the PHOENICS programme (Spalding *et al.*, 1994) carried

out in this study is given in Appendix 3. Other CFD packages include; FLUENT, FLOW3D and STAR-CD. All of these CFD packages utilise the finite volume method of solving the equations necessary to model the flow of fluid in any particular problem. However, the results yielded from CFD simulation rely on three major factors, namely:

- The problem being simulated.
- The CFD code implemented.
- The skill of the user.

In short, CFD analysis is the use of computer-based codes to give information about how fluids flow in given situations. Successful and accurate CFD modelling results are said to be as much an art as a science, from the results obtained this statement would appear vindicated.

The figure 2.3 below shows a simulated airflow pattern within a chamber of similar dimensions to that in Leuven. The airflow comes in through the inlet and stays high across the top of the chamber, hits the opposite end and descends towards the outlet, where some air leaves the chamber and some re-circulates around the chamber due to eddies and thermal buoyancy properties within the chamber. Obviously, different airflow input values will produce different sets of airflow vectors. It should be noted that not all CFD runs produce a steady, stable airflow pattern such as shown in figure 2.3.

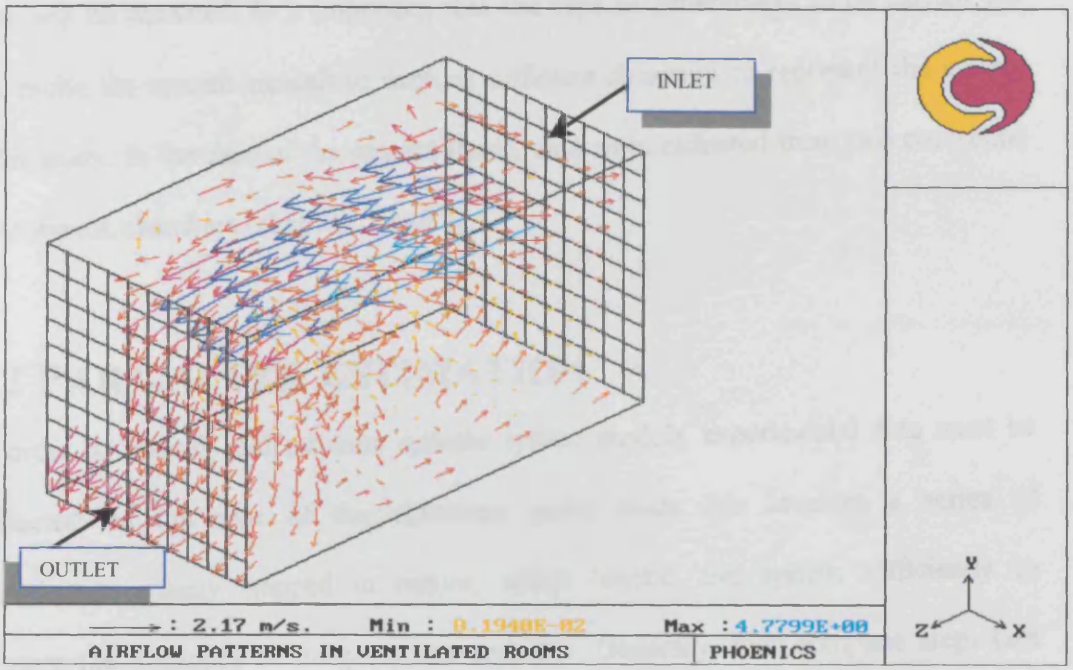

Figure 2.3: Computational Fluid Dynamics (CFD) simulated plot of airflow in Leuven Test Chamber using PHOENICS.

2.1.2 DATA BASED MECHANISTIC MODELS

An alternative to numerical models is the 'grey box' or data based mechanistic modelling method. Data based models, in contrast to physically based models, which are derived from physical, chemical or biological properties, are derived from direct reference to experimental data. In this method, the model structure is identified and the model parameters estimated directly from experimental data via objective, statistically based methods (Young, 1993). Additionally, data based models have been shown to be parametrically efficient compared to physically based mechanistic methods which often have a complex structure, are deterministic in form and require many parameters to describe the system under study.

Additionally, once the control aim has been established, it must be decided what type of open loop experimental data is required from which to estimate a model and how

these will be obtained. It is important that the type of experiments to be carried out will excite the system enough to capture sufficient dynamics to represent the system under study. In the case of the present thesis, data were collected from two controlled environment chambers (chapters 3 and 4).

2.2 PARAMETER ESTIMATION

In order to identify and estimate suitable system models, experimental data must be collected. In the case of the chambers under study this involves a series of experiments mainly stepped in nature, which 'excite' the system sufficiently to capture the dynamics of the particular chamber. Generally, four complete steps (see figure 2.4) were recorded for each experiment in an attempt to capture the dynamics of the system at each particular set point. The airflow rate/temperature was allowed to settle into a 'steady' state at the top and bottom of each step before the step direction was changed.

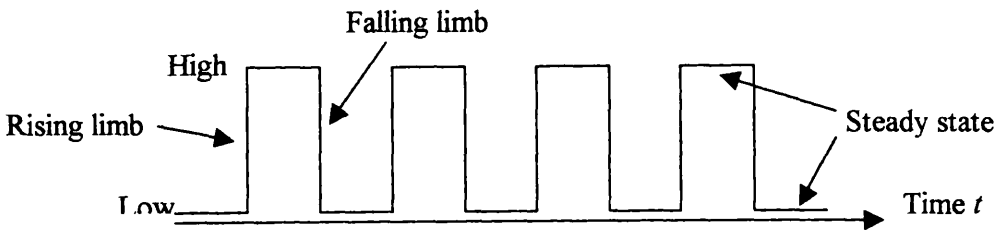

Figure 2.4: Example of step experiments carried out in controlled environment chambers.

The systems under study are non-linear over their whole operating envelopes and in order to design a controller suitable for use in true digital control (TDC) strategy (see section 2.4), a linearised representation of the system is required. For example, the response for the ventilation test chamber in Leuven is shown below (figure 2.5A). It is evident that the response is non-linear, however, close inspection of the plot reveals

that a series of linear or near-linear representations can be found by taking a series of small steps to encompass the whole operating range. Thus, a piece-wise linear representation of the whole system can be made (figure 2.5B).

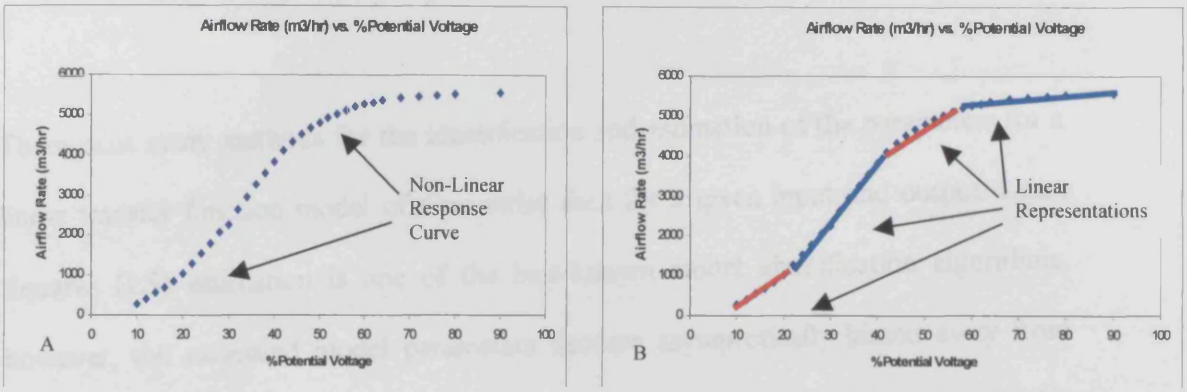

Figure 2.4: Characteristics of airflow rate with increasing percentage voltage input to ventilation test chamber. (a) Non-linear (sigmoid) response curve. (b) Piece-wise linear representation.

Due to the fact the system above can be approximated by a series of linear representations (piece-wise linear representation), (figure 2.5B above), the analysis will initially concentrate on linearised discrete-time transfer function (TF) models, which are identified and estimated from both simulated and measured data. The Simplified Refined Instrumental Variable (SRIV), (Young, 1984; 1985) algorithm used for estimating the model parameters is represented by the discrete-time, backward shift operator $\left(z^{-1}\right)$, where $z^{-1}y(k) = y(k-1)$. The deterministic model for a single input single output (SISO) system takes the following form,

$$y(k) = \frac{B(z^{-1})}{A(z^{-1})}u(k-\tau) \tag{2.1}$$

where y(k) is the measured output to be controlled and u(k) is the control input and $A(z^{-1})$ and $B(z^{-1})$ are the polynomials in the z^{-1}operator. These are defined below:

$$\left.\begin{aligned} A(z^{-1}) &= 1 + a_1 z^{-1} + a_2 z^{-2} + \ldots + a_{n-1} z^{-(n-1)} + a_n z^{-n} \\ B(z^{-1}) &= b_o + b_1 z^{-1} + b_2 z^{-2} + \ldots + b_{m-1} z^{-(m-1)} + b_m z^{-m} \end{aligned}\right] \qquad (2.2)$$

There exist many methods for the identification and estimation of the parameters for a linear transfer function model of time-series data for a given input and output. Least Squares (LS) estimation is one of the best-known model identification algorithms, however, the estimated model parameters become asymptotically biased away from their true values in the presence of measurement noise. Thus, in order to avoid this bias, other more complex methods have been developed such as: Instrumental Variable (IV), Refined Instrument Variable (RIV), and Simplified Refined Instrumental Variable (SRIV) methods (Young and Jakeman, 1980, Young *et al.*, 1980, Young, 1991). Other methods based on maximum likelihood methods (such as the Prediction Error Minimisation (PEM) algorithm in the Matlab Identification Toolbox (see, MATLAB, 1992)) can also be used, but they require concurrent estimation of most model parameters. The IV-based algorithms can be used for identification and estimation of different types of TF data-based models (i.e. linear, time-variant, deterministic, stochastic) in an 'en bloc' or 'recursive' approach. Thus, if the selected TF parameters are constant over time, then 'en bloc' methods can be used. Conversely, if the model parameters are changing over time, such as for time-variable TF models, a recursive identification approach can be used in which the model parameters are updated over time on receipt of additional data. In the following section, the least squares method for a deterministic TF model and the SRIV algorithm

for a stochastic time invariant parameter model are explained. For further information on the SRIV algorithm and other methods for different types of models, the reader is directed to (Young, 1984, Young, 1991).

2.3.2 LEAST SQUARES ESTIMATION

The motivation for developing the least squares method came from Karl Frederick Gauss in the early 1800's, who used it for the estimation of the six constant coefficients that determine the elliptical orbit of a planetary body. Additionally, Gauss developed an algorithm for sequentially or recursively updating the least squares parameter estimates on the receipt of additional data, thus representing the beginnings of recursive least squares theory (from Young, 1984).

The major difficulty in parameter estimation is in defining the parameters such that, the resultant model optimally describes the collected data. For this purpose a cost function is required that shows how well the model describes the data. The most commonly used cost function in this regard is the Least Squares (LS) function (J) which is defined as follows:

$$J = \sum_{k=1}^{k=N} \hat{e}(k)^2 \tag{2.3}$$

where, $\hat{e}(k)$ is the 'response error' and is the difference between the real output and the estimated model output at the kth sampling instance. A discrete-time TF model represented by equation 2.1, $\hat{e}(k)$ can be defined as,

$$\hat{e}(k) = y(k) - \frac{\hat{B}(z^{-1})}{\hat{A}(z^{-1})}u(k-\tau) \tag{2.4}$$

where, $y(k)$ denotes the real output and, $\hat{A}(z^{-1})$ and $\hat{B}(z^{-1})$ are the model estimates of the system polynomials $A(z^{-1})$ and $B(z^{-1})$ (equation 2.2). Therefore, the purpose is to define the values of the parameters such that the cost function (J) is minimised.

2.3.3 THE SIMPLIFIED REFINED INSTRUMENTAL VARIABLE (SRIV) APPROACH

Here it is proposed to use an alternative to the LS algorithm, which uses the response error within its cost function. The alternative equation error is linear in the parameters, compared to the response error equation (2.4), which is non-linear in terms of the model parameters. The equation error (used in this section and also denoted with $\hat{e}(k)$) is formulated as,

$$\hat{e}(k) = \hat{A}(z^{-1})y(k) - \hat{B}(z^{-1})u(k-\tau) \tag{2.5}$$

The IV algorithm utilises the equation error in its iterative, relaxation procedure. The initial response error equation can be linearised by the following mathematical re-arrangement:

$$\hat{e}(k) = \frac{1}{\hat{A}(z^{-1})}\left(\hat{A}(z^{-1})y(k) - \hat{B}(z^{-1})u(k-\tau)\right) \tag{2.6}$$

equation 5.7 can then be rearranged into the following form:

$$\hat{e}(k) = \hat{A}(z^{-1})y^*(k) - \hat{B}(z^{-1})u^*(k-\tau) \tag{2.7}$$

where, y^* and u^* are pre-filtered input (2.9) and output (2.10) signals respectively,

$$y^*(k) = \frac{1}{\hat{A}(z^{-1})} y(k) \tag{2.8}$$

$$u^*(k) = \frac{1}{\hat{A}(z^{-1})} u(k-\tau) \tag{2.9}$$

After the above sequence of mathematical re-arrangements, the response error equation (2.7) is effectively linear in terms of model parameters; however, it requires knowledge of the $A(z^{-1})$ polynomial. This pre-filtering of input and outputs is introduced in the RIV and SRIV algorithms to enhance the statistical efficiency of the parameters (Young, 1992).

The SRIV parameter estimation is based on the above procedure. The stochastic form of the discrete time TF model (2.1) takes the following form,

$$y(k) = \frac{B(z^{-1})}{A(z^{-1})} u(k-\tau) + \xi(k) \tag{2.10}$$

or,

$$y(k) = x(k) + \xi(k) \tag{2.11}$$

where, the term $\xi(k)$ is added to account for the unmeasured stochastic inputs and non-measurable deterministic inputs. The SRIV algorithm incorporates the following three steps:

1. Least Squares provide the initial parameter estimates of the polynomials $A(z^{-1})$ and $B(z^{-1})$. These estimates are then incorporated in the prefilters used in stages 2 and 3.
2. The estimated model obtained from the previous stage is used to generate the noise free outputs known as the auxiliary model, $x(k)$. The inputs $u(k)$, outputs

$y(k)$ and auxiliary model $x(k)$ are filtered, as in equations (2.8) and (2.9) and used in the Instrumental Variable estimation equations in order to re-estimate and update the parameters.

3. SRIV iterates IV using the prefilters, where the prefilter = 1/A, (i.e. part of the auxiliary model found at the IV stage, and used to prefilter data in order to reduce the variance on the noise). The IV algorithm is then repeated until convergence of parameter estimates occurs.

In order to identify the IV algorithm required in this iterative procedure, we first note that the TF equation (2.10) can be written in the following form:

$$y(k)+a_1y(k-1)+\ldots+a_ny(k-n)=b_0u(k-\tau)+b_1u(k-\tau-1)+\ldots \\ +b_mu(k-\tau-m)+\eta(k) \tag{2.12}$$

where, $\eta(k)$ is a noise variable defined as follows in relation to the original noise $\xi(k)$,

$$\eta(k)=\xi(k)+a_1\xi(k-1)+\ldots+a_n\xi(k-n) \tag{2.13}$$

The equation (2.12) can then be re-written in the following vector form, which is more convenient for describing the estimation procedure,

$$y(k)=Z(k)^T\alpha+\eta(k) \tag{2.14}$$

Here, $Z(k)$ and α are the state and parameter vectors, respectively defined as follows,

$$Z(k)=[-y(k-1),-y(k-2),\ldots,-y(k-n),u(k),\ldots,u(k-m)]^T \tag{2.15}$$

$$\alpha=[a_1,a_2,\ldots,a_n,b_0,b_1,\ldots,b_m]^T \tag{2.16}$$

It then follows that the equation error is defined as,

$$\hat{e}(k) = y(k) - Z(k)^T \hat{\alpha}(k) \tag{2.17}$$

where $\hat{\alpha}(k)$ is the estimated vector of parameters at instant k.

Next, by using the LS function (2.4) and setting the gradient, $\nabla_\alpha J = \sum \hat{e}(k)\partial\hat{e}(k)/\partial\alpha^T$ to zero, the following estimation equation is obtained,

$$\hat{\alpha} = \left[\sum_{k=1}^{N} Z(k)Z(k)^T\right]^{-1} - \sum_{k=1}^{N} Z(k)y(k) \tag{2.18}$$

In the IV method, *Z(k)* in equation (2.18) is replaced by the instrumental variable vector χ(k), as follows:

$$\hat{\alpha} = \left[\sum_{k=1}^{N} \chi(k)Z(k)^T\right]^{-1} - \sum_{k=1}^{N} \chi(k)y(k) \tag{2.19}$$

The instrumental variable (IV) vector is defined by,

$$\hat{\chi}(k) = \left[-\hat{x}(k-1), -\hat{x}(k-2), \ldots, -\hat{x}(k-n), u(k), \ldots, u(k-m)\right]^T \tag{2.20}$$

where, $\hat{x}(k)$ is the auxiliary model output obtained as follows,

$$\hat{x}(k) = \frac{\hat{B}(k)}{\hat{A}(k)}u(k) \tag{2.21}$$

Where, $\hat{A}(z^{-1})$ and $\hat{B}(z^{-1})$ are the estimated values of the $A(z^{-1})$ and $B(z^{-1})$ polynomials. In the SRIV algorithm, *u(k)*, *y(k)* and $\chi(k)$ in equation (2.19) are replaced by their pre-filtered values, *u*(k)* and *y*(k)* previously defined by equations (2.8) and (2.9), and $\chi^*(k)$ is defined as,

$$\chi^*(k) = \frac{1}{\hat{A}(z^{-1})}\chi(k) \tag{2.22}$$

The model parameters are then estimated from the following equation in an iterative procedure defined previously, i.e.,

$$\hat{\alpha} = \left[\sum_{k=1}^{N} \chi^*(k)Z(k)^T\right]^{-1} * \sum_{k=1}^{N} \chi^*(k)y^*(k) \tag{2.23}$$

Figure 2.6 below outlines the stages of the discrete time SRIV algorithm described above.

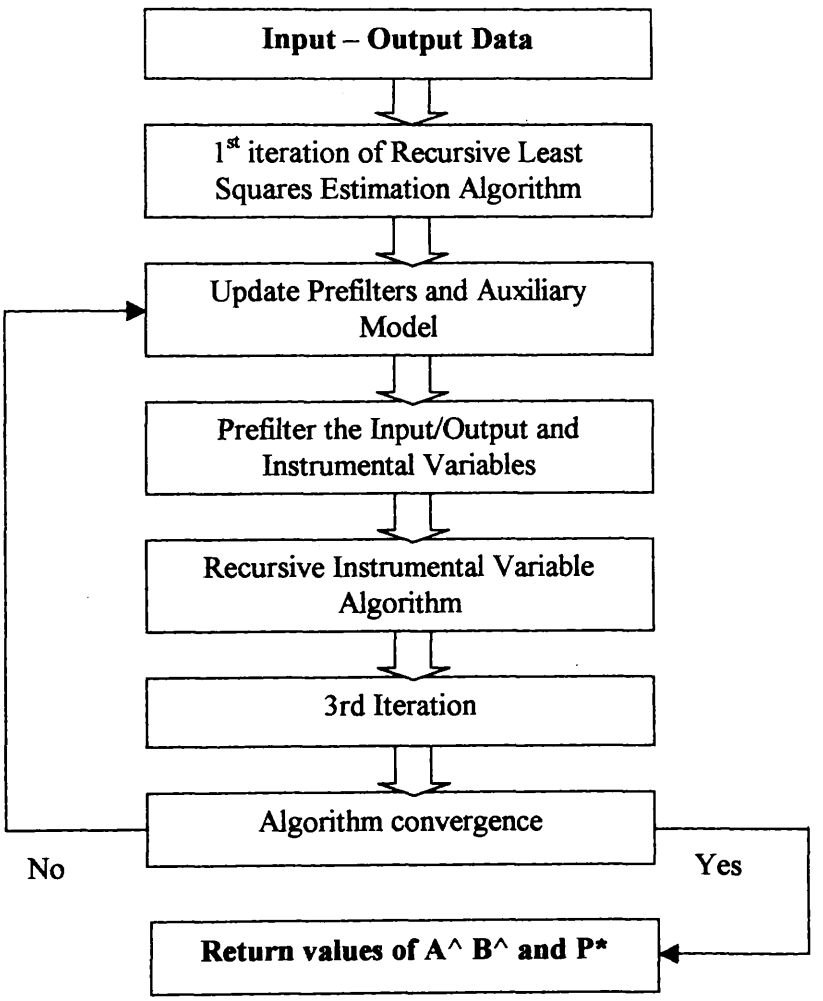

Figure 2.6: Schematic representation of the discrete-time SRIV algorithm

2.3 MODEL IDENTIFICATION

Using the SRIV algorithm described above will result in a set of models which fit the data well. However, some models may be over parameterised, thus to determine the most 'parsimonious' model which also gives an acceptable data fit, a number of statistical criteria can be applied. For input-output data (transfer function (TF)) models, the following criteria are used: the coefficient of determination (R_T^2) and the Young Information Criterion (YIC), (Young, 1988). Model Order Identification gives the most suitable values for the orders of [n and m] of the TF polynomials plus any associated pure time delay that affects the input-output relationship.

2.3.1 COEFFICIENT OF DETERMINATION (R_T^2)

The Coefficient of Determination criterion, is a statistical measure of how well the model explains or fits the data, it is a measure of goodness of fit. The greater the amount of data the model explains, the closer to unity the value will be, for example, an R_T^2 of 0.87 indicates that 87% of the variance in the data is explained by the model. The definition of the R_T^2 statistic is given in (2.24). As a result this *goodness of fit* criterion tends to unity if the variance of the model residuals σ^2 is low compared with the variance of the data σ_y^2 and tends towards zero if σ^2 is of similar magnitude to σ_y^2.

$$R_T^2 = 1 - \frac{\hat{\sigma}^2}{\sigma^2} \tag{2.24}$$

where, σ_y^2 is defined as;

$$\sigma_y^{\,2} = \frac{1}{N}\sum_{k=1}^{k=n}\left(y_k - \bar{y}_k\right)^2 \tag{2.25}$$

and $\bar{y}_k$ is given as;

$$\bar{y}_k = \frac{1}{N}\sum_{k=1}^{k=n} y_k \tag{2.26}$$

and σ^2 is defined as;

$$\hat{\sigma}^{\,2} = \frac{1}{N}\sum_{k=1}^{k=n} \hat{e}_k^2 \tag{2.27}$$

and

$$e_k = y_k - \hat{y}_k \tag{2.28}$$

where, N is the total number of samples; $\bar{y}$ is the mean value of the output series y(k); and e_k is the model residual.

2.3.2 YOUNG INFORMATION CRITERION (YIC)

The use of R_T^2 alone is not recommended as it may result in a model that is over-parameterised. A further more complex, heuristic statistic, namely: the Young Information Criterion (YIC) (Young, 1988), provides information on the number of parameters that an appropriate for a given model. The YIC is defined in the following form,

$$YIC = \ln\left[\frac{\sigma^2}{\sigma_y^2}\right] + \ln\left(NEVN\right) \tag{2.29}$$

where, σ^2 is the sample variance of the model residuals σ_y^2 is the sample variance of the measured system output *y(k)* about its mean value and NEVN is the normalised error variance norm (Young *et al.*, 1980; Young, 1989), NEVN is defined in the following form,

$$NEVN = \frac{1}{np}\sum_{i=1}^{np}\frac{\hat{\sigma}^2\hat{p}_{ii}}{\hat{a}_i^2} \tag{2.30}$$

where, np is equal to $m + n + 1$ (total number of parameters estimated);

$\hat{a}_i$ is the estimate of the ith parameter in the vector α of all the model parameters,

$$\alpha = [a_1\ a_2\ \ldots\ a_n\ b_0\ b_1\ \ldots\ b_m]^T \tag{2.31}$$

and $\hat{\sigma}^2\hat{p}_{ii}$ is an estimate, obtained during the analysis, of the error variance associated with the ith parameter estimate.

The first part of the YIC criterion provides a normalised measure of how well the model explains the data, the smaller the variance of the model residuals in relation to the variance of the measured input, the more negative the first term becomes. While the second part is the normalised measure of the uncertainty in the parameter estimates. The smaller the parameter errors, the better they are defined which results in an increasingly negative value. As the model becomes over parameterised the second term increases, while the first tends to decrease. So the YIC provides a compromise between the ability of the model to explain the data and the order of the model required to achieve this..

Obviously, it would not be prudent to blindly use these statistical criterions in isolation. Further considerations, such as the physical nature of the final model are examined for each estimated and identified model as demonstrated in the practical examples in the following chapters.

2.4 PIP CONTROL DESIGN

The advantage of the Data Based (DB) modelling methodology is its simplicity and ability to characterise the dominant modal behaviour of a dynamic system. This enables such a model to be ideal for model-based control system design. Here, such a model is utilised in the design of an advanced Proportional-Integral-Plus (PIP) control system.

The True Digital Control (TDC) philosophy has been developed by Young *et al.*, (1987 and 1988), where, each part of the control system design are unequivocally digital by nature. In the above papers and many others on the subject such as, Chotai and Young, (1991); Taylor *et al.*, (1998), the TDC control system design analysis is dependent on the definition of an appropriate Non-Minimum State-Space (NMSS) form. The TDC design method can be described as a further advancement of the multi-variable continuous time systems of Young and Willems (1972). The NMSS model representation has a number of advantages over other forms of State Variable Feedback (SVF) control system design. The state vector is defined such that it comprises only of the past and present sampled values of the output signal, the past values of the input signal and an "integral of error" state which allows for the requisite type one servomechanism performance. In addition, the elements of the matrices in the NMSS form are determined directly from the estimated model parameters.

It has been shown by Taylor, *et al.*, (1994) that the PIP control system is similar in design to the Generalised Predictive Controller (GPC), of Clarke *et al.*, (1987a, 1987b) and Clarke, (1994). Thus, the PIP control design may be interpreted in the same model-based predictive control (MBPC) terms, as is the GPC controller.

However, the PIP controller has one main advantage over GPC and other controllers of this period and earlier, in its inherent state-space formulation. This state-space formulation enables linear quadratic (LQ) optimal control or SVF pole-assignment, and, in addition, allows for related stochastic designs and a simple extension to the univariate design process to cover multivariable control systems.

The Proportional-Integral-Plus (PIP) controller can be interpreted as a logical extension of conventional Proportional Integral (PI) and Proportional-Integral Derivative (PID) controllers, with additional dynamic feedback and input compensators introduced automatically when the process has second order or higher dynamics or pure time delays greater than one sampling interval. The block diagram in figure 2.7 shows this extension from the PI and PID controllers, with additional feedback and input compensators added.

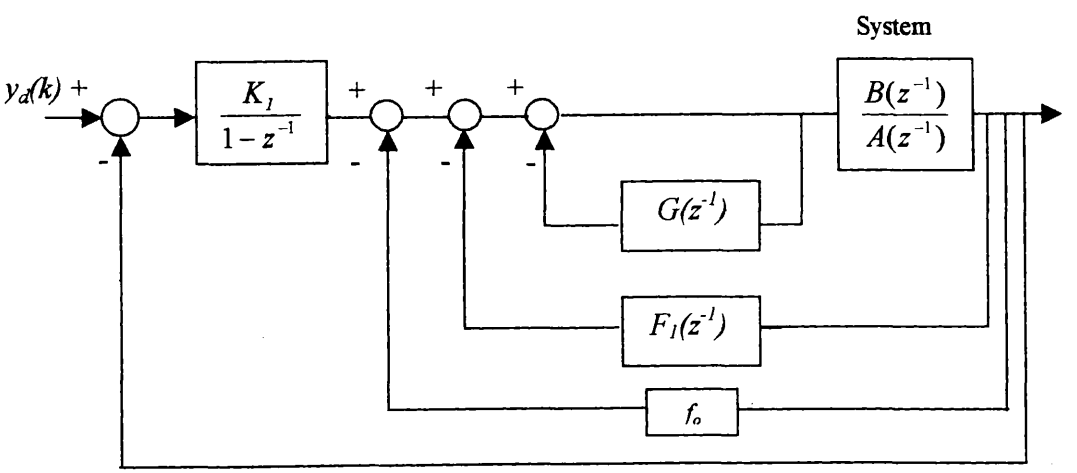

Figure 2.7: The PIP/NMSS controller structure in standard feedback form.

Here, $\frac{B(z^{-1})}{A(z^{-1})}$ represents the system dynamic, K_I is the integral gain of the controller, f_0 is the proportional gain, and $F_1(z^{-1})$ and $G(z^{-1})$ are the feedback compensation polynomials, defined as follows:

$$F_1(z^{-1}) = f_0 + f_1 z^{-1} + f_2 z^{-2} + \ldots + f_{n-1} z^{-(n-1)} \qquad (2.32)$$

$$G(z^{-1}) = 1 + g_1 z^{-1} + g_2 z^{-2} + \ldots + g_{m-1} z^{-(m-1)}$$

where, $f_0, f_1, \ldots, f_{n-1}$ and $g_1, \ldots, g_{m-1}$ are the PIP control gains.

In contrast to conventional PI/PID controllers, however, the PIP design has numerous advantages: in particular, its structure exploits the power of State Variable Feedback (SVF) methods, where the vagaries of manual tuning are replaced by pole assignment or Optimal Linear Quadratic (LQ) design; see e.g. (Taylor *et al* 1998). Because the resulting SVF control law solely utilises the measured input and output variables and their past values, a state reconstructor observer (filter) is not necessary.

The first stage in the formulation of the NMSS representation is to identify and estimate a suitable TF model of the system to be controlled. The resulting discrete-time TF takes the form,

$$y(k) = \frac{b_1 z^{-1} + b_2 z^{-2} + \ldots + b_m z^{-m}}{1 + a_1 z^{-1} + a_2 z^{-2} + \ldots + a_n z^{-n}} u(k) \qquad (2.33)$$

which can be reduced to,

$$y(k) = \frac{B(z^{-1})}{A(z^{-1})} u(k) \qquad (2.34)$$

where,

$$A(z) = 1 + a_1 z^{-1} + a_2 z^{-2} + \ldots + a_n z^{-n}$$

$$B(z) = b_1 z^{-1} + b_2 z^{-2} + \ldots + b_m z^{-m} \qquad (2.35)$$

From equations (2.33) and (2.34), it can be shown that the model can be represented by the following NMSS equations,

$$\begin{aligned} x(k) &= Fx(k-1) + gu(k-1) + dy_d(k) \\ y(k) &= hx(k) \end{aligned} \tag{2.36}$$

The $n+m$ dimensional state vector $x(k)$, consists of both the present and past values of the output variable $y(k)$ and the past sampled values of the input $u(k)$, plus an *integral-of-error* state which is added to give type-1 servomechanism performance,

$$\begin{aligned} x(k) = [\, & y(k)\, y(k-1) \ldots y(k-n+1)\, u(k-1)\, u(k-2) \\ & \ldots u(k-m+1)\, z(k)\,]^T \end{aligned} \tag{2.37}$$

In equation (2.38), the *integral-of-error* state $z(k)$ is defined as the integral of the error between the reference or command input $y_d(k)$ to the servomechanism system and the sampled output $y(k)$,

$$z(k) = z(k-1) + \{y_d(k) - y(k)\} \tag{2.38}$$

The following matrix and vectors can then show the NMSS representation in equation (2.39). Where, the state transition matrix $\boldsymbol{F}$, input vector $\boldsymbol{g}$, command input vector $\boldsymbol{d}$, and output vector $\boldsymbol{h}$ are defined as follows,

$$F = \begin{bmatrix} -a_1 & -a_2 & \ldots & -a_{n-1} & -a_n & b_2 & b_3 & \ldots & b_{m-1} & b_m & 0 \\ 1 & 0 & \ldots & 0 & 0 & 0 & 0 & \ldots & 0 & 0 & 0 \\ 0 & 1 & \ldots & 0 & 0 & 0 & 0 & \ldots & 0 & 0 & 0 \\ \vdots & \vdots & & \vdots & \vdots & \vdots & \vdots & & \vdots & \vdots & \vdots \\ 0 & 0 & \ldots & 1 & 0 & 0 & 0 & \ldots & 0 & 0 & 0 \\ 0 & 0 & \ldots & 0 & 1 & 0 & 0 & \ldots & 0 & 0 & 0 \\ 0 & 0 & \ldots & 0 & 0 & 1 & 0 & \ldots & 0 & 0 & 0 \\ 0 & 0 & \ldots & 0 & 0 & 0 & 1 & \ldots & 0 & 0 & 0 \\ \vdots & \vdots & & \vdots & \vdots & \vdots & \vdots & & \vdots & \vdots & \vdots \\ 0 & 0 & \ldots & 0 & 0 & 0 & 0 & \ldots & 1 & 0 & 0 \\ a_1 & a_2 & \ldots & a_{n-1} & a_n & -b_2 & -b_3 & \ldots & -b_{m-1} & -b_m & 1 \end{bmatrix}$$

and,

$$\begin{aligned} \boldsymbol{g}^T &= [\, b_1, 0, \ldots, 0, 1, 0, 0, \ldots, 0, -b_1 \,] \\ \boldsymbol{h} &= [\, 1, 0, \ldots, 0, 0, 0, 0, \ldots, 0, 0 \,] \\ \boldsymbol{d}^T &= [\, 0, 0, \ldots, 0, 0, 0, 0, \ldots, 0, 1 \,] \end{aligned} \tag{2.39}$$

From the NMSS model (2.39) above, the associated SVF law then takes the form,

$$u(k) = -\boldsymbol{k}\boldsymbol{x}(k) \tag{2.40}$$

where, $\boldsymbol{k}$ is the (n+m) dimensional SVF control gain vector,

$$\boldsymbol{k} = [\, f_0 f_1 \cdots f_{n-1} \cdots g_{m-1} - K_I \,] \tag{2.41}$$

There are two conditions that must be satisfied if the SVF control law based on the above NMSS model is to be controllable, these are given by the following theorem.

Theorem: Proposed by Wang and Young, (1988), states: Given a single-input single-output system as described by (2.36), the non-minimal state space representation (2.40), as described by the pair $\{\boldsymbol{F}, \boldsymbol{g}\}$, is completely controllable, if and only if, the following two conditions are satisfied: 1. the polynomials $A(z^{-1})$ and $B(z^{-1})$ are coprime. 2. $b_1 + b_2 + \ldots + b_m \neq 0$

The coprimeness condition is equivalent to the normal requirement that the TF model (2.33) should have no pole-zero cancellations. The second condition avoids the presence of a zero at unity, which would cancel with the unity pole associated with the integral action.

2.4.1 LINEAR QUADRATIC OPTIMAL CONTROL

Linear Quadratic optimal control is where the PIP control gain vector is computed so that it, will minimise the quadratic cost function (2.42).

$$J = \frac{1}{2}\sum_{i=0}^{\infty} x(i)^T Qx(i) + ru^2(i) \tag{2.42}$$

where, Q is an $(n+m)$ x $(n+m)$ symmetric, positive semi-definite matrix and r is a scalar weight on the input. The Q matrix in (2.42) above has an interesting aspect due to the unique structure of the non-minimal state vector, in that the diagonal elements represent the weights assigned to squared values of not only both the present and past values of the output but, in addition, the past values of the input and the current integral-of-error term. The elements of the Q matrix are defined as follows,

$$Q = diag[q_1, q_2, \ldots, q_n, q_{n+1}, \ldots, q_{n+m-1}, q_{n+m}] \tag{2.43}$$

where,

$$\begin{aligned} q_1 &= q_2 = \ldots = q_n = q_y \\ q_{n+1} &= q_{n+2} = \ldots = q_{n+m-1} = q_u \\ q_{n+m} &= q_z \end{aligned} \tag{2.44}$$

and, due to the special nature of the NMSS form, $r = q_u$. From (2.44) above, q_y, q_u and q_z are *partial* weightings on the output, input and integral-of-error variables in the NMSS vector $x(k)$. Thus, the above partial weightings can be defined as,

$$q_y = \frac{W_y}{n}; q_u = \frac{W_u}{m}; q_z = W_z \tag{2.45}$$

then, W_y, W_u and W_z respectively define the total weightings on the output, input and integral-of-error of the control system. With the fixed gain control design used in this thesis, the three defined scalar weighting factors can be manually tuned for desired closed loop performance of the controller. Utilising the NMSS system description (F, g) plus weighting matrices (Q, r), the optimum SVF gains for the chosen weighting values can be acquired by computing the steady state solution of the associated, discrete-time, matrix Riccati equation (see Borrie, 1986 and Kuo, 1980).

2.4.2 POLE PLACEMENT DESIGN

In pole placement design, the objective is to design the SVF gain vector such that the poles of the closed loop system are at pre-determined positions in the complex z-plane. Choice of suitable closed loop pole locations can be either based on trial and error or some design techniques (see, Franklin *et al.*, 1991). Many algorithms have been proposed to design the SVF gain vector (e.g., Kailath, 1980; Luenberger, 1967; Gopinath, 1971) however, it is possible to compute the gains in a particularly simple manner; by state-space analysis (Young and Willems, 1972); or alternatively, by straightforward polynomial algebra (see Young *et al.*, 1987). For more information and detail of the methods, the reader is directed to the related references.

2.4.3 ALTERNATIVE CONTROL STRUCTURES

There are a number of alternative structures that may be used to implement the SVF control law as opposed to the standard form. For example, a system with disturbances can often be better controlled using forward path control action. Microclimate control is an example of an application that may benefit from forward path control action because the system can be strongly affected by a number of disturbances, such as

wind speed and direction, along with solar radiation, which can create large temperature gradients between the inside and outside of livestock housing.

Additionally, when input constraints apply to the system, the integral wind-up problem may occur. In this case, it is better to implement the '*incremental*' form of the PIP control law, referred to as the incremental form of the PIP controller. In this section, a different structure of the PIP controller, namely the forward path form of the PIP controller is explained. More detailed information on these, and other structures such as the incremental form, filter form, Kalman filter-PIP and feed forward PIP are discussed in; Lees (1996), Dixon (1996) and Taylor (1996).

2.4.3.1 FORWARD PATH FORM OF PIP CONTROLLER

An alternative to the standard form PIP structure is the forward path structure. Here, the measured output of the system is fed back to generate only the error signal necessary for the integrator in the integral of error generation; the model output ($\hat{y}(k)$), rather than the measured output, is fed back to the proportional gain (f_0) and output compensator of the control loop i.e., $F_1(z^{-1})$. This structure is shown in figure 2.9, where $\frac{\hat{B}(z^{-1})}{\hat{A}(z^{-1})}$ denotes the estimated model of the system $\left(\frac{B(z^{-1})}{A(z^{-1})}\right)$. Clearly, when there is no model mismatch, i.e. $\frac{\hat{B}(z^{-1})}{\hat{A}(z^{-1})} = \frac{B(z^{-1})}{A(z^{-1})}$, then both the forward path form and the standard feedback structures are identical. Therefore, both forward path and feedback structures of PIP controller produce the same results when they are implemented on the control model.

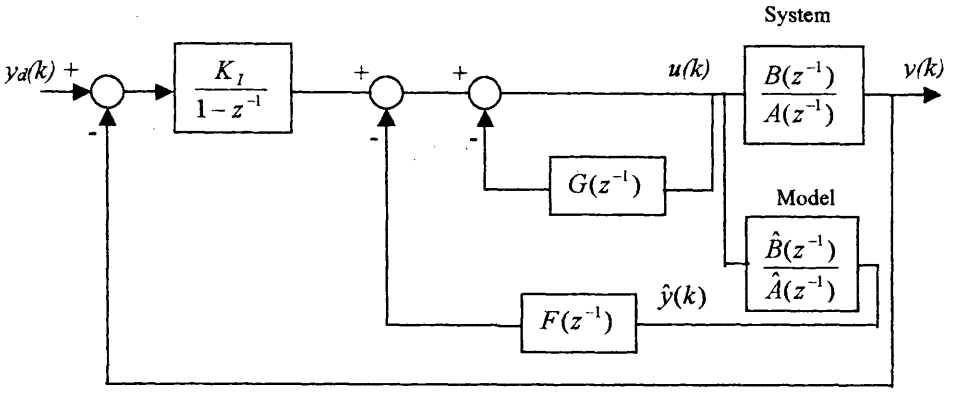

Figure 2.8: Forward path structure of the PIP controller.

The structure presented in figure 2.8 can be easily converted to the form in figure 2.9. Because the pre-compensation appears in the control loop, this form is referred to as the forward path form.

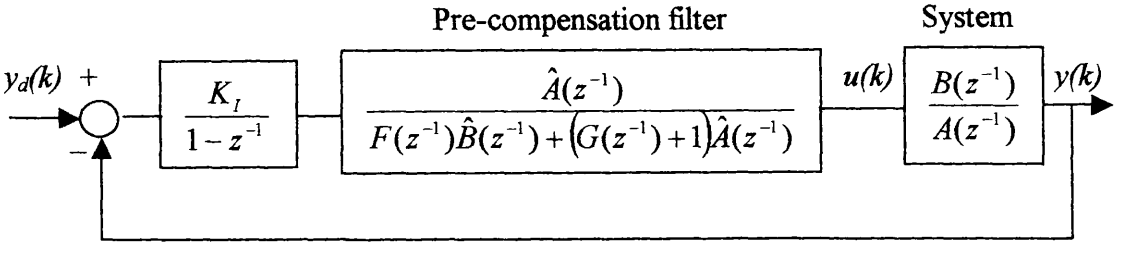

Figure 2.9: The PIP control system in forward path form.

The research implemented by Taylor *et al.* (1996) implies that the standard form structure is more sensitive to modelling errors than the forward path. However, this structure is useful when the output measurements are noisy as it ensures that the noise is not amplified within the controller function thus, providing a smoother control input. However, when the system experiences high amplitude and frequency load disturbances, the standard form is unable to provide as good a closed loop performance as the forward path achieves. The reason is that the model of the system

in the standard form control loop, does not take into account the effects of the load disturbances which affect the real output. In other words, these effects are only being fed to the integrator, not the other compensators of the forward path control loop. In chapter 5 the forward path structure is compared with the feedback structure for both setpoint tracking and disturbance rejection, where the ventilation rate system is controlled using a PIP controller.

2.4.3.2 COMPLETE TRUE DIGITAL CONTROL (TDC)

In previous sections of this chapter, we have considered the identification and estimation of a discrete-time, digital control model of a dynamic system and its subsequent use in PIP control system design. This complete process, plus its implementation, can be considered as a True Digital Control (TDC) design procedure.

The true digital control (TDC) strategy can be summarised with the following flow diagram (figure 2.10):

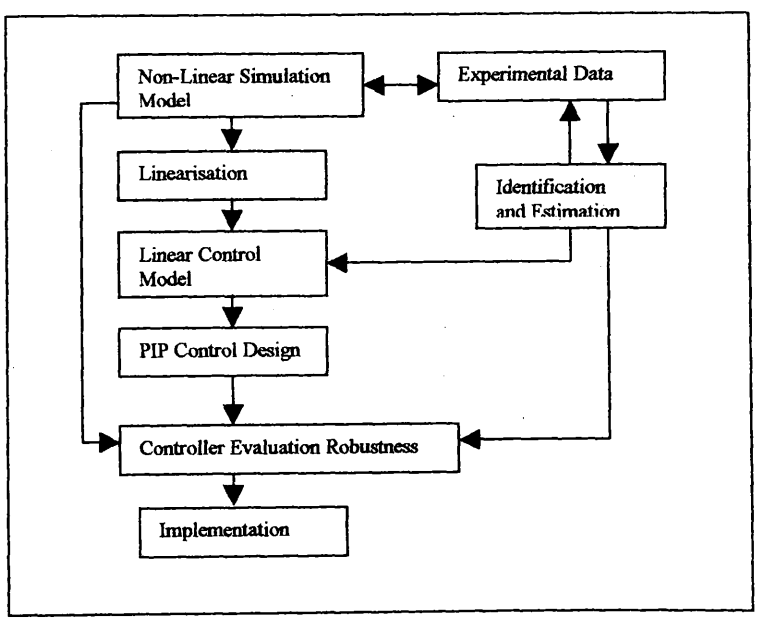

Figure 2.10: Components of True Digital Control (TDC) Design Procedure.

2.5 CONCLUSIONS

This chapter has introduced the techniques of identification and estimation for transfer function models suitable for the advanced digital control methodology utilised in chapters five to eight. Also, other modelling methods such as CFD have been outlined as alternative modelling techniques when digital control is not the end requirement.

The second half of this chapter has considered the control design in True Digital Control approach to control system design for a univariate system (also implemented in chapters 6-7). The multivariable extension of PIP control is described and implemented in chapter 8 of this thesis. In this regard, a Non-Minimum State Space (NMSS) representation of the system, obtained from a databased TF model, has been introduced based on the present and past input-output values. This is an essential part for State Variable Feedback (SVF) control design methods in TDC methodology, such as pole assignment and LQ optimal control design methods. The state variable controller, which is termed a Proportional-Integral-Plus or PIP controller because of its relationship with traditional PI methods (Figure 2.7), is then easily implementable since, the state vector is defined only in terms of the known input and output signals. Furthermore, since all the state variables are available for measurement, there is no general need for a state re-constructor or state estimator, as in normal state variable feedback designs. This yields a more robust controller to uncertainties.

Following the description of the test chambers in chapters 3-4, the next stage is to further improve the modelling and control of the micro-climate chambers by designing, simulating and implementing different forms and designs of control such

as, feed-forward (discussed above), fixed gain, switched gain, scheduled gain, adaptive control (chapters 5-7) and multivariable modelling and control (chapter 8).

Chapter 3

DESIGN AND CONSTRUCTION OF LEUVEN VENTILATION CHAMBER

3.1 INTRODUCTION

This chapter describes the ventilation rate chamber designed and built at the Katholieke Universiteit Leuven, Belgium. The control problem this chamber was designed to address is a single-input, single-output one, with the voltage applied to the axial fan being the actuator and the airflow rate (as measured by the airflow rate sensor) being the controlled input. This is illustrated schematically in figure 3.1. The laboratory test installation

(figure 3.3) was both designed and constructed by the Agricultural Engineering group in order to develop and evaluate new control algorithms and investigate the dynamic influence of external pressure changes that may act as a disturbance on the ventilation rate produced by an axial fan.

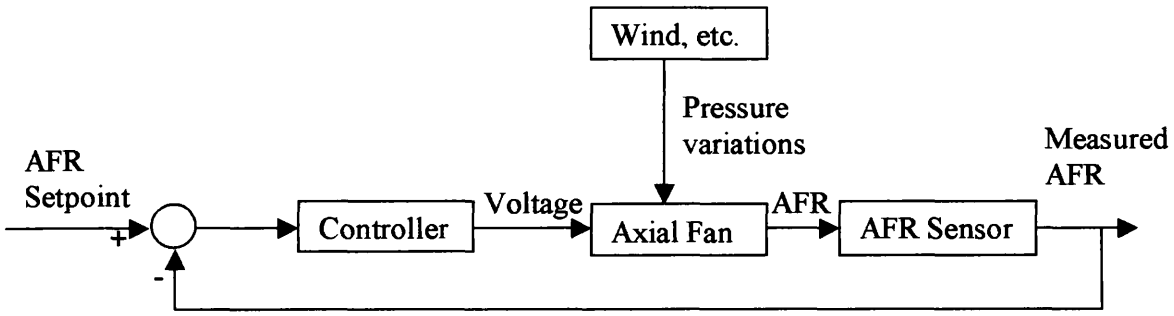

Figure 3.1: Schematic representation of the ventilation system consisting of an axial fan and an airflow rate sensor (AFR).

3.2 LEUVEN CHAMBER LAYOUT

The chamber layout is shown in figures 3.2 and 3.3. The test facility is constructed with a 75mm x 50mm wooden framework, supporting a plywood cube-shaped pressure chamber, (labelled [4] in figure 3.2) (dimensions 2.8m x 2.8m x 2.8m), with smooth inner walls from which air is extracted at one end by the control fan [1] (diameter 0.45m). At the other side of the pressure chamber a second disturbance fan [5] is used to create a dynamic pressure difference over the pressure chamber, thus simulating wind action on the test chamber).

Different disturbance patterns were applied, ranging from simple step functions changing the pressure between two different levels at periodic time steps to more realistic wind pressure simulations, derived from wind pressure measurements in a real full-scale building.

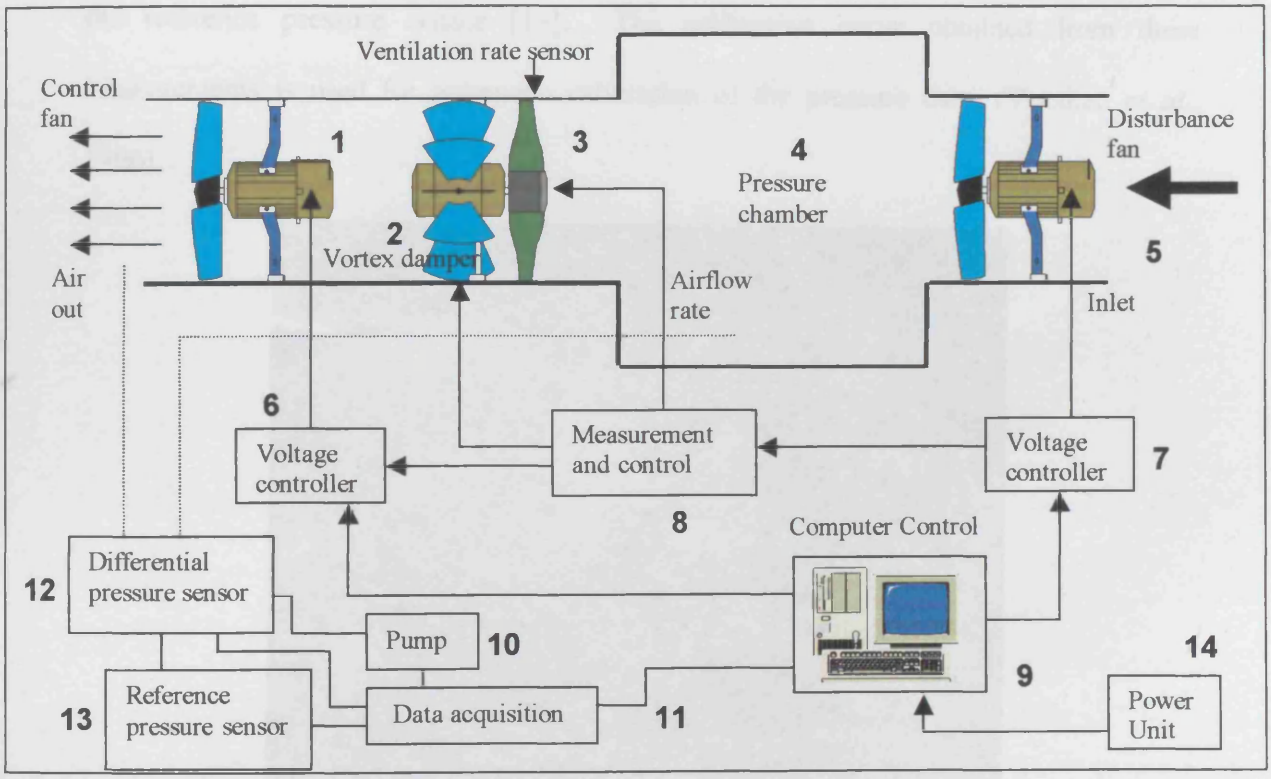

Figure 3.2: Schematic layout of the test chamber and control equipment; the numbers 1-14 are explained in the text.

An accurate ventilation rate sensor [3] (certified accuracy: 50 m^3/h) is used for continuous feedback control. Besides the rotational speed of the fan, a second control actuator has been built in by means of a controllable valve (vortex damper) [2], which can be used to restrict the airflow through the chamber (figures 3.4 and 3.5). The radial blades of the vortex damper can rotate through 90° so that they can be perpendicular or parallel to the airflow direction. Static pressure differences over the test fan are measured with a

differential pressure sensor [12], that is automatically calibrated at the start of each experiment against a reference pressure sensor [13]. During this calibration an air pump [10] is activated by means of an I/O card [11], connected to a PC [9], in order to generate different levels of reference pressure over both the differential pressure sensor [12] and the reference pressure sensor [13]. The calibration curve obtained from these measurements is used for automatic calibration of the pressure data, (Vranken *et al.*, 1996).

Figure 3.3 Leuven Ventilation Test Chamber with axial fan and associated control gear.

The dynamic characteristics of the system also depend upon the static pressure difference over the fan. This pressure difference can fluctuate over time (e.g. moderate wind disturbances) or can change very suddenly (e.g. gusts of wind or by opening a door). Since the pressure difference can only be controlled actively by changing the airflow rate,

pressure difference over the fan is not taken as an input to the system, but variations in pressure difference are considered as a disturbance to the system. Also, since measuring the pressure difference is too costly in real life situations, the controller has to be designed so that it does not require the measured static pressure difference.

The fan has been set to run between 0% (stationary) and 100% (full capacity). In this case, 0% actually represents 90VAC (the amount of voltage required to start the motor turning), while 100% is equivalent to 220VAC (1%=1.3VAC), thus, 0%-100% VAC is equivalent to the whole operating envelope of the axial fan in question. Voltage control is through a variable voltage input device (Triac), the voltage signal is fed to the triac from the control algorithm and its magnitude depends on the desired setpoint. For open loop experiments the voltage may be set automatically or manually altered as required within the respective software MATLAB (control algorithm) and LABVIEW (visualisation software).

The true power consumption P is calculated with the equation:

$$P = v * i * \cos(\varphi) \tag{3.1}$$

Where, v = the voltage (true RMS voltage) applied to the fan (V)

i = the electrical current (A) generated by the applied voltage

φ = the time lag between the voltage and the current (s)

An internal clock within the Labview application measures the phase φ. This clock is activated every time the current i changes from a negative to a positive value and is

stopped when the voltage v changes from a negative to a positive value. The time difference between these events is used to calculate φ.

The data acquisition software from the ventilation rig to the computer is written in a PC-based LABVIEW application and a real time connection with MATLAB has been established. The test installation is operated through a LABVIEW application with all calculations carried out in MATLAB.

Figure 3.4: Cut away view of the fan/valve/airflow rate sensor housing with associated control gear.

Table 3.1 below lists the variables that are continuously measured by the computer interface link to the test chamber and gives the file structure and units of every variable including time measured at each sampling interval (2 seconds).

Table 3.1: File structure: 9 Columns of Data

Number	Parameter	Description	Units
1	Elapsed Time	Time	HH: MM; SS
2	Measured Airflow	The rotational speed of the airflow rate sensor	m^3/hr
3	Airflow Reference Level	Setpoint level	m^3/hr
4	Pressure Difference	The pressure difference over the pressure chamber (inside to outside)	Pa
5	Consumed Power (Main Fan)	The electric energy consumption of the test fan	VA (W)
6	Internal Temperature	The temperature of the incoming air	Degree C
7	Control Fan Voltage	The voltage applied to the test fan	0-100% (% Voltage)
8	Interference Fan	The voltage applied to the disturbance fan	0-100% (% Voltage)
9	Vortex Damper (Valve)	The position of the throttling (restricting) valve	% Closed

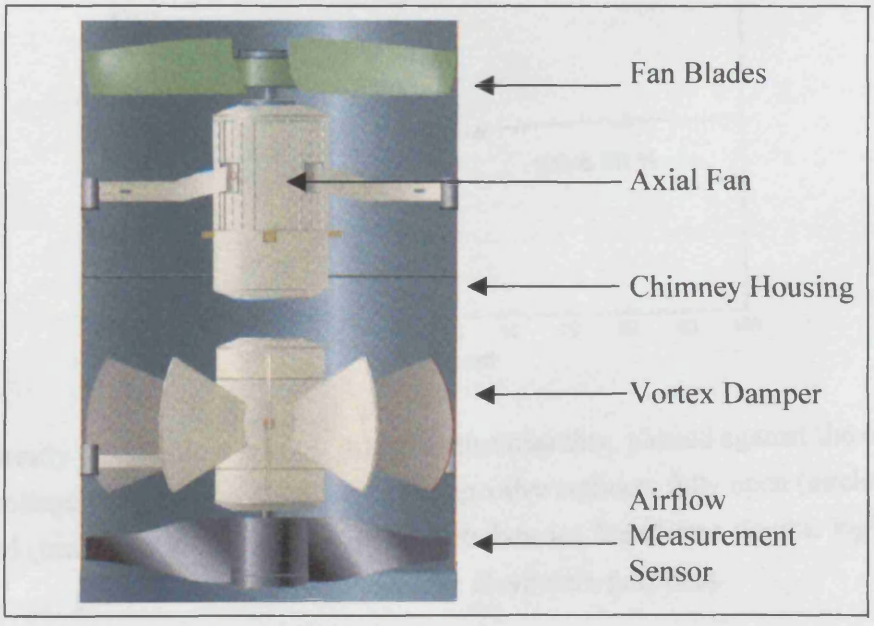

Figure 3.5: Cut away section of chimney housing of main axial fan, vortex damper and free running impeller for volumetric airflow measurement.

3.3 STEADY STATE CHARACTERISTICS OF LEUVEN VENTILATION CHAMBER

The steady state relationship between airflow rate and the potential voltage applied to the main axial control fan takes the form of a conventional non-linear 'S' shaped curve. The curve is illustrated in figure 3.6, where the circles show the measured airflow with the valve fully open (normal conditions) and the triangles illustrate the effect of closing the vortex damper (throttling valve) to 60% closed. A flexible logistic growth function has been fitted to the data (using a least squares approach) in order to further highlight the relationship between these variables.

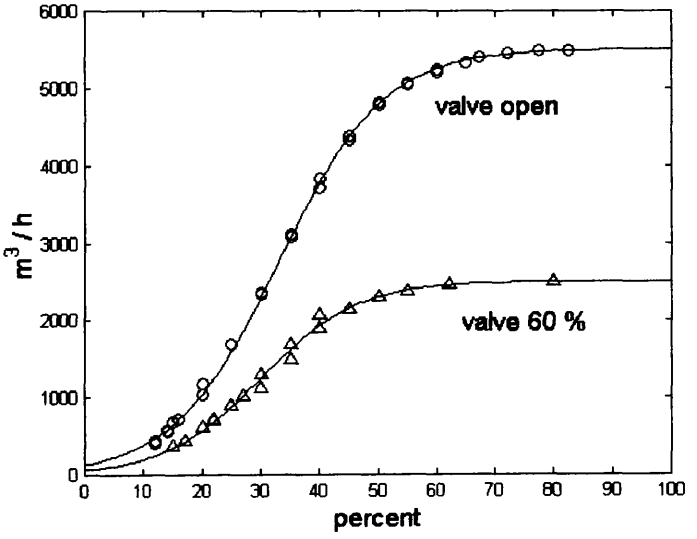

Figure 3.6: Steady state airflow rate (m^3/h) in the test chamber, plotted against the control fan applied voltage (%), for two different throttling valve settings: fully open (circles) and 60% closed (triangles); a least squares fit to each data set, based on a flexible logistic growth curve, is also shown for illustrative purposes.

Figure 3.6 above is a representation of the average airflow rate under steady-state conditions in response to a given voltage. It has been found in practice, however, that stable airflow patterns are not always attained, especially at low ventilation ($<1000 m^3 hr^{-1}$). In order to stabilise airflow at lower ventilation rates the vortex damper (figure 3.5) may be partially closed in order to restrict the airflow through the chamber. However, by reducing the size of the orifice that the air can pass through, the measured airflow is lower than when the damper is fully open. To overcome this, the required ventilation rate can only be achieved by increasing the voltage to the control fan. This is illustrated in figure 3.6, where the triangular data points are obtained from constricting the airflow to 60% of its potential. It can be seen how this clearly prevents the full airflow potential of the axial fan in use being achieved. Due to this fact, the throttling valve is only used for low ventilation rates where the flow may become unstable in response to external disturbances such as a pressure wave caused by a particular wind speed and direction. The major downside to employing the vortex damper (or throttling valve), is the increase in power consumption by the main fan to maintain a desired airflow rate. This obviously increases the overall operating costs of the ventilation/heating control system to the farmer and accordingly should only be utilised at low ventilation rates. There has to be a cost/benefit analysis to compare the benefits of thermal comfort and well being of the animals against animal production costs. This topic is further expanded in chapter 7.

Additionally, utilising the vortex damper to constrict the airflow in conjunction with the axial fan requires careful consideration in the final control algorithm, since it changes both the steady state and the dynamic characteristics of the overall airflow system. This

can be overcome by incorporating a switching, scheduled or adaptive operation of some kind; the result being a more stable airflow across the operating envelope.

3.4 VENTILATION RATE SENSOR

As discussed in the opening chapter, it has been shown that control of airflow rate is probably the most important factor in livestock building control. Vranken (1999) summarises how the ventilation rate affects the following variables:

i) the indoor climate and the micro-environmental conditions around the animals, as a result of energy and mass transfer throughout the building (Carpenter, 1974; Berckmans, 1986a; Randall, 1981),

ii) the spatial distribution of these internal environmental conditions in a non-perfectly mixed fluid, as a result of the obtained airflow pattern (Randall *et al.*, 1979; Berckmans *et al.*, 1993b; De Moor, 1996),

iii) the resulting response of the living organism and the impact on animal welfare, the health and behaviour and the technical production results such as growth rate, feed conversion ratio, etc. (Boon, 1981; Curtis, 1983; Geers *et al.*, 1985),

iv) the energy costs for heating and ventilation (Lilleng, 1989),

v) and finally, the emissions of pollutants from livestock buildings, such as ammonia, carbon dioxide, methane, etc... (Aarnink *et al.*, 1993; Ni, 1998).

It is evident that from the above literature review that accurate airflow measurement is important. However, in practice (i.e. field analysis) it has been shown that poor ventilation control is a major cause of ventilation related health problems. Vranken, (1999), plus various co-workers at the Katholieke Universiteit of Leuven, Belgium have found little advantage in both animal production and welfare in livestock buildings with inaccurate automatic ventilation control compared to low cost, manually operated naturally ventilated animal housing. It was with this in mind that an effective airflow rate sensor was developed that could measure the airflow rate accurately and be used in a feedback loop to improve ventilation control, (Berckmans *et al.*, 1995; Berckmans *et al.*, 1996; Vranken and Berckmans, 1997 and Vranken *et al.*, 1997).

In the Leuven ventilation test rig, a free running impeller with an optimum design is utilised for airflow measurement through the outlet from the chamber ([3] figure 3.2). Due to space limitations, for a full outline of the development and implementation of the novel airflow rate sensor the reader is directed to the above mentioned references and Vranken, (1999). However, it is worth mentioning that generally ventilation rate is measured at either the inlet or outlet depending on whether the system is positively or negatively pressurised with respect to ambient conditions. If the building is a negative pressure system (i.e. the pressure inside is lower than outside), the airflow rate should be measured at the outlet from the livestock housing or chamber etc. in order to measure accurately all the air that leaves the building, (this is the normal situation in most animal housing in Europe). The ventilated space should be as air tight as possible for accurate airflow measurements (lab conditions), it is normal for slight air leakage around doors, windows etc. in a real livestock enclosure. With a positively pressurised system the

airflow rate is measured at the inlet. This avoids errors caused by occasional air leakage through sidewalls, doors or vents. It can be argued that the airflow should be measured at animal height, as this is where the optimum airflow rate is required. With this in mind the Lancaster chamber (chapter 4) has an additional airflow sensor (in this case an air velocity transducer) which can be placed almost anywhere within the 3D airspace. However, it is still essential to know how many volumetric air changes per hour occur throughout the building structure, and with a negative pressure system any number of inlets to a livestock building are permissible. In fact, it is the reduction in pressure within the 3D structure that draws air inside, so more than one inlet can give an enhanced air distribution than only one. Further methods for measuring ventilation rate in livestock buildings are outlined in section 4.5 of chapter 4.

Experimental results in the test chamber have shown the ventilation rate sensor performed as a first order system. However, the time constant was observed to be slightly shorter for the rising (2.3 seconds) and falling limbs (2.7 seconds) during step experimentation (Vranken, 1999).

3.5 CONCLUSIONS

Chapter three has introduced the first of two micro environmental chambers studied within this thesis. The Leuven ventilation chamber is designed primarily to evaluate the modelling and control of airflow through a 3D ventilated space. Chapters 5-7 report a variety of control design and implementation results from this chamber. The next chapter describes in detail the Lancaster micro environmental chamber, which was both, designed

and constructed as part of the present project and consequently is described in greater depth than the Leuven ventilation chamber outlined here.

Chapter 4

DESIGN AND CONSTRUCTION OF LANCASTER CHAMBER

4.1 INTRODUCTION

This chapter describes the design, construction and choice of sensor for the controlled environment chamber in Lancaster, all of which were carried out by the author. This chapter along with Appendix 2 outlines the reasoning behind the numerous decisions required in both construction and data acquisition in order to achieve the aim of obtaining an online micro environmental climate for use in the development and evaluation of multivariable controllers.

4.2 WHY A CONTROLLED ENVIRONMENT CHAMBER IN LANCASTER?

After visiting the Laboratory for Agricultural Buildings Research Unit in the Katholieke University of Leuven, Belgium a number of times in order to carry out experiments and return later to implement control designs, it soon became apparent that such a research facility in Lancaster would be extremely valuable. Thus, the idea was formulated to design and build a test facility in the Engineering Department at Lancaster University, Lancaster in the UK. The Lancaster micro-environment chamber (figure 4.1) is an extension of the ventilation/micro-climate test chambers in Leuven to enable multivariable modelling and control design along with three-dimensional flow observation.

Figure 4.1: Lancaster microenvironment chamber.

In addition to the ventilation rate measurement outlined in the previous chapter, this chamber also incorporates 3D temperature measurements and has a moveable simulated animal present as well as the ability to direct and deflect the airflow upon entry. The airflow speed can also be measured simultaneously in a number of spatial locations and the chamber can be utilised for visualising airflow patterns (simulated smoke experiments) and observing bio-responses (monitoring the effect of an animate or inanimate object within the chamber). As in the Leuven chamber, pressure wind disturbances can be simulated by a disturbance fan, which can apply both positive and negative pressures on the inlet to the chamber. The budget was the main limiting factor on the design and construction of the Lancaster chamber. The chambers in Leuven had been designed, constructed and refined over a period of 10-12 years: whereas in Lancaster, there was little over 12 months to get a working chamber up and running and be in the position to collect sensible, meaningful data. Due to the time constraint, much of the second half of the PhD was dedicated to this purpose.

4.3 LANCASTER MICRO-CLIMATE CHAMBER LAYOUT

The chamber is constructed of a structural aluminium framework in 1m x 1m x 25mm modular sections. The overall size of the chamber is 2m (length) x 2m (height) x 1m (width) (see figures 4.1 - 4.3), while the scale of the Lancaster micro environmental chamber is in the proportions of 1:1:0.5 (length, height and width). Reports from Silsoe research centre (**Ref**) suggest for optimum micro-climate control of an indoor airspace, the model of animal housing should have a length/height ratio of not less than one, and ideally, if possible, it should be greater (i.e. the length should be greater than the height). Also, their findings suggest a length/width ratio of less than 0.5, (i.e.

less than 0.5, (i.e. the length should be at least twice that of the width). The walls are 1m x 1m x 5mm rigid perspex sheets fitted into the framework. The modular construction allows for future design flexibility if a larger or smaller chamber is required to test different dynamic responses to changing airflow rates and heat inputs. The circular inlet ($0.01327m^2$) is at one end of the chamber and cut into the lower modular section (figure 4.2), while the outlet ($0.01327m^2$) (also circular) is in the opposite end in the top modular section.

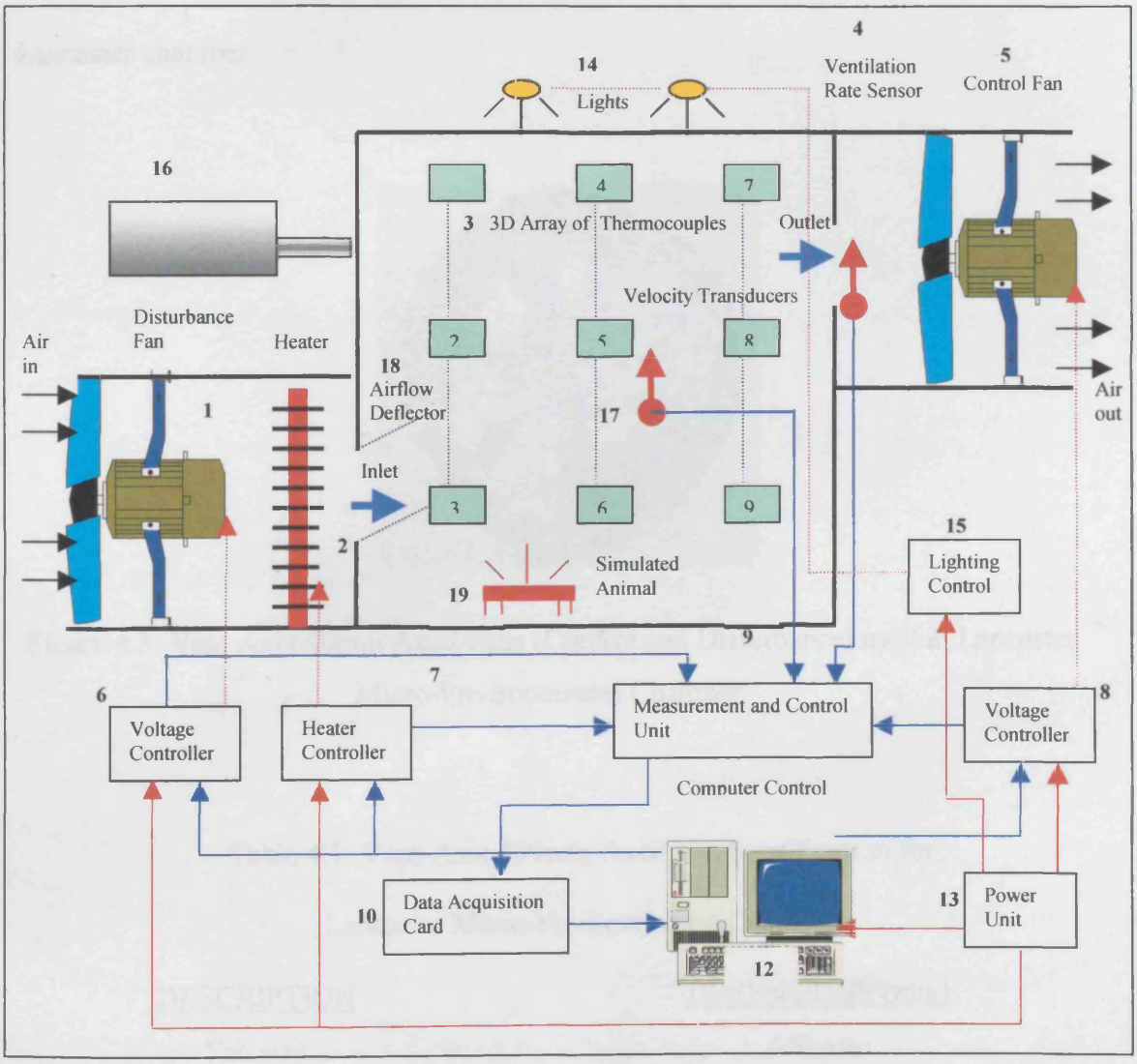

Figure 4.2: Schematic layout of Lancaster micro-environment chamber and associated control equipment; the numbers 1-19 are explained in the text.

The outlet has a 320W axial (Vent Axia) fan [5] (figure 4.1 and 4.3), which can draw the air through the chamber at different ventilation rates (see Appendix 2 for full chamber technical specification). The Vent Axia Axial Fan specified in table 4.1 above and figure 4.3, is suitable for both light and heavy duty use in either ducting or through the wall applications. These fans are constructed from steel plate with a tough epoxy paint finish. The impellers are glass filled polyamide for resistance to outdoor conditions and abrasive airflow. With the above specifications, the fan design and model was chosen to give many years effective and maintenance free service to the Lancaster chamber.

Figure 4.3: Vent Axia 40mm Axial Fans (Control and Disturbance) used in Lancaster Micro-Environmental Chamber.

Table 4.1: Vent-Axia 400mm Axial Fan Specification for Lancaster Micro-Environmental Chamber

DESCRIPTION	DIMENSIONS (mm)
Fan size	400 mm
Depth	170 mm
Diameter	487 mm
Fixing centres	450 mm

FEATURES

- IP65 terminal box and motor allowing units to be washed with water jets
- Greased for life bearings allowing installation at any angle
- Class F motor insulation (-40°C to +70°C) with a ribbed aluminium body for efficient cooling
- Thermal overload motor protection
- Casing dimensions are to DIN 24151 and flange dimensions to ISO 6580

TECHNICAL SPECIFICATION

DESCRIPTION	VALUE
Motor	230V A.C. 4 Pole
RPM	1350
Extract capacity	4940 m^3/hr
Starting current	4·0 A
FLC	1·6 A
Sound level @ 3m	58 dBA

Housed within the inlet is a heating element (500w) [2] to generate heat input to the airflow drawn into the chamber, plus a second axial fan [1] for generating disturbances to the measured airstream within the main body of the chamber. The whole chamber is bolted together and fastened to a blockboard base on industrial standard casters, which makes the whole installation mobile. For maintenance and internal installation access purposes the 1m x 1m panel below the outlet is hinged and can be easily opened. There is a compressible rubber door seal and two catches that tighten the "door" against the main framework to make an airtight seal. The rest of the rig has been sealed with clear flexible silicon to make it as air tight as possible.

Inside the chamber, a 3D-array [3] of 18 thermocouples (type K) measure the temperature distribution of the internal micro-climatic environment (see figure 4.2). In addition, thermocouples are sited at both the inlet and outlet in order to record

reference input and output temperatures against the internal temperature distribution. The thermocouples are hard-wired to a multiplexer (PCLD-789D) and a PCLD-8115 screw terminal board, which is connected via a DB37 way connector to an analogue to digital (AD) board PCL-818L [10] housed in a PC [12]. The outlet airflow rate is measured via an air velocity transducer [4] (see also section 4.4.4), which has been calibrated against the voltage applied to the axial fan (see table 4.?). Both the fans and the heating element are controlled by two Thyristors (type SKKT20B08D, RS Components) that are in turn controlled by a Phase Angle Trigger Module (type SKPC200-240, RS Components) [6, 7, 8].

Figure 4.4: The control equipment associated with the Lancaster micro-environment chamber.

The thyristors and phase angle trigger modules are wired according to the diagram in figure 4.5, then mounted on a back plate inside an adaptable box with appropriate fuse protection (figure 4.4). Each control circuit is then controlled by a 0-5 Volt DC output from the PCL-818L analogue to digital (AD) board [10] housed in a PC [12], and PCLD-8115 screw terminal board or the AD512 AD board (see circuit diagram: figure

4.6). A further air velocity transducer is positioned inside the 3D-airspace [17]. This can be moved around to record the airflow rate in different areas of the chamber in response to varying ventilator speeds and temperatures. A mechanical means of directing the airflow has been added to allow the airflow to be deflected more precisely where it is required for optimum control [18], the angle of deflection is measured in degrees from ~40° to ~140° giving 100° of movement. To add more realism to the chamber an internal heat source (disturbance), designed to simulate animal occupancy has been added. This heat source is in the form of a 60W tubular heater [19], which is controlled via a manual rotary variac. This enables the internal heat source to vary as it would in a real livestock building depending on the animals' thermal state. Additionally, this simulated "pig" is mounted on a set of rails and connected via a pulley system to a variable speed, forward and reversible motor. A schematic layout of the chamber and associated controls is given below in figure 4.3. Finally, tungsten halogen lighting control [14, 15] via a two-gang, single pole switch is included for enhanced visualisation of the internal airflow using smoke [16].

The measurable variables from the ventilation chamber are airflow rate ($m^3\ hr^{-1}$) and temperature (°C). The airflow is recorded in two places at the pre-set sampling interval as a single point measurement: 1. At the centre of the outlet, [4] close to the control fan, (figure 4.2). 2. At a pre-determined point from experimental analysis within the chamber (this can be anywhere within the chamber). However, if necessary, these can be moved to different parts of the chamber to note the air velocity behaviour at a particular point. In contrast, the temperature is measured as a distribution throughout the chamber via a 3D array of thermocouples [3], which detect changes in temperature to 0.1°C at a detection rate of 0.2 seconds.

Reference temperature readings are also recorded at both the inlet and outlet to the chamber. Thus, by altering both heat and airflow rates different thermal mixing patterns within the chamber may be observed and recorded.

In addition, an artificial smoke machine [16] can be positioned at the inlet in order to carry out visualisation experiments of the internal dynamics of airflow. These visualisation experiments allow 'zones' of imperfect mixing or 'dead zones' to be identified. Also, the movement of smoke around the chamber can be photographed and videod for further airflow pattern analysis (see chapter 9).

Finally, the chamber may also be used for investigating bio-responses, i.e. measuring the temperature and airflow changes within the 3D airspace to human occupancy. The initial results of this work can be seen in chapter 8.

4.4 THE SENSORS

The next stage is to select suitable sensors to measure variables such as temperature and airflow velocity. When selecting a sensor for an application such as this controlled climate chamber a number of factors need to be considered:

- The nature of the measurement required, e.g. the variable to be measured:
    - Its nominal value;
    - The range of values;
    - The accuracy required;
    - The environmental conditions under which the measurement is to be made.
- The nature of the output required from the sensor: this determines the signal conditioning requirements in order to give suitable output signals from the measurements.

- Once the above factors have been considered suitable sensors for the Lancaster micro-environment chamber can be identified, taking into account the following;
    - Range;
    - Accuracy;
    - Linearity;
    - Speed of response;
    - Reliability;
    - Maintainability;
    - Life span;
    - Power supply requirements;
    - Ruggedness/robustness;
    - Availability;
    - Cost;
    - Instrument drift.

In addition, the selection of sensors cannot be taken in isolation from the consideration of the form of output that is required from the system under study after signal conditioning. Thus, there has to be a suitable marriage between sensor and signal conditioner.

4.4.1 SIGNAL CONDITIONING

The output signal from a sensor(s) within a measurement system, such as the one under study here, generally has to be processed in some way in order to make it suitable for the next stage. The signal may be too small and require amplification; contain interference which has to be removed; be non-linear and require linearisation; be analogue and have to be made digital; be a voltage change and have to be made into a suitable size current change, etc. All the above are termed *signal conditioning*. In the case of the controlled environmental chamber: the output from a thermocouple

is a very small voltage, a few millivolts. A signal-conditioning module within the multiplexing board is then used to convert this tiny voltage into a current signal, amplify it, provide noise rejection, linearisation and cold junction compensation.

4.4.2 AIRFLOW MEASUREMENT

There are numerous instruments and methods for airflow measurement in a ventilated airspace. These give differing degrees of accuracy and have both advantages and disadvantages depending on their application. Some of these are summarised in table 4.2 for livestock buildings.

Table 4.2: Overview of ventilation rate measurement techniques used in livestock buildings, (Vranken, 1999).

Measuring principle	Ventilation system	Direct or indirect	Accuracy	Reference
Tracer gasses	Mechanical/Natural	Indirect	10 – 30%	Demmers, 1993; 1997 Jung *et al.*, 1994 Muller *et al.*, 1994 Choiniere, 1991 Fisk, 1991 Gustafsson, 1996
Hot wire anemometer	Mechanical/Natural	Direct	25%	De Praetere *et al.*, 1989 Krause *et al.*, 1990 Scholtens *et al.*, 1994
Orifice plates, Nozzles	Mechanical	Direct	1 - 5%	DIN, 1982 ISO, 1993
Vane anemometers	Mechanical	Direct	5 - 10%	Krieger *et al.*, 1993
CO_2-balance	Mechanical/Natural	Indirect	20 - 40%	Van Ouwerkerk *et al.*, 1993 Van 't Klooster, 1994 Pedersen *et al.*, 1996
Heat balance	Mechanical/Natural	Indirect	20 – 40%	Van 't Ooster, 1994
Free running impeller (commercial)	Mechanical	Direct	30%	Heinrichs *et al.*, 1993 Van Ouwerkerk *et al.*, 1995

Table 4.2 above indicates there are two main types of measuring method: direct and indirect. In the direct method the ventilation rate is measured at all inlets or outlets (+ve or –ve system). For example: free running impeller, hot wire anemometer, pitot

tubes, orifice plates etc. By contrast, the indirect method utilises an estimation of ventilation rate from continuous measurements of associated variables, such as temperature, humidity, CO_2 concentration etc. within the ventilated space. Examples of the indirect method include: heat balance, tracer gasses and CO_2 balance methods. The following sub-sections briefly describe the different airflow measurement options available.

4.4.2.1 PITOT TUBE

A Pitot tube is a slender airflow measuring device with twin-walls that is aligned with a fluid flow and measures the fluid velocity by means of a pressure differential (dynamic pressure). The static pressure (p_s) of the airstream is measured through holes in the sidewalls, while the total pressure (p_t) is measured through a hole in the front of the inner tube. The dynamic pressure is the difference between the total pressure and the static pressure. The fluid velocity can then be calculated through the relation:

$$v = \sqrt{\frac{2(p_t - p_s)}{p}} \tag{4.1}$$

Where, p is fluid density; p_t is total pressure and p_s is static pressure.

Equation 4.1 above is a simplification of Bernoulli's equation, which relates pressure, velocity and height of a fluid. While Pitot tubes are excellent for measuring high velocity fluid flows they are less so for low velocities; this makes them less attractive for ventilation measurements in livestock housing where airflows are generally low. For accurate airflow measurements a very sensitive differential pressure sensor is

required. Additionally, the output is not easily converted into a digital signal for use in real-time control algorithms.

4.4.2.2 VANE ANEMOMETER

This method involves the use of small free running impellers. The diameters of the impellers range from 10 mm to 150 mm and is always much smaller than the diameter of the outlet ducting which houses the control fan. The air velocity measurable with a vane anemometer is generally between 0.5 to 10 ms^{-1} and the system has to be calibrated so that the airspeed is measured by the rotational speed of the impeller. This design is only accurate when there is no static pressure difference over the sensor and when the anemometer is placed perpendicular to the air stream direction. This kind of sensor is often used in ventilation system installations but its accuracy cannot be guaranteed.

4.4.2.3 TRACER GAS METHODS

This technique ascertains the air exchange rate in a 3D air space as long as there is an adequate mixing of the internal air mass. There are three main tracer gas methods in use: the Rate Of Decay method (ROD), the Rate Of Accumulation method (ROA) and the Continuous Tracer gas method (CT). However, because all these methods assume perfect mixing within the building volume a mixing fan is sometimes employed. The mixing fan can cause an additional internal airflow that can impact on the overall ventilation rate of the animal housing, causing measurement error (Jung and Zeller, 1994). In the ROD case, a temporary source of tracer gas at a known concentration is employed until a pre-set concentration is attained. The source of the gas is then removed and the decay in concentration is measured over a period of time.

The number of air exchanges (n) within the building volume or at specific locations can then be determined by the equation (4.2):

$$n = \frac{v}{s_v} = \frac{1}{t}\left[\frac{C(t)}{C(o)}\right] \tag{4.2}$$

Where,

N = *air exchange rate* (s^{-1})

V = *ventilation rate* ($m^3\ s^{-1}$)

S_v = *building volume* (m^3)

$C(0)$ = *concentration of the gas when the measurement starts* ($kg^{-1}\ m^3$)

$C(t)$ = *concentration of the gas after time t* ($kg^{-1}\ m^3$)

It is found with this method (ROD) that the concentration of tracer gas decays exponentially with time and by plotting the natural logarithm of gas concentration against time a straight line is obtained and the gradient of the line gives the air exchange within the building volume. However, this method is based on the assumption of a constant airflow rate and in the case of livestock buildings the opposite is true because the ventilation rate in animal housing is affected by a high dynamic wind pressure field (Hoxey, 1989; Bruce, 1982).

The lack of accuracy coupled with the necessity for a reliable gas monitor for gasses such as SF_6, C_4H_8, N_2 or CO_2 make it evident that tracer gas methods are not suitable for use in a continuous feedback control algorithm.

4.4.2.4 HEAT BALANCE METHOD

The heat balance technique uses an energy equation as opposed to the mass balance equation used in the tracer gas methods. Continuous temperature measurements of incoming and outgoing air are recorded and an estimate of the ventilation rate is made from an appropriate form of the energy equation. This method again relies on perfect mixing, plus, empirical models must estimate the input of animal heat production. There are many fluctuations in animal heat production, for example: ventilation rate, temperature, humidity, stress, floor type, feed consumption, etc., and it has been found the majority of models only procure poor estimates. The obvious result is a ventilation rate accuracy that is very low and again unsuitable for the advanced digital control methods employed in this thesis.

4.4.2.5 CO_2 BALANCE METHOD

This is the third method presented here that relies on the assumption of perfect mixing within the building volume. The CO_2 technique is similar to the tracer gas method in all, except that the gas used is naturally produced by the animals instead of the inert gas that is injected into the 3D airspace with the tracer gas method. The limitations are similar to those discussed in section 4.3.3.3.3, while the accuracy is highly dependent on the estimate of the CO_2 production rate. This method is unsuitable for advanced digital control design for similar reasons as the previous two techniques.

4.4.2.6 MICROBRIDGE MASS AIRFLOW SENSOR

The microbridge mass airflow sensor has a unique silicon chip based on advanced microstructure technology. It consists of a thin film, with a thermally isolated bridge structure containing heater and temperature sensing elements. The bridge structure

provides a sensitive and fast response to the flow of air or other gas over the chip. Dual sensing elements positioned on both sides of a central heating element indicate flow direction as well as airflow rate. Laser trimmed thick film and thin film resistors provide consistent inter-changeability from one device to the next.

The microbridge mass airflow sensor operates on the theory of heat transfer. Mass airflow is directed across the surface of the sensing elements. Output voltage varies in proportion to the mass air or other gas flow through the inlet and outlet ports of the arrangement. The specially designed housing precisely directs and controls the airflow across the microstructure sensing element. The microbridge mass airflow sensor uses temperature sensitive resistors deposited within a thin film of silicon nitride. The resistors are suspended in the form of two bridges over an etched cavity in the silicon. The chip is located in a precisely dimensioned airflow channel to provide a repeatable flow response. Etching the cavity space beneath the flow sensor bridges attains highly effective thermal isolation for the heater and sensing resistors. The small size and thermal isolation of the microbridge mass airflow sensor are responsible for the extremely fast response and the high sensitivity to flows.

4.4.2.7 ORIFICE PLATES, VENTURI TUBES AND NOZZLES

Orifice plates, venturi tubes and nozzles are all pressure difference methods. They are based on the principle that the lower pressure energy within an air stream once it has passed a restriction (e.g. a smaller duct diameter) is proportional to the density of kinetic energy. Vranken (1999), shows how Bernoulli's equation can be utilised when corrected with some experimental parameters to show the relationship between the ventilation rate and the pressure difference over the measuring element. While one

differential pressure measurement suffices, in order to obtain accurate measurements the sensor must be placed in a length of duct at least 15 times the diameter of the fan housing. In general, livestock ventilation ducting is 0.5 m diameter, this means a minimum duct length of 7.5 m. Obviously this is not practical in most livestock housing where normal duct lengths are around 1 m. Furthermore, because the axial fans used normally only produce low pressure differences of up to 120 Pa, it has been found this pressure difference is not enough for these techniques to overcome.

4.4.2.8 FREE RUNNING IMPELLER

This method has been mentioned in the previous chapter and a full explanation is given in Vranken (1999), however, a brief explanation is due here for completion. The free running impeller technology was developed to measure the total volumetric flow through a circular duct that also houses the axial fan (Berckmans *et al.*, 1983). The idea being that a pair of specifically designed fan blades could give an improved representation the airflow than a single point measurement. The early designs were combined with a differential pressure sensor, which improved accuracy. However, it was found the costs were too prohibitive, so the final improved design omitted the pressure sensor and the impeller was mounted on a free running axis. The final blade design addressed many corrections to the calibration curve required due to internal pressure influences and removed the need for a pressure sensor feedback signal. The airflow rate is calculated from the rpm of the impeller and fed back to the control algorithm. This is the method used in the chamber described in chapter two and has been found to be accurate over all operating levels, except very low air velocities when a certain airflow is necessary before the impeller will start rotating. Additionally, there can be some inertia overrun when stepping down from high to low

ventilation rates with a subsequently longer time constant on the falling limb when compared to the rising limb of the fan dynamics.

4.4.2.9 HOT WIRE/FILM ANEMOMETERS

An anemometer is an instrument for measuring fluid velocity, whether it be of gases or fluids, hot wire or hot film, anemometers measure fluid speed using a delicate probe made of thin tungsten/platinum wire, or a thin metallic film. This probe is heated to a temperature higher than the average temperature of the fluid. Using sophisticated circuitry, the anemometer stabilises and maintains the probe temperature at a constant level throughout the measurement. Since the fluid flowing past the probe has a lower temperature than the probe, the film/wire is constantly being cooled by the fluid flow (i.e. convection, conduction and radiation). The higher the velocity, the faster the rate of cooling. A Wheatstone bridge measures the electrical resistance variation. A variation on this is to attempt to maintain the wire temperature by controlling the electrical heat supply to the wire. These two methods are shown schematically in figures 4.5A and 4.5B below:

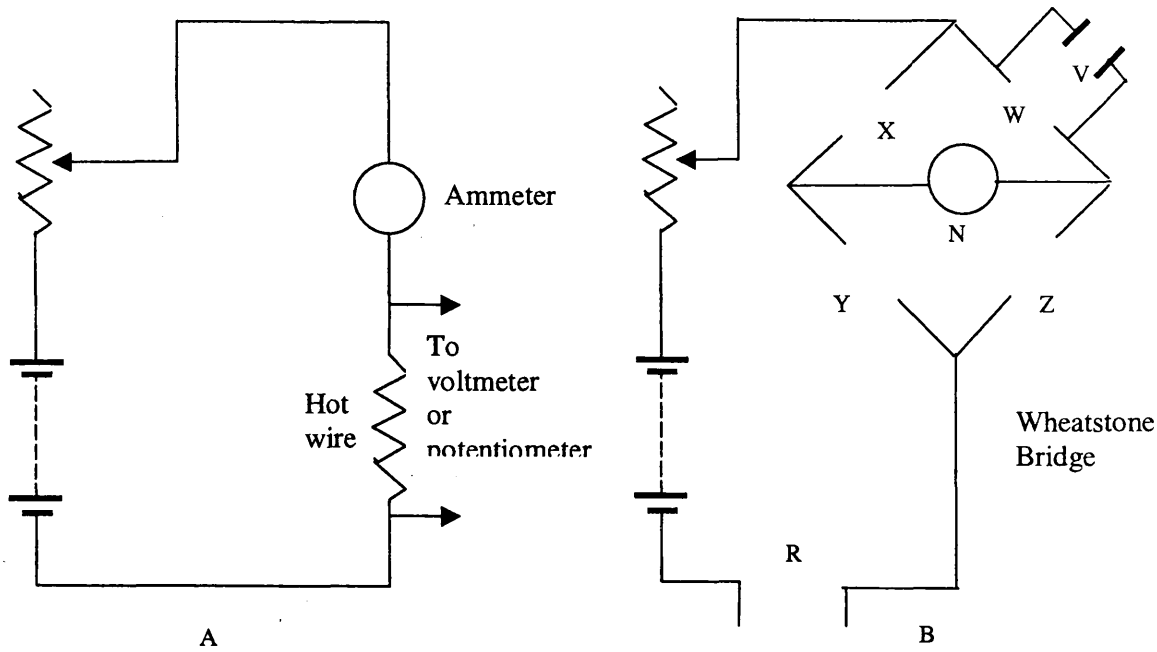

Figure 4.5: Principle of constant-current operation (A); 3. Principle of constant temperature operation (B). Where, W = hot wire; N = null indicator; V = high resistance voltmeter or to potentiometer; R = standard resistance connected to potentiometer and X, Y Z = bridge resistance's.

Since the anemometer must maintain the probe temperature at a constant level, it is therefore sensitive to the rate at which it is being cooled, i.e., the fluid velocity. This velocity is translated to a continuously changing voltage, which has a non-linear relationship with the flowing fluid. This voltage then undergoes signal conditioning, to filter out noise and improve the Signal/Noise ratio.

After proper calibration of the probe channels, it is possible to measure fluid velocities with an accuracy of 0.05% or greater, depending upon the measurement range and the quality of the calibration. The response time between measurement and instrument output is very short in comparison with other methods of fluid flow measurement and can reach a minimum of 1/2 microsecond. Hot wire anemometers are very fragile and

can deteriorate rapidly if placed in polluted air over long periods. However, their versatility and rapid response time along with their accuracy at low ventilation rates make them ideal for use in the advanced digital control methodology used throughout this thesis.

4.4.2.10 AIR VELOCITY METERS

An example of an air velocity meter is the velometer (Ower and Pankhurst, 1977), originally developed by Boyle in the USA, (Poole and Leadbeater, 1939). The velometer consists of a balanced, damped, spring-controlled, pivoted vane, which can be deflected by very light air currents and has a pointer that moves over a graduated scale. The movement is enclosed in a case with two orifices through which the air enters and departs. The vane moves in a chamber shaped so that the scale deflexion is proportional to the velocity. The instrument can be placed in the airflow with the inlet orifice facing upstream and it can measure air velocities as low as 0.1 m s^{-1}. For use in small air inlet or outlets, a probe connected to the meter comprising of a pair of pressure tubes, each with a pressure orifice can be placed in the airstream, with one of the pressure tubes facing upstream and the other downstream. This form of airflow measurement is said to have an error within 3% of the full-scale reading. While it appears suitable for measuring low airflow's, this type of instrument is not in a usable form for advanced digital control methodologies.

4.4.2.11 PARTICLE IMAGE VELOCIMETRY (PIV)

A final technique that does not actually measure directly the ventilation rate is Particle Image Velocimetry (PIV). This is a non-intrusive, full scale and accurate measurement technique for low airflow rates in ventilated airspaces. PIV, a technique

that uses particles and their images to measure flow velocity, is a promising technology to meet the needs of indoor air studies. PIV measures a 2D-velocity vector map of a flow field at an instant time by acquiring and processing images of particles seeded into the flow field. PIV technology needs further development for full-scale buildings. However, this method could be useful in determining aerosol spatial distribution, ventilation effectiveness and aerial contaminant control strategies (Zhao *et al.*, 1999).

4.4.3 OVERVIEW OF AIRFLOW RATE MEASUREMENT IN LIVESTOCK HOUSING

Two main methods were outlined in the introduction to section 4.5: direct and indirect. Indirect methods such as tracer gases or heat balance methods only give an estimation of the airflow rate over a period of several hours. They do not allow for fluctuations in ventilation rate and assume perfect mixing within the building volume. Consequently these methods are neither fast enough nor accurate enough for real-time digital control of the highly fluctuating parameters such as airflow rate found in animal housing.

The direct methods, which depend on velocity, point measurements such as pitot tubes and vane anemometers often require more than one sensor because of non-uniform velocity field in many livestock building inlets. This can make these methods expensive and too complex for use in control systems. Venturi tubes and nozzles require expensive pressure transducers and also need long ventilation ducts to operate in and cannot be combined with axial fans because large pressure differences are needed for optimum performance.

4.4.4 AIRFLOW MEASURMENT IN THE LANCASTER CHAMBER

The means of measuring the airflow within the Lancaster chamber is via an Air Velocity Transducer (AVT), (ITA Model 8455). The TSI air velocity transducers are precision instruments designed specifically to measure air velocity in fixed installations or test facilities. The air velocity transducer was chosen to measure the airflow in the Lancaster micro-environment chamber because of its relative ease of use and installation, along with the fact it has a very fast response to differing inputs and can measure low airflow rates to a high degree of accuracy. Additionally, it is very portable and non-intrusive to the airflow and this allows easy measurement of airflow at any point within the 3D airspace. The Leuven chamber uses a free running impeller, which has been shown to measure the airflow very accurately, especially at medium to high ventilation rates (1500-6000m3/hr); nonetheless, in this installation the decision was taken to use an airflow sensor that had a faster and more accurate response at low ventilation rates. The main drawback being the omni-direction of this particular model, which can make it difficult to measure convective currents in certain locations within the chamber, however, the free running impeller would fair even worse outside the outlet duct it is usually housed in. A second air velocity transducer has been added to allow measurements in different locations compared to the inlet and outlet. Also, a mass balance of airflow through the chamber is possible with a measurement at both inlet and outlet and a choice of measurement location can be made for modelling and control purposes.

The output time constant of the air velocity transducer can be set between 0.05 and 10 seconds. The time constant here is actually an averaging period and the output is the

average of readings taken over the last time-constant period. Readings are taken 20 times per time constant period for a time constant period greater than one second and 20 times per second for time constants of one second or less (TSI, 2000). In order to convert the transducer output signal into a velocity a series of readings were measured over the full range of the main control fan. The transducer was situated in the centre of the outlet for signal conversion purposes. The input voltage data was plotted against the mean transducer output signal (the system was allowed to settle to steady state before a different voltage was applied) in a scatter graph and the results (figure 4.6) show an almost perfect straight line fit. The equation of the line was obtained and incorporated into the SIMULINK diagram, which converts the transducer signal to a velocity. The output now in m s^{-1} was further converted to give a volumetric flow (m^3/hr) over the whole output from the chamber. Multiplying the flow speed (m s^{-1}), and the area (m^2) that the airflow passes over completed this conversion (to m^3/hr). It is a close approximation of the exact volumetric flow that would be passing over the outlet, but for simplicity and practical purposes has deemed to be acceptable for this research. It is possible the airflow rate sensor (free running impeller design) used in Leuven may eventually be added for increased accuracy at higher ventilation rates and a comparison between measurement methods.

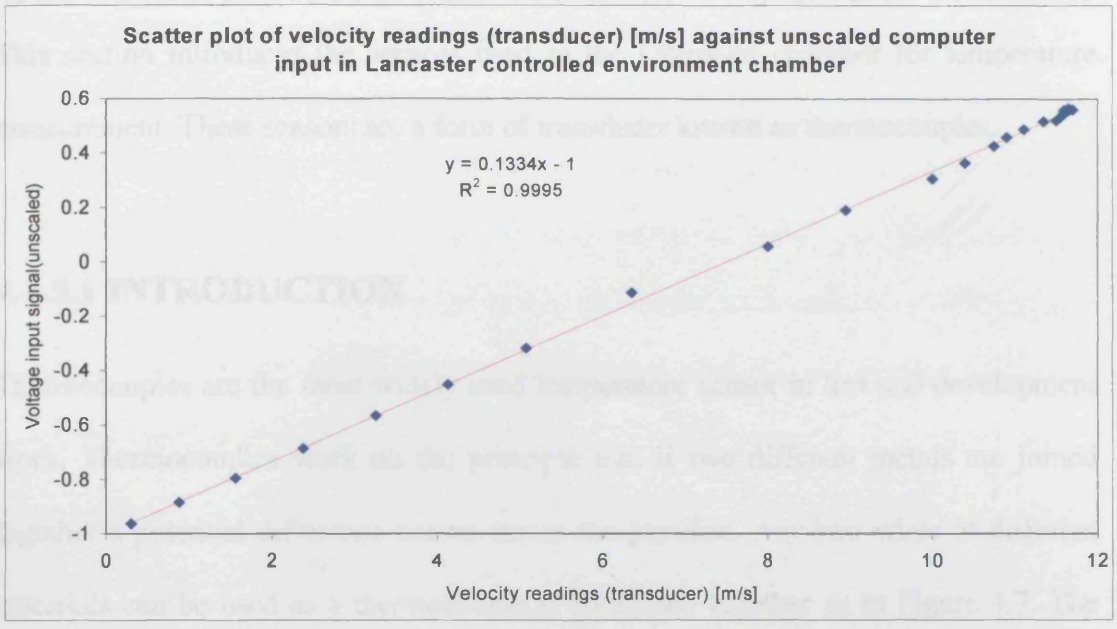

Figure 4.6: Scatter plot and line of best fit of input voltage data plotted against the mean transducer output signal, the equation of the line was incorporated into the Lancaster chamber SIMULINK control diagram.

4.4.4.1 AIRFLOW MEASUREMENT CONCLUSIONS

The free running impeller has shown to perform well in experimentation in the Leuven ventilation chamber, nonetheless, for the Lancaster chamber the decision was taken to use an airflow sensor (air velocity transducer (AVT)) that had a faster and more accurate response at low ventilation rates. The main drawback of the AVT being the omni-direction of this particular model which can make it difficult to measure convective currents in certain locations within the chamber, however, the free running impeller would fair even worse outside the outlet duct it is usually housed in. The AVT was moved to different parts of the 0.13 m diameter outlet and the values observed varied very little wherever it was placed. Thus, the error on the overall accuracy of the AVT compared to a free running impeller was deemed to be minimal and for the ease of use, speed of response and accuracy at low airflow rates the AVT airflow sensor was chosen.

4.4.5 TEMPERATURE MEASUREMENT - THERMOCOUPLES

This section introduces the sensors used in the Lancaster chamber for temperature measurement. These sensors are a form of transducer known as thermocouples.

4.4.5.1 INTRODUCTION

Thermocouples are the most widely used temperature sensor in test and development work. Thermocouples work on the principle that if two different metals are joined together a potential difference occurs across the junction. Any two wires of different materials can be used as a thermocouple if connected together as in Figure 4.7. The AB connection is called the "junction". When the junction temperature, T_{Jct}, is different from the reference temperature, T_{Ref}, a low-level DC voltage, E , will be available at the +/- terminals. The value of E depends on the materials A and B, on the reference temperature, and on the junction temperature. The governing equations for two-wire thermocouples are shown in equations 4.3 and 4.4.

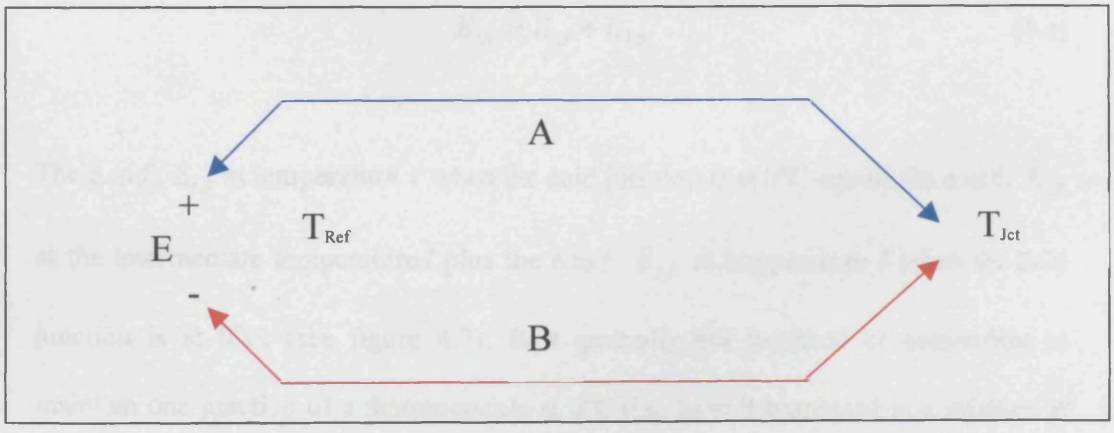

Figure 4.7: The thermocouple.

From equation 4.3, we can see that the EMF is generated by the wires, not the junction: the junction being just an electrical connection between the two wires. The

signal is generated in the wires where the temperature gradient, dt/dx, is not zero: uniform temperature wires do not generate any EMF. If both wires are uniform in calibration, then equation 4.4 can be used, and if the two wires both begin at T_{Ref} and end at T_{Jct}, then equation 4.5 applies. EMF-Temperature tables can only be used when the circuit consists of only two wires, both of which are uniform in calibration, and both of which begin at T_{Ref} and end at T_{Jct}. When only small temperature differences are involved, the values of A and B can be treated as constants, and equation 4.3 gives a good approximation to the EMF.

$$E = \int_{T_{Jct}}^{T_{Ref}} E\frac{dT}{dx} + \int_{1}^{o} T_{Ref}\frac{dT}{dx}dx \tag{4.3}$$

A thermocouple can be used with the reference junction at a temperature other than 0°C. However, standard tables assume a 0°C junction and a correction has to be applied before these tables can be used. The correction is applied using what is known as the *law of intermediate temperatures*, namely

$$E_{t,0} = E_{t,1} + E_{1,0} \tag{4.4}$$

The e.m.f. $E_{t,0}$ at temperature t when the cold junction is at 0°C equals the e.m.f. $E_{t,1}$ at the intermediate temperature 1 plus the e.m.f. $E_{1,0}$ at temperature 1 when the cold junction is at 0°C, (see figure 4.7). It is generally not practical or convenient to maintain one junction of a thermocouple at 0°C (i.e. have it immersed in a mixture of ice and water). Another method is however, to use a compensation circuit to provide an e.m.f. which varies with the temperature of the cold junction in such a way that

when it is added to the thermocouple e.m.f. it generates a combined e.m.f. which is the same as would have been generated if the cold junction had been at 0^0C (figure 4.8). The compensating e.m.f. can be provided by the voltage drop across a resistance thermometer element.

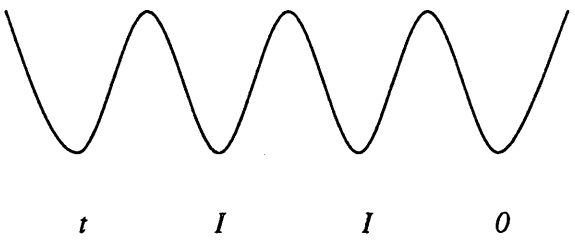

Figure 4.8: Law of intermediate temperatures.

To illustrate the above, consider a type E thermocouple that is to be used for the measurement of temperature with a cold junction at 20°C. What will the thermoelectric e.m.f. at 200°C be? The following is data from standard tables.

Temp. (°C)	0	20	200
e.m.f. (mV)	0	1.192	13.419

Using the law of intermediate temperatures (equation 4.5)

$$E_{200,0} = E_{200,20} + E_{20,0} = 13.419 - 1.192 = 12.227mV \tag{4.5}$$

Note: this is not the e.m.f. given by the tables for a temperature of 180°C with a cold junction at 0°C, namely 11.949 mV.

4.4.5.2 CALIBRATION OF THERMOCOUPLES IN LANCASTER CHAMBER

The calibration of thermocouples in the Lancaster chamber was carried out by initially identifying each thermocouple in turn, and measuring the signal response to a series of hot and cold sources to identify both the speed and magnitude of response (figures 4.9 and 4.10). These were then compared against an accurate pre-calibrated thermometer.

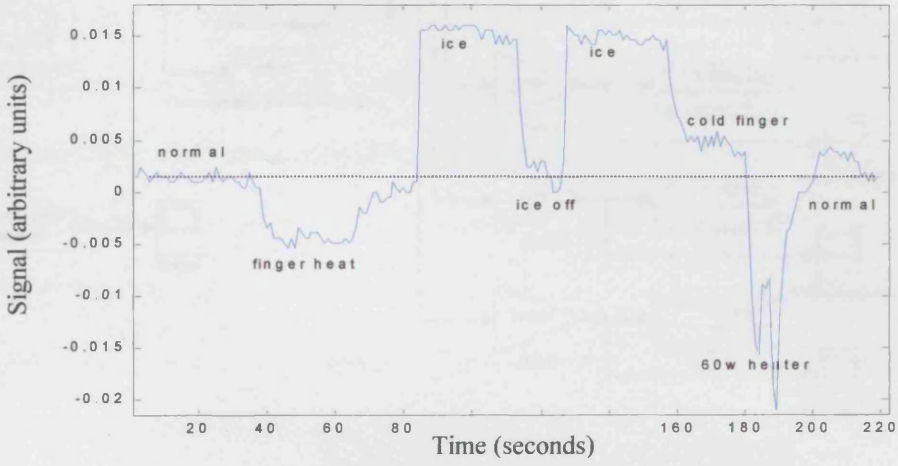

Figure 4.9: Thermocouple response experiment with ice and heater.

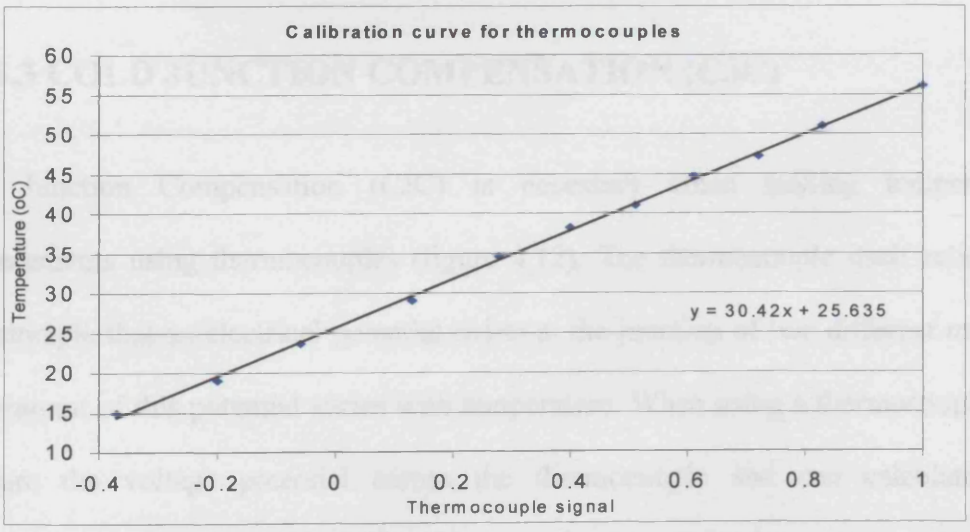

Figure 4.10: Calibration curve for thermocouples.

Figure 4.11 below shows the SIMULINK diagram for thermocouple measurement within the Lancaster microenvironment chamber.

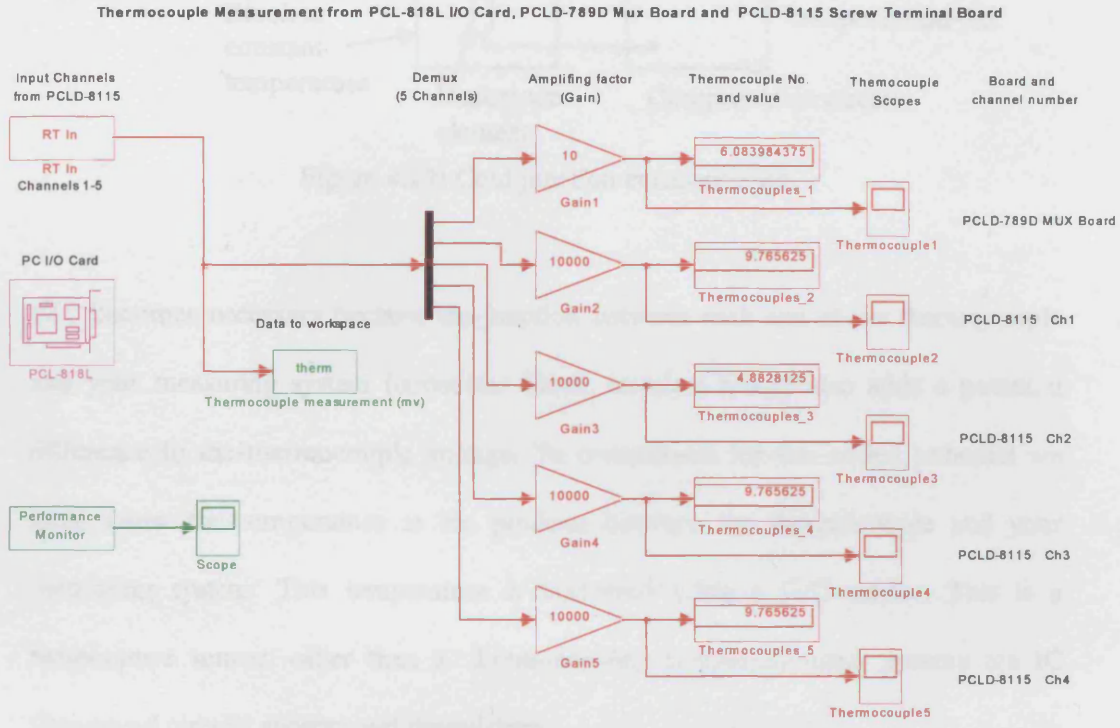

Figure 4.11: SIMULINK diagram of thermocouples.

4.4.5.3 COLD JUNCTION COMPENSATION (CJC)

Cold Junction Compensation (CJC) is necessary when making temperature measurements using thermocouples (figure 4.12). The thermocouple itself relies on the principle that an electrical potential exists at the junction of two different metals. The amount of this potential varies with temperature. When using a thermocouple we measure the voltage potential across the thermocouple and can calculate the temperature causing this potential difference.

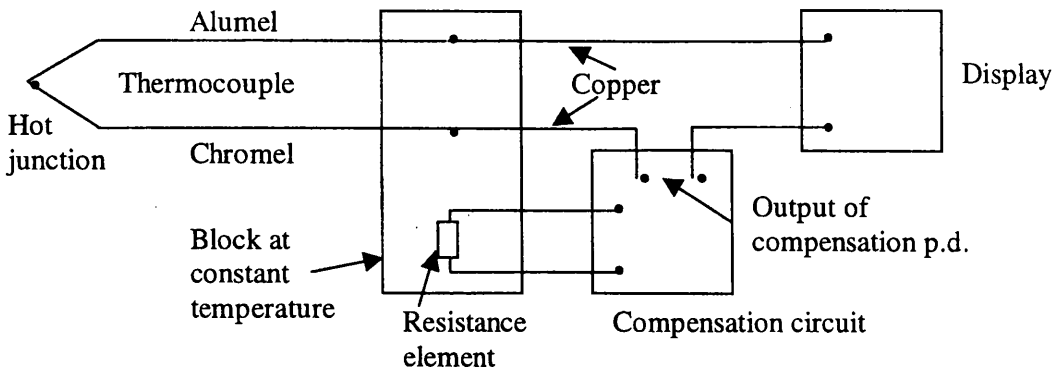

Figure 4.12: Cold junction compensation.

CJC becomes necessary because the junction between each end of the thermocouple and your measuring system (connector block, terminal block) also adds a potential difference to the thermocouple voltage. To compensate for this added potential we must know the temperature at the junction between the thermocouple and your measuring system. This temperature is measured using a CJC sensor. This is a temperature sensor other than a thermocouple; commonly used sensors are IC (integrated circuit) sensors and thermistors.

To make our actual thermocouple temperature measurement we measure the voltage from the thermocouple and CJC sensor. Then we convert the CJC sensor measurement into a CJC temperature and pass the thermocouple voltage and CJC temperature to our conversion function to calculate the thermocouple temperature.

The output of a thermocouple junction must be referred to a reference junction that is at a known temperature. The reference junction or cold junction compensates for the temperature of the junction between thermocouple wire and copper wire at the point at which instrumentation wiring becomes exclusively copper. Hence, the term cold

junction compensation. Standard thermocouple tables assume that the cold junction is at the freezing point of water or 0 degree C.

Conventional practice in industrial thermocouple instrumentation uses the arrangement shown in Figure 4.12. All thermocouple/copper reference junctions are thermally connected to an isothermal (uniform temperature) block, the temperature of which is monitored with a precision temperature sensor such as an RTD. The temperature (TREF) of the isothermal block then is used to compensate the signals (T1...TN) in all thermocouple channels.

Thermocouples are the most popular transducer used to measure the phenomena of temperature due to the transducer's relatively low cost, durability and wide temperature range. Thermocouples, however, need special attention when wiring. Since thermocouples rely on the Seebeck effect (the generation of voltage due to the junction of two dissimilar metals under varying temperatures), terminating the thermocouple wires creates another thermocouple that requires compensation (cold junction compensation). ADAC's thermocouple products (5508TC, TB5800-TC, and 4012TCEX) correct this natural "error" at the termination panel by offsetting the un-wanted voltage using zener diodes as well as housing the terminations in an isothermal environment.

4.5 INTERFACING EXTERNAL DEVICES WITH THE MICROPROCESSOR (PC)

In the controlled environmental chamber, there are a number of external devices, which require interfacing with the microprocessor (PC). These include the control fan, disturbance fan and the heating element. Thus, various outputs from the microprocessor are necessary to operate an actuator, which in turn sends a signal to the external device (e.g. control fan). Also, in this case the actuators for the above mentioned devices require an analogue signal, so the digital output from the PC needs converting to an analogue signal. For this purpose a bridging circuit module (figure 4.13) was designed which has an analogue 0-5 V DC input and a 240 V AC output to the external device to be controlled. This circuit is designed to regulate the AC voltage supplied to the load by a Thyristor pair controlled by a Phase Angle Trigger Module (see figure 4.14 for the output response characteristics of the SKPC200-240 to the 0-5 V analogue input), which is subsequently controlled by the analogue 0-5 V

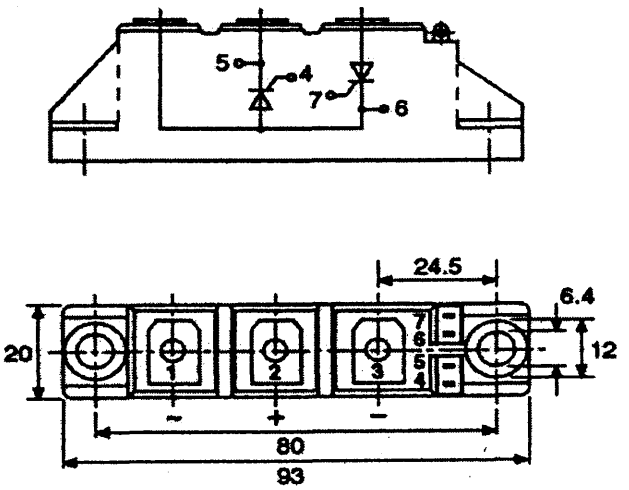

Figure 4.13: Thyristor bridge details.

DC output from the PCL-818L I/O card inside the PC. The bridge in figures 4.15-4.17 is constructed from the thyristor pair (SKKT20B08D) and is controlled by the phase angle trigger module (SKPC200-240), which switches the thyristors in the correct sequence. The circuit diagram is shown in figures 4.15 and 4.17 below.

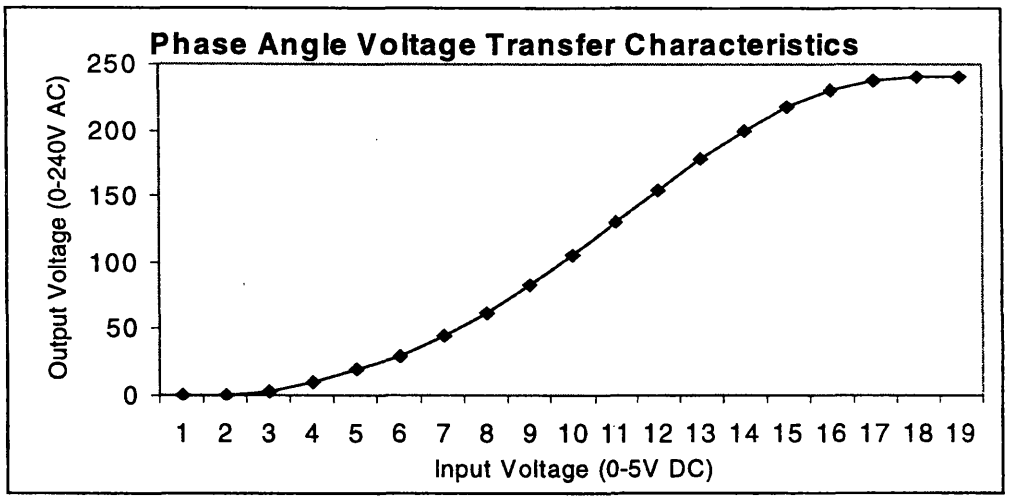

Figure 4.14: Phase angle voltage transfer characteristics.

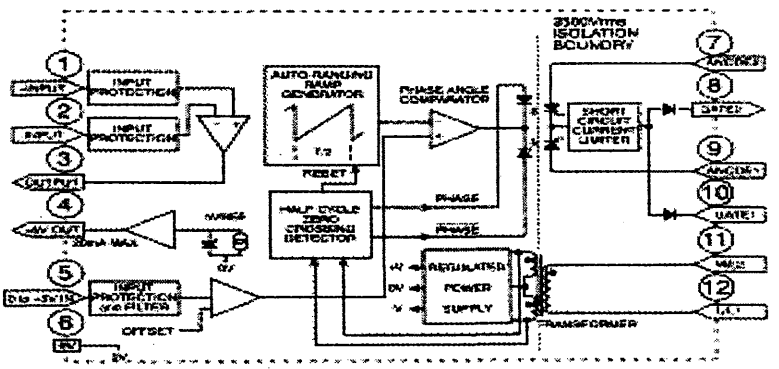

Figure 4.15: AC Power control module for 240V and 400W Loading.

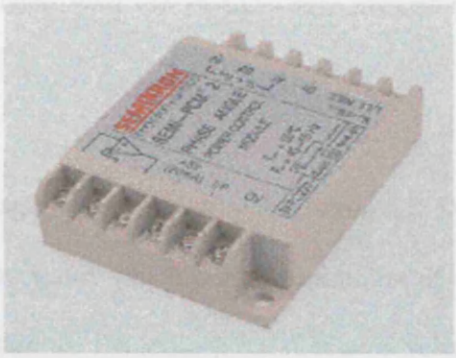

Figure 4.16: Semikron Thyristor Phase Angle Trigger Module (SKPC 200-240V AC).

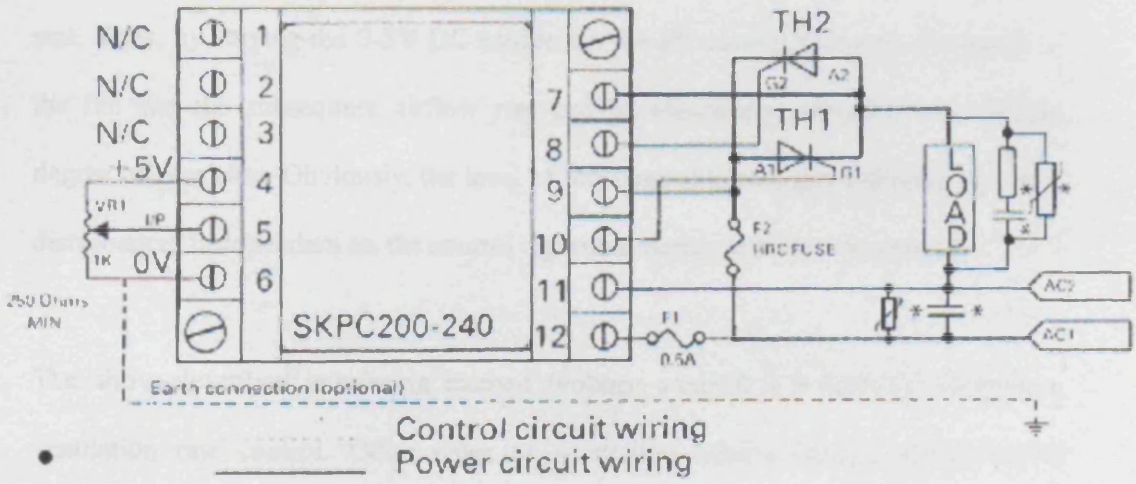

Figure 4.17: Wiring diagram for axial fan control via a phase angle trigger module and pair of thyristors.

In figure 4.17, the output analogue 0-5 V DC voltage is connected across pins 5 (Vout) and 6 (Gnd) of the SKPC200-240. There is a HRC (6A) fuse, which protects the thyristors and load from overcurrent, and a standard 0.5A fuse protects the phase angle trigger module (SKPC200-240). The components were arranged on an insulating board and housed in a suitable enclosure to ensure mechanical and electrical safety. Pins 5 (Vout) and 6 (Gnd) in this power control module were connected to pins

9 (AGND) and 13 (DAO OUT) (digital to analogue output) of the PCLD-8115 connection board associated with the PCLD-789D multiplexer and PCL-818L I/O cards.

This method of AC voltage control (0-240V AC) from a 0-5V DC source, chops the potential AC voltage sine wave, which limits the amount of voltage that reaches the external device (in this case the fan motor). This reduced voltage slows the fan and in turn this produces a lower airflow rate. Conversely, by allowing the voltage output to be undisturbed across the whole sine wave (maximum 5V DC output from PC control) the fan will receive a full 240V AC and the fan will produce its maximum airflow rate. Thus, by varying the 0-5V DC source via the PC control software, the speed of the fan and the subsequent airflow rate can be effectively controlled with a high degree of precision. Obviously, the level of this control to real and simulated pressure disturbances is dependent on the control algorithm design and implementation.

The above-described interfacing method (voltage control) is a form of modulating ventilation rate control. Other types of ventilation control include simple on/off control and stepwise control. These are illustrated below along with modulating control.

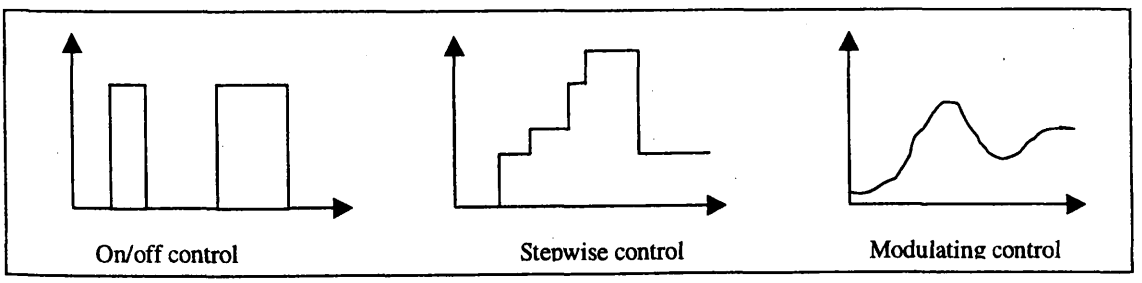

Figure 4.18: Some examples of ventilation rate control.

The first two ventilation control principles in figure 4.18, on/off and stepwise control are cheaper and easier to implement, but when compared to modulating control they result in higher fluctuations of the indoor micro-climate. Both the stepwise and on/off control are mainly used in countries such as the USA, where feed costs are relatively low. By contrast, modulating control is more prevalent in European countries such as, Denmark, Belgium and Holland due to expensive feed costs and more intensive livestock farming. Here, modulating control is used because it provides a more stable ventilation rate and higher probabilities of a more stable indoor ventilation pattern that ultimately results in animals consuming less feed to maintain their optimum temperature.

4.5.1 REAL-TIME CONTROL OF AXIAL FANS AND HEATING ELEMENT

Both the control fan and disturbance fan within the Lancaster chamber along with the heating element all require the capability of automatic feedback into the control algorithm from the advanced digital control design methodology utilised in this thesis. This requirement specifies the voltage to the afore mentioned devices must change (to control the speed of the fans and temperature of the heater) according to a digital output signal from the I/O card and control algorithm.

This can be achieved by various methods:

i) *Pulse Amplitude Modulation (PAM)*: This method chops the dc signal into a series or chain of pulses, the magnitude of the pulse is related to the output voltage; i.e. the higher the pulse the more voltage is applied to the fan and the fan subsequently turns faster.

ii) *Pulse Width Modulation (PWM)*: is where the width, i.e. duration of a pulse rather than its amplitude depends on the size of the voltage applied to the fan.

4.5.2 HEATING CONTROL

The above method of ventilation control was also applied to control the heating element housed in the inlet duct adjacent to the disturbance fan (see figure 4.3). Through trials it was shown a phase angle trigger module (PATM) and a pair of thyristors could effectively regulate the temperature. An analog output (0-5V DC) from the Humusoft AD 512 card was connected to the PATM in exactly the same way as for the fan control (see section 4.2.3.1 for connection details). The heating element is 500W, and has a thermostat housed within the inlet duct, which is wired in series with the heating element that will cut off power in the unlikely event of the duct overheating if the element is left at full voltage with low or no ventilation rate for long periods. A mercury thermometer is also housed inside the duct for monitoring purposes. It is also planned to place an additional thermocouple inside the duct for continuous monitoring within the overall system design.

4.6 SMOKE (VISUALALISATION) EXPERIMENTS IN LANCASTER CONTROLLED ENVIRONMENT CHAMBER

A series of smoke experiments were carried out to investigate the flow patterns in the Lancaster chamber, the following section reports the airflow patterns observed; further figures and analysis can be found in Appendix 7.

4.6.1 EXPERIMENTAL METHOD

A series of planned experiments that introduce imitation smoke into the chamber were carried out in order to determine different airflow patterns within the 3D airspace. The following schematic diagrams illustrate the observed airflow patterns for a range of airflow rates and temperatures. Additionally, an internal heater was used to simulate animal occupancy was moved around the chamber to test the "bio-effects" on airflow within the chamber. The experimental set-up consisted of a flexible duct which was connected to the outlet to transport the smoke outside the laboratory and the smoke machine was aligned to inject smoke directly through the inlet to the chamber.

The smoke machine consists of a heating a block and a water based fluid, which is passed over the pre-heated block that vaporises the fluid producing an injection of a white/grey vapour that simulates smoke.

4.6.2: EXPERIMENTAL RESULTS

Figures 4.19 and 4.20 show two preliminary results of the airflow pattern experiments in this chamber. Further results are presented in Appendix 4.

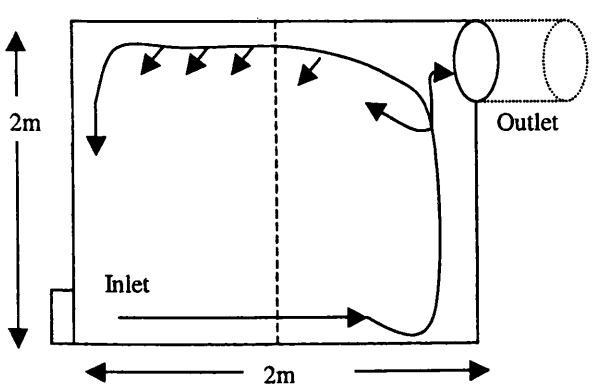

Smoke enters the chamber horizontally, until it reaches the vertical wall on the other side of the chamber. Thereafter smoke rises until the fan is reached where some smoke is removed and the rest continues to move anticlockwise slowly dispersing all the time.

Figure 4.19: Fan 20%, main heater is off, flap fully open, mobile heater is off.

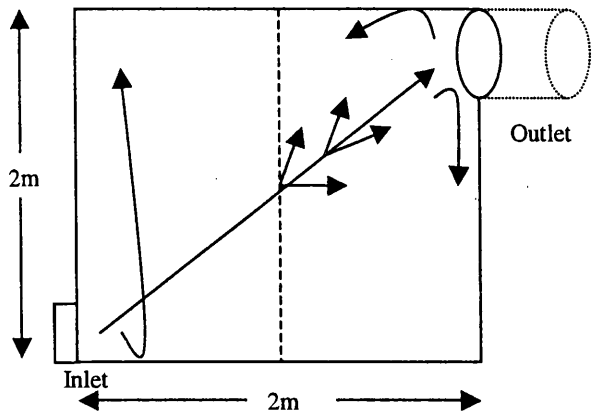

As smoke enters the chamber most follows a relative straight path leading directly to the ventilator, dispersing all the way (noticeable as fan is approached). It should be noted that in the very beginning some smoke immediately rises to the ceiling where it disperses.

Figure 4.20: Fan 30%; Flap Notch 5, Heat is off.

4.7 CONCLUSIONS

This chapter has described the design and construction of the micro environmental chamber in Lancaster. The choice of sensors, along with construction materials has been addressed and the ventilation and heating control methods outlined in detail. The techniques for measuring airflow rate (air velocity transducers) and temperature (thermocouples) within the chamber have also been presented. Appendix 4 continues to expand on the Lancaster chamber theme by introducing the complex subject of data acquisition from the above mentioned hardware devices and sensors which, in practice, is different for each individual application.

The second part of this thesis concentrates on modelling, control and implementation of airflow rate and temperature in both the Leuven ventilation chamber (chapters 5-7) and the Lancaster micro environmental chamber (chapters 6 and 8-9).

Chapter 5

FIXED GAIN PIP CONTROL

5.1 INTRODUCTION

Now the different microclimate chambers have been designed, constructed and described (Chapters 3-4; Appendix 3); and the SISO modelling and control theory has been outlined (chapter 2), this chapter and subsequent chapters focus on the design and implementation of advanced digital control systems in the aforementioned chambers. The design of a fixed gain controller is the next logical stage in the overall aim of control implementation in the ventilation chambers in Leuven and Lancaster. This chapter begins with the design, simulation and finally implementation of the

fixed gain controller in the Leuven ventilation chamber and concludes with the Lancaster microclimate chamber.

5.2 LEUVEN CHAMBER

This section outlines the stages from data collection through to control implementation in Leuven ventilation chamber.

5.2.1 METHODOLOGY

Initially a comprehensive set of open loop experiments were conducted on the ventilation chamber in Leuven in order to identify the dominant dynamics of the axial fan across the whole operating envelope. The experiments that best represent the system under study have been investigated for the purposes of this chapter, (e.g. see table 5.1). The input was potential voltage (PV) (stepped between 10-85%) and the output airflow rate (m^3/hr). The experiments were stepped in nature, ranging from 10-15% of potential voltage applied to the fan to 30-35% and 45-50%, with a few above 60%. However, it was found that, at values much above 50%, the airflow rate did not alter much, but the noise at the end of each step amplified greatly, due partly to the pressure increase within the chamber and its position on the 'S' curve (see figure 2.1). Thus, most of the experiments are concentrated on the three lower ranges. In general, four complete steps were recorded for each experiment in an attempt to capture the dynamics of the system (ventilation chamber) at each particular voltage. The airflow rate was allowed to settle into a 'steady' state before and after each step. In addition, further experiments were carried out where the throttling valve was implemented at different closures, and the disturbance fan set to simulate different disturbances using

a variety of potential voltages both positive and negative. The data were collected at a two second sampling interval for model estimation and control design purposes.

Below, figure 5.1 shows how airflow rate change when an increasing %PV is applied to the ventilation chamber. This data were used to help determine the steady state relationships within the ventilation chamber. The first plot illustrates the measured airflow rate against increasing %PV; the result is a classic non-linear 's' curve. The second bar chart in figure 5.1 indicates where the largest changes in airflow rate occur and emphasises the non-linearity of the system; it is clear from the plot that the largest changes are occurring between 30-40% PV. This is significant for this chamber and is expanded on more in section 5.4 of this chapter. The total sum of the data in plot 2 is 5562m^3/hr which is the absolute maximum the system can produce at 100% PV, with the vortex damper fully open and with the disturbance fan off. Closer inspection of the data reveals that 27.15% of the airflow is produced between 30% and 38% PV while 21.40% and 20.14% are produced for 20-28% PV and 40-48% PV respectively. Added together the airflow from 20-48% accounts for almost 70% of the potential airflow the 45cm diameter axial fan can produce in the Leuven ventilation chamber.

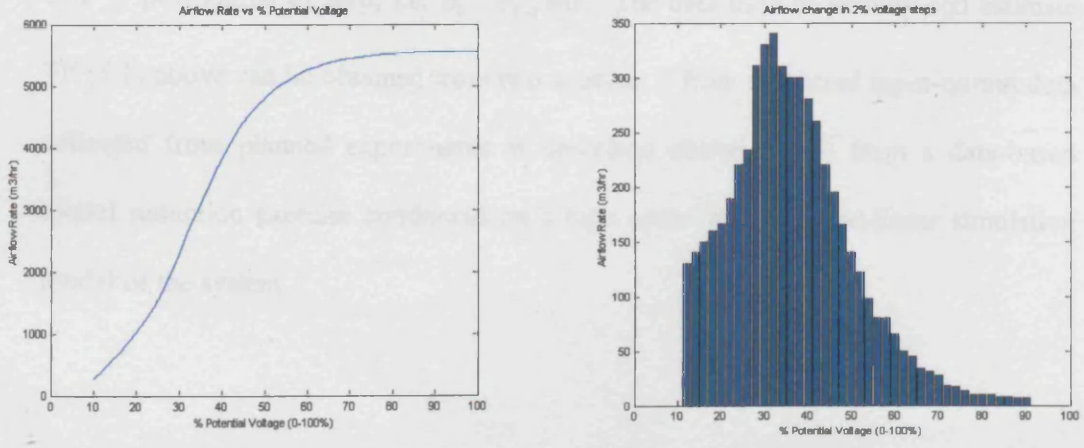

Figure 5.1: Plot showing different parameter characteristics of ventilation chamber to an increasing % potential voltage.

5.2.2 MODEL ESTIMATION

The first stage in developing a PIP control algorithm suitable for use in advanced digital control methodology requires a linearised representation of the system under study. From the discussion in the previous section it is evident that the ventilation chamber is a non-linear system; however, this chapter and further chapters will demonstrate how a straightforward linearised TF model, identified and estimated from either measured or simulated data, can capture the small perturbational behaviour exhibited in the aforementioned data (Young, Parkinson and Lees, 1996 and Young, 1998). For the remainder of this chapter the emphasis will be on the following single-input, single-output (SISO) linear discrete-time system,

$$y(k) = \frac{b_0 + b_1 z^{-1} + ... + b_m z^{-m}}{1 + a_1 z^{-1} + ... + a_n z^{-n}} u(k) = \frac{B(z^{-1})}{A(z^{-1})} u(k) \tag{5.1}$$

where, $y(k)$ is the output variable (to be controlled) and $u(k)$ the control input (actuator signal). $A(z^{-1})$ and $B(z^{-1})$ are appropriately defined polynomials in the backward shift operator z^{-1}; i.e. $z^{-1}y(k) = y(k-1)$. For simplicity, any pure time delay of δ samples will be taken account of by setting the δ initial parameters of the $B(z^{-1})$ polynomial to zero, i.e. $b_0 ... b_{\delta-1} = 0$. The data used to identify and estimate TF (5.1) above can be obtained from two sources: i) from measured input-output data collected from planned experiments as described above, or; ii) from a data-based model reduction exercise conducted on a high order linear or non-linear simulation model of the system.

The model developed from data collected in Leuven is a data-based (DB) TF model, which is both identified (model order) and estimated (parameters) according to the modelling methodology outlined earlier (see chapter 2). The SRIV algorithm identifies a first order model (5.2) as the optimum model after taking into account optimum YIC and R_T^2 statistics for each of the experiments shown in table 5.1 across a wide range of operating conditions (0-5500m^3/hr), i.e.,

$$y(k) = \frac{b_1 z^{-1}}{1 + a_1 z^{-1}} u(k) \tag{5.2}$$

where, b_1 and a_1 are defined as the model parameters, (see table 5.2); and *y(k)* is the airflow rate (m^3 h^{-1}), *u(k)* is the applied voltage (%) and z^{-1} is the backward shift operator.

In the following typical experiment, the throttling valve is set to fully open with the control fan operating in the mid-range of airflow rates (35-40% voltage applied), while the disturbance fan is switched off. The SRIV algorithm (see chapter 2) yields the following discrete-time TF model, where the R_T^2 and *YIC* respectively are 0.9948 and –12.8188,

$$y(k) = \frac{75.9801\ z^{-1}}{1 - 0.4792\ z^{-1}} u(k) \tag{5.3}$$

where $y(k)$ is the airflow rate (m^3/h) and $u(k)$ is the applied voltage (%),

The response of the model (5.3) closely follows the noisy measured data, as illustrated by figure (5.2). The Steady State Gain (SSG) and Time Constant (TC) of the model, which indicate the relative power and speed of response respectively, are 146.12 and 2.72 seconds. Note that the identified time constant (2.72 seconds), relates closely to that obtained from the initial theoretical and empirical investigations into the fan characteristics (Vranken, 1999).

The SRIV algorithm has been applied to each set of experimental time series data; this in turn yields a table such as table 5.1, and the resulting Transfer Function (TF) (equation. 5.3) can now be utilised for model-based control system design (see fixed gain control implementation (section 5.2.4)). Figure 5.2 below, shows the SRIV model fit for the above TF model (5.3).

Table 5.1: Modelling data for ('s') curve (figure 5.3).

Exp. No.	Step in Voltage	Model Order	a_1 Parameter	b_1 Parameter	YIC	RT2	SSG (m^3/%hr)	TC (Seconds)
1	11 to 15	[1 1 1]*	-0.8759	8.1365	-14.1365	0.9928*	65.61	15.10
2	15 to 20	[1 1 1]	-0.7927	19.7482	-14.9338	0.9964	95.28	8.61
3	20 to 25	[1 1 1]	-0.7840	28.2308	-14.1261	0.9950	131.02	8.21
4	25 to 30	[1 1 1]	-0.6724	44.6233	-13.5181	0.9940	136.01	5.03
5	30 to 35	[1 1 1]	-0.5593	65.7757	-13.9049	0.9963	149.27	3.44
6	35 to 40	[1 1 1]	-0.4792	75.9801	-12.8188	0.9948	146.59	2.72
7	40 to 45	[1 1 1]	-0.3777	74.0252	-12.3969	0.9966	119.58	2.05
8	45 to 50	[1 1 1]	-0.4231	46.3089	-10.2430	0.9860	80.27	2.33
9	50 to 55	[1 1 1]	-0.2939	34.3279	-7.2144	0.9623	48.61	1.63
10	55 to 60	[1 1 1]	-0.4427	18.1520	-6.8034	0.9147	32.57	2.45
11	60 to 65	[1 1 1]	-0.2834	16.4255	-4.6524	0.8475	22.92	1.59
12	65 to 70	[1 1 1]	-0.5582	7.7809	-4.0382	0.6160	17.61	3.43
13	70 to 75	[1 1 1]	-0.5039	5.5016	-2.5882	0.2720	11.08	2.92
14	75 to 80	[1 1 1]	-0.5762	4.6487	-2.5421	0.2304	10.96	3.63

* A [1 1 3] model was found to give a better fit (see low ventilation rate control)

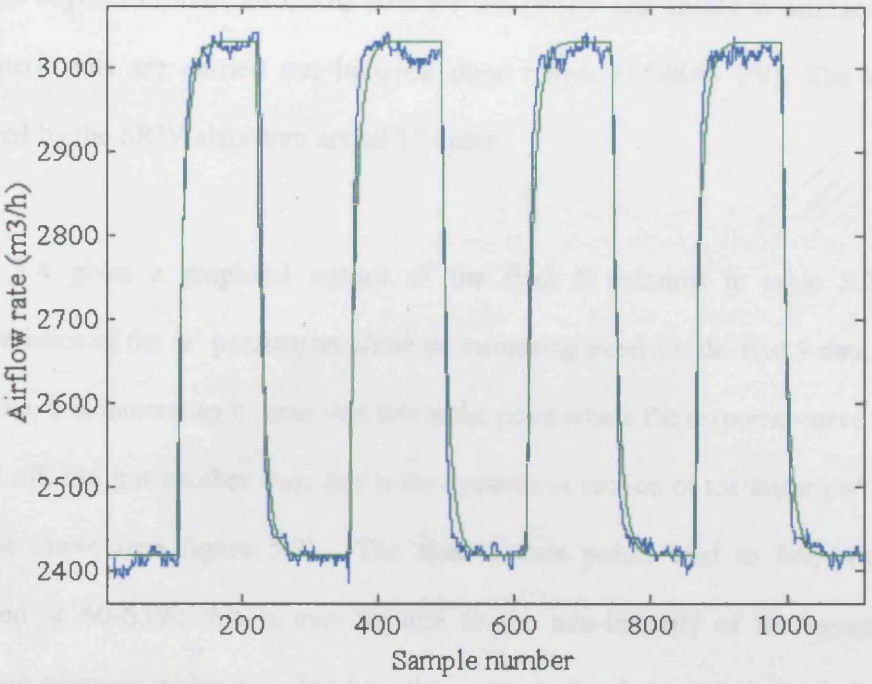

Figure 5.2: Ventilation rate and model fit of a typical experiment (35-40% voltage; YIC = -12.8188; R_T^2 = 0.9948; Model Order =[1, 1, 1]; see table 5.1)).

Once the model has been estimated and identified the model parameters can undergo further statistical analysis. Table 5.1 shows the various parameter values that make up the response (s) curve (figure 5.3) to increasing voltage applied to the axial fan. It is worth noting that figure 5.3 represents the mean ventilation rate for a given voltage.

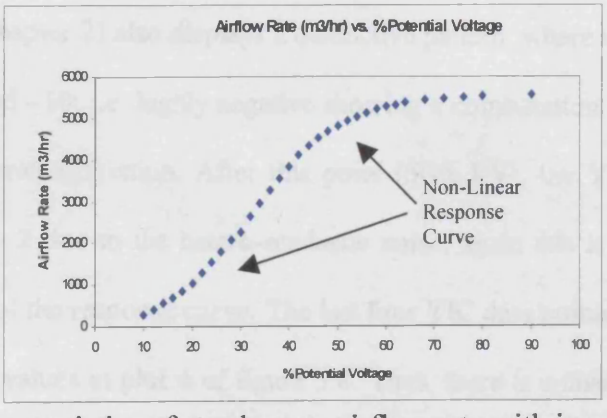

Figure 5.3: Characteristics of steady state airflow rate with increasing percentage voltage input to ventilation test chamber showing a non-linear (sigmoid) response curve.

As mentioned earlier, the axial fan requires >10% potential voltage (PV) before the armature begins to rotate; also, >70-80% PV the airflow rate ceases to increase. Thus the experiments are carried out between these ranges (11-80% PV). The models identified by the SRIV algorithm are all 1st order.

Figure 5.4 gives a graphical output of the final 6 columns in table 5.2. The characteristics of the 'a' parameters show an increasing trend for the first 9 data points (11-55%), it is interesting to note that this is the point where the response curve begins to level off. Or, put another way, this is the uppermost section of the linear part of the response curve (see figure 5.2). The final 5 data points tend to fall, with one exception at 60-65%; this is may be due to the non-linearity of the system and increasing pressure within the chamber (the pressure data becomes increasingly noisy when associated with higher voltages). The 'b' parameters show a similar type of response except the highest values (30-35%; 35-40% and 40-45%) correspond to the area of the curve where there is the greatest rate of change of airflow rate for each percentage change in PV. This is also the centre of the linear part of the curve and shows how the 'b' parameters reflect the dynamic behaviour of the system under study.

The YIC (see chapter 2) also displays a distinctive pattern, where the first 8 values are between –15 and –10; i.e. highly negative showing a combination of a good model fit without over-parameterisation. After this point (50% PV), the YIC for a first order system rises to –2 due to the hetero-scedastic noise; again this is consistent with the non-linear part of the response curve. The last four YIC data points also correspond to the lowest RT2 values in plot 4 of figure 5.4. Thus, there is a change from the model

explaining 98-99% of the data down to 27% and 23% respectively for the last two models. This is hardly surprising given the amount of noise associated with this highly non-linear part of the system.

The final two plots of figure 5.4 show the steady state gain (SSG) and the time constant (TC). The SSG indicates the maximum gain of the system at a particular point and is a function of both the *a* and *b* model parameters; from the plot the highest values are again associated with the linear part of figure 5.3, which in light of the previous discussion is hardly surprising. The TC, which is a function of the model *a* parameters, also drops off towards the linear part of the response curve.

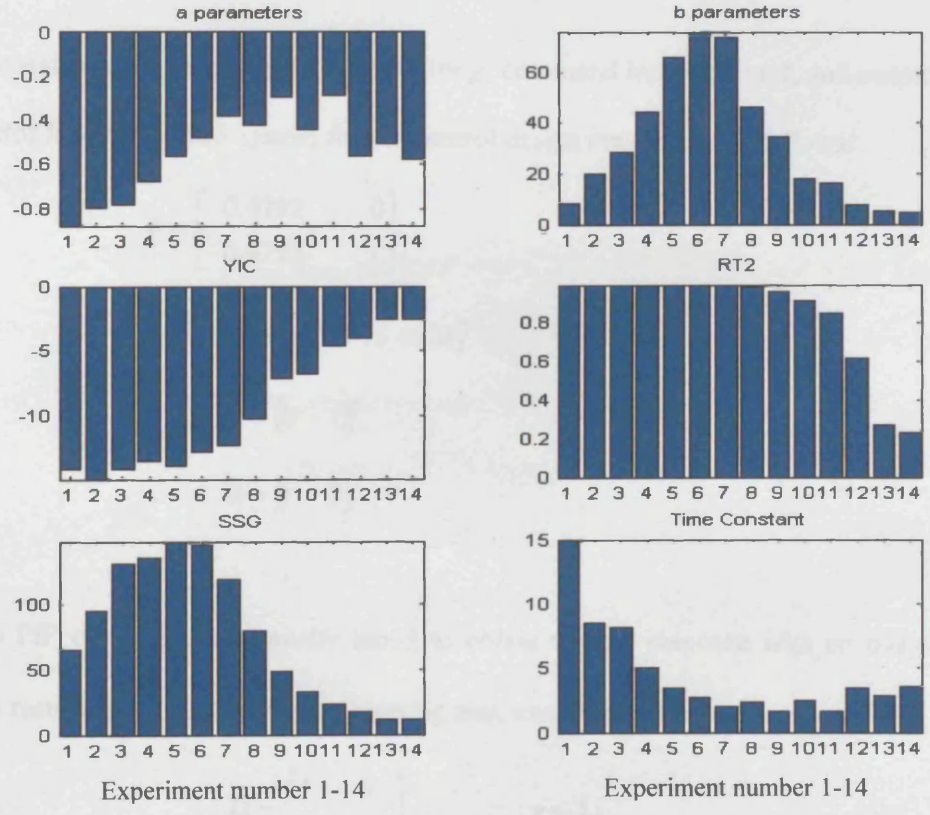

Figure 5.4: Model parameters (*a* and *b*), YIC, R_T^2, SSG and TC values from identifying the response curve to increasing PV% values plotted against the experiment number as defined in table 5.1.

5.2.3 CONTROL DESIGN

The next stage is to design a PIP controller suitable for implementation on the actual system under study. From the experimental data (table 5.1), the model identified earlier (equation 5.3) (experiment 6, table 5.1), which was chosen as a model that represents the most linear part of figure 5.1A, (it has been found through experimental method that a first order model with between one and three time delays very often provides an optimum fit to data across a wide operating envelope). The next step in the PIP control design process is to construct the non-minimum state space (NMSS) representation. Equations 2.36 to 2.41 in chapter two define this procedure. It is sufficient here to directly show the NMSS representation of equation 5.3, (see equation 5.4 below).

The state transition matrix $\boldsymbol{F}$, input vector $\boldsymbol{g}$, command input vector $\boldsymbol{d}$, and output vector $\boldsymbol{h}$ of the NMSS system for the control design are defined as follows:

$$\boldsymbol{F} = \begin{bmatrix} 0.4792 & 0 \\ -0.4792 & 1 \end{bmatrix}$$

$$\boldsymbol{g} = \begin{bmatrix} 75.9801 & -75.9801 \end{bmatrix}^T \qquad (5.4)$$

$$\boldsymbol{d} = \begin{bmatrix} 0 & 1 \end{bmatrix}^T$$

$$\boldsymbol{h} = \begin{bmatrix} 1 & 0 \end{bmatrix}$$

The PIP controller is manually tuned to obtain a rapid response with no overshoot. The resulting LQ cost function weighting matrices $\boldsymbol{Q}$ and $\boldsymbol{r}$ are:

$$\boldsymbol{Q} = \begin{bmatrix} 1 & 0 \\ 0 & 0.01 \end{bmatrix} \qquad \boldsymbol{r} = 1 \qquad (5.5)$$

The SVF control law is then defined as,

$$u(k) = -\boldsymbol{k}\boldsymbol{x}(k) \tag{5.6}$$

And, the resulting matrix of feedback gains $\boldsymbol{k}$ is:

$$\boldsymbol{k} = [f_o \quad -k_I] \tag{5.7}$$

Substituting the gains for f_o and k_I are:

$$\boldsymbol{k} = [0.0073 \quad -0.0013] \tag{5.8}$$

In practice, the PIP control law derived from figure 2.7 (see chapter 2) is always implemented in the following incremental form,

$$u(k) = u(k-1) + k_I\{y_d(k) - y(k)\} - F(z^{-1})\nabla y(k) - \{G(z^{-1}) - 1\}\nabla u(k) \tag{5.9}$$

where, $\nabla = 1 - z^{-1}$ is the difference operator and $F(z^{-1}) = f_0 + F_1(z^{-1})$. Equation 5.12 is not only the most obvious and convenient for digital implementation, but also provides an inherent means of avoiding 'integral windup' in the PIP controller. To avoid such integral windup, which is caused by integration of control errors during periods of actuator saturation, equation 5.5 is employed with the following correction,

$$\begin{aligned} u(k) &= u_{\max} \quad \text{when} \quad u(k) > u_{\max} \qquad (100\%) \\ u(k) &= u_{\min} \quad \text{when} \quad u(k) < u_{\min} \qquad (0\%) \end{aligned} \tag{5.10}$$

In this manner, $u(k)$ and its past values are kept within the practical limits represented by $u_{\min}$ and $u_{\max}$.

Then, the incremental form obtained by substituting the f_o and k_I gains (5.8) into equation 5.9 is,

$$u(k) = u(k-1) + 0.0013\{y_d(k) - y(k)\} - 0.0073\{y(k) - y(k-1)\} \qquad (5.11)$$

5.2.4 MONTE CARLO ANALYSIS

It is important in model-based control system design such as this, that the robustness of the control system is considered with respect to parametric uncertainty (Taylor *et al.*, 1998). Monte Carlo Simulation (MCS) analysis provides an excellent solution to the problem and figure 5.5 shows the results of MCS analysis aimed at assessing the sensitivity of a controller to model uncertainty. Here, the model parameters for each realisation in the MCS analysis, are selected randomly from the joint probability distribution defined by the identified parametric covariance matrix $\boldsymbol{P}$ (Young, 1991), and the sensitivity of the PIP controlled system to parametric uncertainty is evaluated from the ensemble of resulting closed loop response characteristics. The various ensemble results obtained in this manner are normally provided in graphical form: for instance, plots of the closed loop responses as in figure 5.5. It is clear from figure 5.5 that the ventilation rate reaches the desired level in all cases with no unstable realisations. Furthermore, following the imposition of both input and output (load) disturbance signals, the controller rapidly adjusts the applied voltage to return the ventilation rate to the required level for each MC realisation, where it is successfully maintained until the end of the simulation. These disturbances consist of step inputs applied to $u(k)$ and $y(k)$ at the 100^{th} and 150^{th} samples respectively (where both disturbances continue until the end of the simulation).

It should be noted that figure 5.5 shows the sensitivity of the control system to the estimated parametric uncertainty, (as estimated at this particular operating point). In fact, because the model is so well defined for the middle range of airflow rate, i.e. the standard errors on the parameter estimates are very small; the analysis initially yields almost no MCS envelope around the ideal closed loop response. Therefore, in figure 5.5, the parametric covariance matrix has been multiplied by a factor of 100, in order to better evaluate the sensitivity of the response to the inherent non-linearities in the system: even so, the control performance remains excellent and presages the likely robustness of the design when the system is implemented in practice (see section 5.2.5).

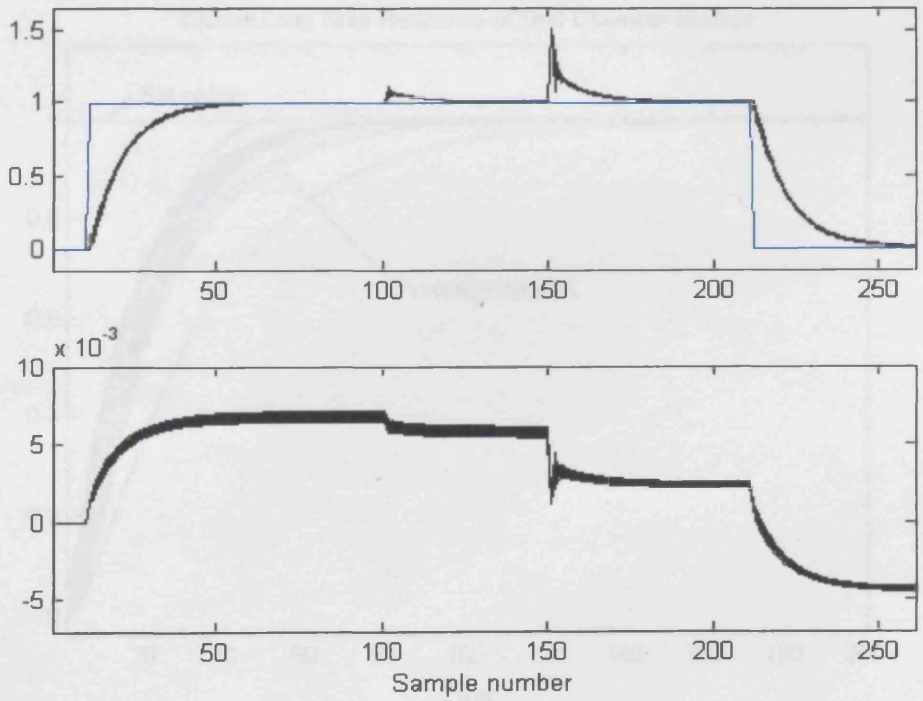

Figure 5.5: PIP-LQ control of ventilation rate with 100 Monte Carlo realisations, showing the response to an input disturbance of 0.001 and a load disturbance of 0.5 at the 100th and 150th sample respectively: *y(k)* and set point (top), together with *u(k)* (bottom), with all the variables plotted against sample number.

Of course, the parameters could change much more than indicated by the covariance **P** matrix based on just an operating point. For instance, Table 5.1 and figure 5.4 reveal large parameter changes over the whole operating envelope. It is necessary, therefore, to consider the robustness to such large parameter variances. In this regard Figure 5.6, below, shows the control robustness to a unity step reference input for the 14 models in table 5.1 compared to the average model controller (dots). It is evident from the plot that the average model results in robust control design with the output reaching the set point for all 14 models with no unstable realisations. In fact, most of the responses are similar to the mean control system response, which results in 'bunching' around that profile. However, if the system parameters are significantly different to the expected values, then substantially faster or slower responses arise.

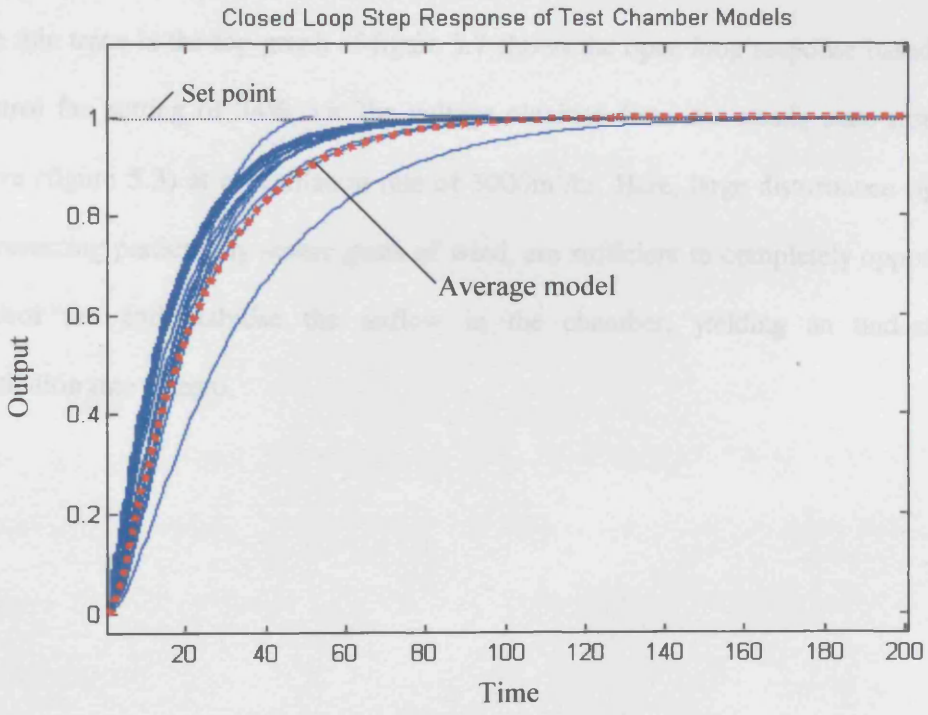

Figure 5.6: Step response of different models in table (5.1).

5.2.5 CONTROL IMPLEMENTATION

The previous section has shown how robust the PIP control design can be with respect to parametric uncertainty. Now, the above PIP design (section 5.2.3) is implemented on the Leuven ventilation chamber. The first example (figure 5.7) shows why feedback control is essential to maintain an even airstream within a building envelope, especially in the presence of a disturbance. In many of the subsequent closed loop experiments presented, the second fan (see figure 5.14) is turned on to generate different disturbance patterns, ranging from simple step functions to more realistic wind pressure simulations. Figure 5.7 shows the PIP control response, where the disturbance is derived from wind pressure measurements obtained from a real building (Vranken, 1999).

The thin trace in the top graph of figure 5.7 shows the open loop response based on a control fan setting of 34%, i.e. the voltage obtained from the steady state response curve (figure 5.3) at a ventilation rate of 3000m^3/hr. Here, large disturbance signals, representing particularly severe gusts of wind, are sufficient to completely oppose the control fan and stabilise the airflow in the chamber, yielding an undesirable ventilation rate of zero.

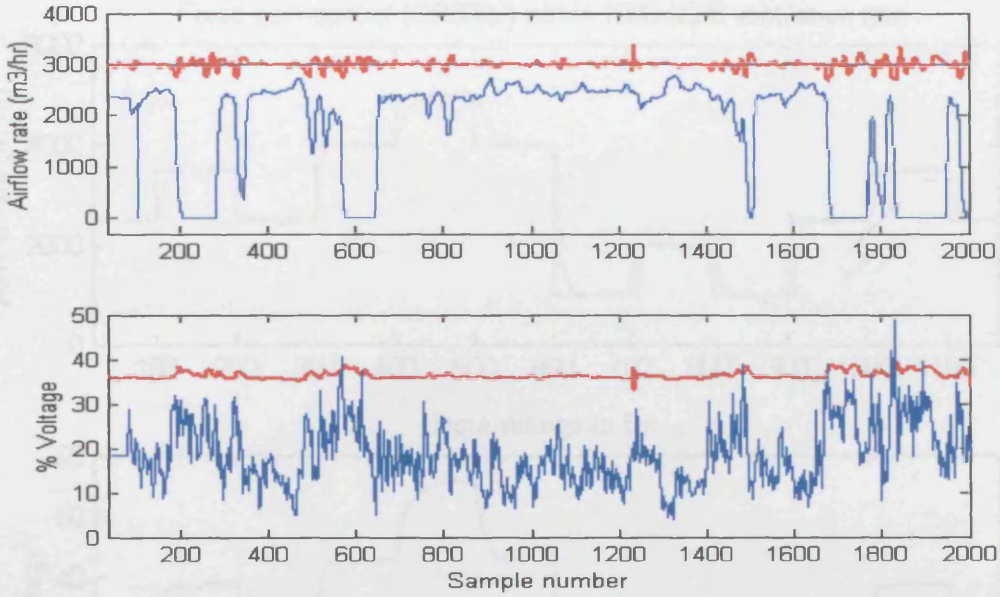

Figure 5.7: PIP-LQ (thick trace) and open loop (thin) control of ventilation rate (m^3/h) for a set point of $3000m^3/h$ (top); control fan (thick trace) and disturbance fan inputs (%; bottom), all plotted against sample number (seconds); the constant open loop control input of 34% is not shown.

It is clear from figure 5.7, however that the ventilation rate is successfully regulated by the PIP feedback control, with the input voltage responding rapidly to the high frequency wind disturbances.

The next example (figure 5.8) shows the same fixed gain controller applied across a wide operating envelope ($1000\text{-}5000m^3/hr$) with no disturbance input applied (i.e. disturbance fan off): it shows tight tracking of the varying set point with little or no overshoot present.

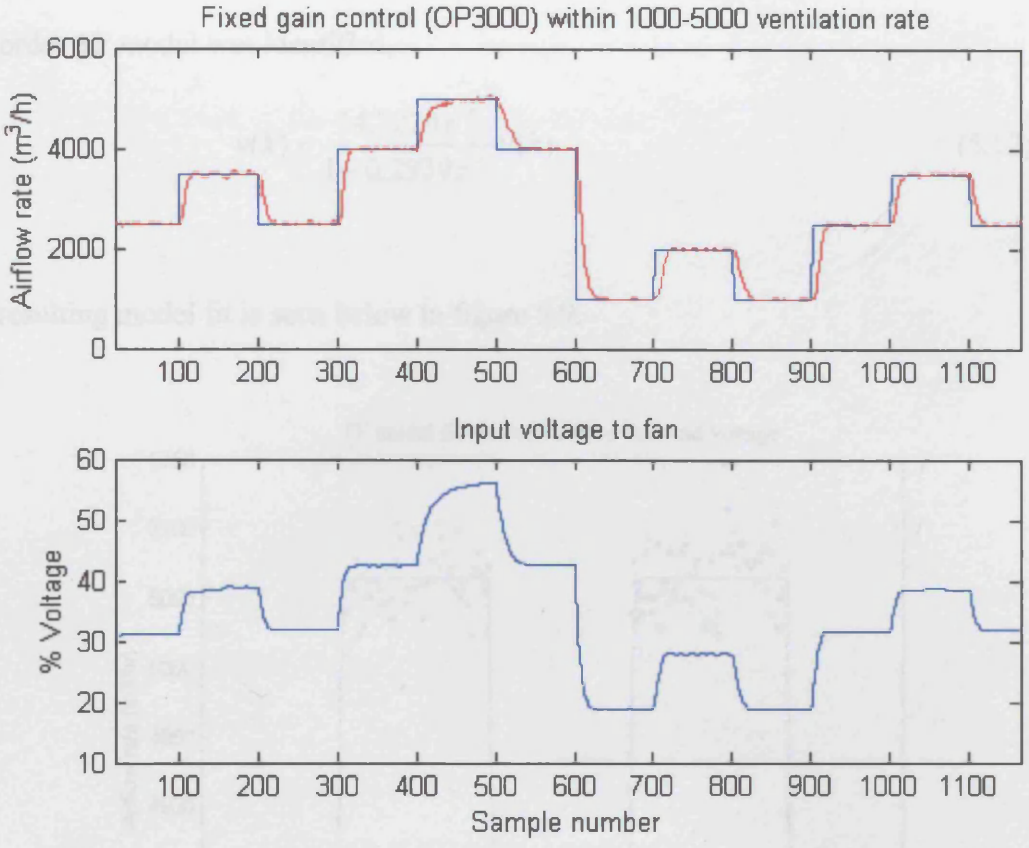

Figure 5.8: Fixed gain control over a wide operating envelope (model based on 3000m^3/hr). The upper plot shows the tight tracking (red) of the set point (blue); while the lower plot is the voltage applied to the fan required to attain the aforementioned control response.

5.2.5.1 HIGH VENTILATION RATE CONTROL

Closer inspection of figure 5.8 shows that the response to the set point change above 4000m^3/hr and below 2000m^3/hr is slower than the range the controller was designed for (i.e. 3000m^3/hr). This slow response is caused by model mismatch, since equation (5.3) does not adequately represent the airflow dynamics at the higher operating point. However in both cases the airflow does reach the desired level. In order to improve on this a second controller was designed for operation at high ventilation rates. Following

an experiment carried out between 50%PV and 55%PV (see table 5.1), the following first order TF model was identified,

$$y(k) = \frac{34.3279z^{-1}}{1-0.2939z^{-1}}u(k) \tag{5.12}$$

The resulting model fit is seen below in figure 5.9.

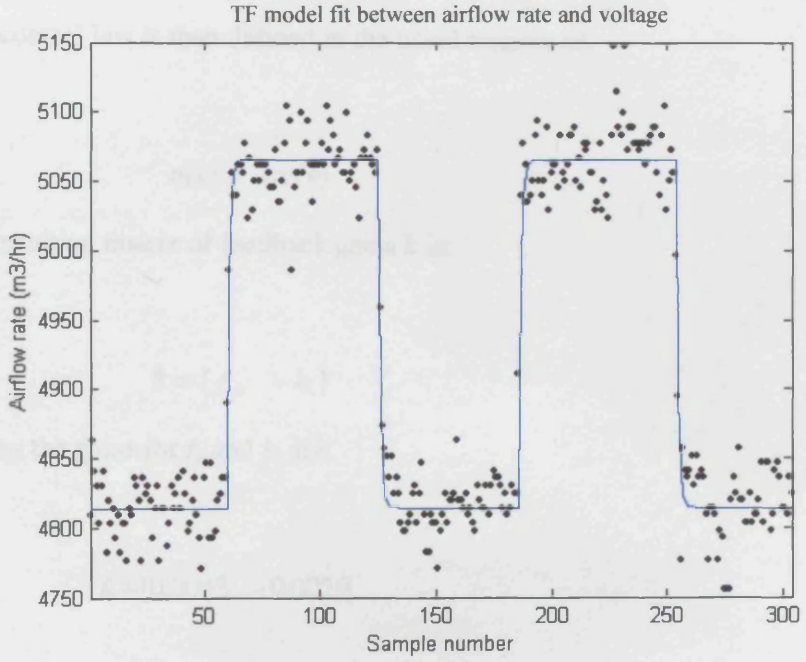

Figure 5.9: Ventilation rate and model fit of a typical experiment (50-55% voltage; YIC = -7.2145; R_T^2 = 0.9623; Model Order =[1, 1, 1]; see table 5.2)).

The state transition matrix $\boldsymbol{F}$, input vector $\boldsymbol{g}$, command input vector $\boldsymbol{d}$, and output vector $\boldsymbol{h}$ of the NMSS system for the control design based on parameters estimated in TF (5.12) above, are defined as before (5.4):

$$\boldsymbol{F} = \begin{bmatrix} 0.2939 & 0 \\ -0.2939 & 1 \end{bmatrix}$$

$$\boldsymbol{g} = \begin{bmatrix} 34.3279 & -34.3279 \end{bmatrix}^T \tag{5.13}$$

$$\boldsymbol{d} = [0 \quad 1]^T$$

$$\boldsymbol{h} = [1 \quad 0]$$

The PIP controller is manually tuned and the same LQ cost function weighting matrices $\boldsymbol{Q}$ and $\boldsymbol{r}$ are found to give optimal reference tracking:

$$\boldsymbol{Q} = \begin{bmatrix} 1 & 0 \\ 0 & 0.01 \end{bmatrix} \qquad \boldsymbol{r} = 1 \tag{5.14}$$

The SVF control law is then defined in the usual manner as,

$$u(k) = -\boldsymbol{k}\boldsymbol{x}(k) \tag{5.15}$$

And, the resulting matrix of feedback gains $\boldsymbol{k}$ is:

$$\boldsymbol{k} = [f_o \quad -k_I] \tag{5.16}$$

Substituting the gains for f_o and k_I are:

$$\boldsymbol{k} = [0.0083 \quad -0.0029] \tag{5.17}$$

Then, the incremental form obtained by substituting the f_o and k_I gains (5.8) into equation 5.9 is,

$$u(k) = u(k-1) + 0.0029\{y_d(k) - y(k)\} - 0.0083\{y(k) - y(k-1)\} \tag{5.18}$$

The next figure (5.10), demonstrates the benefit of designing a controller for the region it will operate over. It is clear from figure 5.10 that the control designed at an operating point of 5050m^3/hr (blue thick line) rapidly handles changes in set point; both on the rising and falling limb. By contrast, the tracking performance of the

controller designed at 3000m^3/hr (red line) is poor because the controller does not generate a large enough signal to the control actuator (i.e. voltage to the control fan). This is clear from the lower plot of figure 5.10 where the input voltage to the fan for the higher set point (5300m^3/hr) is insufficient; whereas for the lower set point (4800m^3/hr) the gains produce a slow response that does reach the desired level.

A further factor that makes the system more difficult to control at high ventilation rates is the fact (as discussed earlier) that the overall system is non-linear and at this airflow rate the system is at the top of the 's' curve; thus it is not so surprising that a control designed around a much lower operating point does not control the airflow optimally.

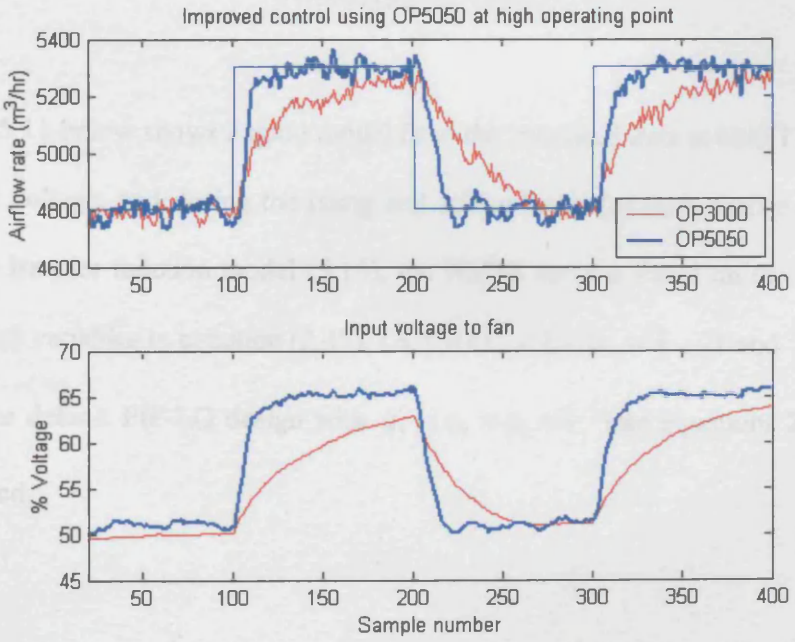

Figure 5.10: Comparison of two control designs controlling at high operating points.

5.2.5.2 LOW VENTILATION RATE CONTROL

The previous discussion has highlighted the problems that can occur at high ventilation rates; here, we direct the emphasis to low ventilation rate control, which as

will become apparent in this and subsequent chapters comes with its own set of difficulties. The following TF model was estimated and identified before being implemented on the Leuven ventilation chamber. The experiment in question models the 'bottom' end of the sigmoid curve in figure 5.3, i.e. from 11% to 15% voltage (very low airflow rates (400-1000m^3/hr). Further detailed modelling at low ventilation rates revealed slower dynamics than those found at higher ventilation rates; and a first order model with three time delays gave an improved fit. For control purposes this improved model was utilised. This results in the following first order TF model with three time delays [1 1 3]. Table 5.1 gives the results solely for first order models with a single time delay with a *YIC* value of -14.84 and R_T^2 of 0.9957,

$$y(k) = \frac{10.8543z^{-3}}{1-0.8323z^{-1}}u(k) \tag{5.19}$$

Figure 5.11 below shows a good model fit to the measured data at both 11% and 15% applied voltage; and during the rising and falling limbs for each change in set point. For the transfer function model (5.19), the NMSS form is based on the definition of four state variables in equation (2.40), i.e. [$y(k)$, $u(k-1)$, $u(k-2)$ and $z(k)$]. In this case, the default PIP-LQ design with $q_y = q_u = q_z = 1$ (see equations 2.33-2.35) is employed.

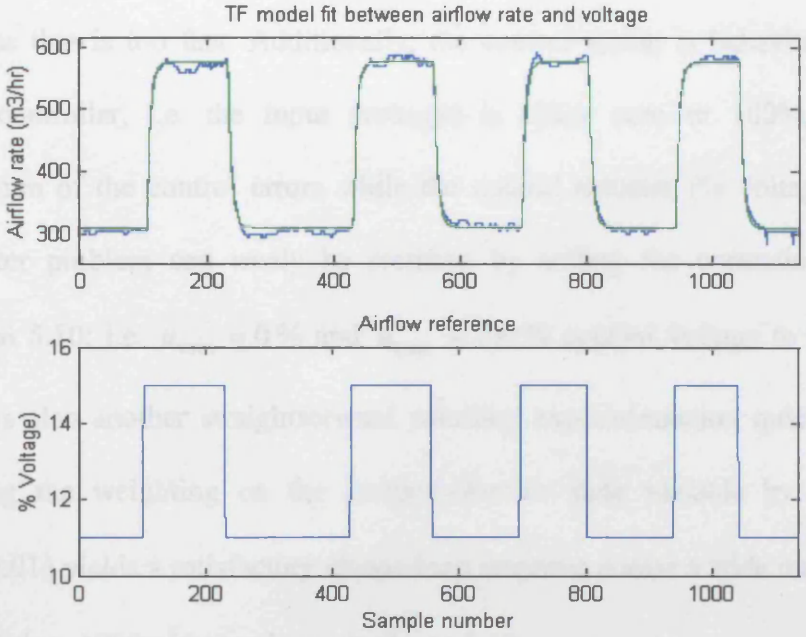

Figure 5.11: TF model fit between airflow rate and voltage (top plot) and airflow reference (lower plot).

In this case, due to the extra time delays the control gain vector is defined as follows,

$$\boldsymbol{k} = [f_0 \quad g_1 \quad g_2 \quad -k_I] \tag{5.20}$$

Substituting the gains for f_0, g_1, g_2 *and* k_I gives:

$$\boldsymbol{k} = [0.1398 \quad 1.4478 \quad 1.8247 \quad -0.0564] \tag{5.21}$$

while the incremental form obtained by substituting these gains into equation (5.15) is,

$$\begin{aligned} u(k) = u(k-1) &+ 0.0564\{y_d(k) - y(k)\} - 0.1398\{y(k) - y(k-1)\} \\ &-1.4478\{u(k-1) - u(k-2)\} - 1.8247\{u(k-2) - u(k-3)\} \end{aligned} \tag{5.22}$$

The above PIP design is then again implemented on the Leuven ventilation chamber, of which the initial result around a low operating point can be seen to be very

oscillatory. The LQ weightings of [1 1 1] have in this instance clearly produced a response that is too fast. Additionally, the control action is behaving like a 'bang-bang' controller, i.e. the input (voltage) is either zero or 100%, which allows integration of the control errors while the control actuator (% voltage) is saturated. The later problem can easily be rectified by adding the correction described by equation 5.10; i.e. $u_{\min} = 0\,\%$ and $u_{\max} = 100\,\%$ applied voltage to the control fan. There is also another straightforward solution: experimentation quickly reveals that reducing the weighting on the integral-of-error state variable by a factor of 10 ($q_z = 0.01$) yields a satisfactory closed loop response across a wide range of operating points below 1000m^3/hr as shown in figure 5.13.

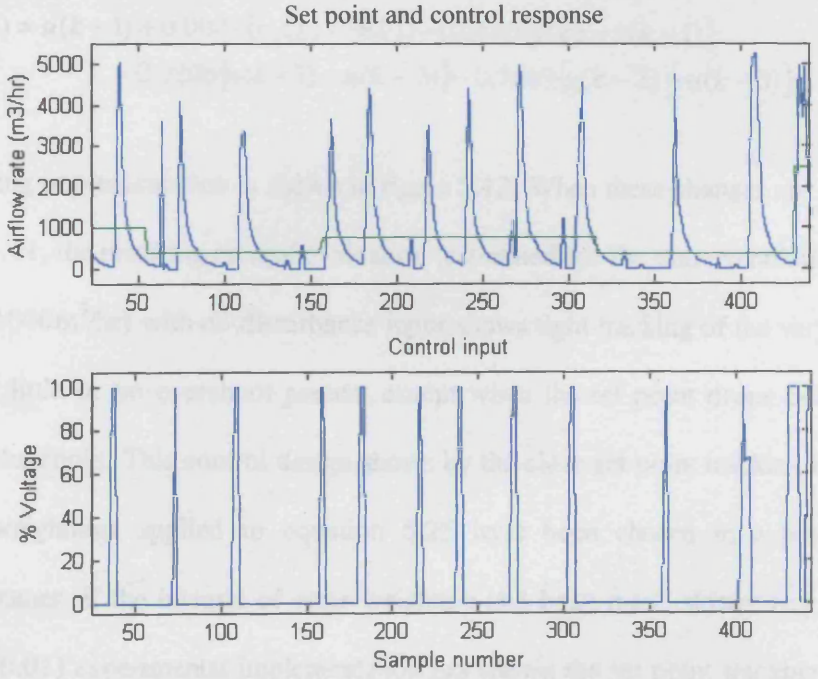

Figure 5.12: Initial fixed gain control (upper plot (showing reference airflow (green) and control response (blue)) of Leuven ventilation chamber with 'Bang-Bang' actuator behaviour (lower plot).

Thus, in figure 5.13 the diagonal weighting coefficients are $q_y = 1$; $q_u = 1$; *and* $q_z = 0.01$. And this yields a new control gain vector of,

$$\boldsymbol{k} = [f_o \quad g_1 \quad g_2 \quad -k_I] \tag{5.23}$$

And again, substituting the gains for f_0, g_1, g_2 *and* k_I gives:

$$\boldsymbol{k} = [0.0660 \quad 0.9206 \quad 0.8609 \quad -0.0087] \tag{5.24}$$

While the incremental form is again obtained by substituting these gains into equation 5.12,

$$\begin{aligned} u(k) = u(k-1) &+ 0.0087\{y_d(k) - y(k)\} - 0.0660\{y(k) - y(k-1)\} \\ &- 0.9206\{u(k-1) - u(k-2)\} - 0.8609\{u(k-2) - u(k-3)\} \end{aligned} \tag{5.25}$$

The resulting implementation is shown in figure 5.13. When these changes are applied to figure 5.11, the resulting control evaluation (estimated for the same ventilation rate, i.e. ~400-1000m^3/hr) with no disturbance input shows tight tracking of the varying set point with little or no overshoot present except when the set point drops below the 400m^3/hr threshold. This control design shows by the close set point tracking how the diagonal weightings applied to equation 5.25 have been chosen in a practically optimal manner. If the integral of error weighting had been made slower (e.g. 0.001 instead of 0.01) experimental implementation has shown the set point tracking would reach each new desired level eventually but it would take more than 100 time steps (200 seconds) for it to reach it.

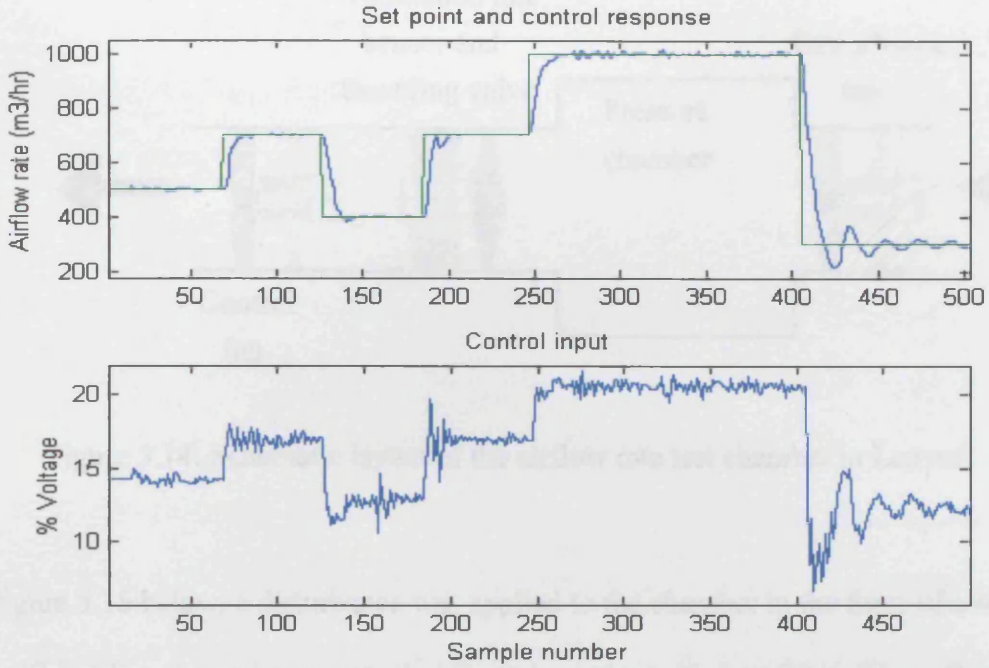

Figure 5.13: Fixed gain control (upper plot (showing reference airflow (green) and control response (blue)) of Leuven ventilation chamber and control input (lower plot)

5.2.5.3 DISTURBANCE REJECTION

The experimental implementations to date have not been subjected to any kind of disturbance. In order to further test the robustness of the control design, in this section and the following sections the control experiments described have been subjected to a random wind disturbance derived from real wind data (Silsoe, 1999).

The position of the disturbance fan can be seen in the simplified schematic layout of figure 3.2 and below in figure 5.14, the disturbance fan is positioned in the region of the air inlet.

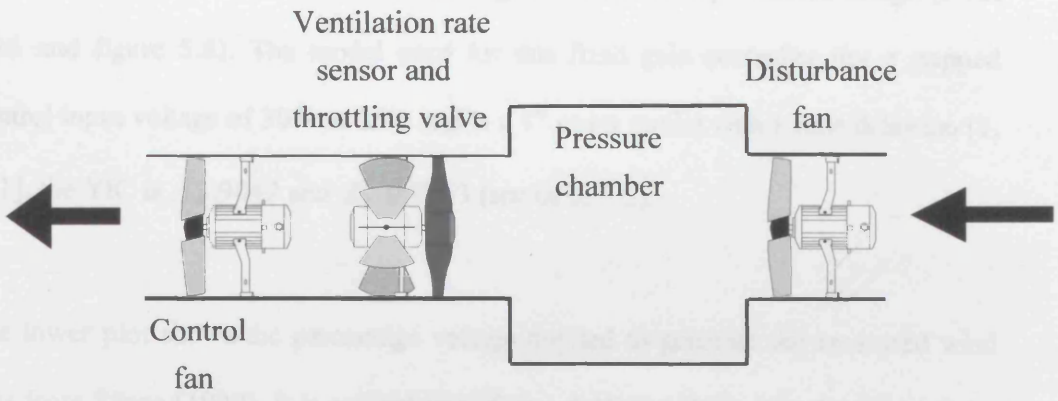

Figure 5.14: Schematic layout of the airflow rate test chamber in Leuven.

In figure 5.15 below, a disturbance was applied to the chamber in the form of a second fan. This 'disturbance' was actual collected wind speed data from Silsoe Research Laboratory that was converted into a digital signal by, (Vranken, 1999). The upper plot shows the magnitude of deviation from the set point of 3000m^3/ hr caused by the

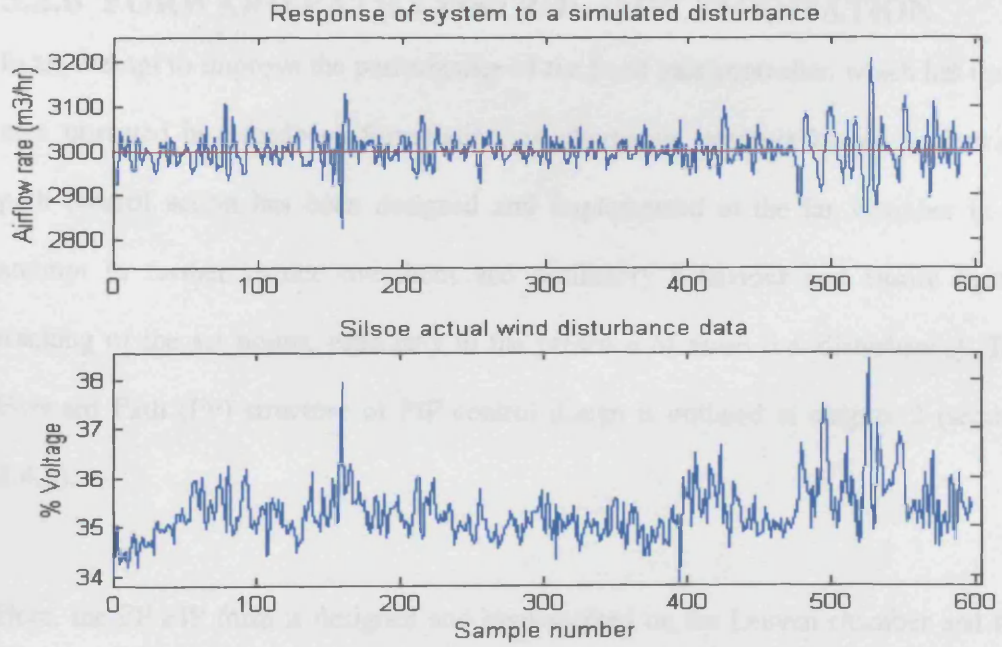

Figure 5.15: The top plot shows the set point at 3000m^3/hr (red) and the airflow tracking response (blue), while the lower plot is the Silsoe wind disturbance simulation data.

disturbance with the fixed gain control design from above implemented design (5.15; 5.16 and figure 5.8). The model used for this fixed gain controller has a stepped control input voltage of 30% to 35% and is a 1st order model with 1 time delay i.e. [1, 1, 1], the YIC is -13.9049 and R_T^2 0.9963 (see table 5.2).

The lower plot shows the percentage voltage applied to generate the measured wind data from Silsoe (1999). It is evident from figure 5.15 that the largest deviations from the set point occur during the highest wind gusts. This is not unexpected, however, the fixed gain controller works well in restricting these oscillations to a maximum of $\pm 200 m^3/hr$ from the highest set point during the highest gust of 50mph (38% applied voltage) and the controller quickly returns the ventilation rate to its desired level. This is well within 10% of the ventilation rate and the deviation from the set point is less than 3% for the majority of the duration of the experiment (1200 seconds).

5.2.6 FORWARD PATH CONTROL IMPLEMENTATION

In an attempt to improve the performance of the fixed gain controller, which has up to now operated in a feedback formulation, an alternative structure known as forward path control action has been designed and implemented in the fan chamber in an attempt to further reduce overshoot and oscillatory behaviour and ensure tighter tracking of the set points, especially in the presence of noise (i.e. disturbance). The Forward Path (FP) structure of PIP control design is outlined in chapter 2 (section 2.4.3).

Here, the FP PIP form is designed and implemented on the Leuven chamber and for comparison it is compared with the FB form. The implemented experiments are

summarised in table 5.2 below. The SRIV model based on a ventilation rate of 3000m^3/hr was used in the LQ control design for table 5.2 and figures 5.16 and 5.17 respectively.

The table of results (5.2) (below) shows the experiments used to determine differences between feedback and forward-path PIP control with two different LQ designs values over both a small and large ventilation rate range. In all experiments the Silsoe wind disturbance data was applied to further evaluate the robustness of the control designs, as in lower plot of figure 5.14.

Table 5.2: Results of FB and FP comparison experiments.

FB or FP Control	*Feed-back*	*Forward-path*
PIPOPT (erw,uw,xw) weighting values	(0.05; 1; 1)	(0.05; 1; 1)
Control gains	0.0072; 0.0028	0.0072; 0.0028
Model order	[1 1 1]	[1 1 1]
1500-4600m3/hr	Exp 30	Exp 29
2200-3000m3/hr	Exp 23	Exp 25
Disturbance fan	On	On
Vortex damper	Fully open	Fully open

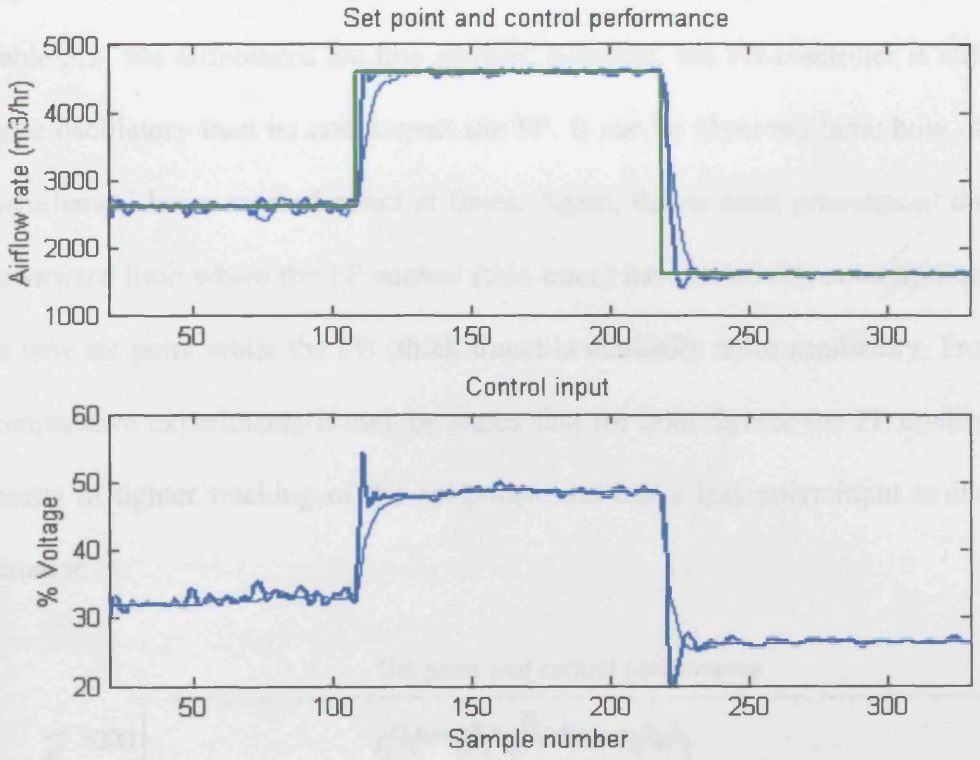

Figure 5.16: Comparison plot of feedback (thick trace; exp. 30) and forward path (thin trace; exp. 29) PIP control of ventilation chamber.

The step response in figure 5.16 shows how both the FB and FP designs handle a large step in ventilation rate (>3000m^3/hr). The FB design (thick trace) shows a fast response which is slightly oscillatory on the downward step, while the input to the control actuator (voltage) has a spike of ~6% voltage at each set point change. In contrast the FP control design has a slightly slower response that is smooth for both the rising and falling limb. Additionally, the actuator input is also smooth with no overshoot. Overall, the FP control response is smoother, especially when, as is the case here, a disturbance has been applied.

Figure 5.17 below, has a smaller 'step' (800m^3/hr) and the upper airflow level is lower (table 5.2) the differences are less marked; however, the FB controller is still a little more oscillatory than its counterpart the FP. It can be observed here, how the 'wind disturbance' has a marked effect at times. Again, this is most pronounced during the downward limb where the FP control (thin trace) has a relatively smooth transition to its new set point while the FB (thick trace) is markedly more oscillatory. From these comparative experiments it may be stated that for both figures the FP control design results in tighter tracking of the set points and has a less noisy input to its control actuator.

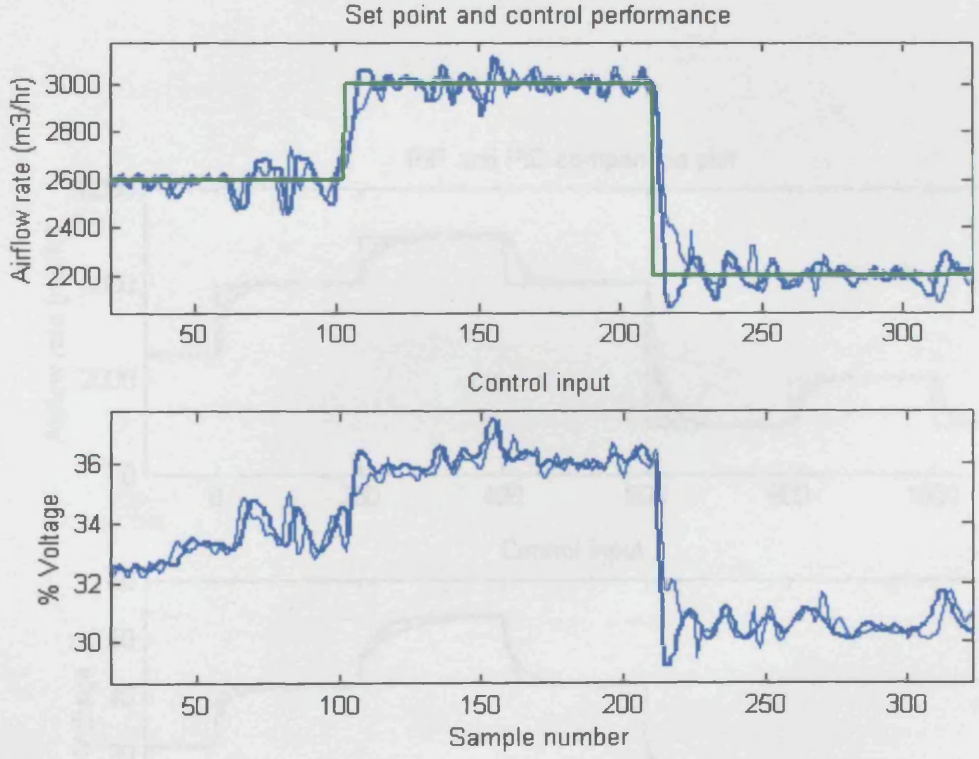

Figure 5.17: Comparison plot of feedback (thick trace; exp. 23) and forward path (thin trace; exp. 25) PIP control of ventilation chamber.

5.2.7 COMPARISON OF PIP WITH PID CONTROL

For comparison purposes, a conventional PID controller is designed for this system using the Ziegler-Nichols method (e.g. Kreider & Rabl, 1996) for tuning the PID

control parameters. The response is shown as the thin trace in figure 5.18. Here, the measured step response in figure 5.2 is employed to estimate the three PID control parameters, while the final algorithm is converted to a discrete-time form for implementation on the available digital computer system. In fact, the final algorithm proved rather sensitive to the discretisation method utilised in the analysis, with the simplest backward difference approximation yielding the most successful results illustrated in this section. Finally, the Ziegler-Nichols control parameters are further optimised by trial and error to improve the robustness of the algorithm over the range of operating points shown in figure 5.18. With no disturbances, the controlled ventilation rates for both the PIP and PID cases are similar.

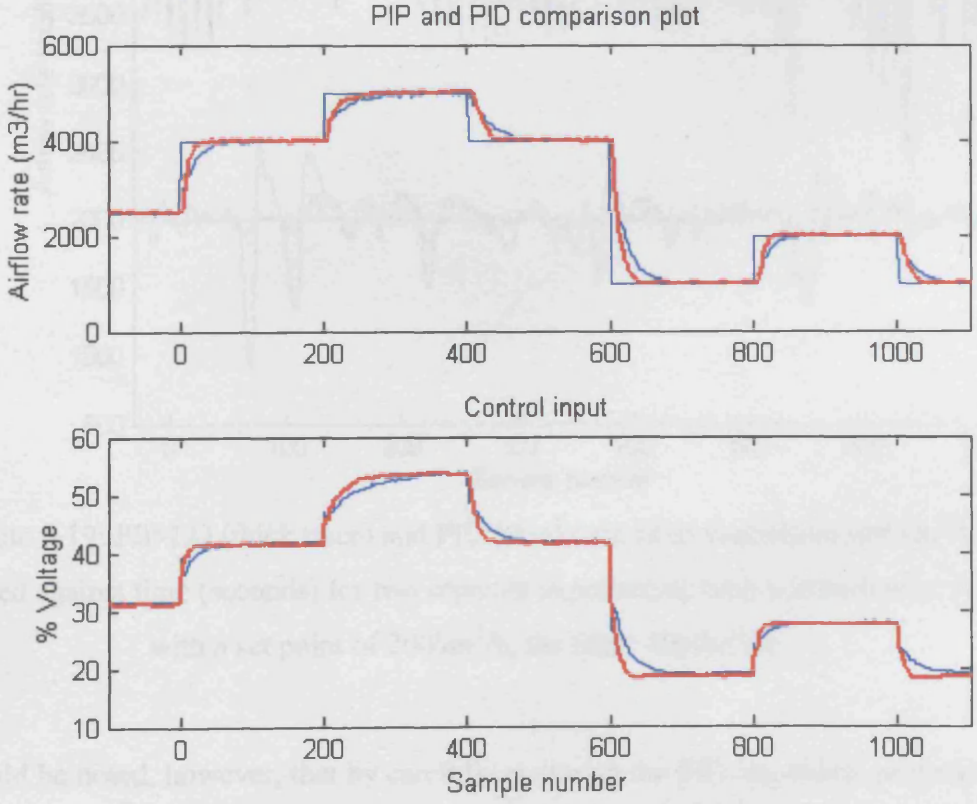

Figure 5.18: PIP-LQ (thick trace) and PID (thin) control of ventilation rate together with set point (top); control input (% bottom), all plotted against sample number (seconds).

When the ventilation rate set point is very close to the operating level for which the PIP and PID control systems are designed, i.e. 3000m^3/hr, then the response of the two control strategies is very similar. In fact, the PID disturbance response is almost indistinguishable from the PIP case shown in figure 5.18 and so is not plotted. However, at higher or lower ventilation rates the PIP design proves considerably more robust to these realistic wind disturbances, as illustrated in figure 5.19. In particular, at a ventilation rate of 4000m^3/hr, the PID design yields a highly oscillatory response.

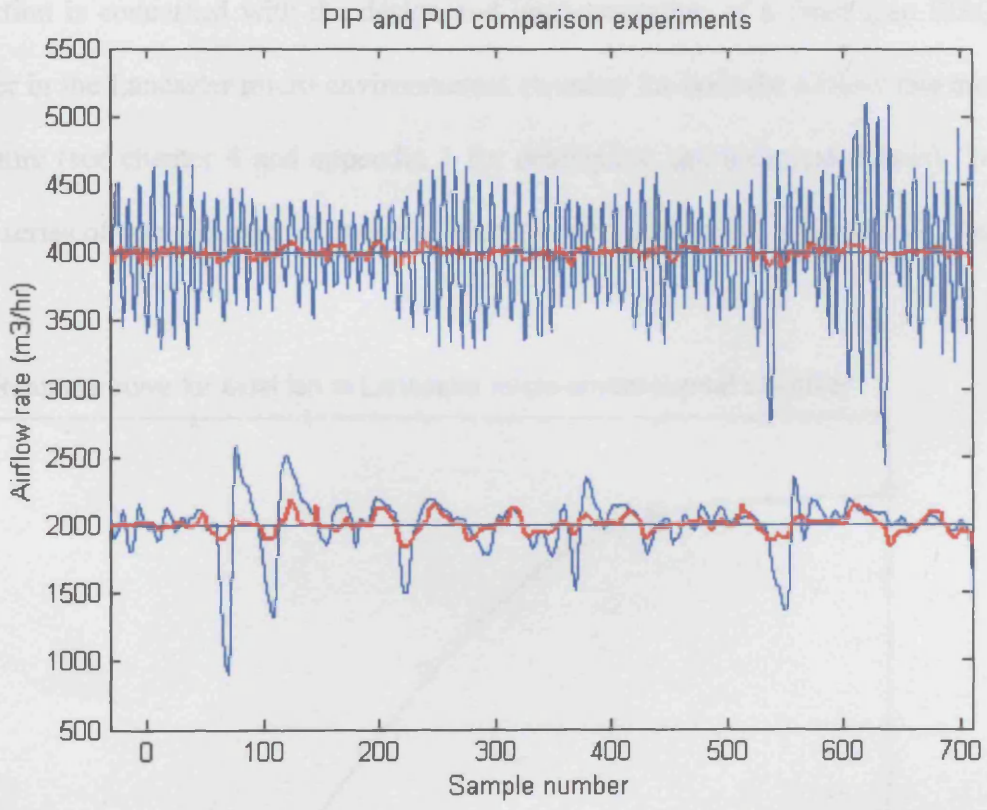

Figure 5.19: PIP-LQ (thick trace) and PID (thin) control of ventilation rate (m^3/h) plotted against time (seconds) for two separate experiments with a disturbance, one with a set point of 2000m^3/h, the other 4000m^3/hr.

It should be noted, however, that by carefully re-tuning the PID algorithm on the basis of numerous laboratory experiments, such as those shown in figures 5.18-5.19, an improved closed loop response can be obtained at both the higher and lower operating levels. However, while there are numerous approaches to automatically tuning such

PID control systems, the NMSS/PIP methodology seems particularly straightforward in the present application: the transfer function model is selected on the basis of one simple experiment (figure 5.2), while the PIP-LQ control gains are obtained after adjustment of just the integral-of-error weight. The final PIP design immediately performs well both with and without disturbances.

5.3 LANCASTER CHAMBER

This section is concerned with the design and implementation of a fixed gain SISO controller in the Lancaster micro-environmental chamber for both the airflow rate and temperature (see chapter 4 and appendix 1 for descriptive and technical details). To begin, a series of open-loop experiments to identify the steady state behaviour of the

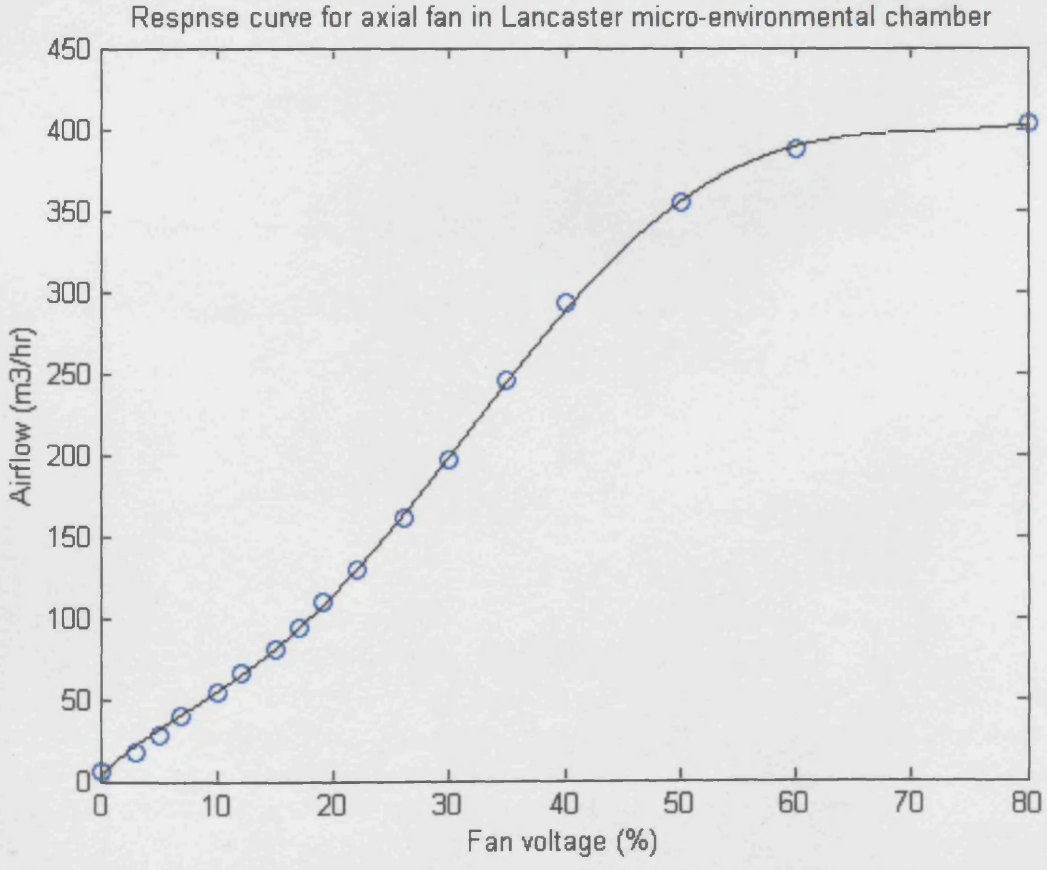

Figure 5.20: Response curve for Lancaster micro-environmental chamber.

chamber were carried out in the same way as those for Leuven chamber. These produced the following non-linear response curve (figure 5.20), (i.e. similar to the one in figure 5.3 for the Leuven chamber).

5.3.1 MODEL ESTIMATION

A series of SRIV models were identified at different operating points for the Lancaster chamber. Figure 5.21 shows a series of modelled data at step changes from 10-20% voltage through to 50-60% voltage (the voltage is measured in the same way as in Leuven, i.e. potential % voltage). It should be noted that the airflow rate measurable in this smaller chamber ($4m^3$ cf. Leuven, ($22m^3$)) is considerably lower and has a range of ~10 to $450m^3/hr$, this is approximately an order of magnitude lower than that measurable in Leuven.

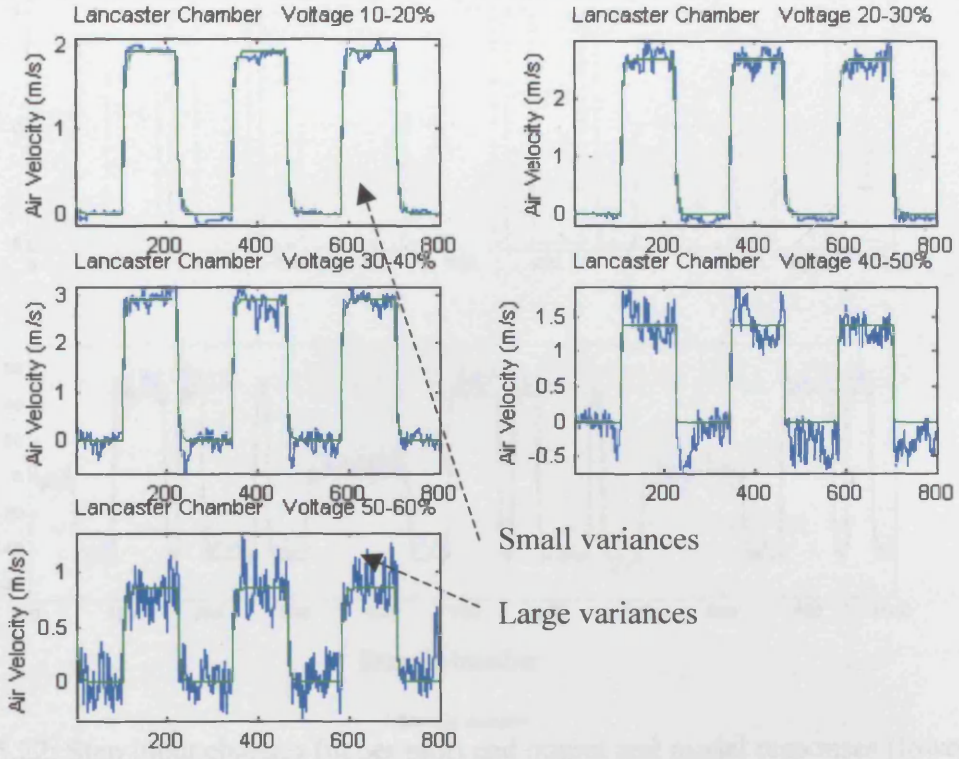

Figure 5.21: The plots shows modelling results of airflow rate (blue) against desired output (green) for 5 different step inputs (10-20% to 50-60%). Also, there is distinct evidence of hetero-scedastic noise present (see text above).

The following first order TF model with two time delays (5.22) was estimated and identified using the SRIV algorithm with a *YIC* of –10.5498 and an R_T^2 of 0.9717;

$$y(k) = \frac{4.5262\ z^{-2}}{1 - 0.5067\ z^{-1}} u(k) \tag{5.22}$$

The model fit is shown in figure (5.22) below (lower plot) where again the hetero-scedastic noise is present. The upper plot shows the random stepping sequence chosen which highlights how well the first order TF model fits the data.

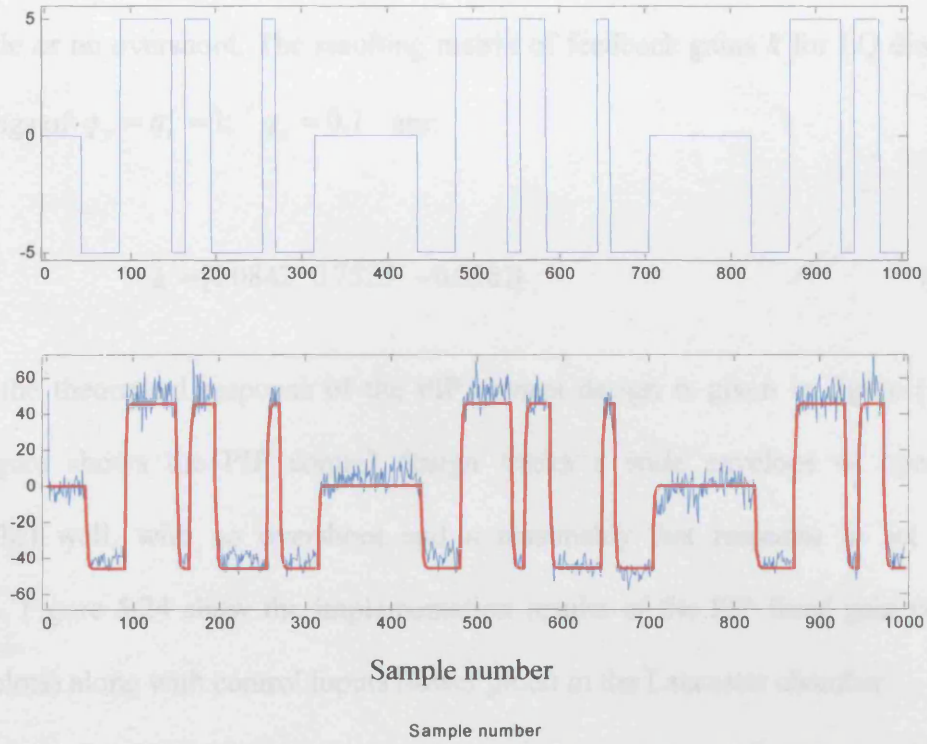

Figure 5.22: Step input changes (upper plot) and output and model responses (lower plot).

5.3.2 CONTROL DESIGN

The fixed gain control design follows the same process as outlined in section (5.6) of this chapter; where, the state transition matrix $\boldsymbol{F}$, input vector $\boldsymbol{g}$, command input vector $\boldsymbol{d}$, and output vector $\boldsymbol{h}$ of the NMSS system for the control design are defined as follows:

$$\boldsymbol{F} = \begin{bmatrix} 0.5067 & 4.5262 & 0 \\ 0 & 0 & 0 \\ -0.5067 & -4.5262 & 0 \end{bmatrix}$$

$$\boldsymbol{g} = \begin{bmatrix} 0 & 1 & 0 \end{bmatrix}^T \tag{5.25}$$

$$\boldsymbol{d} = \begin{bmatrix} 0 & 0 & 1 \end{bmatrix}^T$$

$$\boldsymbol{h} = \begin{bmatrix} 1 & 0 & 0 \end{bmatrix}$$

The PIP-LQ control weightings are manually tuned in order to obtain a rapid response with little or no overshoot. The resulting matrix of feedback gains $\boldsymbol{k}$ for LQ diagonal weightings of $q_y = q_u = 1; \quad q_z = 0.1$ are:

$$\boldsymbol{k} = [0.0842 \quad 0.7525 \quad -0.0581] \tag{5.26}$$

Firstly, the theoretical response of the PIP control design is given in figure (5.23). This figure shows the PIP control design tracks a wide envelope of operation (200m^3/hr) well, with no overshoot and a reasonably fast response to set point changes. Figure 5.24 show the implementation results of the PIP fixed gain control (upper plots) along with control inputs (lower plots) in the Lancaster chamber.

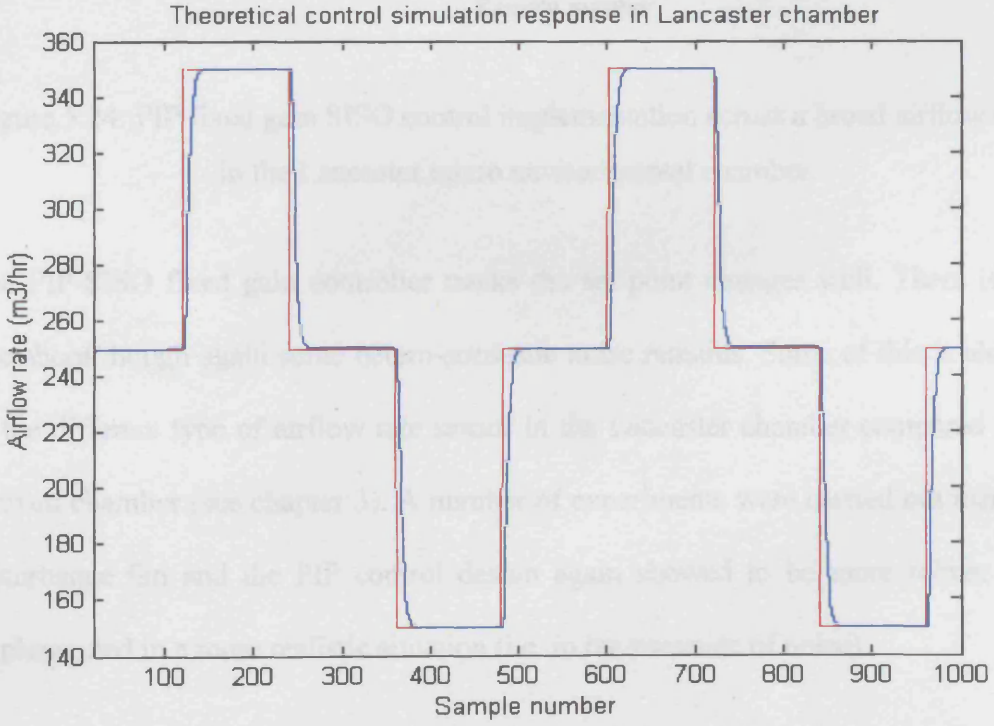

Figure 5.23: Theoretical simulation response of PIP control design in Lancaster micro environmental chamber.

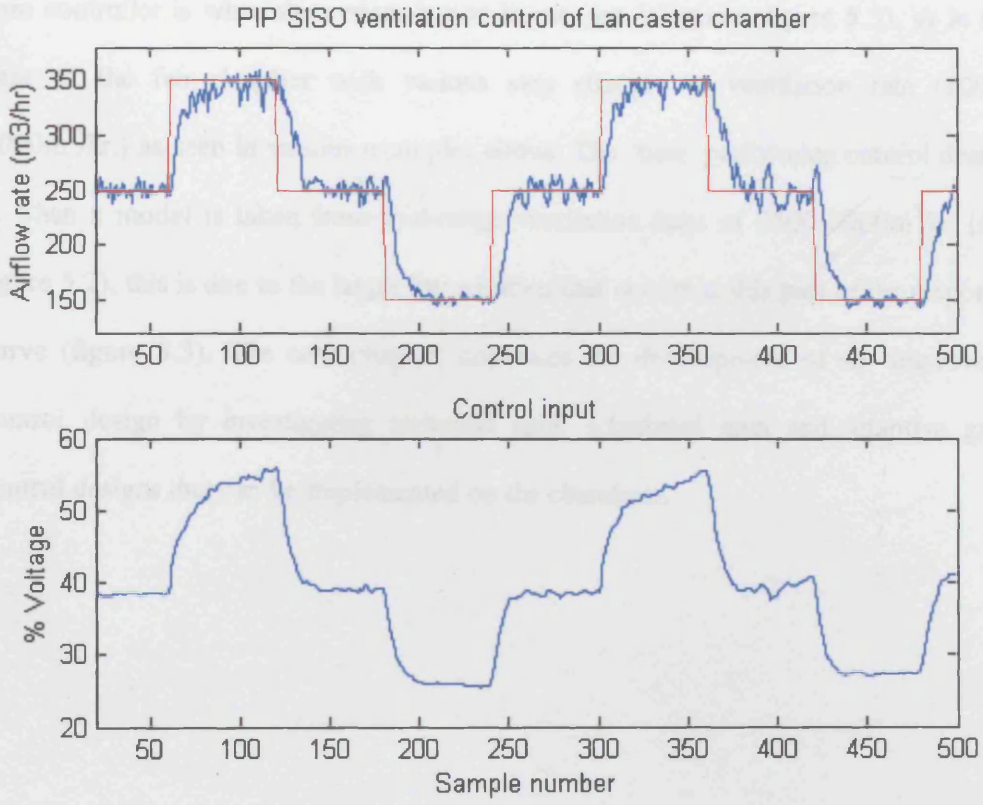

Figure 5.24: PIP fixed gain SISO control implementation across a broad airflow range in the Lancaster micro environmental chamber.

The PIP-SISO fixed gain controller tracks the set point changes well. There is little overshoot though again some hetero-scedastic noise remains. Some of this is also due to the different type of airflow rate sensor in the Lancaster chamber compared to the Leuven chamber (see chapter 3). A number of experiments were carried out using the disturbance fan and the PIP control design again showed to be more robust when implemented in a more realistic situation (i.e. in the presence of noise).

5.4 CONCLUSIONS

The fixed gain controller has shown to have both advantages and disadvantages. The main advantages include straightforward implementation and a closed loop system

that is linear, and thus simpler to analyse. While the major disadvantage of a fixed gain controller is when the system is non-linear (see 's' curve; figure 5.3), as in the case of the fan chamber with various step changes in ventilation rate (1000-5000m^3/hr.) as seen in various examples above. The 'best' performing control design is when a model is taken from mid-range ventilation rates of 2500-3000m^3/hr (see figure 5.2), this is due to the larger linearisation that occurs at this part of the response curve (figure 5.3). The next chapter, continues the development of an 'improved' control design by investigating switched gain, scheduled gain and adaptive gain control designs that can be implemented on the chambers.

Chapter 6

SCHEDULED AND ADAPTIVE PIP CONTROL

6.1 INTRODUCTION

This chapter expands on the relatively straightforward fixed gain control design described in the previous chapter, into more advanced control design techniques that can handle the non-linear behaviour of the chambers more readily than the fixed gain controller. Firstly, the *scheduled gain* PIP control design is shown, followed by the

implementation of an adaptive gain control design; and finally, a simulation comparison between fixed gain, scheduled gain and adaptive gain control is presented.

6.2 SCHEDULED GAIN CONTROL

Gain scheduling is a popular approach to nonlinear control design and has been widely and successfully applied in fields ranging from vehicle speed control, aerospace flight control to process control (e.g. Johansen *et al.*, 1998; Sharmma and Athans, 1992; Åström and Wittenmark, 1990). Although a wide variety of control methods are often described as "gain-scheduling" approaches, these are usually linked by a 'divide and conquer' type of design procedure whereby the nonlinear control design task is decomposed into a number of linear sub-problems. This 'divide and conquer' approach is the source of much of the popularity of gain scheduling methods since it enables well established linear design methods to be applied to nonlinear problems (Leith, D.J., Leithead, W.E., 1998). Consequently the common method of gain scheduling is to derive a finite set of linear time-invariant controllers, which when constructed form a non-linear controller with a suitable interpolation method between each linear controller.

The systems under study (Lancaster and Leuven chambers) are non-linear over their whole operating envelopes. Thus, in order to design a controller suitable for use over the full operating range, a linearised representation of the system is required. For example, the response for the ventilation test chamber in Leuven is shown below (figure 6.1A). It is evident, as discussed in previous chapters that the response is non-linear, however, close inspection of the plot reveals that a series of linear or near-linear representation can be found by taking a series of small steps to encompass the

whole operating range. Thus, a piece-wise linear representation of the whole system can be made (figure 6.1B). Due to the fact the afore mentioned system can be approximated by a series of linear representations (piece-wise linear representation), (figure 6.1B below), the analysis in this chapter will concentrate on linearised discrete-time transfer function (TF) models across the operating envelope.

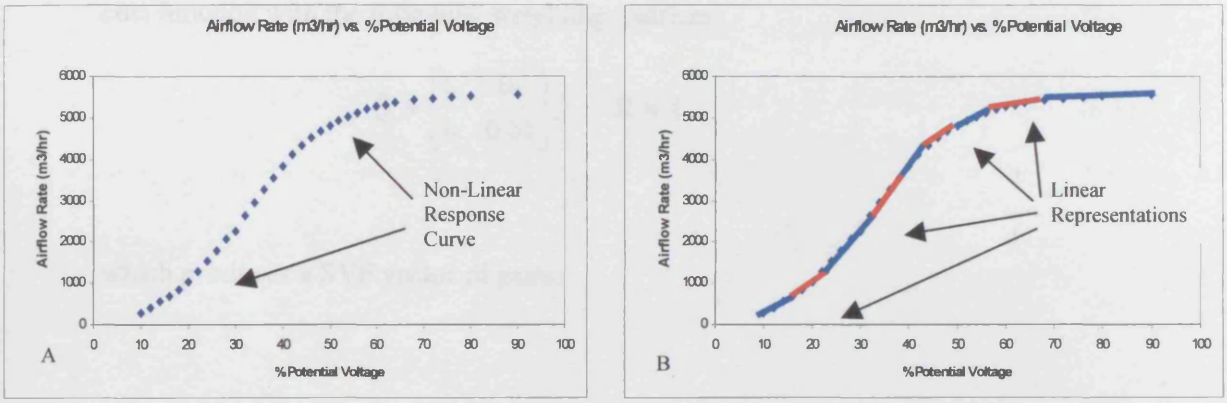

Figure 6.1: Characteristics of airflow rate with increasing % voltage input to ventilation test chamber. (a) Non-linear (sigmoid) response curve. (b) Piece-wise linear representation.

It is evident from the previous chapter that although the fixed gain controller can control the airflow well around the operating point it is designed for, above and below this level the set point tracking often tends to deteriorate. Thus, it was found the best way to control the airflow rate around a local operating point was to collect data around that operating point (step experiment), estimate a suitable model and calculate control gains based on the model parameters; then finally the control gains derived would be implemented on the chamber. In order to improve on this a series of models and control designs can be evaluated and the value of the operating point to be 'tracked' determines which set of control gains is selected (see table 6.1).

6.2.1 MODELLING AND CONTROL DESIGN

As a result of SRIV modelling, a series of first order models with a single time delay were estimated and the LQ-control design applied to the model parameters; this gave the following proportional and integral control gains (shown graphically in figure 6.2 against operating voltage, with the values listed in table 6.1) optimised using an LQ cost function with the following weighting matrices:

$$\boldsymbol{Q} = \begin{bmatrix} 1 & 0 \\ 0 & 0.01 \end{bmatrix}, \qquad R = 1 \tag{6.1}$$

which produces a SVF vector of gains:

$$\boldsymbol{k} = [f_o \quad -k_1] \tag{6.2}$$

These gains were then calculated at each operating point in figures 6.2 and 6.3. In this example the same LQ weighting matrices have been applied for each operating point. However, if different weighting matrices are applied for each operating point over the whole operating envelope there may be a risk of experiencing 'jumps' in the gain schedule. It is not uncommon to experience closed-loop instability if there are relatively large changes in the gains over small changes in the scheduling variable. In such situations, the scheduling variable may require higher-order linear, or possibly even non-linear interpolation functions. In order to reduce the probability of this scenario, Leith and Leithead, (1998) maintain that the scheduling variable should change slowly.

Consequently, for a particular airflow rate, the corresponding set of proportional and integral gains are implemented from a look-up table (table 6.1); this may be as little as 3 or the full range depending on the application. Closer inspection of figure 6.2 shows how the proportional gain in the upper plot vary more than the integral gains when moving from a low applied voltage (11-15%) through to a high value (80-85%). In fact, the values at the extreme ends of both f_o and k_I are similar; with the values dropping towards the mid-airflow range (35-45%). The region with lower gain values corresponds to the region where the greatest change in airflow rate occurs for each percentage change in voltage (see figure 5.1), while the greatest change is where the system displays the greatest non-linearity.

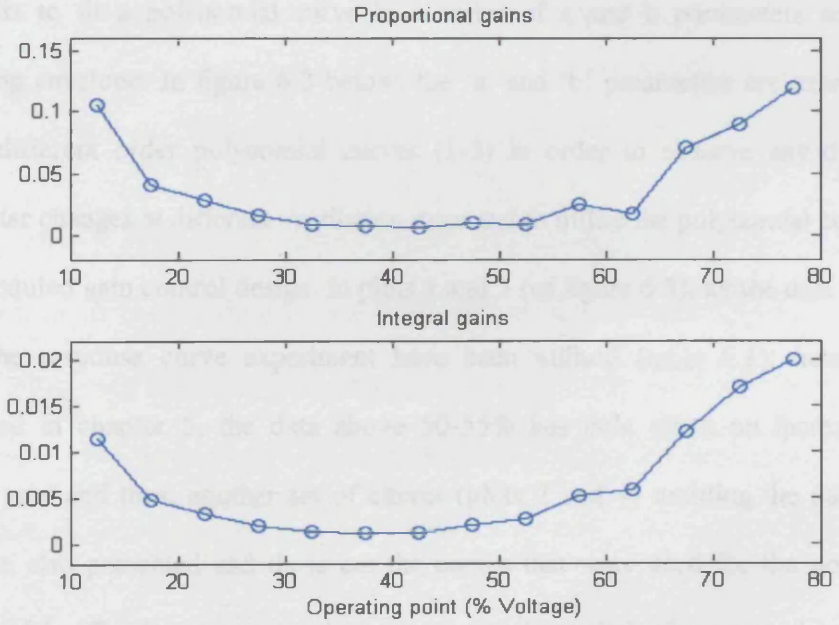

Figure 6.2: Proportional and integral schedule gains obtained from PIP-LQ control design at each operating point (10-80% voltage).

Table 6.1: Controller gains at each operating point.

Airflow rate (m^3/hr)	Operating Voltage (%)	Proportional Gain (f_o)	Integral Gain (k_I)	Model Order	PIP-LQ weights
0-500	11 to 15	0.10622	0.01154	[1 1 1]*	[1 0.01]
1000	15 to 20	0.04005	0.00480	[1 1 1]	[1 0.01]
1500	20 to 25	0.02774	0.00336	[1 1 1]	[1 0.01]
2250	25 to 30	0.01506	0.00213	[1 1 1]	[1 0.01]
3000	30 to 35	0.00850	0.00144	[1 1 1]	[1 0.01]
3850	35 to 40	0.00631	0.00125	[1 1 1]	[1 0.01]
4400	40 to 45	0.00510	0.00128	[1 1 1]	[1 0.01]
4800	45 to 50	0.00913	0.00205	[1 1 1]	[1 0.01]
5100	50 to 55	0.00855	0.00277	[1 1 1]	[1 0.01]
5250	55 to 60	0.02432	0.00523	[1 1 1]	[1 0.01]
5350	60 to 65	0.01719	0.00578	[1 1 1]	[1 0.01]
5450	65 to 70	0.07069	0.01209	[1 1 1]	[1 0.01]
5500	70 to 75	0.08896	0.01695	[1 1 1]	[1 0.01]
5550	75 to 80	0.11905	0.01987	[1 1 1]	[1 0.01]
5575	80 to 85	0.88527	0.08342	[1 1 1]	[1 0.01]

Another method of identifying a suitable lookup table for scheduled gain control design is to fit a polynomial curve to a series of a and b parameters across the operating envelope. In figure 6.3 below, the 'a' and 'b' parameters are examined by fitting different order polynomial curves (1-3) in order to observe any dynamical parameter changes at different ventilation rates and to utilise the polynomial curve in the scheduled gain control design. In plots 1 and 3 (of figure 6.3), all the data gathered from the response curve experiment have been utilised (table 5.1); however, as discussed in chapter 5, the data above 50-55% has little effect on increasing the airflow rate and thus, another set of curves (plots 2 and 4) omitting the data above 55% are also presented and these are the curves that were used for the polynomial lookup table. The 'a' parameter shows an almost linear behaviour over the specified ventilation range, while the 'b' parameters increase up to a peak (35-40%) before dropping away in a uniform manner.

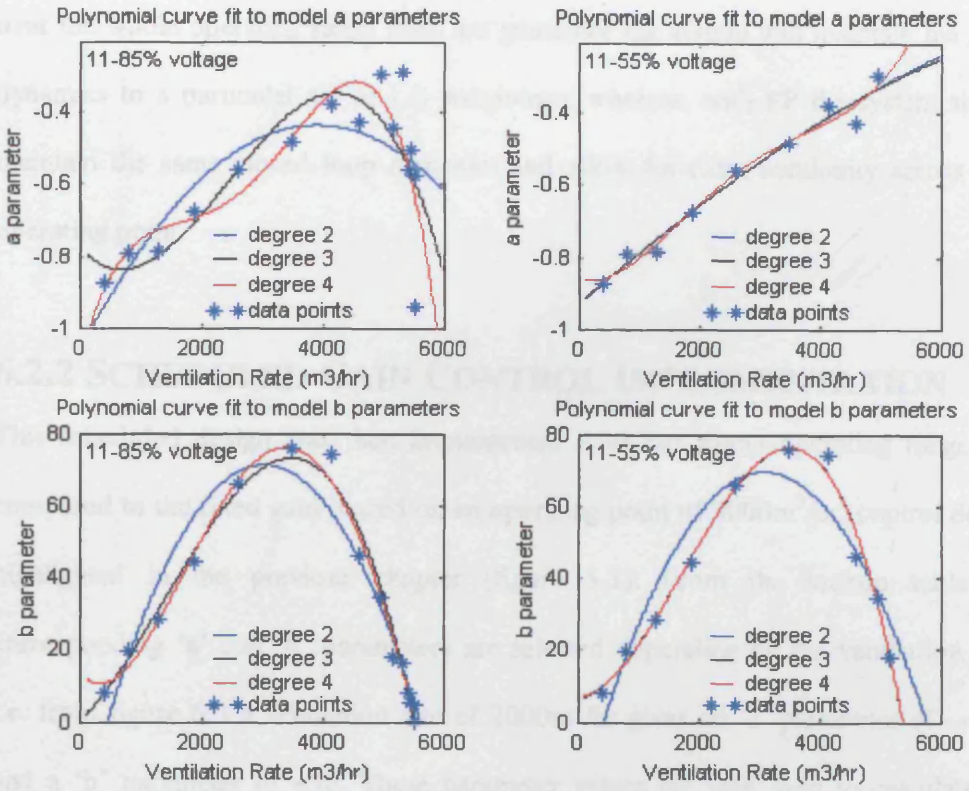

Figure 6.3: Polynomial curve fit for 'a' and 'b' parameters associated with ventilation chamber 's' (sigmoid) curve for two different voltage ranges.

The peak in the 'b' parameters (as described in chapter 5) is due to the area of the curve where there is the greatest rate of change of airflow rate for each percentage change in PV. From figure 6.3, the best polynomial fit of the lowest order is a first order for the 'a' parameters and a third order for the 'b' parameters. These polynomial fits were then chosen for scheduled gain control purposes in the rest of this chapter.

The scheduled PIP control was designed for use with a continuous lookup table based on the 'a' (denominator) and 'b' (numerator) values from the polynomial fit described above. The PIP control design utilises pole placement design (see chapter 2), with poles optimised at 0.7 and 0.8 after experimental analysis. Pole placement (PP) design

* A [1 1 3] model was found to give a better fit (see low ventilation rate control, chapter 5)

was chosen over the LQ design in this instance, because selecting the same LQ design over the whole operating range does not guarantee the system will maintain the same dynamics to a particular set of LQ weightings; whereas, with PP the system should maintain the same closed loop dynamics and allow for extra continuity across each operating point.

6.2.2 SCHEDULED GAIN CONTROL IMPLEMENTATION

This scheduled design was then implemented over the whole operating range and compared to the fixed gain (based on an operating point of 3000m^3/hr) control design highlighted in the previous chapter (figure 5.7). From the lookup table the corresponding 'a' and 'b' parameters are selected depending on the ventilation rate, i.e. from figure 6.3 a ventilation rate of 2000m^3/hr gives an 'a' parameter of ~-0.68 and a 'b' parameter of ~50. These parameter values are then used to calculate the control gains on line, which are subsequently implemented on the ventilation system.

The implementation of the scheduled gain control compared to the above mentioned fixed gain controller is shown in figure 6.4, below. While the fixed gain control exhibits a slow response at high ventilation rates (see also figure 5.8), the scheduled gain controller set point tracking with this method shows a faster response, except that it has a tendency to both over and under shoot at certain set point changes and is clearly unsuitable to step changes in set point values. This can be attributed to the fact that as a change in desired level occurs, the airflow rate quickly tries to change to this new level.

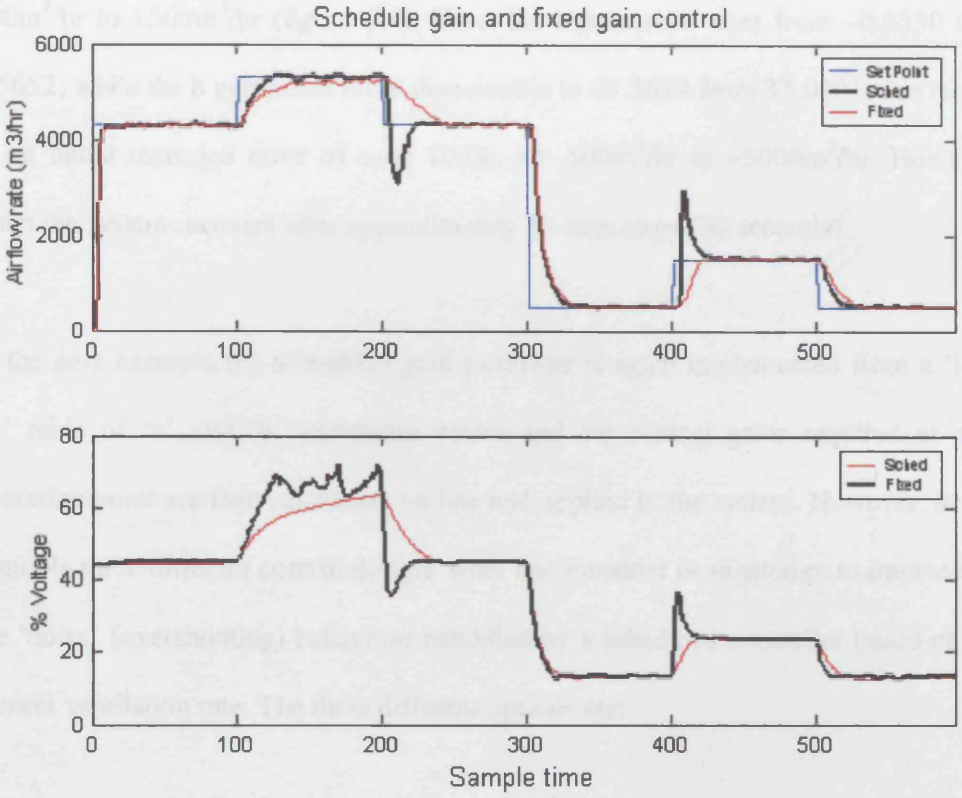

Figure 6.4: Fixed gain control designed at (OP=3000) and scheduled gain controller over wide operating envelope. Control over 1000-5000m^3/hr operating points. In the upper plot the black (scheduled gain) and red (fixed gain) lines are the reference tracking and the blue the set point level. The lower plot shows the % voltage input to the main fan.

Additionally, where the airflow rate has dropped (5300m^3/hr – 4300m^3/hr) the a and b parameters initially read off the polynomial curve (lookup table) are lower and higher respectively, than they should be when compared to the values adjacent to the reference level (a, -0.4064 to –0.551); (b, 63.6500 to 74.2685). This results in the obvious calculation of control gains that are unsuitable for tight reference tracking at that particular point and the measured airflow has a large error compared to the desired (1000m^3/hr). Nonetheless, it can be seen after around 15 time steps (30 seconds) the system recovers and resumes close reference tracking.

A further example of this overshoot is observed when the system steps up from 500m^3/hr to 1500m^3/hr (figure 6.4). Here, the a parameter rises from –0.8530 to –5.5652; while the b parameter more than double to 69.3699 from 33.0201; this results in an initial recorded error of over 100%, i.e. 500m^3/hr to ~3000m^3/hr. However, again the system recovers after approximately 20 time steps (40 seconds).

In the next example the scheduled gain controller is again implemented from a 'look up' table of 'a' and 'b' parameter values and the control gains required at each operating point are then calculated on-line and applied to the system. However, in this example three different control designs were implemented in an attempt to improve on the 'noisy' (overshooting) behaviour exhibited by a scheduled controller based on the current ventilation rate. The three different options are:

i) the operating point is a function of the set point (reference level) (op = ref);

ii) the operating point is a function of ventilation rate as used in figure 6.4 (op = vent), and ;

iii) the operating point is at the mid point between the current ventilation rate and the current operating point (op = vent+(ref-vent) / 2).

Figure 6.5, below shows how well each control design tracks the changing set points. Additional to the set point tracking, the lower two plots indicate what the value of each 'a' and 'b' parameter are at each set point for the above three control strategies. The first option, where the operating point is a function of the set point shows good control at 4300m^3/hr; and when it steps up a 1000m^3/hr to 5300m^3/hr it still manages

to reach the set point, albeit after >50 time steps when it is >100m^3/hr over the desired level. The set point tracking is fairly slow when stepping back down to 4300m^3/hr, but nonetheless gives tight tracking once it is reached.

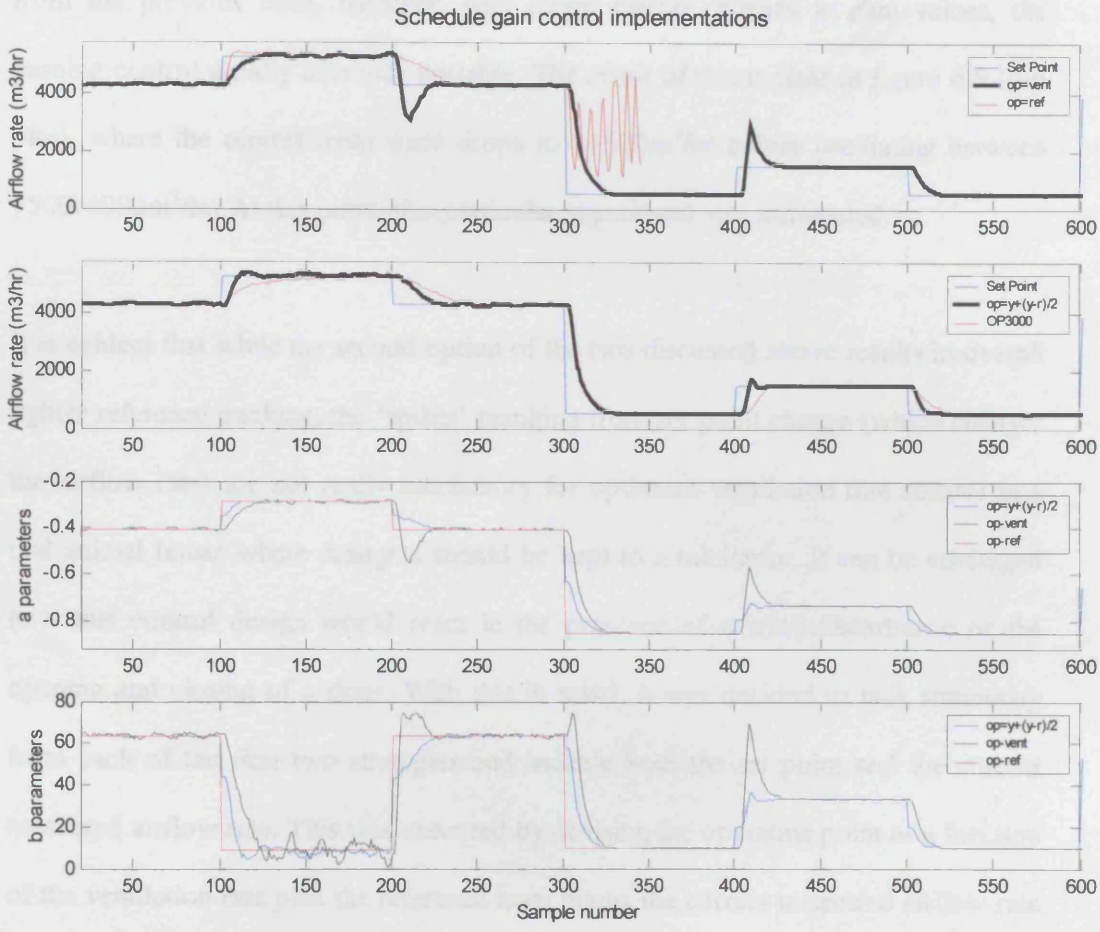

Figure 6.5: Comparison of three different types of scheduled gain control design: the two upper plots show 3 different scheduled gain control design implementations; while the lower plots show the varying nature of the a and b parameters to step changes by each control design. The legend explains which trace belongs to each controller.

However, this control strategy breaks down when asked to make a large step on the downward limb (4300-500m^3/hr); because the control design is based on 'a' and 'b' parameters at the current set point, it is clear from the lower plots of figure 6.5 that the denominator and numerator cannot deviate from the value read off from figure 6.3 and

thus, when the set point changes the parameter value changes to a new value instantly; and in the same instant a new set of control gains are calculated which are immediately implemented on the system. With small steps up to ~1000m^3/hr the resulting control is reasonable because the new control gains will not be too different from the previous ones, however, with larger instant changes in gain values, the ensuing control rapidly becomes unstable. The result of this is clear in figure 6.5 (top plot), where the op=ref (red) trace drops to ~1500m^3/hr before oscillating between 1500-4000m^3/hr. At this point, this particular experiment was terminated.

It is evident that while the second option of the two discussed above results in overall tighter reference tracking, the 'spikes' resulting from set point change (which changes the airflow rate) are not really satisfactory for optimum ventilation rate control in a real animal house where draughts should be kept to a minimum. It can be envisaged how this control design would react in the presence of a wind disturbance or the opening and closing of a door. With this in mind, it was decided to tack something from each of the first two strategies and include both the set point and the current measured airflow rate. This was executed by devising the operating point as a function of the ventilation rate plus the reference level minus the current measured airflow rate divided by two. This results in a taking values of a and b in-between the two previous methods.

This third method, described in the last paragraph and in figure 6.5 above gives good control over the whole operating envelope. Here, because the control design takes into account both the current ventilation rate and the set point, the a and b parameters read off from the polynomial plot (lookup table) will always be within reasonable

bounds; i.e. it cannot ever exceed halfway between the measured airflow and reference level. The (Op = vent + (ref-vent) /2) final scheduled gain method presented (figure 6.5) displays tight reference tracking to the changing set points and in the second plot is compared to the fixed gain control design for reference. Both a and b parameter values change smoothly between steps, with little or no over and undershoot present.

The scheduled gain controller has shown at both the higher and lower levels to give a faster and less noisy response than the fixed gain controller designed at a single operating point. Effectively, this result is a sophisticated combination of the mid, high and low control designs described in the last chapter. Another more straightforward way of achieving similar results to figure 6.5 would be to use a switched gain control design, where, say, three or more fixed gain controllers are designed as in chapter 5 for a range of set points. Then, it is simply a case of the controller switching between different sets of control gains depending on where the current desired level is required. A more advanced form of this type of control is described in the next chapter (7) (see three operating point controller).

6.3 ADAPTIVE CONTROL

The last section showed that a scheduled gain control design can maintain reference tracking to a measurable degree of accuracy over a broad range of ventilation rates. In this section, a further method of controlling the airflow is presented, namely: adaptive control. This control design is similar to the scheduled gain controller with a lookup table, except here the lookup table is replaced by a recursive algorithm which updates the a and b parameters using Recursive Least Squares (RLS) (Young, 1984).

Here, the parameters are estimated recursively on line, using the recursive least squares (RLS) algorithm of Young (1984). From the parameter estimates, the control gains are calculated and applied in an attempt to control the system. The P matrix is given an initial Noise Variance Ratio (NVR) value of 100 to 'kick' start the system. Early results indicate a rapid convergence after 2 or 3 time steps, this has the result of very little parameter change in both 'a' and 'b' parameters compared to what is expected from modelling results of open-loop experiments across the whole operating envelope. The 'a' parameters are converging rapidly to ~-0.8 and then, at subsequent step changes to the desired set-point; a small 'blip' occurs in the parameter value before it continues at ~-0.8, irrespective of the step change, magnitude or direction.

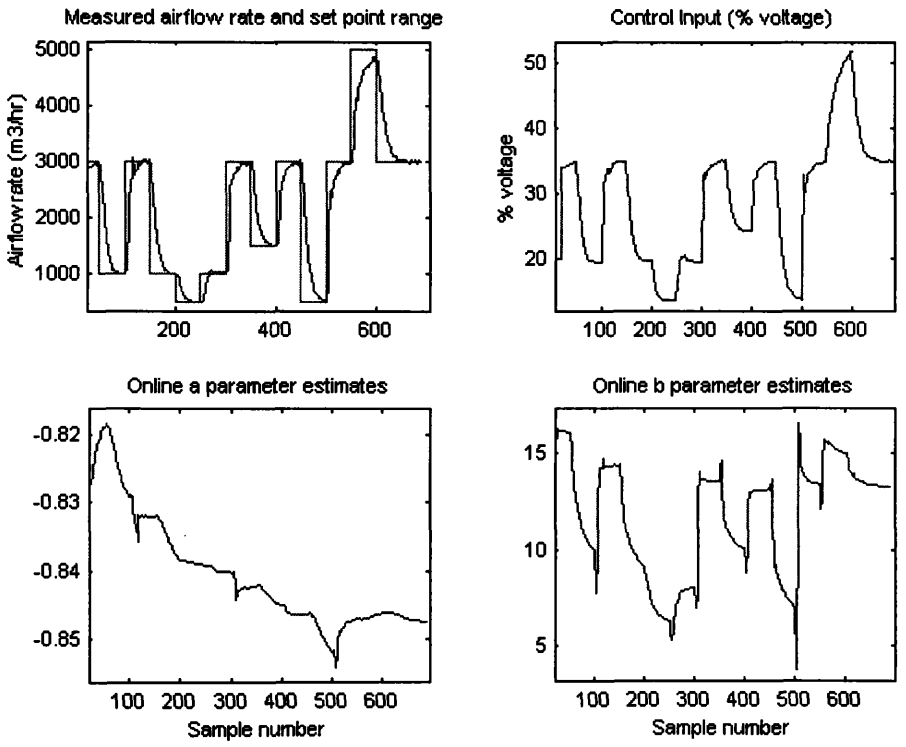

Figure 6.6: Implementation of adaptive controller on Leuven ventilation chamber. The a and b parameters are the online estimates from the RLS algorithm (Young, 1984).

The NVR was set to different values to come on at set-point changes, and while momentarily the P matrix was 'excited', it would still rapidly converge back to zero, often after only 1 time step. Again, this only produced a 'blip' in the parameter values. Subsequently the result is a control system not as robust and/or accurate as was expected.

This RLS algorithm was then run in a simulation comparison with both the fixed gain and scheduled gain control designs. The results of this simulation are presented in the next section.

6.4 SIMULATION COMPARISON OF 3 DIFFERENT PIP CONTROL DESIGNS

Here, a simulation comparison of three different PIP control designs is presented. For effectiveness the simulation covers the whole operating range of the Leuven ventilation chamber. The SIMULINK model below (figure 6.7) has three distinct PIP control designs incorporated within it, namely:

i) fixed gain;

ii) scheduled gain; and

iii) adaptive gain.

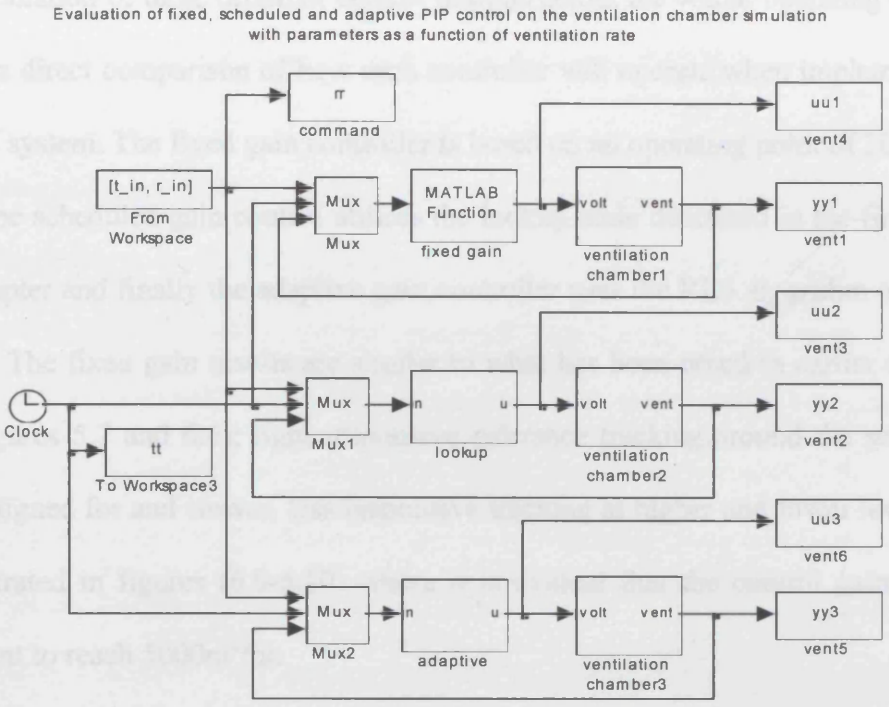

Figure 6.7: Simulation comparison across whole operating range of Leuven ventilation chamber of fixed gain, scheduled gain and adaptive gain controllers.

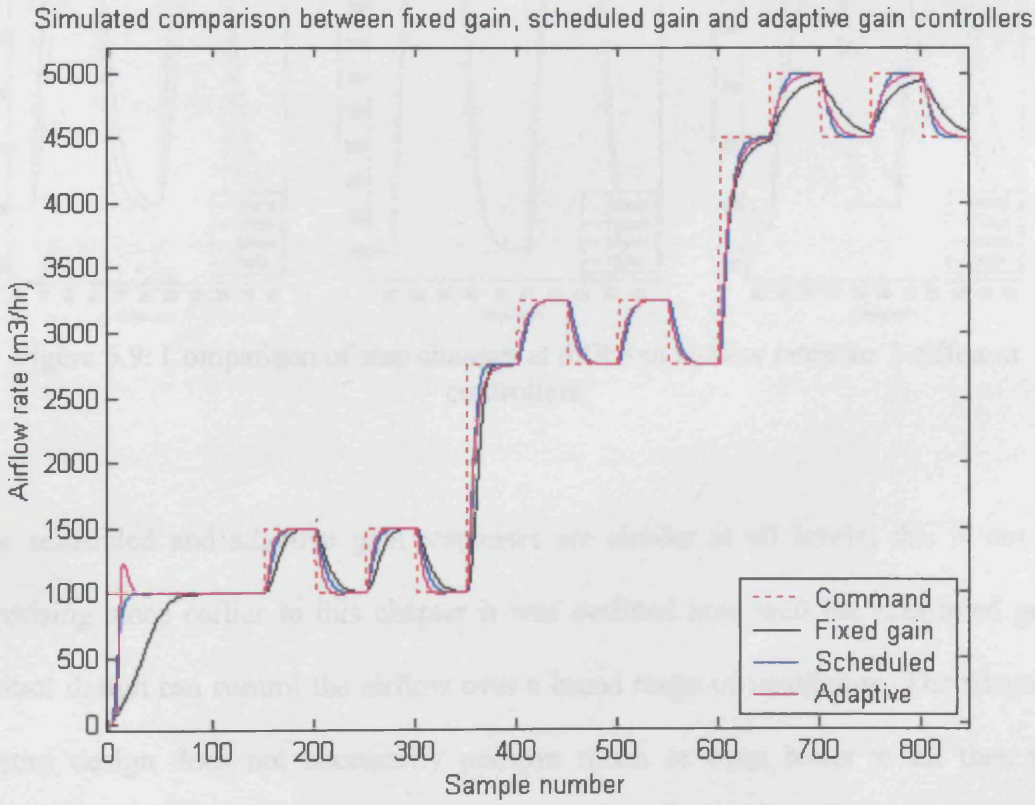

Figure 6.8: Simulated comparison between three different PIP control designs.

The simulation of three different control designs across the whole operating envelope allows a direct comparison of how each controller will operate when implemented on the real system. The fixed gain controller is based on an operating point of $3000m^3/hr$, while the scheduled gain control utilises the lookup table described in the first part of this chapter and finally the adaptive gain controller uses the RLS algorithm of Young, (1984). The fixed gain results are similar to what has been noted in earlier examples (e.g. figures 5.7 and 6.6); tight responsive reference tracking around the set point it was designed for and slower, less responsive tracking at higher and lower levels. This is illustrated in figures (6.9-6.10) where it is evident that the control gains are not sufficient to reach $5000m^3/hr$.

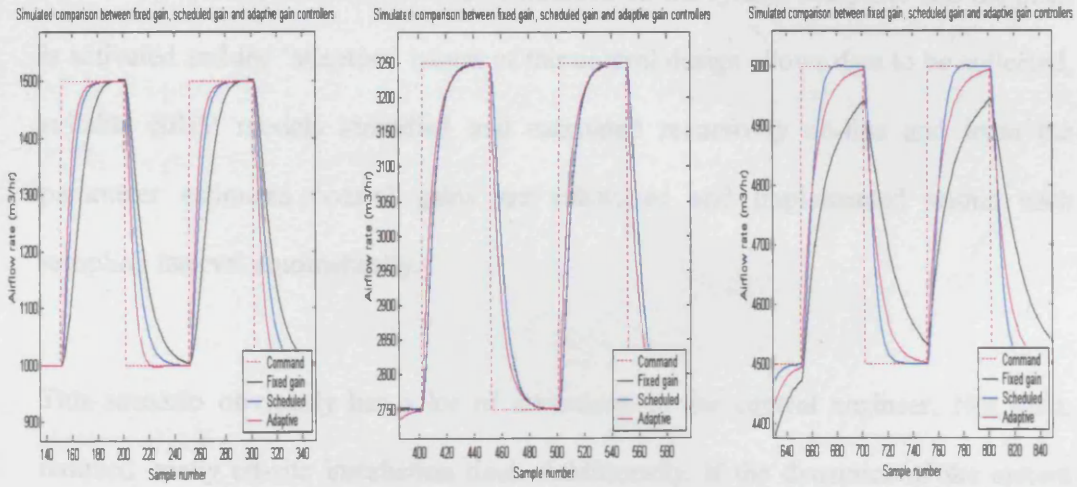

Figure 6.9: Comparison of step changes at different airflow rates for 3 different controllers.

The scheduled and adaptive gain responses are similar at all levels; this is not so surprising since earlier in this chapter it was outlined how well the scheduled gain control design can control the airflow over a broad range of ventilation. The adaptive control design does not necessarily perform much or even better at all than the scheduled gain, but it is has been shown to be a more flexible and easily implemented

control design on many installations. The next chapter outlines the implementation of this simulated adaptive design on the Leuven ventilation chamber.

Comparison experiments of scheduled gain and adaptive gain control design do not show conclusively that either system is superior in terms of reference tracking. However, it was noted how the scheduled gain design has the requirement of calculating all the necessary model parameters to make up a suitable polynomial curve from which to build a lookup table; from which the control gains needed for optimum control over a broad operating envelope can be calculated online and implemented. It is with automating this process further that the adaptive control design becomes an attractive alternative. The adaptive controller has the ability to be a fully operational self tuning system, i.e. the controller is installed on the system computer and the plant is activated and the 'adaptive' nature of this control design allows data to be collected, suitable SRIV models identified and estimated recursively on-line and from the parameter estimates control gains are calculated and implemented within each sampling interval automatically.

This scenario obviously has a lot of attractions to the control engineer. Not least, reduced costly on-site installation time. Additionally, if the dynamics of the system change due to expansion of the plant under control or the introduction of new inlets or outlets the system will automatically recalculate the necessary model parameters and gains without the costly and time consuming (closing the plant) necessity of collecting experimental data and re-modelling etc.

6.6 CONCLUSIONS

It is evident from figure 6.2 that the values of f_o and k_I do not change too much at each operating point change which assists for a smooth transition between airflow rates. However, although it can be concluded the scheduled gain control design is relatively effective at improving control across a broad range of operating points, it is still a relatively drawn out process to execute from data collection through to model identification and control design at each operating point. The systems under study are relatively small compared to some complex non-linear industrial processes; and if there were 50 or a 100 or more operating points the process of setting up a switched gain control could be rather laborious in the extreme. Furthermore, if the system was modified in any way the whole process would require repeating because the dynamics of the system would undoubtedly change. Thus, while the scheduled gain controller is an ideal option for a relatively small system a more sophisticated control design such as the adaptive gain is preferable.

Chapter 7

IMPLEMENTATION OF COMBINED FAN AND VALVE CONTROLLERS

7.1 INTRODUCTION

The desired airflow rate within agricultural buildings is typically set at a relatively low level. It is reasonably straightforward to maintain these low airflow rates in open loop control; however, when disturbances, such as wind, eddy currents or thermals are present to perturb the system, a closed loop control mechanism is required. Also, at low airflow rates with disturbances present, the system under study can be hard to stabilise because

the airflow drawn through the 3D airspace is not robust to external influences. This can result in a system, which simply goes unstable, producing a fluctuating ventilation rate that is unsuitable for maintaining the welfare of the animals housed within. Microclimate control typically amounts to ~15% of production costs, (Vranken, 1999), if these costs can be lowered to 10% or less, the instant increased profits to the farmer are obvious. It is with this in mind that the issue of developing a low (operating) cost controller, which is stable at low airflow rates even in the presence of wind disturbances, is addressed here. In this chapter, the development and implementation of a unique fan and valve configuration using proportional integral plus (PIP) control of airflow rate within the ventilation chamber in Leuven, Belgium is presented.

As outlined in chapter three, the ventilation rate throughput can be restricted using the vortex damper (see figure 3.1) to minimise the effects of thermal buoyancy and wind disturbances. Figure 7.1, shows the typical performance characteristics of an axial fan; it can be seen how (curved lines 1-7) the airflow rate increases as the static pressure decreases. Two working curves (A and B) are also indicated on figure 7.1; these represent the static pressure change for two different building envelopes at varying ventilation rates. The resulting ventilation rate and pressure difference is found at the intersection of both curves for each voltage. These data show that the obtained ventilation rate is a function of both the applied voltage and the static pressure difference over the ventilation opening in which the fan is placed. Consequently, to modify the ventilation rate in a mechanical ventilation system different basic methods can be applied (Randall and Boon., 1994); i.e.:

i) maintain fan voltage and re-circulate a proportion of the building air,

ii) maintain fan voltage and alter the pressure difference by restricting the throughput of the fan (see influence of pressure in figure 7.1),

iii) varying the voltage applied to the fan (see influence of voltage in figure 7.1),

iv) add to or reduce the number of fans in operation.

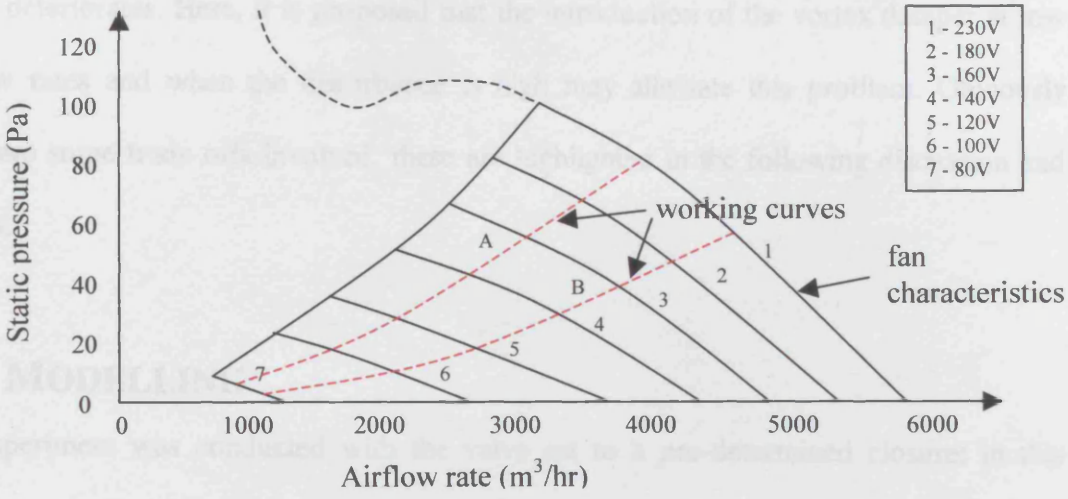

Figure 7.1: Static pressure produced by an axial fan as a function of voltage and ventilation rate.

In short, the more power (voltage) applied to a ventilation (axial) fan, the faster and more energetically it runs. In order to produce the same airflow rate as the voltage increases, the throttling valve has to close more and more. For a very stable airflow rate at low ventilation rates with a moderate disturbance (lee-type) applied, the voltage applied to the control fan needs to be large. Thus, if the voltage can be held constant while the valve takes over control, it is argued the overall stability will improve and power consumption decrease.

7.2 FIXED GAIN FAN CONTROL INCORPORATING THE VORTEX DAMPER

The previous two chapters outlined that a range of control designs from straightforward (fixed gain) to more sophisticated (adaptive gain) could be used to regulate the airflow well inside the ventilation chamber. However, it was noted that at low airflow rates and under high disturbance conditions the control algorithm's ability to maintain set-point levels deteriorates. Here, it is proposed that the introduction of the vortex damper at low airflow rates and when the disturbance is high may alleviate this problem. Obviously there are some trade offs involved, these are highlighted in the following discussion and results.

7.2.1 MODELLING

An experiment was conducted with the valve set to a pre-determined closure; in this preliminary case the vortex damper is set to 75% closed and a series of steps in the voltage to the fan from 15-20% (i.e. low airflow rate) and back down are executed (see figure 3.6). This results in the following first order TF model with two time delays [1 1 2], with a *YIC* value of −16.68 and R_T^2 of 0.9984,

$$y(k) = \frac{4.1987z^{-2}}{1-0.8868z^{-1}}u(k) \tag{7.1}$$

where $y(k)$ is the airflow rate (m^3/h) and $u(k)$ is the applied voltage (%). The model parameters and associated errors are,

$$a_1 = -0.8868(0.0026)$$
$$b_1 = 4.1987(0.0138)$$

and the Steady State Gain (SSG) and Time Constant (TC) of the model are,

$$SSG = \frac{4.1987}{1-0.8868} = 37.08 \tag{7.2}$$

$$TC = -\frac{\Delta t}{\ln(-a_1)} = -\frac{2}{\ln(0.8868)} = 16.64 \text{ seconds} \tag{7.3}$$

where Δt is the sampling rate. Figure 7.2 below shows the excellent model fit to the measured data. This good model fit is also partially due to the amount the vortex damper was closed, which in this case is 75%; this has the effect of damping most of the oscillations out due to the increased stability of the airflow through the increased voltage sent to the fan.

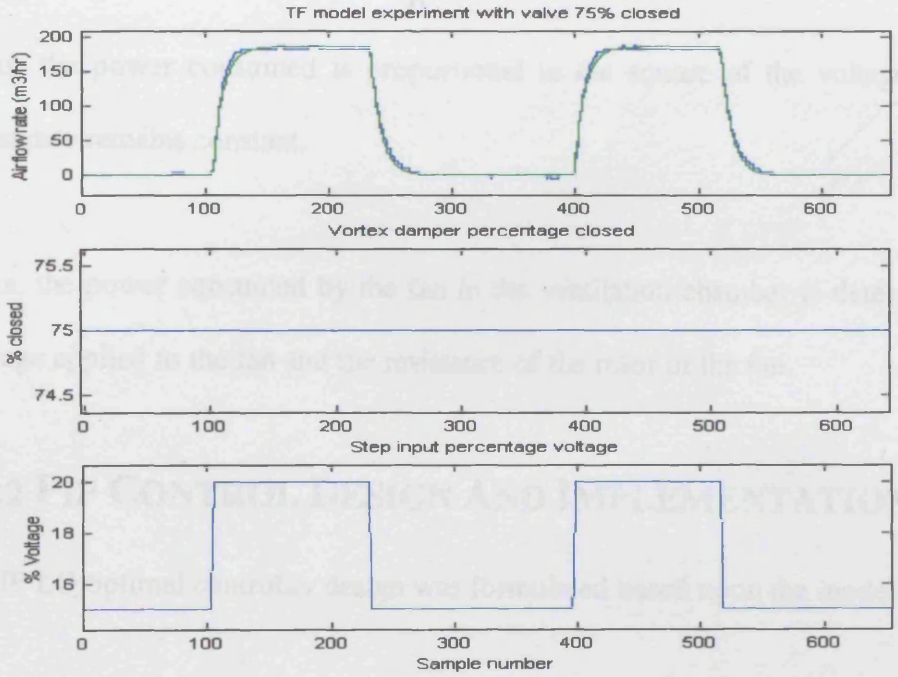

Figure 7.2: TF model experiment with valve 75% closed. The upper plot shows the model fit (blue) to the measured data (green); the middle plot indicates the position of the vortex damper; and the lower plot shows the % voltage step changes applied. The sampling interval is 2 seconds.

There also exists a relationship between applied voltage and consumed power. Ohms Law states,

$$V = I * R \tag{7.4}$$

where, V = Voltage (Volts); I = Current (Amps) and R = Resistance (Ohms). And, power consumed (Watts) can be determined by rearranging equation 7.6.

$$I = \frac{V}{R} \tag{7.5}$$

The power can be found by using equation (7.7),

$$P = V * I \tag{7.6}$$

Substituting (7.6) into (7.7) gives,

$$P = \frac{V^2}{R} \tag{7.7}$$

Thus, the power consumed is proportional to the square of the voltage applied if the resistance remains constant.

Thus, the power consumed by the fan in the ventilation chamber is determined from the voltage applied to the fan and the resistance of the rotor of the fan.

7.2.2 PIP CONTROL DESIGN AND IMPLEMENTATION

A PIP LQ optimal controller design was formulated based upon the model in (7.1), with

$$\mathbf{Q} = \begin{bmatrix} 1 & 0 & 0 \\ 0 & 1 & 0 \\ 0 & 0 & 0.01 \end{bmatrix} \quad and \quad , \quad r = 1 \tag{7.8}$$

This results in the control gain vector,

$$\boldsymbol{k} = [0.1977 \quad 0.9361 \quad -0.0218] \tag{7.9}$$

The control gains (7.9) were then incorporated into the PIP control design and the controller was implemented in its standard formulation on the airflow test rig. The control response can be seen in figure (7.3) below. The control is good in the region where the control design was intended, but the set point tracking performance below and at 500 m^3/hr is oscillatory; this is to be expected because the control design is operating in a region below its lower limits. If we refer to the sigmoidal response curve (figure 5.2) it

can be seen that the lowest 1000 m^3/hr of measurable airflow is in a region that is highly non-linear. Thus, this result perhaps expected. The purpose of this has been to highlight the shortcomings of the airflow rate control design at low airflow rates without damping.

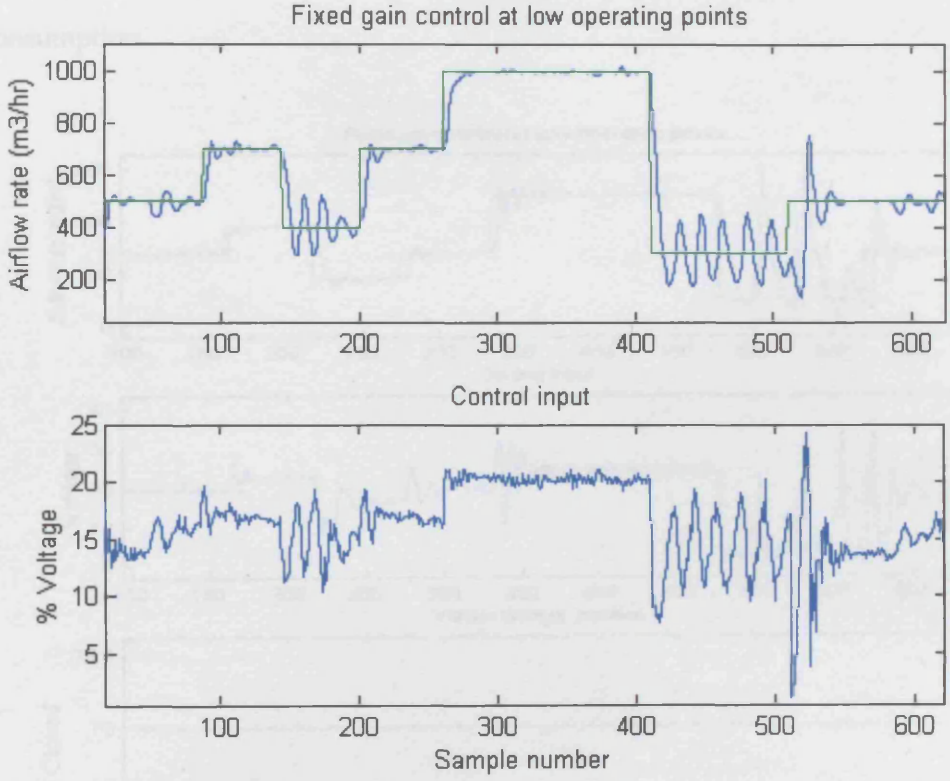

Figure 7.3: Fixed gain control at low airflow rate with vortex damper fully open.

The next stage involves incorporating the throttling valve in some form in order to attempt to improve ventilation rate control at low airflow rates. In figure 7.4 below, the control gains are the same as those used in figure 7.3, but with the throttling valve set to 75% closed and the set point range is 100-500 m^3/hr. With the vortex damper partially closed the airflow is now controllable down to ~180 m^3/hr. The reason the control improves is due to the narrowing of the orifice the air has to pass through, the smaller the orifice, the faster, more stable the airflow. However, to obtain the correct airflow to

maintain the required set point, the fan requires more voltage, and therefore consumes more power. Also, in figure 7.4 it is evident that if the set point is much below 200 m^3/hr the controller becomes oscillatory again. In order to control the airflow at this level, the throttling valve would require closing up to around 90%, which will further increase power consumption.

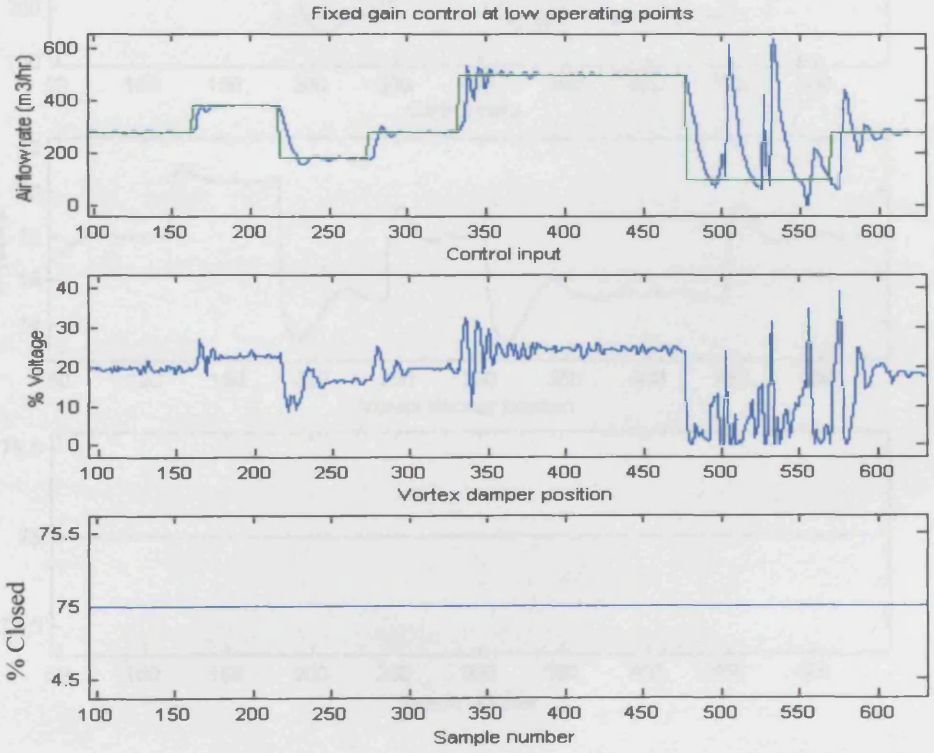

Figure 7.4: Fixed gain control at low airflow rate with vortex damper 75% closed.

The same control design as used in figure 7.6 was implemented in the forward path (FP) PIP control design; the resulting set point tracking at 400-180 m^3/hr is presented in figure 7.5 below. The corresponding tracking of the stepped desired levels is good, with slight overshoots at step changes; but the control action rapidly controls the axial fan output to the required airflow level. The control input is less noisy in the FP implementation

compared to that in the FB case in figure 7.4 above and the overall model output is also less oscillatory.

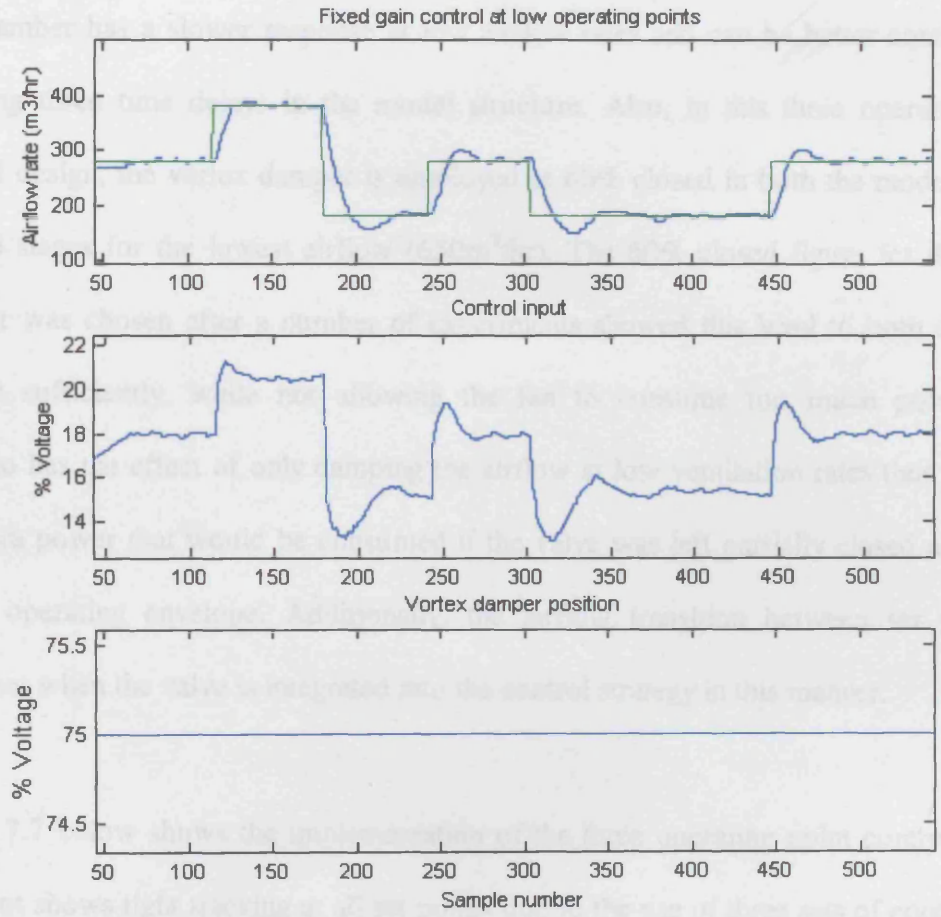

Figure 7.5: Comparison plots of forward path PIP control implementation using the same model and control gains as in figure 7.6 above.

A further sophistication of this method is to partially close the fan only when the desired airflow drops below a certain level. The following figure (7.6) illustrates this for a step down (and back up) from a medium range ventilation rate (2750 m^3/hr) to one below 1000 m^3/hr. Here, the controller uses what has been termed the 'three operating point' control design, which is a controller that is designed for three different operating points

across the operating envelope (Low (650m^3/hr), medium (3000m^3/hr) and high (5050m^3/hr)). Both the medium and high airflow rate controllers are first order TF with a unity time delay, while the low (650m^3/hr) control gains are derived from again a first order TF model, but this time with a time delay of three samples. It has been found that the chamber has a slower response at low airflow rates and can be better controlled by allowing three time delays in the model structure. Also, in this three operating point control design, the vortex damper is employed at 60% closed in both the modelling and control stages for the lowest airflow (650m^3/hr). The 60% closed figure for the vortex damper was chosen after a number of experiments showed this level to both damp the airflow sufficiently, while not allowing the fan to consume too much power. This scenario has the effect of only damping the airflow at low ventilation rates thus reducing the extra power that would be consumed if the valve was left partially closed across the whole operating envelope. Additionally, the airflow transition between set points is smoother when the valve is integrated into the control strategy in this manner.

Figure 7.7 below shows the implementation of the three operating point control design. This plot shows tight tracking at all set points due to the use of three sets of control gains calculated for 2500-3000m^3/hr; 1000-1500m^3/hr and 300-800m^3/hr ventilation rates. The implemented control design (figure 7.7) is described as a switched gain control; i.e. the control design simply switches to a new set of control gains when the set point changes to a higher or lower reference level. The idea with this type of controller is that it can be programmed relatively easily. The schematic layout in figure 7.6 below shows the TF and vector of control gains used at each switching point for the three operating controller and the three regions of ventilation control.

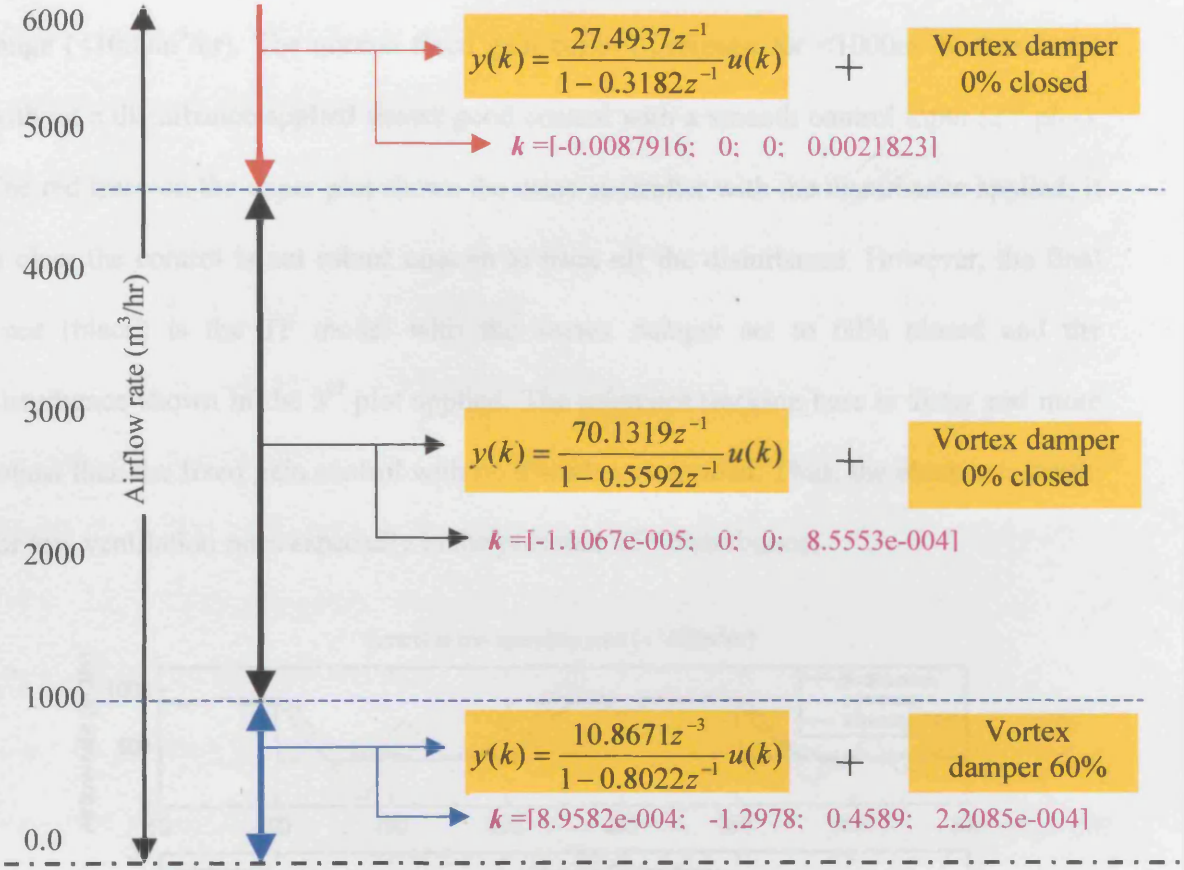

Figure 7.6: Schematic of three operating point controller.

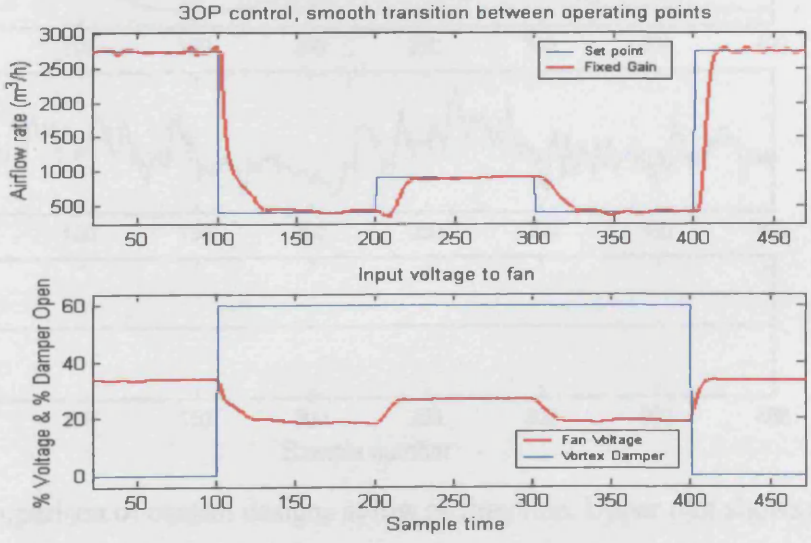

Figure 7.7: Three operating point control with valve partially closed for smoother transition between operating points.

The figure 7.8 below, shows a comparison at the lowest part of the three operating control range (<1000m^3/hr). The normal fixed gain control designed for <1000m^3/hr (magenta) without a disturbance applied shows good control with a smooth control input (2nd plot). The red trace on the upper plot shows the same controller with the disturbance applied; it is clear the control is not robust enough to back off the disturbance. However, the final trace (black) is the TF model with the vortex damper set to 60% closed and the disturbance shown in the 3rd plot applied. The reference tracking here is faster and more robust than the fixed gain control with no disturbance applied. Thus, the damper is useful for low ventilation rates especially in the presence of a disturbance.

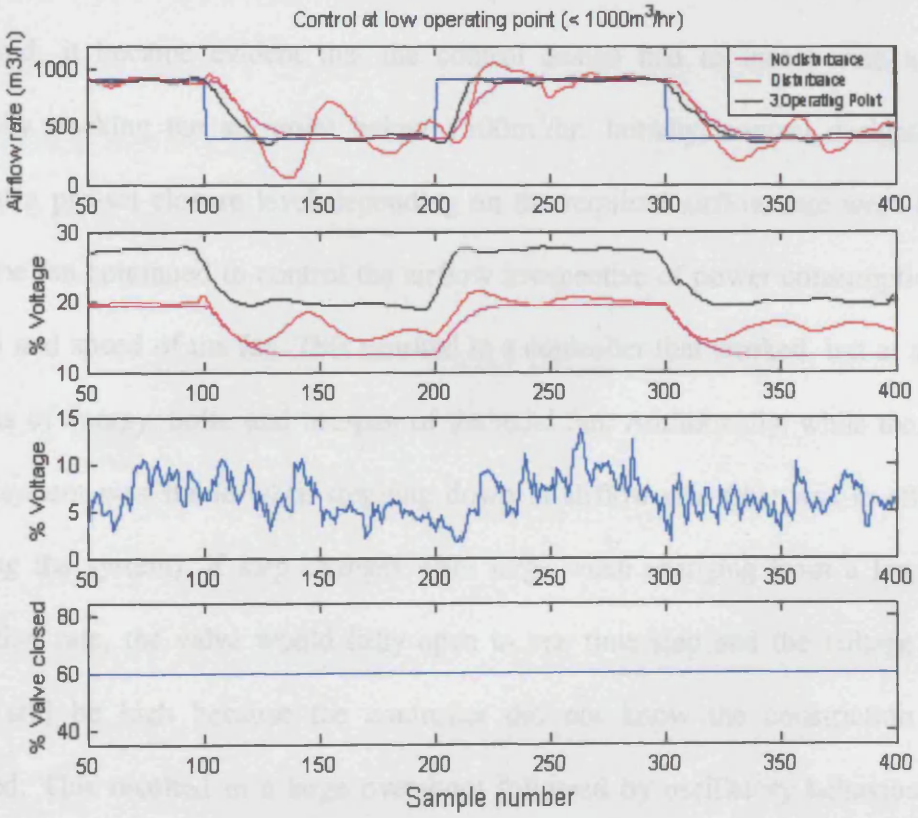

Figure 7.8: Comparison of control designs at low airflow rate. Upper plot shows the set point change (blue); 3 operating point control (black) with disturbance and valve; fixed gain with disturbance (red) and fixed gain no disturbance (magenta).

This methodology certainly appears to work, but obviously requires a higher voltage applied to the fan, thus increasing costs to the farmer. So, with this in mind, the following section outlines the full fan/valve control design and implementation in an attempt to both improve control and reduce power consumption when controlling the airflow at low ventilation rates.

7.3 FAN-VALVE CONTROL

The previous section has shown how the ventilation rate at low operating points in the presence of a disturbance can become unstable. This thesis has shown that ventilation rate can be controlled well, even in the presence of a disturbance when the airflow rate is above $1500m^3/hr$. However, because in practice lower ventilation rates are often employed, it became evident that the control design had to incorporate a means of optimally tracking the set point below $1500m^3/hr$. Initially, control designs using the valve at a pre-set closure level depending on the required airflow rate were developed; while the fan continued to control the airflow irrespective of power consumption, voltage applied and speed of the fan. This resulted in a controller that worked, but at a huge cost in terms of energy, noise and lifespan of the axial fan. Additionally, while the behaviour of the system was stable when stepping down in airflow rate (this was in effect simply damping the system), if step changes were large when changing from a low to a high ventilation rate, the valve would fully open in one time step and the voltage to the fan would still be high because the controller did not know the constriction had been removed. This resulted in a large overshoot followed by oscillatory behaviour until the system stabilised. Obviously this was an unacceptable scenario and a better solution is required.

Other work was carried out by Gevers *et al.* (2000), using a model based predictive control (MBPC) algorithm based on Van den Boom (1996) in which the key to the algorithm is the minimisation of a cost function. In this MBPC design, the valve was set to a pre-determined closure and they found increased stability in the airflow rate, with a corresponding increase in power consumption. Their MBPC algorithm only allowed the valve to remain at one position and was tested over a constant airflow rate of 1500 m^3/hr. While showing improved stability at 1500 m^3/hr, this control design was obviously not sufficient to control airflow across the whole operating envelope of the system under study; and more specifically was not tested at very low (<1000 m^3/hr) ventilation levels. Additionally, Gevers *et al.* (2000), compared a PI controller based on the measured airflow rate and a P controller based on estimated pressure difference. They found the PI controller did not increase accuracy or decrease the power consumption, but an increase in the control accuracy was found when using the estimated pressure difference (along with an increase in power consumption).

The original fan/valve controller outlined in the previous section where the valve was pre-set to close partially when the airflow rate was below 1000 m^3/hr was clearly unsuitable on economic grounds. However, it was evident that in order to stabilise the airflow below 1000 m^3/hr the valve would be required to close in some manner. It was decided that the valve would have to take a more dynamic role in the control action. For this initial control design it was deemed easier to remain with a single input/single output (SISO) controller, rather than use a multivariable multi input/single output control (MISO) design. This was because it was uncertain how the cross coupling between the two inputs would behave.

Future controllers of this sort would probably take the MISO route, but for the purposes of this example the more straightforward SISO control design will be used.

From earlier experiments and prior work in Leigh *et al.*, (1999; 2000), Taylor *et al.*, (2000) and Vranken *et al.*, (2000) which have shown how the ventilation rate at low operating points in the presence of a disturbance can become unpredictable, it can be seen that the main component in controlling the ventilation chamber was the voltage applied to the control fan. Because it was evident the system could be controlled adequately above 1000-1500 m^3/hr, that part of the controller could be the same as in previous fixed gain and scheduled gain controllers outlined in chapter six (also, see Taylor *et al.*, (2001)). The new controller would feature a fan voltage that was held constant when the set point called for a ventilation rate of 1000 m^3/hr or below and the valve then becomes the actuator below this level. The block diagram in figure (7.9) below outlines the principal of the control action, however, this does not take into account effects of hysteresis around 1000m^3/hr when switching from one control design to the other.

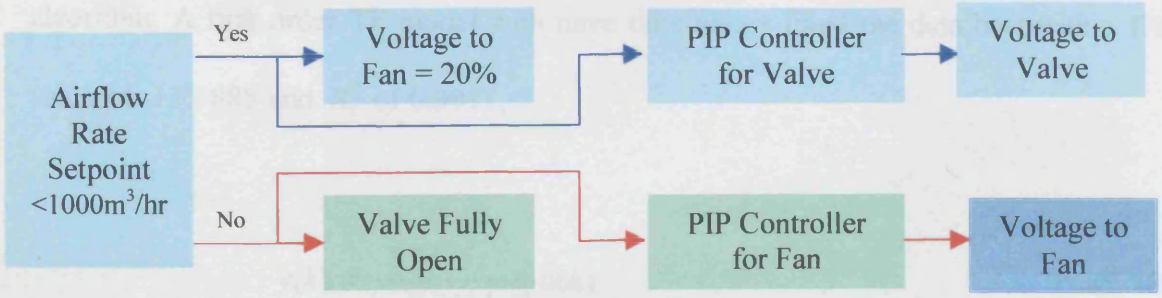

Figure 7.9: Block diagram of combined fan/valve PIP controller where there are two modes of control: 1. <20% voltage (<1000 m^3/hr), the valve takes over control and fan stays constant at 20%; 2. >20% voltage the valve opens fully (0% valve) and the main fan controls the airflow.

Before the control design could be finalised a model of the throttling valve was required. Thus, open loop experiments with the valve position stepping between different stages of closure with a constant voltage applied to the control fan throughout were carried out. From these, the model that captured most of the dynamics of the system was chosen. The LABVIEW/MATLAB interface (see chapter 3) enables real time viewing of the output of open loop experiments and this allowed the user to get a direct assessment of how each percentage closure of the valve affected the measured airflow rate. It soon became evident that between 0-30% closed there was very little effect on the airflow, so it was decided to use the model for the control design from steps of 50% to 70% closed, with a constant voltage of 20% (potential voltage) applied to the control fan.

7.3.1 MODELLING

The models for the fan/valve control system design were identified and estimated by following a similar procedure to that described in chapters two and six. The valve was stepped between different closures (e.g. 50% to 70% closed), while the fan speed was maintained at a constant 20% voltage. The collected data were modelled with the SRIV algorithm. A first order TF model with three time delays fitted the data best with a *YIC* value of -12.3888 and R_T^2 of 0.9911,

$$y(k) = \frac{3.6415z^{-3}}{1-0.7314z^{-1}}u(k) \tag{7.10}$$

Figure 7.10 below shows the model fit to the measured data, where $y(k)$ is the airflow rate (m^3/h) and $u(k)$ is the applied voltage (%).

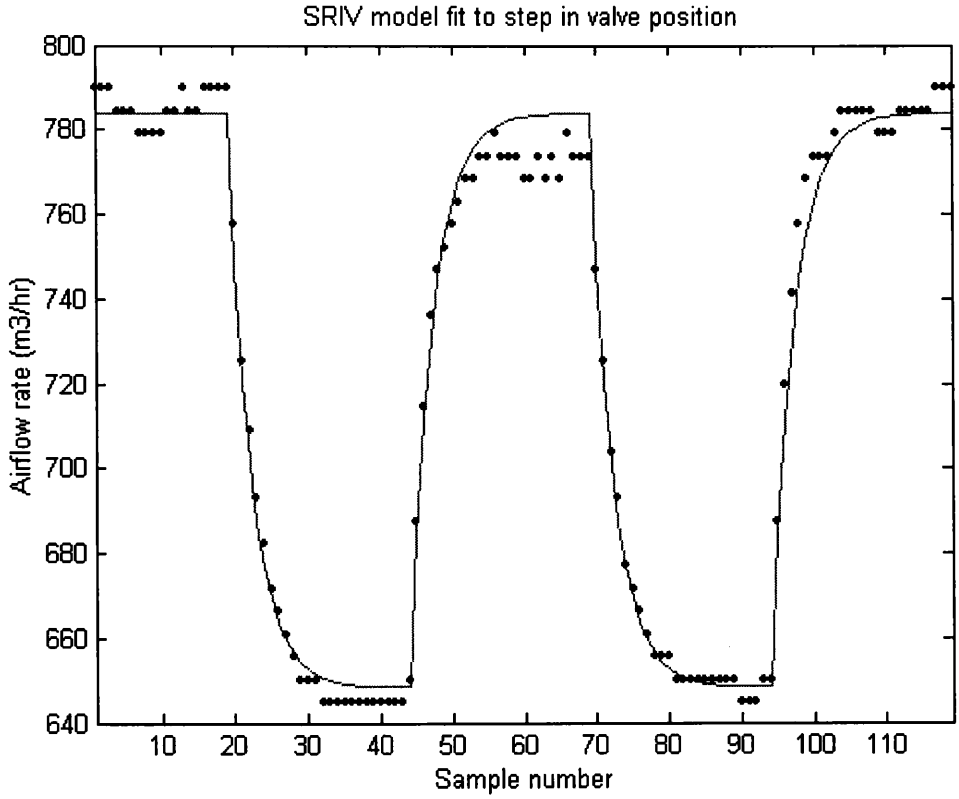

Figure 7.10: Example of valve only SRIV model fit, the valve step is 50-60% and the airflow is provided by the main fan at a constant (20%). The blue dots are the data and the red line is the model fit.

7.3.2 PIP CONTROL DESIGN

Using the above model (7.10) and the use of LQ optimal design with the following cost function diagonal weights,

$$Q=\begin{bmatrix}1 & 0 & 0 & 0\\ 0 & 1 & 0 & 0\\ 0 & 0 & 1 & 0\\ 0 & 0 & 0 & 0.01\end{bmatrix}, \qquad r=1 \tag{7.11}$$

This yields the following SVF gains

$$\boldsymbol{k} = [-0.1322\ 0.7767\ 0.6583\ -4.0248] \tag{7.12}$$

The control gains were then incorporated into the PIP control design and figure 7.11, below, shows the control response to a unity step change.

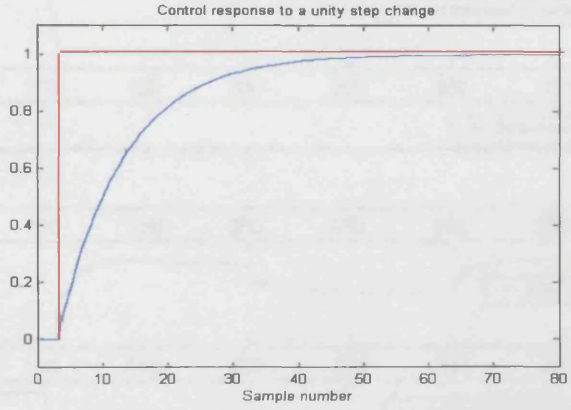

Figure 7.11: LQ optimal control response to a unity step change.

The controller was now ready to be implemented on the airflow test rig.

7.3.3 IMPLEMENTATION

Various LQ weightings were tried and an optimum response was obtained when LQ weightings of $w_y = 1, w_u = 1$ *and* $w_z = 0.01$ were applied. The control implementation results for this design are shown in figure 7.12. It is clear from this plot the control system is working well and the combination of the control fan and throttling valve design has been shown to give good control at low ventilation rates while the transition between high and low airflow is smooth with almost no overshoots or oscillatory behaviour. The next

test on this control design was to apply a disturbance to the system to see how robust the control design was and how efficiently it could deal with a fluctuating airflow.

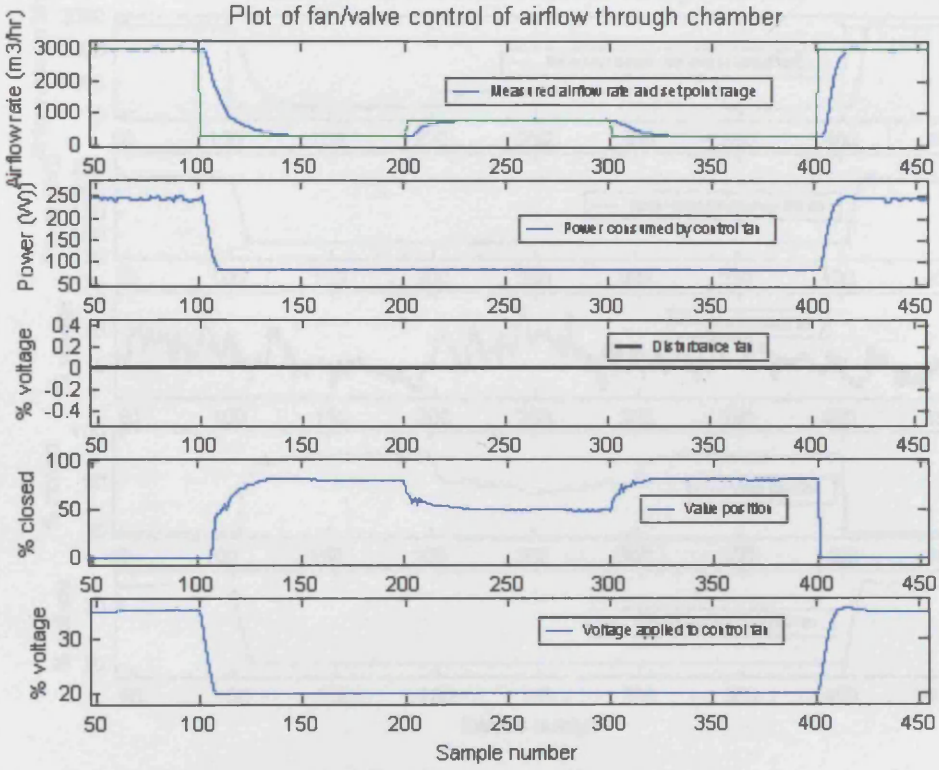

Figure 7.12: Plot of fan/valve control in Leuven chamber.

Figure 7.13 is the same plot as figure 7.12, but the centre plot now has the disturbance signal turned on. There is very little difference between the two responses, except for the region where the disturbance is largest; here the maximum deviation from the set point is <2% without the disturbance; and peaks at 10% with the disturbance. Thus, the airflow is maintained within acceptable 10% limits around the desired level. The amount the valve is closed also deviates a little more in figure 7.13 to allow for the fluctuating disturbance

signal. However, overall the control design has shown a robust response to a disturbance signal.

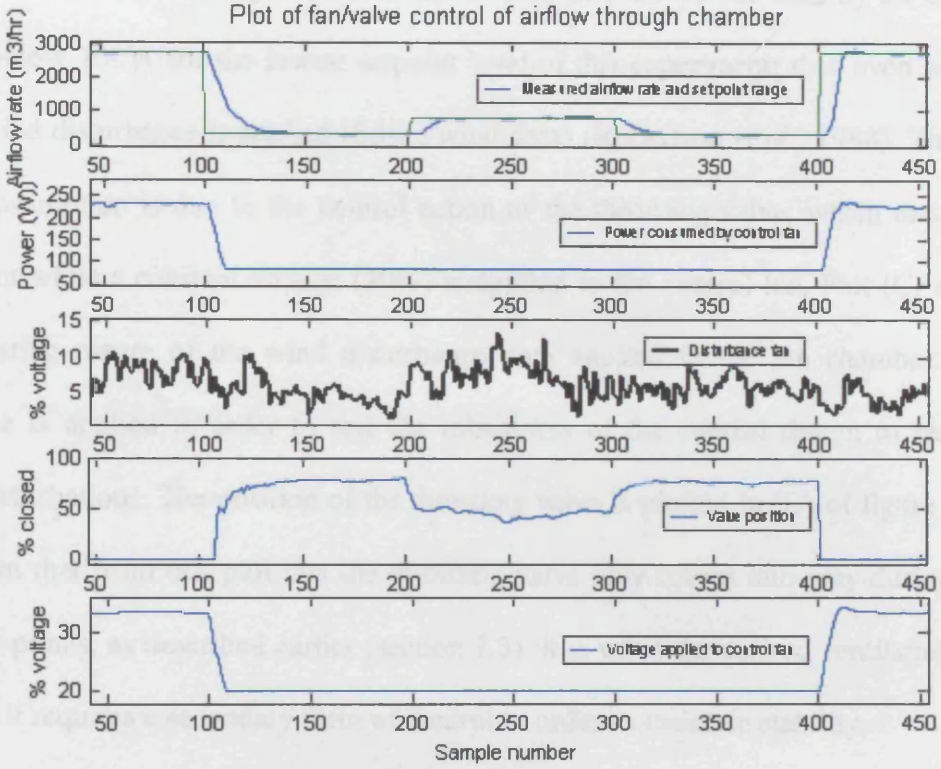

Figure 7.13: Plot of fan/valve control in Leuven chamber with disturbance signal on (LQ and pole placement design [0.01 1 1]; [07/0.8]).

Figure 7.14, is the output from an experiment across the high and low operating levels of the fan chamber, the fan control is optimised from the (operating point of 3000m^3/hr) fixed gain controller described in chapter six. The experiment had a realistic wind disturbance applied. The results in figure 7.14 show how this controller works well across the whole operating envelope of the system under study. The initial set point is 4250m^3/hr, which changes every 100 time steps (200 seconds) (see figure 7.14) to follow the programmed setpoint changes. From the upper plot in figure 7.14A, it can be clearly seen how well the controller tracks both the setpoint and setpoint changes. There is a

smooth transition between high and low ventilation rates where the different modes of control switch in and out. This is evident on both (large and small steps) the rising and falling limbs of the plot. Plot (B) of figure 7.14 shows the power consumed by the control fan for the duration of the experiment. It can be seen how the power used by the control fan dips below 100W for the lowest setpoint level of this experiment; this, even when a realistic wind disturbance is applied (Silsoe wind data) (Robertson *et al.*, 1988). The low power consumption is due to the control action of the throttling valve, which maintains the setpoint while a constant voltage (20%) is applied to the control fan. Plot (C) shows the fluctuating nature of the wind disturbance data applied to the fan chamber. This disturbance is applied in order to test the robustness of the control design to realistic outside perturbations. The position of the throttling valve is plotted in (D) of figure 7.14. It is evident that from this plot that the throttling valve only comes into play during low airflow set points, as described earlier (section 7.3), it is when the desired ventilation rate is low that it requires a secondary form of control in order to maintain stability.

From figure 7.14D, it can be seen that the valve had to close to just over 70% (0% = fully open; 100% = fully closed). Also, it can be seen how the setpoint tracking controlled by the valve only, with a constant control voltage of 20% applied is very accurate with very little deviation from the setpoint. The few small oscillations seen in the valve position plot are due to the disturbance fan, while the output ventilation rate remains smooth and constant showing the efficiency and robustness of this control design for low airflow rates. This, in the presence of a disturbance is a vast improvement over the fan-only control design and the fan-only with a pre-set valve position to improve stability. The final plot of figure 7.14E, shows the voltage applied to the control fan throughout the

experiment over all operating ranges. The constant values at 20% coincide with the periods when the valve control is operating.

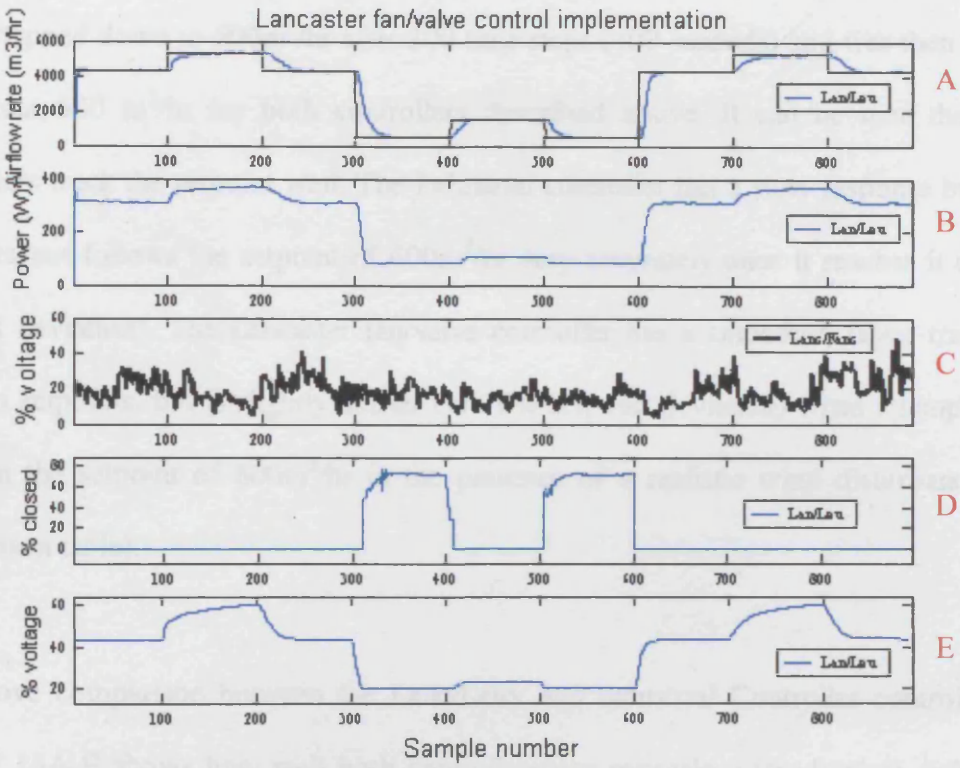

Figure 7.14: Combined Lancaster fan/valve FB controller with full disturbance applied over a wide operating envelope (letters A-E are described in the text above).

7.4 COMPARISON OF FAN/VALVE CONTROLLERS

[1]Installed on the ventilation rig was an existing Industrial fan/valve controller. However, it was unclear what the exact mode of operation was for this particular controller. It was possible to extract the measured ventilation rate and the power consumption; thus, it was deemed able to make a direct comparison of the performance of this Industrial controller

[1] The Industrial fan/valve controller referred to above is named as such for reasons of confidentiality.

and the proposed PIP fan/valve controller over a range of criteria (e.g. speed of response; setpoint tracking (deviation from setpoint) and power consumption).

Figure 7.15 shows the output from an experiment with a starting setpoint of $3000m^3/hr$ which stepped down to $600m^3/hr$ after 200 time steps (400 seconds) and was then held at a constant 600 m^3/hr for both controllers described above. It can be seen that both controllers track the setpoint well. The Industrial controller has a slow response between setpoints but follows the setpoint of $600m^3/hr$ very accurately once it reaches it (+/-1% setpoint deviation). The Lancaster fan/valve controller has a smoother, faster transition between setpoints, but is slightly noisier (+/-10% setpoint deviation) when attempting to maintain the setpoint of $600m^3/hr$ in the presence of a realistic wind disturbance (see comparison table).

The above comparison between the Lanc/Leuv and Industrial Controller controllers in figure 7.15A-E shows how well both controllers can maintain a steady state airflow of $600m^3/hr$ while being subjected to a disturbance (figure 7.15C) with minimum deviations from the setpoint. The mean and standard deviation for the airflow rate along with mean and standard deviation for power consumption in both control designs are shown in table (7.2).

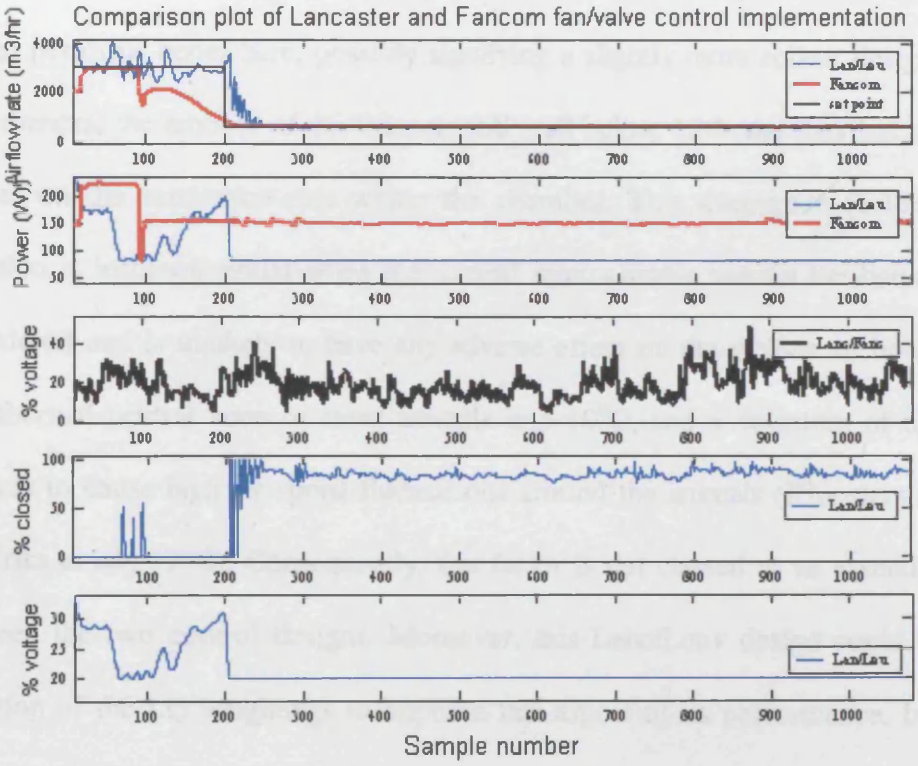

Figure 7.15: Comparison plot of Lanc/Leuv and Industrial Controller controllers (A-E; see text for details).

Table 7.2: Table showing statistical comparison between the Lanc/Leuv and Industrial Controller controllers.

Controller	Parameter	Mean	Std. deviation
Lanc/Leuv	Airflow rate	602.27 m^3/hr	36.78 m^3/hr
Industrial Controller	Airflow rate	596.87 m^3/hr	7.80 m^3/hr
Lanc/Leuv	Power consumed	81.40 W	0.67 W
Industrial Controller	Power consumed	149.982 W	2.35 W

Here, the airflow mean values (597 and 602m^3/hr) are very close to the desired (600m^3/hr) setpoint level; however, there is a difference in the standard deviations (σ). The Lanc/Leuv design gives an σ of 36.8m^3/hr, which equates to a 6.1% deviation from

the mean, while the Industrial Controller design has a very low σ of 7.81m^3/hr, which gives a deviation of just over 1% (1.3%). While conceding the Industrial Controller design performs better here, possibly signifying a slightly more robust design to external disturbances, the amount of deviation is still well below 10% and thus has no significant impact on the ventilation rate within the chamber. This magnitude (6.1%) of airflow variation is inconsequential when the overall microclimate around the housed animal is considered and is unlikely to have any adverse effect on the welfare of housed animals. The thermal neutral zone of most animals is 5-10°C, and a deviation of up to 10% is unlikely to cause high air speed fluctuations around the animals (Kloosters *et al.*, 1989; Hendriks *et al.*, 1990). Consequently, this factor is not classed as an essential difference between the two control designs. Moreover, this Lanc/Leuv design could be tuned by selection of the LQ weightings to improve this aspect of its performance. Indeed multi-objective tuning (see Chotai, *et al.*, 1998) could be used.

A very noteworthy difference between the Lanc/Leuv and Industrial Controller systems was observed when the power consumption was compared. As was shown earlier with this type of controller, where it really stands out from the Industrial Controller is in its power consumption (table 7.2). The Industrial Controller uses 150W to maintain the setpoint at 600m^3/hr with a realistic wind disturbance applied, while the Lanc/Leuv design requires only 81.5W. Thus, the Lancaster fan/valve controller utilises only 54% of the power needed by the Industrial Controller control design, resulting in a power saving of 46%. The logical conclusion from this analysis is to propose that the Lancaster fan/valve controller has a far greater efficiency than the Industrial Controller design. The exact internal details of the Industrial Controller are unknown, and while it evidently

performs well within the context of setpoint tracking, the power consumption is far higher when a direct comparison with the Lancaster fan/valve controller is made.

Further inspection of figure 7.15D and 7.15E show the extent to which the valve is used to damp the airflow while the control fan simply requires a constant and modest 20% potential voltage. Visual observations of the Industrial Controller controller suggest the control fan and vortex damper are working in tandem to control the airflow and the method employed requires the control fan to work at a level around 35-40% voltage. While this method has advantages when the external disturbance is large, it has been found that for normal operation it is unnecessarily high and a lower voltage will suffice when integrated into an optimal control design such as the one presented. The major savings, as highlighted earlier are in microclimate control running costs (power consumption): the proposed Lancaster fan/valve design could make savings of 7-10% on overall production costs per housed animal, which obviously makes it a viable proposition since the controllers complexity is no greater than in the Industrial Controller case.

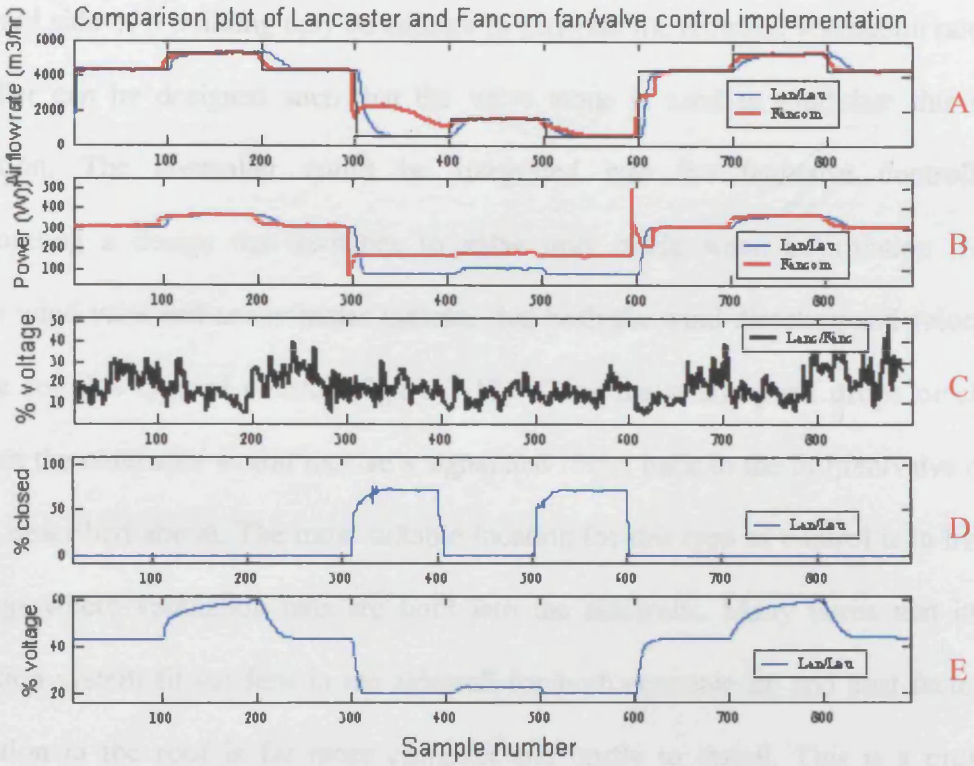

Figure 7.16 is another comparison plot of the two fan/valve controllers and the main difference here is the visual differences at the set point changes. While the power consumption is very similar at high ventilation rates it again shows the marked difference during low airflow rates.

7.5 VALVE ONLY CONTROL

The chimney effect in a building tends to produce natural ventilation, especially when there is a temperature difference between inside and outside. Generally, inside will be warmer, the warm air will be drawn from the building interior towards any chimney structure to outside the building. Thus, a natural air-circulation can occur. This is natural ventilation and requires no electro/mechanical fan to drive it. The simplest and cheapest

way of controlling this natural ventilation is to use the valve as the actuator, with information fed to it directly from the airflow rate sensor. The disturbance against the windward side of a building may be enough to generate the required ventilation rate and a controller can be designed such that the valve alone is used to modulate this natural ventilation. The controller could be integrated into the fan/valve controller by incorporating a design that switches to valve only mode when information from an outside wind vane and anemometer indicate that both the wind direction and velocity are suitable for this type of control (figure 7.17). Once the wind speed drops or changes direction the controller would receive a signal and revert back to the full fan/valve control system described above. The most suitable location for this type of control is in livestock buildings where ventilation fans are built into the sidewalls. Many farms that install a ventilation system fit the fans in the sidewall for both convenience and cost factors. An installation in the roof is far more complex and costly to install. This is a prominent feature of livestock farming in the low countries of Europe, i.e. Belgium and Holland, where many farms are built along the coast of the North Sea and are subjected to strong prevailing westerly winds. The obvious spin off with this type of combined control design is the power savings through eliminating the need for a control fan during windy conditions. Figure 7.17 below, gives a schematic overview of ideal conditions when the throttling valve only control could be used.

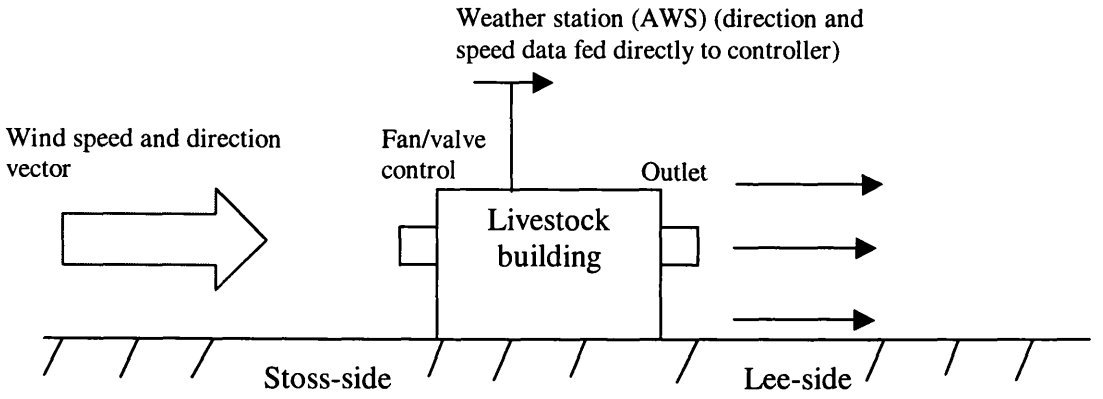

Figure 7.17: Schematic of livestock building and indicating wind direction for suitable throttling valve only control.

7.5.1 MODELLING AND PIP CONTROL DESIGN

A series of open loop experiments were carried out as in chapters 5 and 6, the disturbance fan was set at 27.75% (150% of the mean value from a set of real wind disturbance data) and the valve aperture was stepped between two different percentage openings, 55-60%. The data were collected and the following first order TF model with three time delays was identified,

$$y(k) = \frac{59.0z^{-3}}{1 - 0.4234\ z^{-1}}u(k) \tag{7.17}$$

where $y(k)$ is the airflow rate (m^3/h) and $u(k)$ is the percentage closed position of the vortex damper (% closed). The result of the valve only modelling are shown in figure 7.18 below.

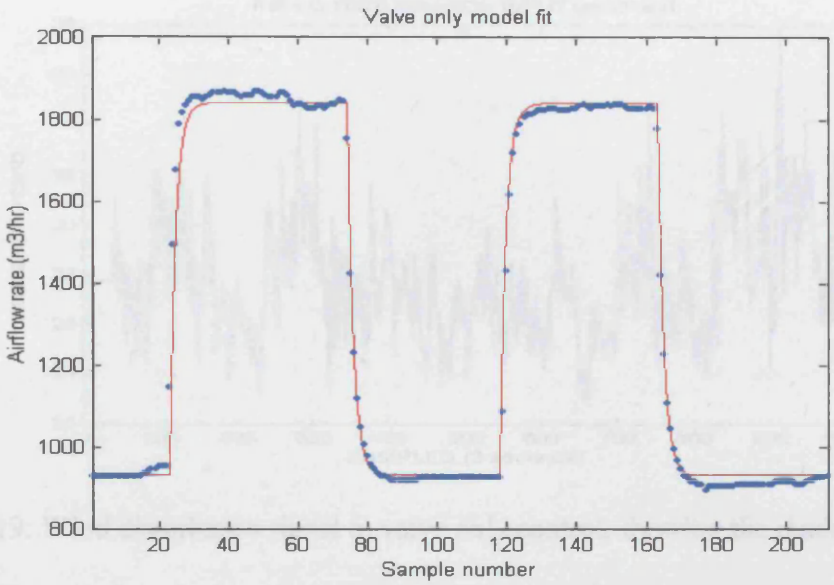

Figure 7.18: Example of valve only SRIV model fit, the valve step is 50-70% and the airflow is provided by the mean of the disturbance signal (18.5%).

The following LQ diagonal weights were chosen, Q = diag. [1, 1, 0.01] and r = 1, which yields the following SVF gain vector:

$$\boldsymbol{k} = [-0.004,\ 0.6934,\ 0.5637,\ -0.0046] \tag{7.18}$$

5.5.3 IMPLEMENTATION

The control gains were then incorporated into the PIP control design and the controller was implemented in FB form on the airflow test rig. Figure 7.20 shows one of the first valve only control implementations with the wind being the disturbance fan programmed to run the noisy Silsoe wind speed data (see figure 7.19). The initial results are very promising over the three set points in figure 7.20 below.

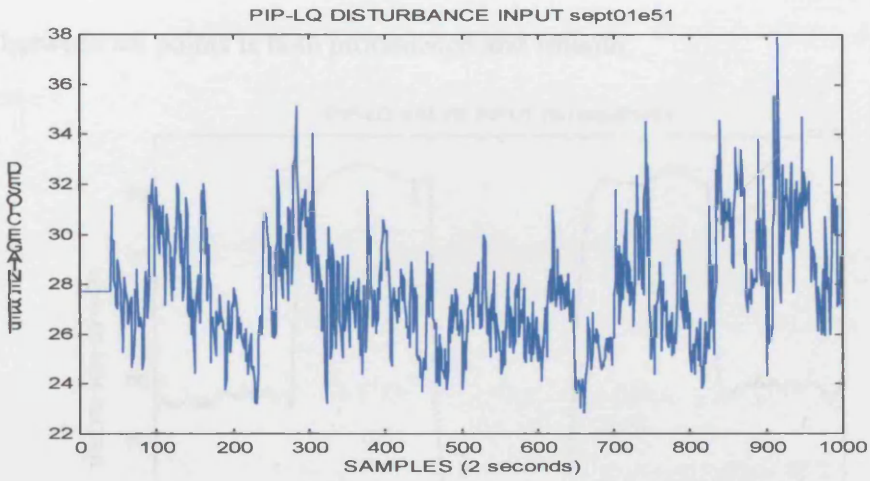

Figure 7.19: Wind disturbance signal to valve only control, showing the random nature of the disturbance.

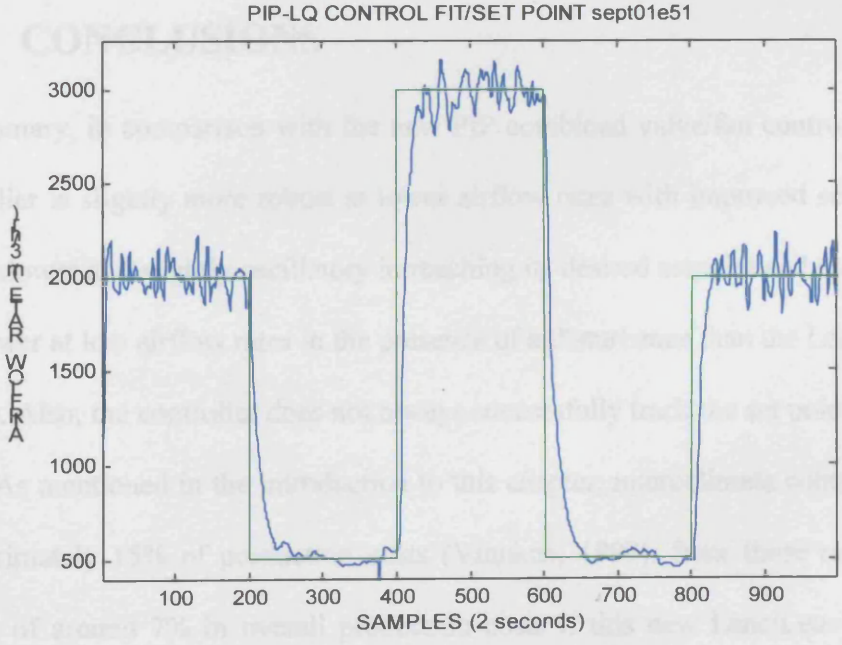

Figure 7.20: Control response to setpoint tracking with valve only control.

Figure 7.21 shows the valve position during the control implementation experiment. The transition between set points is both pronounced and smooth.

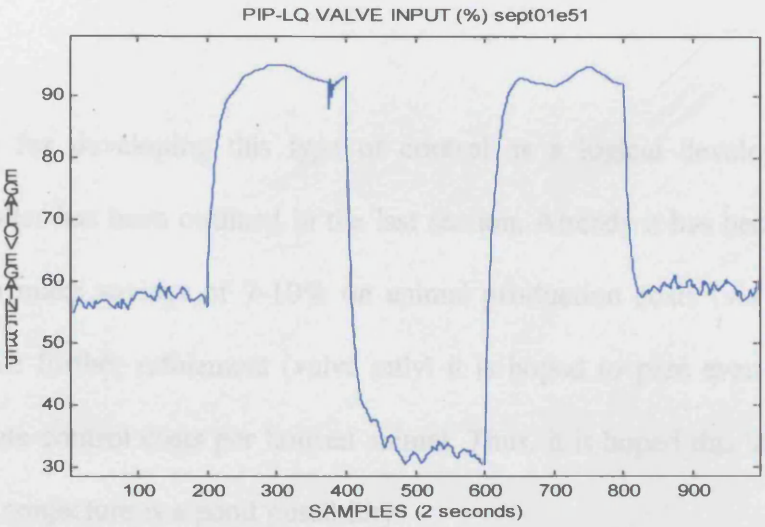

Figure 7.21: Valve input signal to maintain setpoint tracking with valve only control.

7.6 CONCLUSIONS

In summary, in comparison with the new PIP combined valve/fan control, the Industrial controller is slightly more robust at lower airflow rates with improved setpoint tracking, but is slower and slightly oscillatory in reaching its desired setpoint and uses up to double the power at low airflow rates in the presence of a disturbance than the Lanc/Leuv control design. Also, the controller does not always successfully track the set point at low airflow rates. As mentioned in the introduction to this chapter, microclimate control accounts for approximately 15% of production costs (Vranken, 1999), from these results there is a saving of around 7% in overall production costs if this new Lanc/Leuv control design should be installed in place of the current Industrial controller. Further refinements to this type of control; include utilising the throttling valve only control during high wind

disturbances from a particular direction (the previous section has shown this to be viable) and a combination type controller would produce further cost savings and should be tested in the field. Multi-objective PIP design could also produce advantageous improvements.

The motivation for developing this type of control as a logical development to the fan/valve controller has been outlined in the last section. Already it has been shown how it is possible to make savings of 7-10% on animal production costs (via microclimate control); with the further refinement (valve only) it is hoped to pare even more off the 15% microclimate control costs per housed animal. Thus, it is hoped this last section has shown how that conjecture is a good possibility.

Chapter 8

MULTIVARIABLE PIP CONTROL OF THE LANCASTER CHAMBER

This chapter demonstrates the utility of the Lancaster micro-climate chamber by implementing multivariable Proportional-Integral-Plus (PIP) control systems for ventilation rate and temperature. The control inputs are the voltages to the main fan and the heating element. As for the single input, single output examples considered in earlier chapters, it will be seen that such PIP controllers are able to exploit the full power of

optimal state variable feedback, here within a *multivariable* Non-Minimum State Space (NMSS) setting.

Since multivariable PIP control is not the focus of the present thesis, the author has worked closely with colleagues to design the actual control algorithm, which is implemented in its most basic form largely with default settings. In this regard, it should be pointed out that the primary objective of the chapter is to illustrate the feasibility of developing general multivariable control systems, such as PIP, using the on-line data acquisition hardware and software implementing by the author (see Chapter 3). However, as will be seen, this research also provides an initial step in the design of a complete multivariable micro-climate control system.

8.1 MULTIVARIABLE PIP CONTROL SYSTEM DESIGN

Multivariable PIP control can be applied to systems represented by either discrete-time, backward shift (Young *et al.*, 1994) and delta (δ) operator (Chotai *et al.*, 1997) or continuous-time (derivative operator) models (Young, 1996). However, in keeping with the earlier examples in this thesis, backward shift methods are employed for the research described below since they are so straightforward, yet are found to yield very good control of the ventilation system. In this case, consider the following 2-input, 2-output, discrete time system represented in terms of the left Matrix Fraction Description or MFD:

$$\boldsymbol{y}(k) = [\boldsymbol{A}(z^{-1})]^{-1}\boldsymbol{B}(z^{-1})\boldsymbol{u}(k) \tag{8.1}$$

where,

$$\boldsymbol{y}(k) = [y_1(k) \quad y_2(k)]^T \qquad \boldsymbol{A}(z^{-1}) = \boldsymbol{I} + \boldsymbol{A}_1 z^{-1} + \ldots\ldots + \boldsymbol{A}_n z^{-n}$$

$$\boldsymbol{u}(k) = [u_1(k) \quad u_2(k)]^T \qquad \boldsymbol{B}(z^{-1}) = \boldsymbol{B}_1 z^{-1} + \ldots\ldots + \boldsymbol{B}_m z^{-m}$$

Here, $\boldsymbol{y}(k)$ and $\boldsymbol{u}(k)$ are vectors of system outputs and control inputs respectively, $\boldsymbol{A}_i (i = 1,2,\ldots,n)$ and $\boldsymbol{B}_i (i = 1,2,\ldots,m)$ are 2 by 2 matrices of parameters, while z^{-i} is the backward shift operator, i.e., $z^{-i} y(k) = y(k-i)$. In this case, the ventilation rate $y_1(k)$ (m^3/hour) and temperature $y_2(k)$ (C) are controlled by the voltages applied to the main fan $u_1(k)$ and heating element $u_2(k)$. Note that some of the initial $\boldsymbol{B}_i$ terms can take null values to accommodate pure time delays in the system if necessary.

The model in equation (8.1) is formulated from the transfer functions identified for each input-output pathway of the multivariable system. In the present research, these transfer functions are identified from measured input-output data collected from planned experiments on the chamber, while the required identification and estimation analysis utilises the Simplified Refined Instrumental Variable (SRIV) algorithm (Young 1991, 1996).

8.1.1 MULTIVARIABLE NON-MINIMAL STATE SPACE FORM

The state vector for the NMSS form of equation (8.1) is defined as,

$$\boldsymbol{x}(k)^T = [\, \boldsymbol{y}(k)^T \;\; \boldsymbol{y}(k-1)^T \;\; \ldots \;\; \boldsymbol{y}(k-n+1)^T \;\; \boldsymbol{u}(k-1)^T \;\; \ldots \;\; \boldsymbol{u}(k-m+1)^T \;\; \boldsymbol{z}(k)^T \,] \qquad (8.2)$$

where $\boldsymbol{z}(k) = [z_1(k) \quad z_2(k)]^T$ is the following integral-of-error vector,

$$z(k) = z(k-1) + [\, y_d(k) - y(k)]$$ (8.3)

in which $y_d(k) = [y_{d1}(k) \quad y_{d2}(k)]^T$ is the reference or command input vector, where $y_{d1}(k)$ is the desired ventilation rate and $y_{d2}(k)$ the desired temperature. Having defined the above state vector, the NMSS representation can be formulated directly in the following form,

$$\begin{aligned} \boldsymbol{x}(k) &= \boldsymbol{F}\boldsymbol{x}(k-1) + \boldsymbol{G}\boldsymbol{u}(k-1) + \boldsymbol{D}\boldsymbol{y}_d(k) \\ \boldsymbol{y}(k) &= \boldsymbol{H}\boldsymbol{x}(k) \end{aligned}$$ (8.4)

where the state matrices are defined below.

$$\boldsymbol{F} = \begin{bmatrix} -\boldsymbol{A}_1 & -\boldsymbol{A}_2 & \cdots & -\boldsymbol{A}_{n-1} & -\boldsymbol{A}_n & \boldsymbol{B}_2 & \cdots & \boldsymbol{B}_{m-1} & \boldsymbol{B}_m & \boldsymbol{0} \\ \boldsymbol{I}_p & \boldsymbol{0} & \cdots & \boldsymbol{0} & \boldsymbol{0} & \boldsymbol{0} & \cdots & \boldsymbol{0} & \boldsymbol{0} & \boldsymbol{0} \\ \boldsymbol{0} & \boldsymbol{I}_p & \cdots & \boldsymbol{0} & \boldsymbol{0} & \boldsymbol{0} & \cdots & \boldsymbol{0} & \boldsymbol{0} & \boldsymbol{0} \\ \vdots & \vdots & \ddots & \vdots & \vdots & \vdots & \ddots & \vdots & \vdots & \vdots \\ \boldsymbol{0} & \boldsymbol{0} & \cdots & \boldsymbol{I}_p & \boldsymbol{0} & \boldsymbol{0} & \cdots & \boldsymbol{0} & \boldsymbol{0} & \boldsymbol{0} \\ \boldsymbol{0} & \boldsymbol{0} & \cdots & \boldsymbol{0} & \boldsymbol{0} & \boldsymbol{0} & \cdots & \boldsymbol{0} & \boldsymbol{0} & \boldsymbol{0} \\ \boldsymbol{0} & \boldsymbol{0} & \cdots & \boldsymbol{0} & \boldsymbol{0} & \boldsymbol{I}_r & \cdots & \boldsymbol{0} & \boldsymbol{0} & \boldsymbol{0} \\ \vdots & \vdots & \ddots & \vdots & \vdots & \vdots & \ddots & \vdots & \vdots & \vdots \\ \boldsymbol{0} & \boldsymbol{0} & \cdots & \boldsymbol{0} & \boldsymbol{0} & \boldsymbol{0} & \cdots & \boldsymbol{I}_r & \boldsymbol{0} & \boldsymbol{0} \\ \boldsymbol{A}_1 & \boldsymbol{A}_2 & \cdots & \boldsymbol{A}_{n-1} & \boldsymbol{A}_n & -\boldsymbol{B}_2 & \cdots & -\boldsymbol{B}_{m-1} & -\boldsymbol{B}_m & \boldsymbol{I}_p \end{bmatrix} \quad \boldsymbol{G} = \begin{bmatrix} \boldsymbol{B}_1 \\ \boldsymbol{0} \\ \boldsymbol{0} \\ \vdots \\ \boldsymbol{0} \\ \boldsymbol{I}_r \\ \boldsymbol{0} \\ \vdots \\ \boldsymbol{0} \\ -\boldsymbol{B}_1 \end{bmatrix} \quad \boldsymbol{D} = \begin{bmatrix} \boldsymbol{0} \\ \boldsymbol{0} \\ \boldsymbol{0} \\ \vdots \\ \boldsymbol{0} \\ \boldsymbol{0} \\ \boldsymbol{0} \\ \vdots \\ \boldsymbol{0} \\ \boldsymbol{I}_p \end{bmatrix}$$

and $\boldsymbol{H} = [\boldsymbol{I}_p \quad \boldsymbol{0} \quad \ldots \quad \boldsymbol{0}]$. Inherent type 1 servomechanism performance is introduced by means of the integral-of-error part of the state vector, $z(k)$. If the closed-loop system is stable, then this ensures that steady-state decoupling is inherent in the basic design (Young *et al.*, 1994). The controllability conditions for the NMSS model are described by Chotai *et al.* (1992).

8.1.2 MULTIVARIABLE PIP CONTROL

The state variable feedback (SVF) control law associated with the NMSS model (8.4) is defined in the usual fashion, i.e.,

$$\boldsymbol{u}(k) = -\boldsymbol{K}\boldsymbol{x}(k) \tag{8.5}$$

where $\boldsymbol{K}$ is the control gain matrix. This strategy results in a control system which can be structurally related to more conventional designs, such as multivariable PI and PID controllers, as illustrated in Figure 8.1.

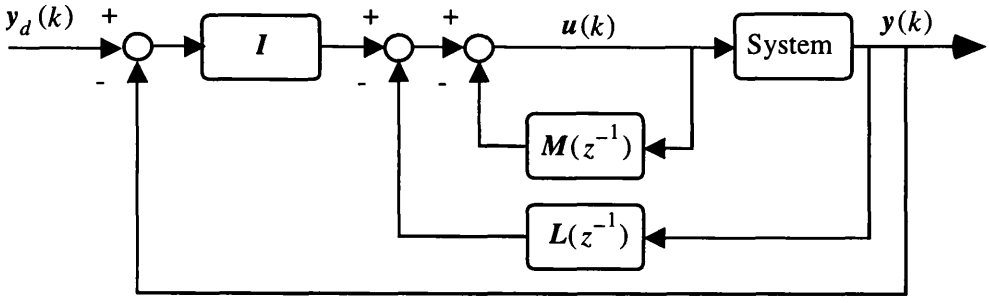

Figure 8.1: Multivariable PIP control in feedback form.

Here,

$$\begin{aligned}
\boldsymbol{L}(z^{-1}) &= \boldsymbol{L}_0 + \boldsymbol{L}_1 z^{-1} + \cdots + \boldsymbol{L}_{n-1} z^{-n+1} \\
\boldsymbol{M}(z^{-1}) &= \boldsymbol{M}_1 z^{-1} + \cdots + \boldsymbol{M}_{m-1} z^{-m+1} \\
\boldsymbol{I} &= \boldsymbol{k}_I (1 - z^{-1})^{-1}
\end{aligned} \tag{8.6}$$

This SVF approach can be used as a foundation for the design of PIP Linear Quadratic (PIP-LQ) controllers. Here, the requirement is to design a control gain matrix which minimises the following quadratic performance criterion,

$$J = \sum_{i=0}^{\infty} \boldsymbol{x}(i)^T \boldsymbol{Q}\boldsymbol{x}(i) + \boldsymbol{u}(i)^T \boldsymbol{R}\boldsymbol{u}(i) \tag{8.7}$$

where $\boldsymbol{Q}$ and $\boldsymbol{R}$ are symmetric positive semi-definite and symmetric positive definite weighting matrices, respectively. The feedback gain matrix which minimises the cost function can be determined by the steady state solution of the discrete time matrix Riccati equation (see e.g. Borrie, 1986).

It is clear that, due to the special structure of the non-minimal state vector, the elements of the LQ weighting matrices have a particularly simple interpretation, since the diagonal elements directly define the weights assigned to the measured input and output variables, together with the integral-of-error states. In this regard, the following convention is employed for the choice of the multivariable weighting matrices $\boldsymbol{Q}$ and $\boldsymbol{R}$ (Taylor *et al.*, 2000),

$$\boldsymbol{Q} = diag[\bar{y}_1 \ \ldots \ \bar{y}_n \ \bar{u}_1 \ \ldots \ \bar{u}_{m-1} \ \bar{z}] \tag{8.8}$$

where, in this 2 input, 2 output case, $\bar{y}_i (i = 1 \ldots n)$, $\bar{u}_i (i = 1 \ldots m-1)$ and $\bar{z}$ are all vectors with two elements each,

$$\begin{aligned}
\bar{y}_i (i = 1 \ldots n) &= \left[\frac{y_1^w}{n} \quad \frac{y_2^w}{n} \right] \\
\bar{u}_i (i = 1 \ldots m-1) &= \left[\frac{u_1^w}{n} \quad \frac{u_2^w}{n} \right] \\
\bar{z} &= \left[z_1^w \quad z_2^w \right]
\end{aligned} \tag{8.9}$$

in which, finally, y_1^w, y_2^w, u_1^w, u_2^w, z_1^w and z_2^w are the user selected weighting parameters. The corresponding input weighting matrix takes the following form,

$$\boldsymbol{R} = diag\left[\frac{u_1^w}{m} \quad \frac{u_2^w}{m}\right] \tag{8.10}$$

Although convoluted in description, the purpose of (8.8) to (8.10) is to simplify the choice of the LQ weightings, so that the designer selects only a total weight for (all the present and past values of) each input and output signal together with each integral of error state. The 'default' weightings are obtained by setting each of the user selected parameters to unity.

8.2 HEATING ELEMENT POWER CURVE

As discussed in Chapter 4, temperature in the chamber is controlled by a heating element at the inlet. For the present analysis, the control signal to this heating element is a scaled voltage in the range -0.8 (off) to 1.0 (maximum heating). Note that the inlet air is drawn from the laboratory in which the chamber is housed, so with the heating element turned off, the temperature of the chamber returns to room temperature.

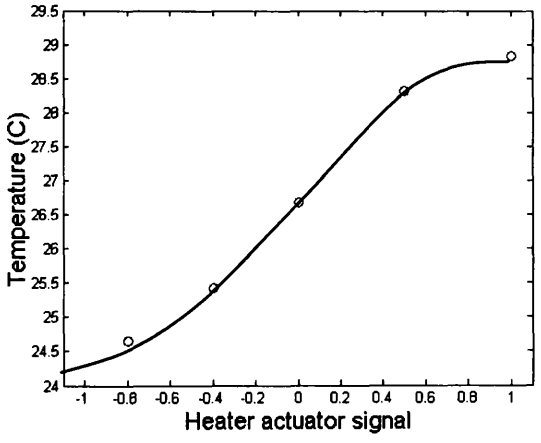

Figure 8.2: Heating element power curve showing the steady state temperature.

In this regard, a steady state S-curve showing the power of the heater is illustrated by Figure 8.2. Here, a constant voltage of 30% is applied to the main fan, so as to draw the heated air steadily through the chamber. For this particular ventilation rate and for the external temperature at the time of the experiments, it is evident the heating element is able to raise the temperature of the chamber by 4C.

8.3 MODELLING VENTILATION RATE AND TEMPERATURE

The multivariable PIP control algorithm discussed below is designed for the mid-range operating point of both the fan and heating element, corresponding to a ventilation rate of ~200m^3/hour (see Chapter 5) and a temperature elevated by ~2C above room temperature (see Figure 8.2). In this regard, the top two plots of Figure 8.3 below, illustrate the response of ventilation rate (left) and temperature (right) to an open loop experiment utilising a sequence of steps in the fan voltage between 25 and 35 percent, while the signal to the heating element is specified as zero. Similarly, the lower two plots of Figure 8.2 are for an experiment utilising a sequence of steps to the heating element signal in the range -0.8 and +0.8, while the voltage to the fan is fixed at 30%.

As for the single input, single output designs, a sampling rate of 2 second is employed throughout this chapter, since this yields adequate control performance and is within the capabilities of the current hardware implementation. Utilising the data in Figure 8.2, the following transfer function matrix is identified for the micro-climate system,

$$\begin{bmatrix} y_1(k) \\ y_2(k) \end{bmatrix} = \begin{bmatrix} \dfrac{2.6117z^{-1}}{1-0.6305z^{-1}} & \dfrac{-0.1177z^{-1}}{1-0.8044z^{-1}} \\ \dfrac{-0.0131z^{-1}}{1-0.8755z^{-1}} & \dfrac{0.0045z^{-1}}{1-0.9812z^{-1}} \end{bmatrix} \begin{bmatrix} u_1(k) \\ u_2(k) \end{bmatrix} \tag{8.11}$$

where $y_1(k)$ is the ventilation rate (m^3/hour), $y_2(k)$ the temperature (C), and $u_1(k)$ and $u_2(k)$ are the main fan and heating element input signals respectively.

In order to ensure a low order control algorithm that is straightforward to implement, a 1st order transfer function model has been specified for each input-output pathway. This yields a good model fit between the fan and both the ventilation rate and temperature ($R_T^2 = 0.9976$ and $R_T^2 = 0.9517$ respectively), as illustrated by the top two figures of Fig. 8.3. However, the same model structure is less successful for when the heating element is the driving input to the system, as illustrated by the bottom two plots of Figure 8.3; here, $R_T^2 = 0.3458$ and $R_T^2 = 0.9575$ for ventilation rate and temperature respectively. In this regard, it should be pointed out that the heating element has only a very small influence on the ventilation rate, while it is clear from the implementation results discussed below that the model for temperature is satisfactory for control system design purposes.

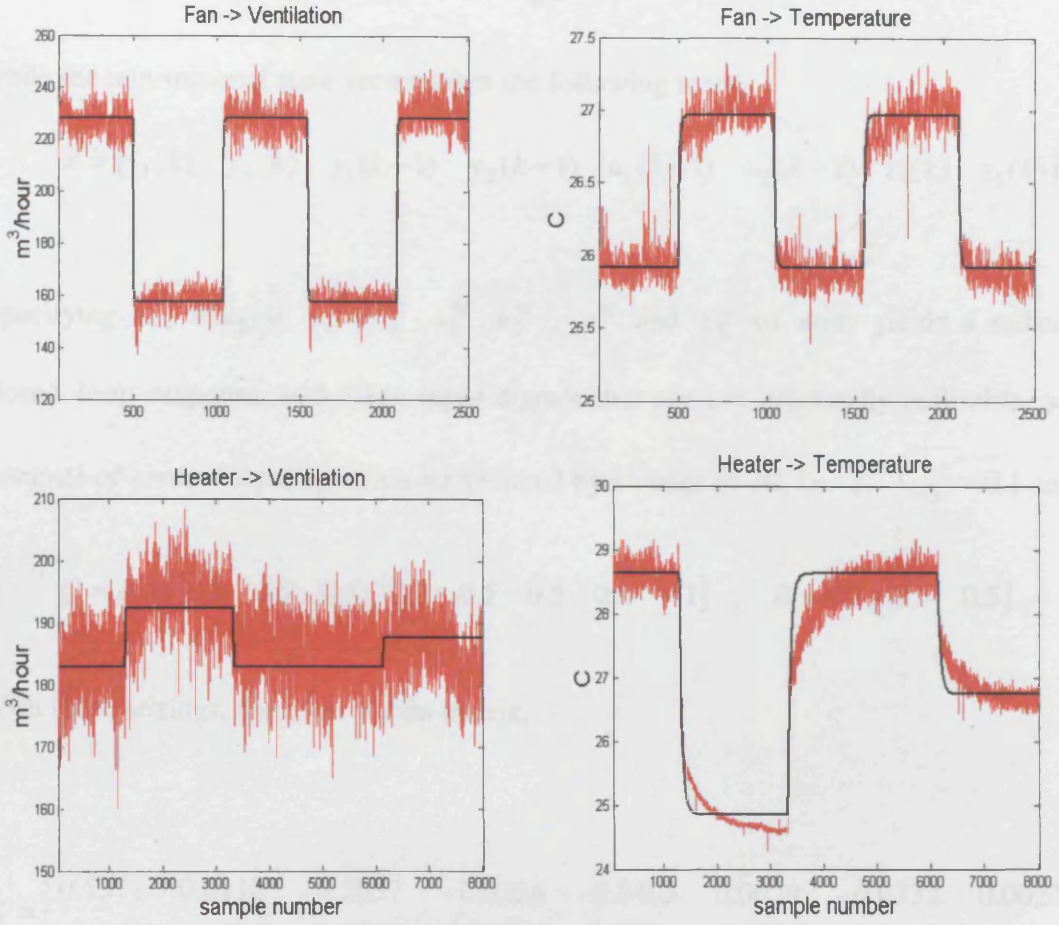

Figure 8.3: Response of ventilation rate (left) and temperature (right) to an open loop experiments utilising a sequence of steps in the fan voltage (top) and heating element (bottom); the 1st order transfer function response is also shown as the smooth thick trace in each plot.

8.4 CONTROL DESIGN FOR VENTILATION RATE AND TEMPERATURE

The transfer function models (8.11) are written in MFD form (8.1) as follows,

$$A_1 = \begin{bmatrix} -1.5060 & 0 \\ 0 & -1.7855 \end{bmatrix} \; ; \; A_2 = \begin{bmatrix} 0.5520 & 0 \\ 0 & 0.7892 \end{bmatrix} \tag{8.12}$$

$$\boldsymbol{B}_1 = \begin{bmatrix} 2.6117 & -0.0131 \\ -0.1177 & 0.0045 \end{bmatrix} \; ; \; \boldsymbol{B}_2 = \begin{bmatrix} -2.2865 & 0.0083 \\ 0.1155 & -0.0036 \end{bmatrix}$$

while the non-minimal state vector takes the following form,

$$\boldsymbol{x} = [y_1(k) \quad y_2(k) \quad y_1(k-1) \quad y_2(k-1) \quad u_1(k-1) \quad u_2(k-1) \quad z_1(k) \quad z_1(k)]^T \tag{8.13}$$

Specifying LQ weights y_1^w, y_2^w, u_1^w, u_2^w, z_1^w and z_2^w of unity yields a rather fast closed loop response with large input signals that are not practically realisable, so the *integral-of-error* weighting terms are reduced by a factor of 10, i.e. $z_1^w = z_2^w = 0.1$ so that,

$$\boldsymbol{Q} = diag[0.5 \quad 0.5 \quad 0.5 \quad 0.5 \quad 0.5 \quad 0.5 \quad 0.1 \quad 0.1] \; ; \; \boldsymbol{R} = diag[0.5 \quad 0.5] \tag{8.14}$$

With these settings, the control gain matrix,

$$\boldsymbol{K} = \begin{bmatrix} 0.5371 & 0.0110 & -0.2037 & -0.0234 & -0.8403 & 0.0029 & -0.0332 & 0.0023 \\ 0.1701 & 18.7751 & -0.0987 & -14.7667 & 1.7527 & -0.0655 & -0.0081 & -0.0989 \end{bmatrix}$$

(8.15)

and the theoretical closed loop response is illustrated in Fig. 8.4 below. Here, the top two plots show the predicted response of ventilation rate (left) and temperature (right) to a unit step in the desired ventilation rate $y_{d1}(k)$, with $y_{d2}(k) = 0$. Similarly, the lower two plots show the response to a unit step in the desired temperature $y_{d2}(k)$, with $y_{d1}(k) = 0$. In this manner, Fig. 8.4 shows the response to a change in the demand (diagonal plots) and the associated cross coupling in each case (off-diagonal plots).

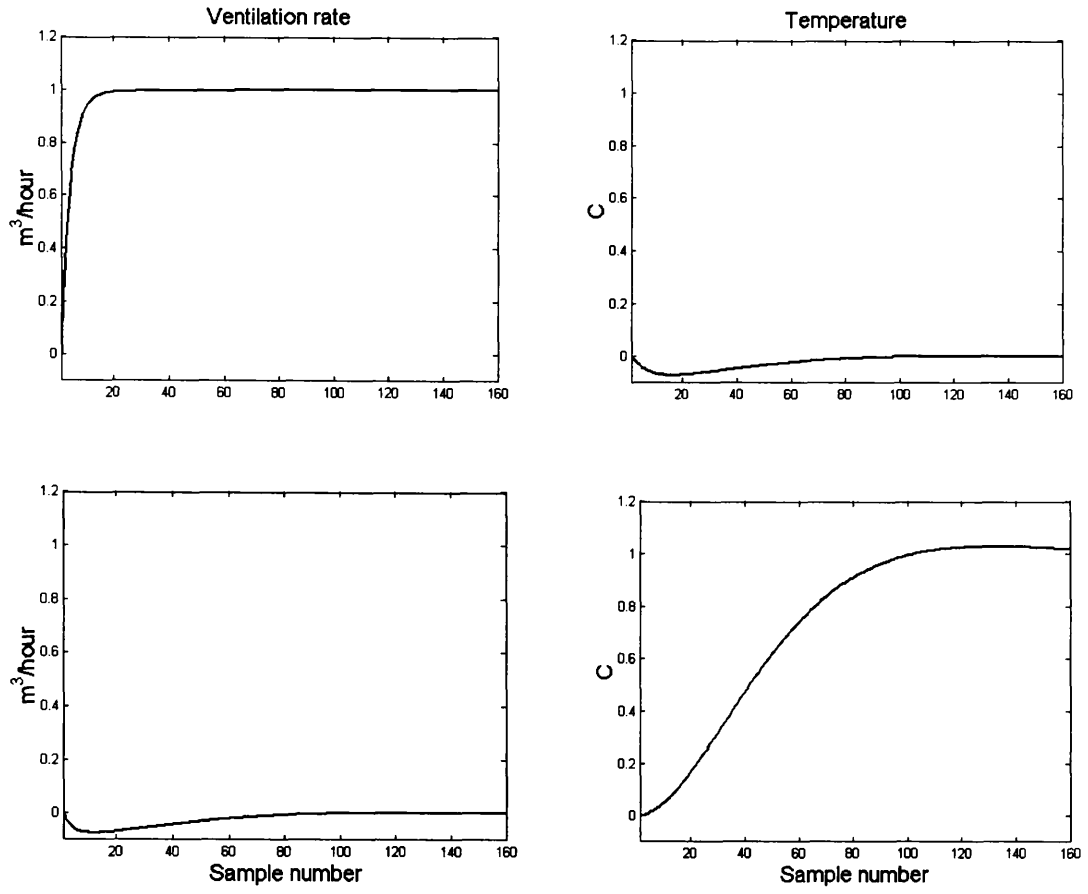

Figure 8.4: Theoretical closed loop response.

In the present research, adequate *steady state* closed loop control responses were quickly obtained by manually tuning the weighting parameters as discussed above. However, it is clear from Fig. 8.4 that some transient cross coupling between the variables occurs, which presages certain problems when the controller is implemented on the chamber (see section 8.5 below). One recently developed technique available for *automatically* mapping the various control requirements into elements of the $\boldsymbol{Q}$ and $\boldsymbol{R}$ matrices (including the off-diagonal elements), is multi-objective optimisation in its goal attainment form (Chotai *et al.*, 1997). This method optimises the Cholesky factors of the weighting matrices and hence generates only guaranteed stable optimal solutions. Such an

approach would be a useful starting point for future research into the multivariable climate control problem.

8.5 CONTROL IMPLEMENTATION

Figure 8.5 illustrates the response of the multivariable PIP controller with the disturbance fan turned off. It is clear that both ventilation rate and temperature are adequately controlled, with steady state decoupling between the variables. The airflow stays within 10% of the its point for the entire experiment, while the temperature also tracks the desired level well, fluctuating by around 1°C, well within acceptable limits required by a climate control system. Furthermore, both variables respond quickly to changes in their demanded level.

Note that the high temperatures requested towards the end of the experiment are not realisable in practice, since the heating element is at its maximum power (1.0 on the bottom right plot). However, the incremental form of the PIP algorithm ensures that integral wind up does not occur and, in each case, control is smoothly restored once a more realistic lower temperature is demanded.

As expected from the theoretical response, there is a degree of transient coupling between ventilation rate and temperature, although for the most part this is well within acceptable limits. One exception appears to be the 2-3 °C change in temperature following the large steps in ventilation rate after 300 and 680 samples. Of course, temperature is particularly sensitive to such changes in ventilation rate and it is clear that further investigation is required to reduce these cross coupling affects. In this regard, an improvement in the

heating element to temperature model is one possible avenue of improvement (Figure 8.3).

Finally, consider Figure 8.6, which shows the response of the control system when the disturbance fan is activated to represent a time varying pressure disturbance, as shown in Figure 8.7. Although large disturbances clearly do cause a temporary deviation from the set point, the control fan and heating element are quickly adjusted to maintain the demanded environment.

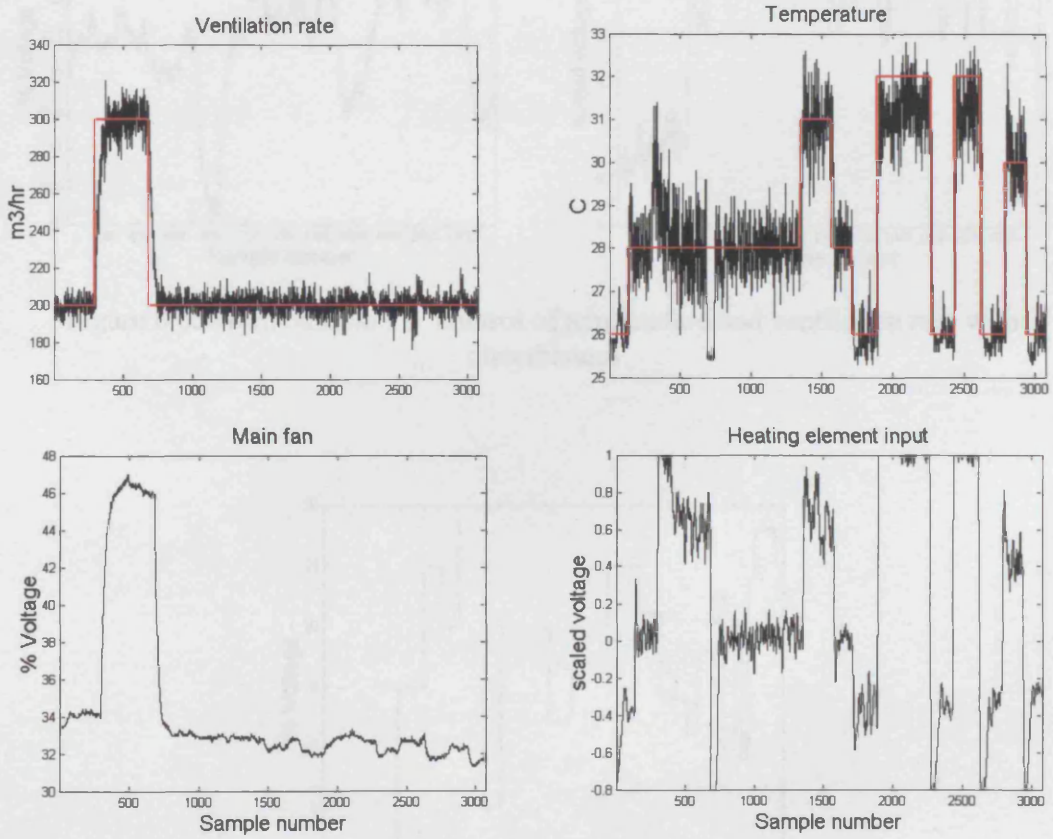

Figure 8.5: Multivariable PIP control of temperature and ventilation rate.

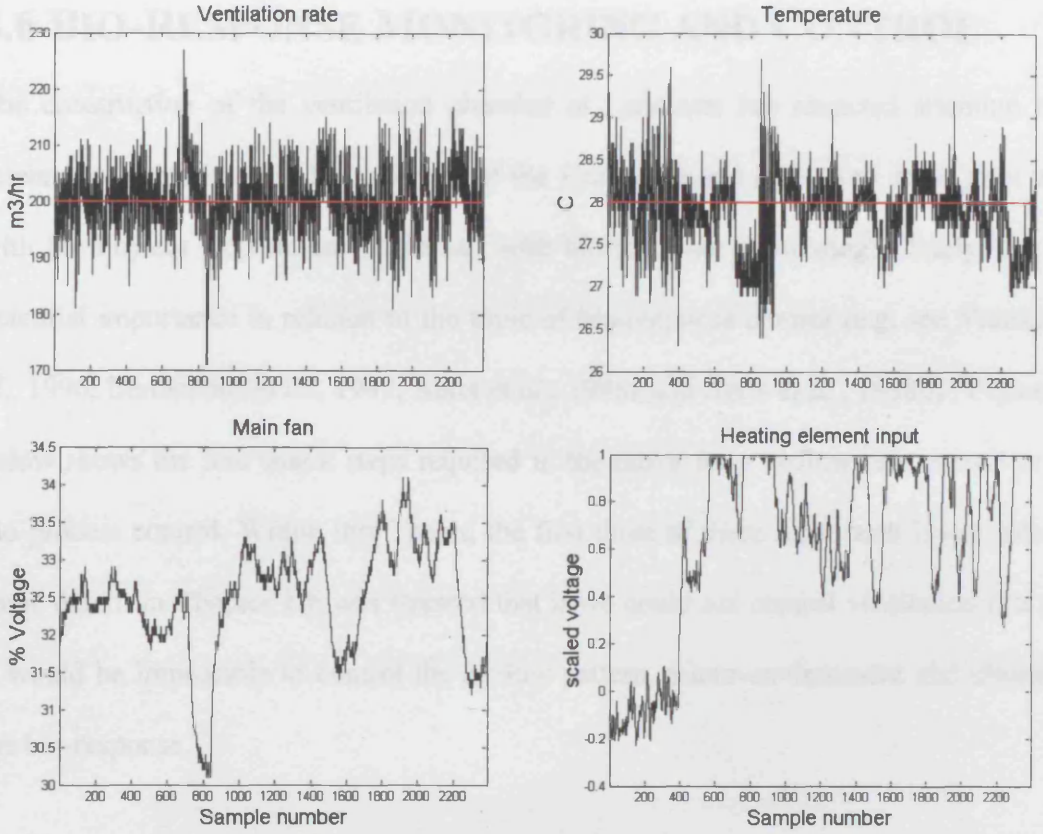

Figure 8.6: Multivariable PIP control of temperature and ventilation rate with disturbances

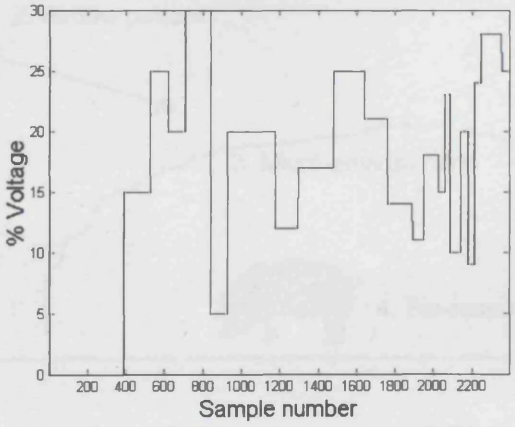

Figure 8.7: Disturbance fan input utilised for Figure 8.6.

8.6 BIO-RESPONSE MONITORING AND CONTROL

The construction of the ventilation chamber at Lancaster has attracted attention from research workers in other Departments at the University and has led to some joint work with the Physics Department concerned with bio-response monitoring. Clearly, this has potential importance in relation to the topic of bio-response control (e.g. see Vranken *et al.*, 1996; Berckmans *et al.*, 1997; Aerts *et al.*, 1998a and Aerts *et al.*, 1998b) . Figure 8.8 below shows the four major steps required in the move from airflow rate control to full bio-process control. Within this Thesis, the first three of these have been investigated in some detail. In Chapter 1 it was stressed that if we could not control ventilation rate then it would be impossible to control the airflow pattern, micro-environment and ultimately the bio-response.

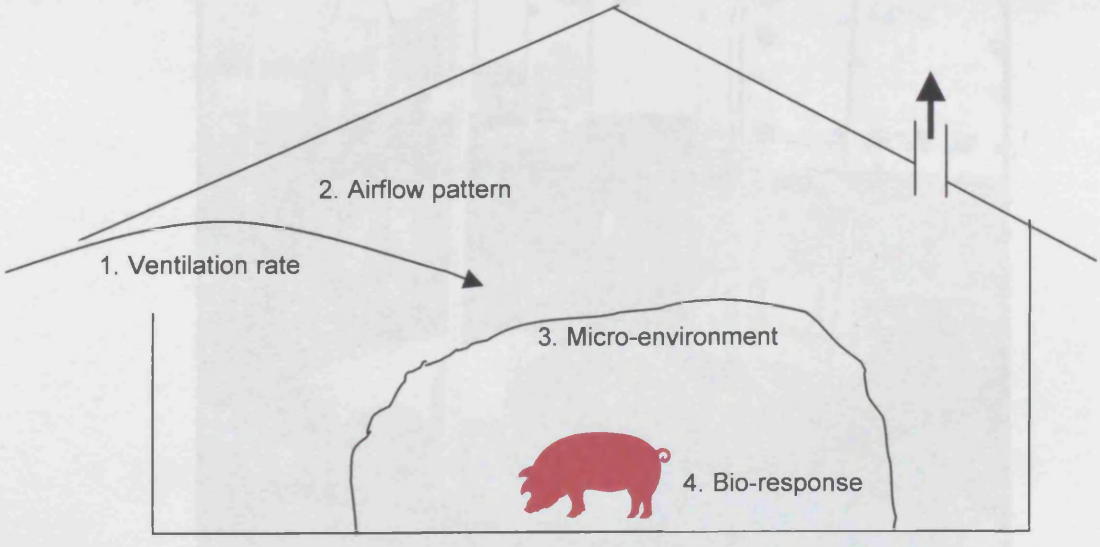

Figure 8.8: Four steps in bio-process control (Vranken, 1999).

Table 8.1: Measured parameters and their sampling interval for bio-response experiments.

Parameter	Units	Sampling interval (Hz)
Temperature 1 (air)	Degrees centigrade	10
Temperature 2 (air)	Degrees centigrade	400
Body temperature 3 (skin)	Degrees centigrade	400
Airflow above head	m^3/hr	10
Airflow in chamber	m^3/hr	10
Heart rate (ECG)	BPM	400
Breathing rate	BPM	400
Blood volume flow	L/min	400

Table 8.2: Details of bio-response experiments.

File name	Chamber contents	Experiment type
Stef1	Volunteer + fan (airflow of ~65-70m^3/hr)	Volunteer in chamber with control fan at 15% voltage
Stef2	Just the Volunteer	Volunteer in completely isolated chamber (no fan)
Stef3	Just Air	An empty completely isolated chamber (no fan)

The initial results from this set of experiments show that temperature and air velocity oscillations are caused by the human body inside the chamber and the work will continue to further evaluate these and other phenomena. The importance to the present project is the demonstration that such monitoring is already feasible and it could open the way to research on bio-response control along the above lines.

8.7 CONCLUSIONS

A multivariable Proportional-Integral-Plus (PIP) control system for ventilation rate and temperature, utilising the main fan and the heating element as control inputs, has been designed and implemented for the Lancaster micro-climate chamber. The preliminary

results presented in this chapter are very promising, with the airflow typically maintained within 5% of the its point and the temperature within 1°C. However, it is clear that further research is required in order to reduce the cross coupling between these variables and to investigate the performance of the system across a wide range of operating conditions.

The present chapter demonstrates the multivariable functionality of the Lancaster chamber, with the on-line data acquisition hardware and software framework developed by the author allowing for the simultaneous monitoring and control of two or more climate variables. In this regard, it is anticipated that the chamber will be used intensively over the next few years for further research into multivariable and nonlinear control.

Chapter 9

CONCLUSIONS AND FURTHER WORK

9.1 CONCLUSIONS

The main contributions and objectives of the research project described in this Thesis relate to developments in the modelling and advanced control of ventilation systems in two different micro-environment chambers. This has included the design and implementation of model-based fixed gain, schedule adaptive and fully adaptive PIP control systems on the Leuven chamber; control systems that have not previously been

implemented in a test chamber of this kind. In addition, a fan/valve control system has been designed that provides a novel and practical approach to problems of stability at low airflow rates, especially in the presence of disturbances. The fan/valve system design has also proven to be a very cost-effective method of instilling robustness at low airflow rates.

The other main contribution is the design and construction of an experimental ventilation chamber in Lancaster. This has been used for the initial studies on the multivariable (MIMO) control of ventilation rate and temperature in the chamber, as described in Chapter 8. It will now be used for future research on multivariable and nonlinear control system design, as well as providing a potential facility for other, unrelated research (see later). Previously no similar facility of this kind has existed at Lancaster and the chamber is now an integrated high quality adaptable research test chamber for carrying out research into the modelling and control of micro-climate systems. As such, the chamber has already allowed us to initiate experimental research on forced ventilation and heating in a simulated experimental agricultural building, adding to the experience of previous research in this area[1].

In addition to these main contributions, a series of experiments were carried out on the Leuven chamber in an attempt to capture the non-linear dynamics of the system for non-linear modelling and, ultimately, control purposes. Although time constraints and problems with experimental design have prevented further work on these results, they

[1] Incidentally, the facility also serves as a teaching aid for control courses in both Engineering and Environmental Science at Lancaster.

will be the subject of future research (see later). As reported briefly in Chapter 8, the author has also helped colleagues in the Physics Department at Lancaster to exploit the Lancaster chamber for monitoring human response. The importance of this work to the present project is the demonstration that such monitoring is already feasible and it could open the way to research on bio-response control (see later).

9.2 FUTURE RESEARCH

There is plenty of scope for further research designed to exploit either of the chambers utilised in the present project. Full use of the 3D array of thermocouple has not been realised to date in the Lancaster chamber but the recent purchase of new data logging equipment should help facilitate this and so enable 3D representations of the temperature distributions in the chamber to be investigated. Additionally, a vortex damper is ready to be installed in the chamber so that the unique fan/valve control design can be evaluated and possible developed further in Lancaster. Additionally, our links to the Katholieke Universität of Leuven remain strong and it is hoped that collaboration will continue on topics currently being pursued there, such as "Process control of intensive cattle farming"; "Development of a quantitative method for a more objective evaluation of the animal welfare in existing and new housing systems for broiler chickens"; "Air Recycling Pig System: research on a sustainable profitable system for the Dutch pig industry"; and "Automatic adaptive control of the climate in pig houses based on biomarkers as informers of infection processes". It is intended that the techniques acquired during this research can be put to use in a collaborative manner in some of the above mentioned projects or other projects as they come online.

Future research based on the Lancaster microclimate chamber is already planned and funded. It will be concerned with the further development of the current MIMO PIP control system designs, as well as research on nonlinear modelling, control system design and implementation. Currently, airflow and temperature are the measurable outputs, while an axial fan and heating element provide the inputs. A useful extension of this design could involve an additional inlet, with or without fan assistance, by which cold air (via an air conditioning unit) could be pumped into the chamber, as well as warm/hot air. This would allow the scenario of temperature regulation to be faster and more controllable in applications where such tight control is required: for example: an adaptation of this system could be fitted in motor vehicles for hot or cold climates. Clean rooms, incubators, a controlled microclimate for certain foods and the storage of foods such as grain within a warehouse environment. Such control could involve a valve that switches between warm and cold air depending on what the controller calls for at a particular operating level and temperature.

There is considerable current interest in nonlinear modelling and control. At Lancaster, for instance, research in this regard has centred on modelling and control of a widely applicable *State Dependent Parameter* (SDP) class of nonlinear stochastic system (e.g. Young, 2000, 2001; McCabe, 2000; Young *et al*, 2001, 2002). Initial work in the present project (see above) has established that the Leuven experimental chamber can be modelled in this manner, so an obvious topic of future research is the continuation of these initial studies, with a view to the design and implementation of a fully nonlinear SDP control system on either the Leuven or the Lancaster chamber. The initial studies have revealed that an important aspect of such research will be the design of experiments

that produce data suitable for comprehensive SDP model, identification and estimation (the main reason why more work on this was not possible in the present project). Also, the research reported in McCabe (2001) and Young *et al* (2002b) has established the need for more theoretical research on the global controllability of SDP systems, so any applied research will need to go hand-in-hand with such theoretical studies.

Future work could include implementing the control designs proposed in this thesis on a real livestock building. An ideal scenario would be to have a number of identical buildings with the same orientation and for example test the adaptive and scheduled gain controllers. The "plug and play" ability of the adaptive control design may make this an attractive option to the livestock farmer. Additionally, an implementation of the fan/valve arrangement in a real building would be an interesting advancement of this particular design.

Another option is to utilise the 3D facility within the Lancaster chamber for temperature distribution within the chamber envelope. Within this scenario, use of the "simulated" animal could be investigated. Also, for the purposes of this thesis, the airflow was measured close to the inlet and outlets; however, due to the mobility of the air velocity transducer the airflow could be measured at any pre-defined point within the chamber.

A further research line could be to utilise the methods described in this work and apply them to air conditioning control of buildings and offices. These methods may be able to help alleviate symptoms of "sick building syndrome" often present in large office blocks.

This thesis has also investigated CFD modelling as an alternative to DBM. Perhaps another avenue of research could be to investigate the problems of calibrating CFD for future use in ventilation control.

The bio-response experiments described in chapter 8 (section 8.5) could be expanded and a collaborative experiment between Leuven and Lancaster should be possible to further this.

A number of unrelated research projects have also taken advantage of the micro-environmental chamber in Lancaster. These include: "Investigation into the effects of windspeed on the performance of novel passive air samplers for persistent organic pollutants" and "The calibration of a number of anemometers for a wind shear experiment in the lower boundary layer". Further details on these collaborative projects can be found on a web page relating to work done with the Lancaster micro-environmental chamber (Taylor, 2003).

REFERENCES

REFERENCES

Andonov, K.J., Daskalov, P.I., and Martev, K.V. 1989, Microclimate system for livestock building with controlled natural ventilation. *Agric. Eng., Bulgaria.*, **2**, 55-62.

Aarnink, A.J.A, Wagemans, M.J.M. and Keen, A., 1993, Factors Affecting Ammonia Emission from Housing of Weaned Piglets, Proc. 1st Int. Sympp. On Nitrogen Flow in Pig Production and Environmental Consequences, *Ed. Verstegen M.W.A., Pudoc Scientific Publishers*, Wageningen, Netherlands, pp.286-294.

Attwood, P., Brouwer, R., Ruigiwaard, P., Versloot, P., De Wit, R., Heederik, D., and Boleij, J.S.M., 1987, A study of the Relationship between Airborne Contaminants and Environmental Factors in Dutch Swine Containment Buildings. *Am. Ind. Hyg. Assoc. Jnl.*, **48**, 745.

Awbi, H.B., 1989, Application of Computational Fluid Dynamics in Room Ventilation, *Bldg. Envir.* **24**, 73-84.

Barber, E.M., 1981, Scale Model Study of Incomplete Mixing in a Ventilated Airspace, *Unpublished Ph.D. Thesis, University of Guelph*, Ont.

Barber, E.M., and Ogilvie, J.R., 1982, Incomplete Mixing in Ventilated Airspace's. Part 1. Theoretical Considerations, *Canadian Agric. Engng.*, **24**, No. 1, pp.25-29.

Berckmans, D. and Goedseels, V. 1986, Development of New Control Techniques for the Ventilation and Heating of Livestock Buildings, *J. Agric. Engng. Res.* **33**, 1-12.

Berckmans, D. and Goedseels, V. 1988, Modelling and Controlling Ventilated Agricultural Structures, *Building Systems and Air Contaminant Distribution*, Ed. Christianson, L.L., University of Illinois at Urbana-Champaign.

Berckmans, D., De Moor, M. and De Moor B. 1992, Test Installation to Develop a New Model Concept to Model and Control the Energy and Mass Transfer in a Three Dimensional Imperfectly Mixed Space, *Proceedings of Roomvent 92: Air distribution in rooms,* Aalborg, Denmark.

Berckmans, D., Ni, J.Q., Coengegrachts, J. and Vranken, E., 1994, Influence of the Control of Ventilation Rate on Ammonia Emission in a Pig House, International Winter Meeting ASAE, Atlanta, USA, (Paper no. 94-4589).

Bird, R.B., Stewart, W.E. and Lightfoot, E.N., 1960, Transport Phenomena, *John Wiley & Sons, Inc.* London, UK.

Boon, C.R., 1978, Airflow Patterns and Temperature Distribution in an Experimental Piggery, *J. Agric. Engng. Res.* 23, 129-139.

Borrie, J.A., 1986, Modern Control Systems: A Manual of Design Methods, *Prentice Hall*, New York).

Brockett, B.L. and T.D. Albright. (1983). Natural ventilation in single airspace buildings. *J. Agric. Eng. Res.*, 37, 141-154.

Bruce, J.M., 1979, Automatically controlled natural ventilation. *Farm Building Progress*, 58, 1-2.

Bruce, J.M., 1981, Ventilation and temperature control criteria for pigs. In: *Environmental Aspects of Housing for Animal production*, (Ed. J.A. Clark). pp. 197-216. London. Butterworths.

Bruce, J.M. and Clarke, J.J., 1979, Models of Heat Production and Critical Temperature for Growing Pigs, *Animal Production*, **28**, 353-369.

Buyse, J., Simons, P.C.M., Boshouwers, F.M.G. and Decuypere, E., 1996, Effect of Intermittent Lighting. Light intensity and source on the performance and welfare of broilers, *World Poultry Science Journal*, **52**, 121-130.

Callendar, A., Hartree, D.R. and Porter, A., 1936, Time Lag, in a Control System, in Philos. Trans. R. Soc. London A. London: Cambridge University Press.

Carpenter, G.A. 1986, Effects of Internal Air Filtration on the Performance of Broilers and the Aerial Concentrations of Dust and Bacteria, *British Poultry Science*, **27** (3), 471-480.

Cockshull, K.E., 1988, The integration of plant physiology with physical changes in the greenhouse climate. *Acta Horticulturae.* pp. 113-123.

Chotai, A. and Young, P.C., 1993, Glasshouse Systems: Automatic Control, *Concise Encyclopaedia of Environmental Systems*, Ed. Young, P.C. pp.263-267.

Chotai, A. and Young, P.C., 1991, Self adaptive and self tuning control of a nutrient film technique (NFT) system, *IFAC Workshop on Mathematical Control Applications in Agriculture and Horticulture*, Matsuyama, Japan.

Chotai, A., Young, P.C. and Tych, W., 1992, Dynamic decoupling, pole assignment and servo-mechanism design for multivariable NMSS discrete-time systems. *6th IMA Conference on Control, Modelling, Computation and Information*, (UMIST).

Chotai, A., Young, P.C., Mckenna, P.G. and Tych, W., 1997, Proportional-Integral-Plus (PIP) design for delta (δ) operator systems: Part 2, MIMO systems. *Int. J. Control*, 70, 149-168.

Cole, G.W., 1980, The Derivation and Analysis of The Differential Equations for the Air Temperature of the Confined Animal Housing System, *American Society of Agricultural Engineers*, pp.712-720.

Cole, G.H.A., 1962, Fluid Dynamics. *Methuen & Co. Ltd.* London, UK.

Clarke, D.W., Mohtadi, C. and Tuffs, P.S. 1987. Generalised Predictive Control – Part 1. The Basic Algorithm. *Automatica*, Vol. 23, **2**, 137-148.

Clarke, D.W., Mohtadi, C. and Tuffs, P.S., 1987, Generalised Predictive Control – Part 2. Extensions and Interpretations. *Automatica*, Vol. 23, **2**, 149-160.

Curtis, S.E., 1983, Environmental Management in Animal Agriculture, Ames: The IOWA State University Press, Iowa.

Daskalov, Daskalov, P.I., 1997, Prediction of Temperature and Humidity in a Naturally Ventilated Pig Building. *J. Agric. Eng. Res.* 68, 329-339.

Davis, P.F., & Hooper, A.W., 1991, Improvement of greenhouse heating control. IEE Proceedings, Control Theory and Applications 138, 249.

Davis, P.F. and Bailey, B.J., 1993, Glasshouse Crops: Control of Environment, AFRC Institute of Engineering Research, Silsoe, UK. *Concise Encyclopaedia of Environmental Systems*, Ed. Young, P.C. pp.260-263.

De Moor, M. and Berckmans, D., 1993, Visualisation of measured three dimensional well mixed zones of temperature in a ventilated space, *Energy impact of Ventilation and Air infiltration*, 14th AIVC Conference, Copenhagen, Denmark.

De Moor, M. and Berckmans, D., 1993, Analysis of the Control of Livestock Environment by Mathematical Identification on Measured Data, *ASEA Meeting Presentation*, Paper No. 934574. Chicago, Illinois, USA.

De Moor, M. and Berckmans, D., 1993, Visualisation of measured three-dimensional well-mixed zones of temperature in a ventilated space. Energy impact of Ventilation and Air infiltration. *14th AIVC Conference*, Copenhagen, Denmark.

De Moor, M., 1996, Modelling and control of energy and mass transfer in imperfectly mixed fluids. *Dissertationes de Agricultura*. Katholieke Universiteit Leuven, Belgium.

Doering, C.R., and Gibbon, J.D., 1995, Applied analysis of the Navier-Stokes Equations. *Cambridge University Press*, Cambridge, UK.

Gates, R.S., Chao, K., and Sigrimis, N., 2001, Identifying Design Parameters for Fuzzy Control of Staged Ventilation Control Systems, Computers and Electronics in Agriculture, **31** (1), 61-74.

Geers, R., Berckmans, D., Goedseels, V., Wynhoven, J., and Maes, F., 1984, A case study of fattening pigs in Belgian contract farming. *Animal Production*, **38**, 105-111.

Geers, R., Goedseels, V., Berckmans, D., and Huybrechts, D., 1984, Effect of season and environmental control on mortality and feed conversion of pigs. *Livestock Production Science*, **11**, 235-241.

Geers, R., Dellaert, B., Goedseels, V., Vranken, E., Maes, F., and Berckmans, D., 1989, An Assessment of Optimal Air Temperatures in Pig Houses by the Quantification of Behavioural and Health-Related Problems. *Animal Production*, **48**, 491-578.

Gilham, S., Deaves, D.M., Hoxey, R.P., Boon, C.R. and Mercer, A., 1997, Gas build-up within a single building volume - comparison of measurements with both CFD and simple zone modelling. *J. of Hazardous Materials*. 53, 93-114.

Gloster, J. Donaldson, I., and Hough, M.N., 1984, Analysis of a series of Outbreaks of Aujeszky's Disease in Yorkshire (1981-82): The Possibility of Airborne Disease Spread, Veterinary Record, **114**, 234-239.

Gosman, A.D., P.V. Neilson, A Revisto and J.H. Whitlaw.,1980,The flow properties of rooms with small ventilation openings. *J. Fluids Engineering, ASME Trans.* 102, 316-323.

Gunn, H.M. and Wilson, B. 1991, Observations on Outbreaks of Respiratory Disease in Intensively Housed Feedlot Cattle and Climatic Considerations, *Irish Veterinary Journal*, 44 (4-6), 41-42.

Guss, S.B.,1973, Effects of Housing on the Health of Dairy Cows, *National Dairy Housing Conference*, ASME, 120-127.

Hartung, E., Buscher, W. and Jungbluth, T., 1994, Basic Research on Ammonia Release in Livestock Production using Liquid Manure Pits, Procc. Int. Conference on Agricultural Engineering, AGENG 1994, Milan, 1901, pp. 197-198.

Harral, B.B. and Boon, C.R.,1997,Comparison of predicted and measured air flow patterns in a mechanically ventilated livestock building without animals. *J. Agric. Eng. Res.* 66, 221-228.

Hebner, A.J., Boon, C.R. and Peugh, G.H.,1996,Air patterns and turbulence in an experimental livestock building. *J. Agric. Eng. Res.* 64, 209-226.

Heitman, H and E.H. Hughes, 1949,The effects of air temperature and relative humidity on the physiological well-being of swine. *Journal of Animal Science*, 8, 171-181.

Jouini, D.B., Said, M.N. and Pletts, E.G.,1994,Measurement of Room Air Distribution in a Ventilated Office Environment, *Building and Environment*, 29, No. 4, pp. 511-521.

Julian, R.J., 1993, Ascietes in Poultry, *Avian Pathology*, **22**, 419-454.

Kreider, J.F. and Rabl, A.,1994,Heating and Cooling of Buildings: Design for Efficiency. *McGraw-Hill Book Co.* Singapore.

Kuo, B.C., 1980, Digital Control Systems, Holt Reinhart and Winston, New York.

Lees, M.J.,1996,Multivariable Modelling and PIP Control of Greenhouse Climate., *PhD Thesis*, Lancaster University, UK.

Leigh, P.A.,1999,Modelling and Control of Forced Ventilation in Agricultural Livestock Buildings. *Tech. Report No. TR/227*, Centre for Research on Environmental Systems and Statistics, Lancaster University, UK.

Leigh, P., Young, P., Chotai, A., Price, L., Taylor, J., Vranken, E., Berckmans, D., 1999,Modelling and control of forced ventilation in agricultural livestock buildings, *Proc. Int. Conf. On Biometeorology at the turn of the Century*. Sydney, Australia. **1**, 365-370.

Leigh, P., Taylor, C.J., Price, L., Chotai, A., Young, P.C., Vranken, E., Gevers, R. and Berckmans, D., 2000, Modelling and Proportional Integral Plus (PIP) control of ventilation rate in a Fan Test Chamber. *15th International Conference on Systems Engineering*, 12-14 September, Coventry University. 366-371.

Lush, D.M., 1993, Air Conditioning Control Systems, *Concise Encyclopaedia of Environmental Systems*, Ed. Young, P.C. pp.30-37.

McCabe, A., 2000, Proportional-Integral-Plus Control of Non-Linear Systems, Systems Science, **26** (3), 25-46.

McCabe, A., 2001, Proportional-Integral-Plus Control of Non-Linear Systems, *PhD Thesis*, Lancaster University, UK.

McKenna, P.G., Van Brecht, A., & Janssens, K., 2002, Deflection of incoming airflow as a controllable input in ventilation experiments, CRES Technical Report TR/180

Mistriotis, A., Bot, G.P.A., P. Picuno and G. Scarascia-Mugnozza.,1997,Analysis of the efficiency of greenhouse ventilation using computational fluid dynamics. *J. of Agric. and Forest Meteorology*, 85, 217-228.

Mistriotis, A., De Jong, T., Wagemans, M.J.M. and Bot, G.P.A.,1997, Computational Fluid Dynamics (CFD) as a Tool for the Analysis of Ventilation and Indoor Microclimate in Agricultural Buildings, *Netherlands J. of Agric. Science*, 45, 81-96.

Mistriotis, A. *et al.* 1997. Computational Fluid Dynamics (CFD) as a Tool for the Analysis of Ventilation and Indoor Microclimate in Agricultural Buildings, Netherlands *J. of Agric. Science.* 45, 81-96.

Monteith, J.L., and Mount, L.E., 1973, Heat Loss from Animal and Man, *Butterworths*, London.

Mount, L.E., 1968, The Climatic Physiology of the Pig, *Edward Arnold*, London.

Norris, T.S., B.J. Bailey, M. Lees and P.C. Young., (1996), Design of a controlled ventilation open-top chamber for climate change research, *J. Agric. Eng. Res.*, 64, 279-288.

Neilson, P.V., A. Revisto and J.H. Whitlaw, (1978), The speed characteristics of ventilated rooms, *J. Fluids Eng., ASME Trans.* 100, 291-298.

Neinaber, J. A., Hahn, G.L. *et al.*, 1993, Eating Behaviour of Swine as Influenced by Environmental Temperature, Proceedings of the Forth International Symposium of Livestock Environment, University of Warwick, England, pp. 937-944.

Ogilvie, J.R., 1993, Operant Response of Weaning Pigs to Temperature and Air Speed, *Proc. of Fourth International Symposium of Livestock Environment*, University of Warwick, England, 6-9 July, pp.779-787.

Price, L. E., 1999, Imperfect Mixing in Energy and Mass Transport: A Data-Based Mechanistic Modelling Approach. *Ph.D. Thesis.*, Lancaster University, UK.

Price, L. E., Young, P.C., Berckmans, D., Janssens, K. and Taylor, C.J., 1999, Data-Based Mechanistic (DBM) Modelling and Control of Mass and Energy Transfer in Agricultural Buildings. *Annual Reviews in Control.* (Pergamon) 23, 71-82.

Randall, J.M. 1975, The Prediction of Airflow Patterns in Livestock Buildings, *J. Agric. Eng. Res.* 20,199-215.

Randall, J.M., 1975, The Prediction of Airflow Patterns in Livestock Buildings, *J. Agric. Eng. Res.*, 20,199-215.

Randall, J.M., 1981, Ventilation System Design, In: *Environmental Aspects of Housing for Animal Production*, ed. J.A. Clark, Butterworths, London., pp. 351-369.

Randall, J.M. and V.A.Battams., 1979, Stability criteria for airflow patterns in livestock buildings. *J. of Agric. Eng. Res.*, 24, 361-374.

Rostern, H.I. and Spalding, D.B., 1987, The PHOENICS beginners guide. *CHAM T/R100, Concentration, Heat and Momentum Ltd.*, London, UK.

Scokaert, P. O. M., 1994, Constrained Predictive Control. *PhD Thesis*, Department of Engineering Science, University of Oxford.

Seginer, I., 1997, Alternative Design Formulae for the Ventilation Rate of Greenhouses, *J. of Agric. Eng. Res.*, **68**, 355-365.

Shaw, C.T., 1992, Using Computational Fluid Dynamics. *Prentice Hall.* London, UK.

Sigrimis, N., Arvanitis, K.G., Kookos, I.K., and Paraskevopoulos, P.N., 2000, H∞-PI Controller Tuning for Greenhouse Temperature Control, 14th World Congress of IFAC.

Smith, J.H., Wather, C.M. and Baldwin, B.A., 1996, The Preference of Pigs for Fresh Air over Ammoniated Air, *Applied Animal Behaviour Science*, **49**, 417-424.

Spalding, D.B., Ludwig, J and Qin, H.Q. (1994) PHOENICS Reference Manual. *CHAM Report TR200.* London, UK.

Spalding, D.B. (1994). The Beginner's Guide. *CHAM Report TR100.* London, UK.

Taylor, C.J., Chotai, A. and Young, P.C., 1998, Proportional-Integral-Plus (PIP) control of time delay systems, *Proc. Inst. Of Mech. Engrs*, Part 1, Journal of Systems and Control Engineering, **212**(11), 37-48.

Taylor, C.J., 1996, Generalised Proportional-Integral-Plus control, *PhD thesis, Environmental Science Division, Lancaster University.*

Taylor, C.J., McCabe, A.P., Young P.C. and Chotai, A., 2000, Proportional-Integral-Plus (PIP) control of the ALSTOM gasifier problem, *Proceedings of the Institution of Mechanical Engineers, Journal of Systems and Control Engineering*, 214, Part I, 469-480.

Taylor, C.J., 2003, Web page on Lancaster Micro-environmental chamber: http://www.lancs.ac.uk/staff/taylorcj/ventilation.htm

Timmons, M.B., 1980, The use of Models to Predict Fluid Motions in Mechanically Ventilated Structures, *ASAE*, **80**, 4018.

Tritton, D.J., 1988, Physical Fluid dynamics, Second Ed. *Clarendon Press*. Oxford, UK.

Van den Boom T.J.J., 1996, Model Based Predictive Control: Status and Perspectives. *Proceedings of CESA'96 IMACS Multiconference*: Symposium on control, optimisation and supervision., Lille, France, 1996, July 9th. Vol. 1, pp. 1-12.

Versteeg, H.K. and Malalasekera, W. (1995) An introduction to Computational Fluid Dynamics, The Finite Volume Method, *Longman Group Ltd.* Harlow, UK.

Verstegen, M.W.A., Brascamp, E.W. and Van der Hel, W., 1978, Growing and Fattening of pigs in Relation to Temperature of Housing and Feeding Level, *Canadian Journal of Animal Science*, **58**, 1-13.

Vranken, E., K. Janssens, R. Gevers and D. Berckmans. (1998) Model Based Control of the Ventilation Rate in Agricultural Buildings. *ASAE Annual International Meeting*, Orlando, Florida, USA. 1998. Paper No. 984046.

Vranken, E.K. 1999. Analysis and Optimisation of Ventilation Control in Livestock Buildings., PhD Thesis., Katholieke Universiteit, Leuven, Belgium.

Webster, A.J.F. 1985, Animal Health and the Housing Environment, *Animal Health and Productivity*, Royal Society of England, pp.227-242.

White, W., Hughes, H.C., Singh, S.B., and Lang, C.M. 1983, Evaluation of a Cubicle Containment System in Preventing Gaseous and Particulate Airborne Cross-Contamination, *Laboratory Animal Science*, **33** (6), 571-576.

Young, P.C., 1981, Parameter Estimation for Continuos-Time Models - A Survey, *Automatica*, Vol. 17, No. 1, pp. 1-23.

Young, P.C. 1984, Recursive Estimation and Time Series Analysis. (Springer-Verlag: Berlin).

Young. P.C., 1985, The Instrumental Variable Method: a practical approach to identification and system parameter estimation, in: H.A. Barker and P.C. Young (eds.) *Identification and System Parameter Estimation* 1985, Pergamon Press, Oxford.

Young P.C. 1991, Simplified Refined Instrumental Variable (SRIV) estimation and True Digital Control (TDC): a tutorial introduction. *1st European Control Conference*, 1991, 1295-1306 (Grenoble).

Young, P.C., 1996, Identification, estimation and control of continuous-time and delta operator systems. In *Identification in Engineering Systems* (Eds. M.I. Friswell and J.E. Mottershead), pp. 1-17 (University of Wales, Swansea).

Young, P. C., 2000, Stochastic, dynamic modelling and signal processing: Time variable and state dependent parameter estimation. In W. J. Fitzgerald, A. Walden, R. Smith, & P. C. Young (Eds.), *Nonstationary and Nonlinear Signal Processing*. Cambridge: Cambridge University Press, 74-114.

Young, P. C., 2001, The identification and estimation of nonlinear stochastic systems. In A. I. Mees (Ed.), *Nonlinear Dynamics and Statistics*. Boston: Birkhauser, 127-166.

Young, P.C. and Lees, M., 1993, The Active Mixing Volume: A new Concept in Modelling Environmental Systems, in: V. Barnett and K.F. Turkman, (Eds.) *Statistics for the Environment.* (Wiley, Chichester.) 3-44.

Young, P.C. and Wallis, S.G., 1993, Solute Transport and Dispersion in Channels, *Channel Network Hydrology*, Ed. Beven, K and Kirkby, M.J., John Wiley & Sons Ltd, pp. 129-173.

Young, P.C. and Beven, K.J., 1994, Data-Based Mechanistic Modelling and the Rainfall-Flow Non-Linearity, *Environmetrics*, Vol. 5, 335-363.

Young, P.C., Jakeman, A.J. and Post, D.A., 1997, Recent Advances in the Data-Based Modelling and Analysis of Hydrological Systems, *Wat. Sci. Tech.*, Vol. 36, No. 5, pp. 99-116.

Young, P.C., Jakeman, A.J. and McMurtrie, R., 1980, An Instrumental Variable method for model Order Identification, *Automatica*, Vol. 16, pp. 281-294.

Young, P.C. and Wallis, S.G., 1994, Solute transport and dispersion in channels. Chapter 6, in K.J Beven and M.J. Kirby (Eds.) *Channel Networks.* Wiley, Chichester, 129-173.

Young, P.C., Behzadi, M.A., Wang, C.L. and Chotai, A., 1987, Direct digital and adaptive control by input – output state variable feedback pole assignment, *Int. J. Control*, **46** (6), 1867-1881.

Young, P.C., M.J. Lees. A. Chotai, W. Tych and Z. Chalabi., 1994, Modelling and PIP control of a glasshouse microclimate, *Control Eng. Practice*, 2, 591-604.

Young, P.C., Price, L., Berckmans, D. and Janssens, K., 1998, Recent Developments in the Modelling and Control of Climate and Ventilation in Agricultural Buildings.

Young, P.C., Parkinson, S. and Lees, M. (1996) Simplicity out of Complexity in Environmental Modelling: Occam's Razor Revisited, *J. of Applied Statistics*, **23**, No.'s 2 & 3, 165-210.

Young, P.C., Behzadi, M.A., and Chotai, A., 1988, Self tuning and self adaptive PIP control systems., *Implementation of self-tuning controllers*, K. Warwick (Ed.). Peter Perigrinus, London, 220-259.

Young, P.C. and Willems, J.C., 1972, *Int. J. Control*, **15**, 961.

Young, P.C., Chotai, A., Price, L., McKenna, P. and Leigh, P. 2002. Modelling and control of imperfectly mixed mass and energy flow processes with agricultural and biological applications. *Final report.*

Young, P.C., McKenna, P. and Bruun, J., 2001, Identification of nonlinear stochastic systems by state dependent parameter estimation, *Int. Jnl. Control*, **74**,1837-1857.

Young, P.C., Lees, M., Chotai, A., Tych, W. and Chalabi, Z.S. 1994, Modelling and PIP control of a glasshouse micro-climate. *Control Engineering Practice*, **2** (4), 591-604.

Zhang, Y. and Barber, E.M., 1995, An evaluation of heating and ventilation control strategies for livestock buildings. *J. Agric. Engng. Res.*, **60**, 217-225.

Zhang, Y., Barber, E.M. and Sokhansanj, S., 1992, A Model of the Dynamic Thermal Environment in Livestock Buildings, *J. Agric. Engng. Res.*, **53**, 103-122.

Zuidof, M., Feddes, J.J.R., and Robinson, F.E., 1993, Effects of Ventilation Rate and Stocking Density on Turkey Health and Performance. *J. of Applied Poultry Research.*

LIST OF APPENDICES

Appendix 1

COMMON ACRONYMS AND NOTATION

A1.1: Common Acronyms

AC	Alternating Current
AVT	Air Velocity Transducer
DBM	Data Based Mechanistic
DC	Direct Current
LQ	Linear Quadratic
MIMO	Multi-Input Multi-Output
NMSS	Non-Minimum State Space
PI	Proportional-Integral
PID	Proportional-Integral-Derivative
PIP	Proportional-Integral-Plus
PIP-FB	PIP with Feedback configuration
PIP-FP	PIP with forward-Path configuration
SISO	Single-Input Single-Output
SVF	State Variable Feedback
TF	Transfer Function
TDC	True Digital Control
YIC	Young's Identification Criteria

A1.2: List of symbols

Notation

$a_1 \ldots a_n$	Coefficients of the system denominator polynomial
$A(z^{-1})$	System denominator polynomial
$b_1 \ldots b_m$	Coefficients of the system numerator polynomial
$\boldsymbol{d}$	SISO NMSS reference input vector
Δt	Sampling interval
$f_0 \ldots f_{n-1}$	Coefficients of the controller output feedback polynomial
$F(z^{-1})=f_0+f(z^{-1})$	Controller output feedback polynomial
$\boldsymbol{F, g, d, h}$	Non-minimal state-space (NMSS) form
$\boldsymbol{F}$	NMSS system matrix
$\boldsymbol{g}$	SISO NMSS input matrix
$g_1 \ldots g_{m-1}$	Coefficients of the controller polynomial
$G(z^{-1})$	Controller input polynomial
$\boldsymbol{h}$	SISO NMSS output vector
J	Linear Quadratic cost function
K_I	Integral control gain
$\boldsymbol{k}$	Control gain vector
m	Order of the system numerator
Q, Q_s	Heat supply of heating element (W)
$\boldsymbol{Q}$	Linear quadratic optimal control state weighting matrix
$\boldsymbol{q}_i$	Index vector of LQ cost function state weightings
R^2	Coefficient of determination (measure of model fit)
r	Linear quadratic optimal control input weighting scalar
$\boldsymbol{R}$	Matrix of LQ cost function input weightings
t	Time (s)
T	Matrix/vector transpose operator
$u(k)$	Control input signal (0-100% voltage)
V	Voltage applied to the fan (volt)
v_{oo}	Voltage at minimum airflow rate (volt)
V	Ventilation rate (m^3/s)
V_{ref}	Airflow rate setpoint (m^3/s)

w	Wind speed (m/s)
$x(k)$	Non-minimal state vector
$y(k)$	Controller output at time step k
$y(k)$	System output (Airflow rate m^3/hr)
$y_d(k)$	Command input or set point
$z(k)$	Integral-of-error state variable
z^{-1}	Backward shift operator $z^{-1}\, y(k) = y(k-1)$

Appendix 2

PHOENICS - COMPUTATIONAL FLUID DYNAMICS (CFD) PROGRAM OVERVIEW

A2.1 INTRODUCTION

PHOENICS is a sophisticated computer code that can simulate a whole series of phenomena, such as heat transfer, fluid flow and chemical reactions. The PHOENICS computing environment is a powerful computational fluid dynamics simulation tool, which can be used to model fluids such as, airflow in and around buildings. It can be utilised in the facilitation of behaviour in both natural and man-made environments.

PHOENICS computes mathematical inferences from accepted physical principles. Thus a whole image of what occurs within the given environment may be modelled, this assists the user to expand both their imagination and insight into a particular problem and aids further comprehension of it.

PHOENICS and its associated computer codes are written in standard FORTRAN computer language, (ANSI 66, but with '77' character handling) for maximum portability.

PHOENICS stands for **P**arabolic, **H**yperbolic **O**r **E**lliptical **N**umerical **I**ntegration **C**ode **S**eries. The PHOENICS program sets up and solves finite-domain equivalents of the basic

differential equations and embodies the laws of conservation of mass, momentum and energy, for either one or two phases. In addition, PHOENICS contains solvers for sets of linear simultaneous equations, options include, point-by-point, slabwise and whole-3D-field. The coupled hydrodynamic equations are solved by the SIMPLEST procedure, (Spalding, 1980) which is an extension from the SIMPLE algorithms (Semi-Implicit Procedure for Pressure-Linked Equations) developed by the same author in conjunction with Patankar, (i.e. Spalding and Patankar, 1980).

PHOENICS also has two turbulence models built into it. The command 'TURMOD' followed by either 'KLMODL' or 'KEMODL' activates each of the two models. The KLMODL selects the KE-LENI model where, KE is the kinetic energy and LENI is its length scale. While KEMODL selects the KE-EP model where KE is again the kinetic energy and EP is the rate of dissipation of kinetic energy.

A2.2 LIMITATIONS OF PHOENICS

It is important to understand the limitations of PHOENICS as well as its abilities. There are three main limitations that must be taken into account:

- The realism of any simulation cannot exceed the assumptions on which its use is based.
- The accuracy of a given simulation is dependent on the amount of computer time the user has spent.
- PHOENICS will not necessarily provide a converged solution to every problem without the user implementing the settings of solution-control switches.

An example of the first limitation is if the flow to be simulated is turbulent. In such a case PHOENICS must be instructed to use one of the turbulence models, these approximately express the physical laws of such flows. However, when the selected models are a poor approximation to reality then any predictions will be defective. For the second limitation, if a coarse grid is used to model an intricate process then only a rough estimation of the real system will result. Thus to ensure the simulation encompasses as much detail as possible, as finer grid as possible must be implemented. The final limitation is largely confined to the skill of the user. Further research and future versions of PHOENICS will attempt to incorporate more devices that can make these settings automatically.

In addition, irrespective of how finely the computational grid is defined and how well converged and numerically accurate the solutions produced by PHOENICS are, the realism of the flow simulation is inherently restricted by limitations of realism within the modelled equations.

In general, CFD methods are iterative, this entails continual adjustments resulting in a 'converged' set of values which adequately satisfy the balance equations (Figure A2.1). However, without proof that refining the grid (i.e. reducing time and space steps) does not alter the results, then even well converged results cannot be accepted as numerically accurate.

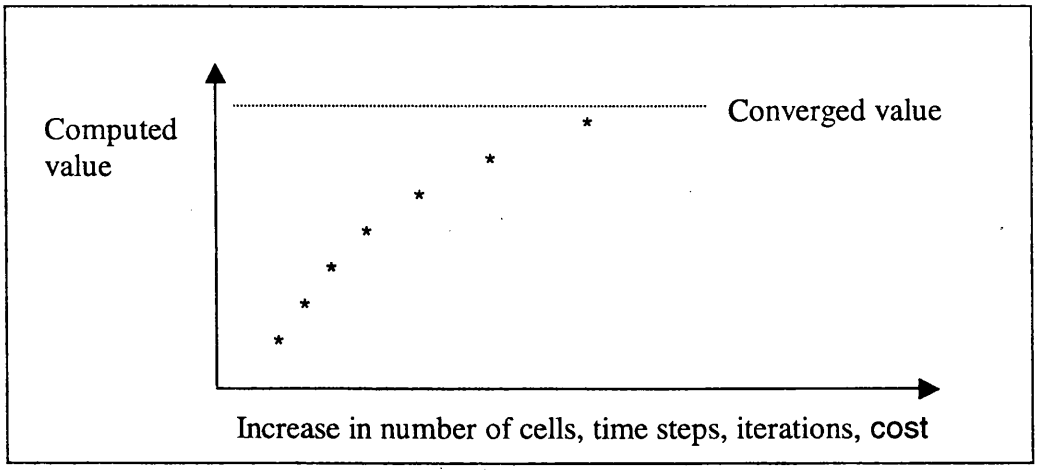

Figure A2.1: An idealised plot showing a converged value.

A2.3 WHAT ARE THE COMPONENTS THAT MAKE UP PHOENICS?

PHOENICS is composed of six computer codes, two essential ones and four auxiliary ones. A pre-processor called SATELLITE and a processor EARTH make up the essential codes. The auxiliary codes are PHOTON, AUTOPLOT and PINTO, which are post-processors, plus a self-instruction program named GUIDE. The flow diagram (Figure A2.2) shows the principle components of PHOENICS.

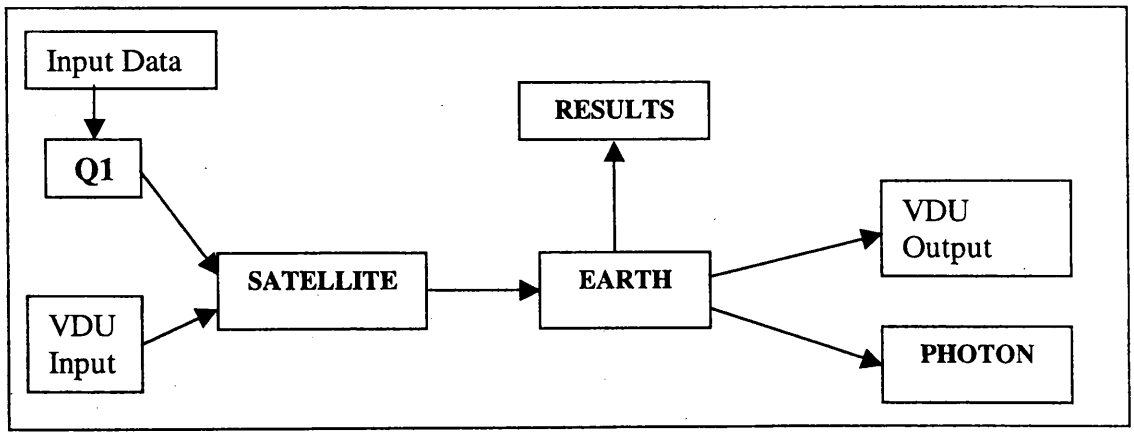

Figure A2.2: Flow diagram of the main components within the PHOENICS CFD package.

A2.4 ESSENTIAL CODES OF PHOENICS

The following is a description of the essential codes of PHOENICS:

A2.4.1 SATELLITE

SATELLITE takes its instructions by means of a Q1 file, inputted by the user, or loads an instruction file from the PHOENICS input library, or communicates with the keyboard during an interactive session with the user. Also any combination of the above. In addition SATELLITE contains FORTRAN *subroutines*, SATLIT and MAIN which allow data-setting statements and dimension changes to be made.

A2.4.2 EARTH

EARTH is the second essential code that makes up PHOENICS. EARTH reads the data file sent by SATELLITE and carries out the necessary computations, an output file named RESULT is created, which may be read by the user. The results of any fluid flow computation can then be read by PHOTON, which is one of the auxiliary codes within PHOENICS. EARTH contains sequences for:

- Storage allocation
- Formulation of finite-volume equations
- Iterative solution of finite-volume equations
- Calling GROUND when required
- Termination of iteration sequences
- Output of results

A2.4.3 AUXILIARY CODES OF PHOENICS

The following is a brief description of the four auxiliary codes within the PHOENICS program.

A2.4.4 PHOTON

PHOTON, one of the auxiliary codes within PHOENICS, defined as (PHoenics OuTput optiON), is a interactive graphics program, designed to display the results of fluid flow simulations via a PHIDA file written by EARTH. A variety of plots such as, contour, vector, relief maps, 'blown up' views, streamlines and perspective views from arbitrary viewpoints can all be produced by PHOTON.

A2.4.5 AUTOPLOT

Labelled plots of data illustrating one or more variable against another are produced in AUTOPLOT. This program is a self-contained interactive-graphics program which can produce a graphical display of numerical data.

A2.4.6 PINTO

In PINTO it is possible to move PHOENICS data between grids of different degrees of fineness. PINTO is a stand-alone computer code within the PHOENICS CFD program.

A2.4.7 GUIDE

GUIDE is another stand-alone computer code in PHOENICS, which is a useful help guide for both beginners and experienced users.

A2.5 VARIABLES WITHIN PHOENICS

There are three types of variables in PHOENICS, namely:

- Independent variables
- Dependent variables
- Auxiliary variables

A2.5.1 INDEPENDENT VARIABLES

The independent variables are the dimensions of any grid shape, which is simulated within the program. There are three dimensions in space and one in time. These are:

- North-south,
- East-west,
- High-low, and
- Time

Here, 't' measures time in the early to late direction, 'x' measures distance (or angle) in the west-east direction, 'y' measures distance in the south-north direction while 'z' measures the distance from high to low. See figure A2.3 below.

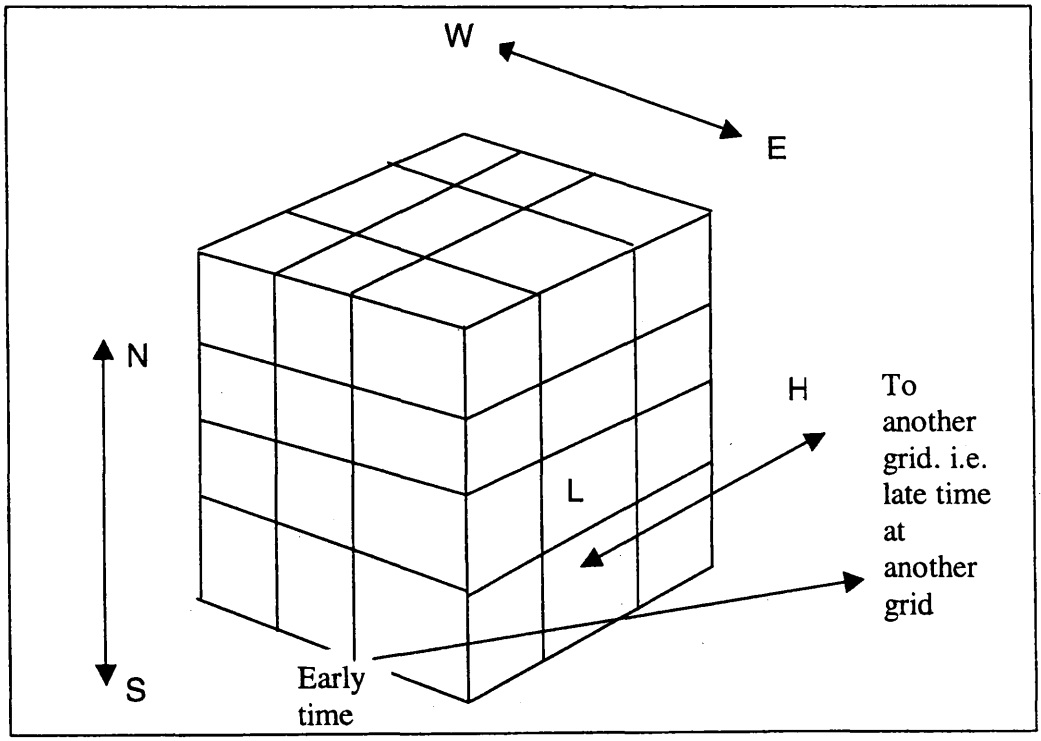

Figure A2.3: Illustration of the independent variables within PHOENICS.

Figure A2.3 is an illustration of the locations in both time and space of how dependent variables such as, temperature and velocity are computed. They are finite in number and as such are visualised to fall within a finite set of 'cells' which if added combine to make up the whole time-space domain in a particular problem. The above figure, A2.3 shows this concept. However, in many problems the cell sizes will not always be equal, or their shape symmetrical.

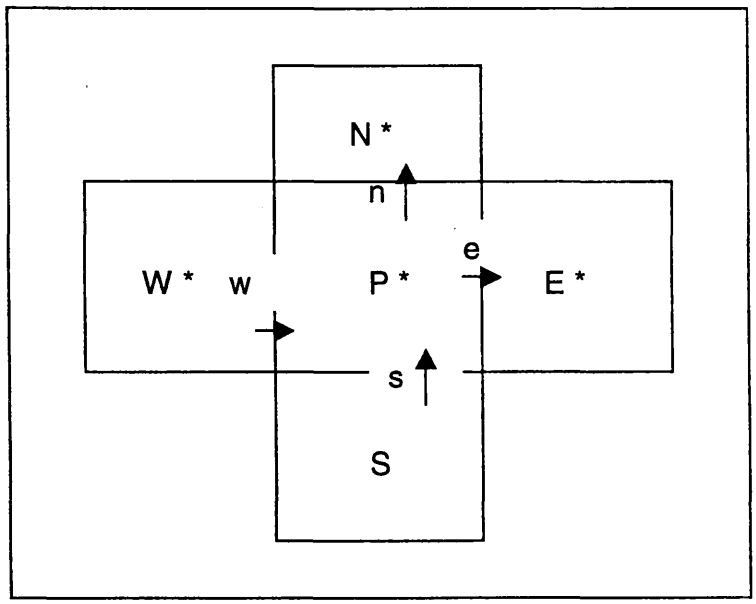

Figure A2.4: Illustration of where PHOENICS computes values in individual cells.

The actual location of all the dependent variables is not strictly within the cells, the velocities are evaluated on the cell walls. Inspection of figure A2.4 illustrates this point, Here, a single cell 'P' with four adjacent cells N, S, E, and W is shown. The pressures, concentrations and temperatures are computed for the previously mentioned locations within the cells by PHOENICS, however, west-to-east velocities are computed at the cell

wall locations as shown by lower-case 'w and e'. Likewise south-to-north velocities are computed as indicated by lower-case 's and n' on the cell walls. Figure (6.4) shows a plan view, a 3-dimensional diagram would indicate also the high and low points for pressure etc.

A2.5.2 DEPENDENT VARIABLES

Variables such as temperature, velocity and pressure are dependent variables, which occur at each nodal space and must be specified by the user. Up to two 'phases' can be specified in PHOENICS, air-flow is classed as one phase as is water, thus a combination of the two can be modelled in PHOENICS. E.g. air mixed with water droplets. Up to 50 dependent variables can be solved in EARTH, plus any further ones the user specifies. A few examples are shown in table (A2.1) below.

Table A2.1: Dependent variables within PHOENICS.

NAME	VARIABLE
P1	Pressure of both the phases
U1	X-direction velocity of the first phase
U2	X-direction velocity of the second phase
V1	Y-direction velocity of the first phase
V2	Y-direction velocity of the second phase
W1	Z-direction velocity of the first phase
W2	Z-direction velocity of the second phase
R1	Volume fraction of the first phase
R2	Volume fraction of the second phase
RS	Volume fraction of the 'shadow' of the second phase
KE	Turbulence kinetic energy of one of the phases
EP	Rate of dissipation of turbulent kinetic energy for the same phase
H1	Specific enthalpy of the first phase
H2	Specific enthalpy of the second phase
C1	Concentration variable of the first phase
C2	Concentration variable of the second phase
C3	Another concentration variable of the first phase
C4	Another concentration variable of the first phase
.....	..... and so on until
C35	Another concentration variable of the first phase

A2.5.3 AUXILIARY VARIABLES

Auxiliary variables are derived from algebraic equations over differential equations, for example, laminar viscosity, diffusivity and Prandtl number. In addition the state of

turbulence may be characterised by parameters such as, the turbulent kinematic viscosity, length scale and generation rate. A further example of auxiliary variables is inter-phase transport, with parameters such as, coefficient of inter-phase heat transfer and friction, and rates of condensation and evaporation.

A2.6 EQUATIONS SOLVED BY THE PHOENICS CFD PROGRAM.

The differential equations within PHOENICS gives solutions to discretised versions of sets of differential equations having the general form:

$$\frac{\partial(r_i \rho_i \varphi_i}{\partial t} + div\,(r_i \rho_i v_i \varphi_i - r_i \Gamma_{\varphi i}\, grad\ \varphi_i) = r_i S_i \qquad \text{(A2.1)}$$

transient convection diffusion source

Where, t = time; r_i = volume fraction of phase i; ρ_i = density of phase i; φ_i = any conserved property of phase i, such as enthalpy, momentum per unit mass, turbulent energy etc.; v_i = the velocity vector of phase i; $\Gamma_{\varphi i}$ = the exchange coefficient of the entity φ in phase i; and $S_{\varphi i}$ = the source rate of φ_i.

Appendix 3

DATA ACQUISITION FOR LANCASTER CONTROLLED ENVIRONMENT CHAMBER

A3.1 INTRODUCTION

This chapter describes the methods used for data acquisition in the Lancaster controlled environment chamber and outlines how and why the different data acquisition (DAQ's) boards were chosen. In order to communicate in real-time with the DAQ's, sensors and external devices a suitable PC software application was required, this is also described.

A3.2 DATA ACQUISITION

In the modern world of data acquisition and advanced control techniques, digital computers and other microprocessor based devices have replaced analog recording and display technologies in almost all but the simplest data acquisition applications. During this digital revolution it is evident that computers have had a positive role to play in data acquisition and digital control. However, computers only speak in a binary language of ones and zeroes, while sensors etc. in manufacturing processes and natural phenomena are still by their very nature analog. The difference being, natural processes tend to vary smoothly over time, whereas in the digital world it is a series of changing states from

black to white or on to off. This section introduces and addresses some of the background fundamentals to data acquisition for the Lancaster micro-environmental chamber.

It is evident that if analog measurements such as temperature, pressure and flow rate are to be of true value they must be converted into digital representations. Even inherently digital events such as the tripping of a motor or a pulse generated by a positive displacement must be made interpretable as transistor-to-transistor (TTL) changes in voltage, (Mechatronics, 1999). This is the motivation for the origination and continuing development of input/output (I/O) systems, which can convert analog and digital information about real-world process and events into the binary language of computers (figure A3.2). The term *data acquisition*, or DAQ is used for the process of taking data from sensors and inputting that data into a computer for processing. The sensors are generally connected via some signal conditioning, to a data acquisition board that is plugged into the back of a computer and reads data into the PC.

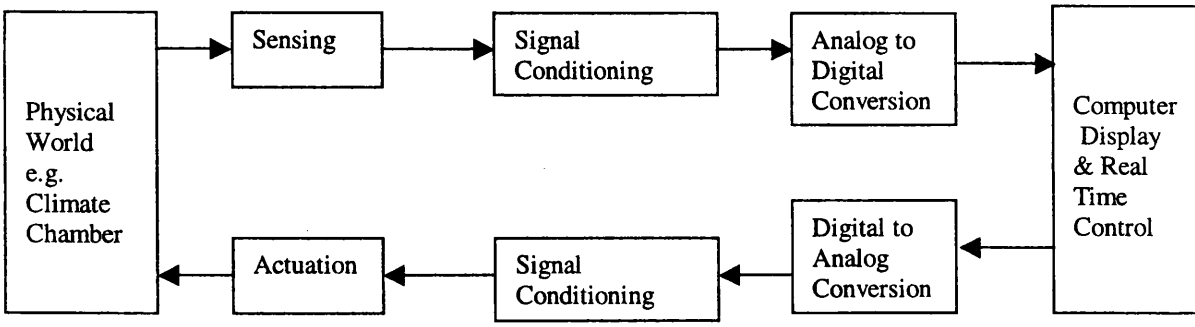

Figure A3.1: Functional diagram for data acquisition and control.

The data acquisition is controlled by computer software via the DAQ board. This process occurs in the following manner: when the program requires an input from a particular sensor, it activates the board by sending a control word to the control and status register.

Such a word indicates the type of operation the board has to carry out. As a consequence the board switches the multiplexer to the appropriate input channel. The input from the sensor connected to that input channel is then passed via an amplifier to the analog-to-digital (A/D) converter. After conversion the resulting digital signal is passed to the data register and the word in the control and status register changes to indicate that the signal has arrived. Following that signal, the computer then issues a signal for the data to be read and taken into the computer for processing. This signal is necessary to ensure the computer does not wait doing nothing while the board carries out its data acquisition, but uses this signal to the computer when the acquisition is complete and then the computer can interrupt any program it is implementing, read the data from the DAQ and then continue with its program.

A3.2.1 RESOLUTION AND ALIASING

In general, sensors for measuring temperature, pressure and other continuous variables produce a continuously varying electrical output (voltage or current), which represents the magnitude of the variable in question. in order to make this electrical signal interpretable by a microprocessor, it must be converted from a smooth, continuous analog value into a discrete, digital binary number (figure A3.2).

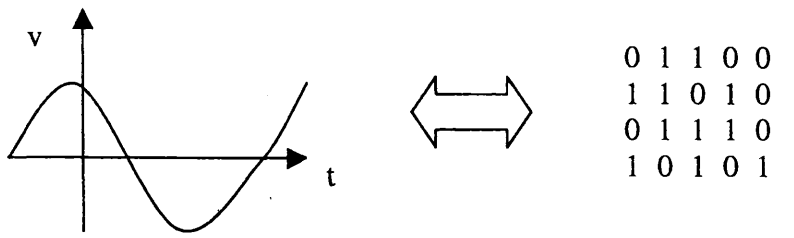

Figure A3.2: Analog to Digital Interface.

With A/D conversion there are two issues to address: namely that of quantisation and sampling over time (figure A3.3). Quantisation is the uncertainty that is introduced when an analog voltage is converted to a digital number. The typical continuously varying signals provided by measurement transducers (e.g. thermocouples) are typically 0-10 V dc, 0-5 C dc, 0-100 mV dc or 4-20mA dc. However, once this analog signal is represented as a digital number the continuous resolution is now limited to discrete steps. The resolution of an A/D conversion is generally stated in terms of "bits", and the more bits the finer the resolution. The number of bits determines the number of divisions into which a full-scale input range can be divided to approximate an analog input voltage. For example, 8-bit resolution of a 0-10 V input signal means that the range is divided into 2^8 = 256 steps. This yields a step or interval size of 10 V/256 = 0.039 V. Thus, a 10 V input is equal to the digital number 255 and 0 V input corresponds to 0. Consequently, each 0.039 V change in the output is indicated by adding or subtracting 1 from the previous number (e.g. 9.961 V is digitally represented by 254).

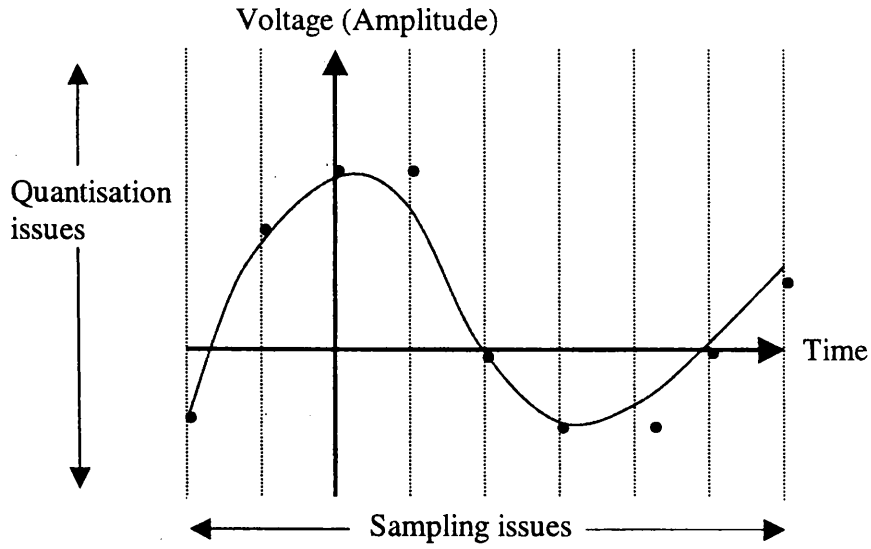

Figure A3.3: A/D Conversion issues.

Close inspection of figure A3.3 above, shows how digital data acquisition systems quantise data not only in terms of magnitude (y-axis), but time (x-axis) is also allotted into discrete intervals. Generally there is no information about the behaviour of the process between gathered data points. Thus, precautions to ensure no meaningful data is lost must be taken, and any interpolation between recorded data points remains a valid assumption.

A method to define the minimum sampling interval is the Nyquist theorem. This defines the relationship between the highest frequency contained within a signal and the minimum required sampling frequency. Nyquist stated that the sampling rate must be at least twice the highest frequency component contained in the input signal. Or, stated another way, the Nyquist theory cannot be applied to the sampled waveforms unless their bandwidth is limited to less than half of the sampling rate. For example, for a 1 Hz sine

wave the sampling interval must be at least 2 Hz; a sampling rate of 8-12 Hz would be even better for resolving the true shape of the output wave.

The primary implications of ignoring the Nyquist criterion include not only missing the high frequency information, but of introducing aliasing. This is illustrated in figure A3.4, where it can be seen that if the sampling rate is not fast enough the presence of non-existent frequencies may be indicated at the expense of the real signal frequencies. Low-pass or anti-aliasing filters can be used to limit the measured waveform's frequency spectrum to ensure no detectable component equals or exceeds half the sampling rate.

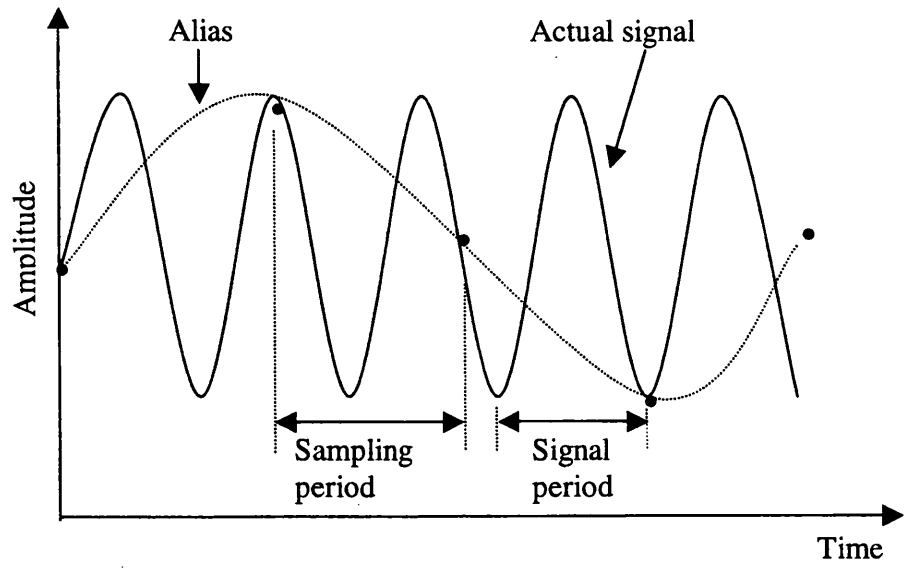

Figure A3.4: Aliasing due to too slow sampling rate.

In short, designing or specifying a device for A/D conversion consists of a series of trade-offs. The next section will demonstrate how a higher resolution (more bits), means a higher level of accuracy in the A/D conversion; but more expensive hardware. Similarly, slower sampling rates mean cheaper A/D conversion, but the Nyquist criterion must still be satisfied. For optimum performance of the hardware it is worth remembering that the

Nyquist criterion is an absolute minimum in terms of defining the sampling rate. And, if the users of such hardware conclude there is no need to sample any higher than say 200 Hz for a signal of around 100 Hz, then such conclusions will generally lead to disappointing results at best.

A3.2.2 ANALOG TO DIGITAL (A/D) CONVERSION

As mentioned in the previous sections, continuous electrical signals from sensors such as thermocouples are converted into binary digits. This is carried out via an analog-to-digital (A/D) converter. The A/D converter may be housed either on a PC motherboard or in a variety of remote or networked configurations. In addition to the A/D converter there may be a combination of multiplexer and screw terminal boards, an amplifier, sample and hold circuits, timing, synchronisation and signal conditioning elements (figure A3.5). Also, within the above configuration are logic circuits for controlling the transfer of data to the internal register and computer memory.

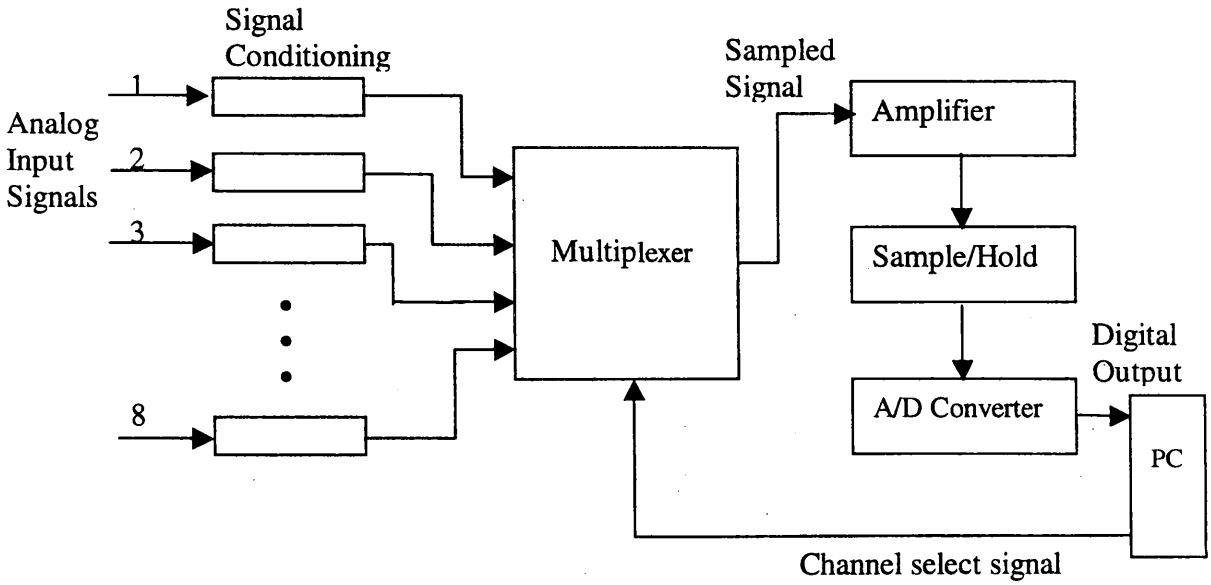

Figure A3.5: Analog to Digital (A/D) flow diagram through a multiplexer.

When determining what type of A/D converter to use for a given application, it is important to ensure that performance is closely matched to the requirements of the analog input of the transducers to be used. Accuracy, signal frequency content, maximum signal level and dynamic range should all be considered. Central to the performance of the chosen A/D converter is its resolution, which is generally expressed in bits. An A/D converter essentially divides the analog input range into 2^n bins, where n is the number of bits. Or more plainly, resolution is a measure of the number of levels used to represent the analog input range and determines the converter's sensitivity to a change in analog input. This is different from the absolute accuracy of the converter and should not be confused. Amplification of the signal or input gain (e.g. on a multiplexer to amplify the micro-voltage signal from a thermocouple), can be applied to increase the apparent sensitivity if the expected maximum range of the signal concerned is less than the input range of the A/D converter.

Another cost/benefit consideration is the amount of resolution required. High-resolution converters are expensive, and if, for example, your application has around 1% accuracy (1 in 100) on its external devices (e.g. temperature transducers and/or air velocity transducers) then a 16 bit (i.e. 1 in 65536) A/D converter will have more than enough resolution.

Additional to the resolution, the other primary A/D converter performance parameter that must be considered is speed or through put of data for a multi-channel device. Overall, system speed depends on the conversion time, acquisition time, transfer time and the number of channels being served by the system.

i) Acquisition is the time required by the front-end analog circuitry to acquire a signal. This is also known as aperture time and is the time the converter must see the analog voltage in order to complete a conversion.

ii) Conversion is the time required to produce a digital value corresponding to the analog value.

iii) Transfer is the time required to send the digital value to the computer memory.

iv) Throughput then, equals the number of channels being served divided by the time it takes to carry out all three functions.

A3.2.3 A/D CONVERTER OPTIONS

Analog-to-digital converters are classified by their resolution or number of bits, however, the method the A/D circuitry achieves this resolution varies from device to device. There are four primary types of A/D converters used for industrial and laboratory applications: i) *Successive approximation*; ii) *Flash/Parallel*; iii) *Integrating*, and finally; iv) *Ramp/Counting*. Some are optimised for speed, others for economy, while some opt for a compromise among the competing priorities (table A3.1). Most industrial and laboratory data acquisition tasks typically require 12 to 16 bits. Generally, increasing the resolution results in higher costs and slower conversion speed.

Table A3.1: Alternative A/D converter designs.

DESIGN	SPEED	RESOLUTION	NOISY IMMUNITY	COST
Successive approximation	Medium	10-16 bits	Poor	Low
Integrating	Slow	12-18 bits	Good	Low
Ramp/counting	Slow	14-24 bits	Good	Medium
Flash/parallel	Fast	4-8 bits	None	High

The method of A/D conversion used in the data acquisition cards in the Lancaster micro environmental chamber is successive approximation; this is also the most common A/D converter design for general industrial and laboratory applications. This design offers an effective compromise between resolution, speed and cost. In this design (figure A3.6), an internal D/A converter and a single comparator, (essentially a circuit that determines which of two voltages is higher, a known voltage generated by a clock emitting a regular sequence of pulses and the unknown voltage which is the incoming signal) are used to close in on the unknown voltage by turning bits in the A/D converter on until the voltages match to within the least significant bit. For example, for a 4-bit system, the comparison may start at 1000, if this is too large try 0100, if this is too small, then try 0110 and finally if this is too large try 0101. From the above it is found that because each of the bits in the word is tried in sequence, with an n-bit word it only takes n steps to make the comparison. Thus, if the clock has a frequency f, the time between pulses is $1/f$. Hence, the time taken to generate the word, i.e. the conversion time is n/f. Raw sampling speeds for successive approximation converters is in the 50 kHz to 1 MHz range. In order to achieve higher sampling rates with this method, a fast initial conversion followed by a correction step that adjusts the least significant bit after allowing sufficient settling time. The conversion is therefore completed faster at the expense of additional hardware. Redundancy is useful when both fast sampling rates and high resolution are desirable.

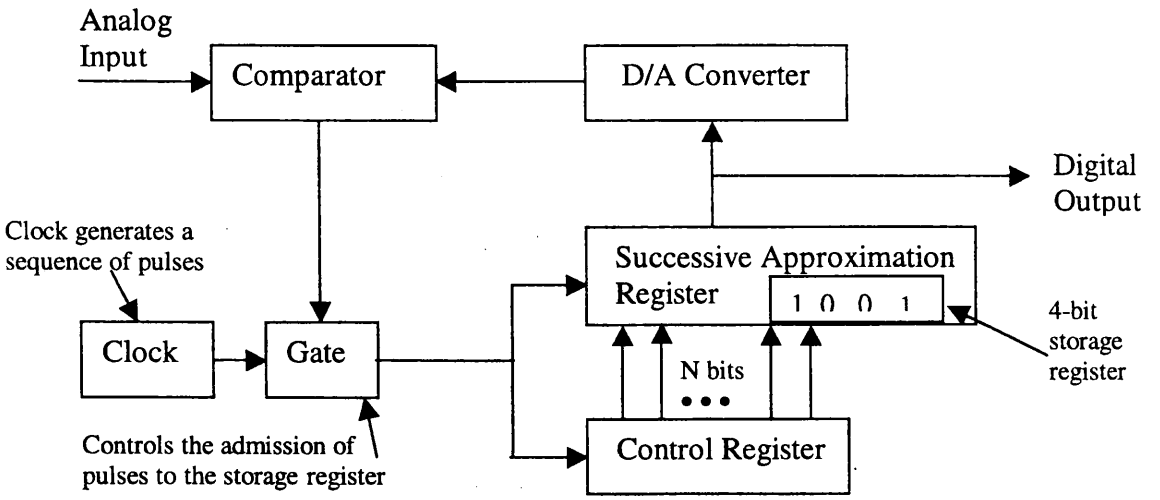

Figure A3.6: A/D Conversion by successive approximation.

If faster sampling and/or higher resolutions are required the flash/parallel method is required. However, because this method uses multiple comparators in parallel to process data at more than 100 MHz with 8-12 bits resolution, a large number of relatively expensive comparators are needed (e.g. a 12 bit converter requires 4095 comparators). Integrating and ramp/counter methods are used when sampling rates are slow. The integrating A/D converter integrates an unknown input voltage for a specific period of time, then integrates it back down to zero. This time is compared to the amount of time taken to perform a similar integration on a known reference voltage. Finally, the ramp/counter method is similar to the successive approximation designs, where one comparator circuit and an A/D converter are utilised. The ramp/counter design progressively increments a digital counter and with each new count generates the corresponding analog voltage and compares it to the unknown input voltage. When agreement is indicated, the counter contains the digital equivalent of the unknown signal.

A3.3 MULTIPLEXING AND SIGNAL CONDITIONING

As shown in figure A3.5, A/D converters seldom function alone and must be considered in a systems context with associated circuitry for signal conditioning, multiplexing, amplification and other functions. Every application will dictate a unique mix of add-ons that may be implemented in a variety of physical configurations; on a PC I/O board, inside a remote transmitter or at a local termination panel.

A3.3.1 MULTIPLEXING

In many industrial and laboratory applications, multiple analog signals must be converted to digital form. If speed is not a limiting factor, a single A/D converter can be shared with multiple input channels via a switching mechanism called a multiplexer. Multiple signals are captured this way in order to eliminate the requirement for multiple converters, which would prove prohibitive in terms of cost for most applications. Additionally, multiplexers allow amplification and other signal conditioning circuitry to be shared among multiple channels. Software or auxiliary hardware controls the switch selection. A multiplexer is essentially an electronic switching device that enables each of the inputs (e.g. a 3D array of thermocouples) to be sampled in turn. For example, the Advantech PCLD-789D utilised in the Lancaster microenvironment chamber has 16 input channels with each channel having a 4-bit binary address for selection purposes.

A3.3.2 SAMPLE AND HOLD

It is important to note that a multiplexer reduces the frequency with which data points are acquired and the Nyquist sampling rate criterion must still be observed. During a typical

data acquisition process, individual channels are read in turn sequentially. This is known as standard or distributed sampling, while a reading of all samples is called a scan. However, because each channel is acquired and converted at a slightly different time, a skew in sampling time is created between data points (figure A3.7). If time synchronisation is important, some data acquisition cards offer "burst" mode operation or simultaneous "sample and hold" circuitry. Burst mode or pseudo-simultaneous sampling acquires each channel at the maximum rate of the board, and then waits for a user-specified amount of time before sampling again.

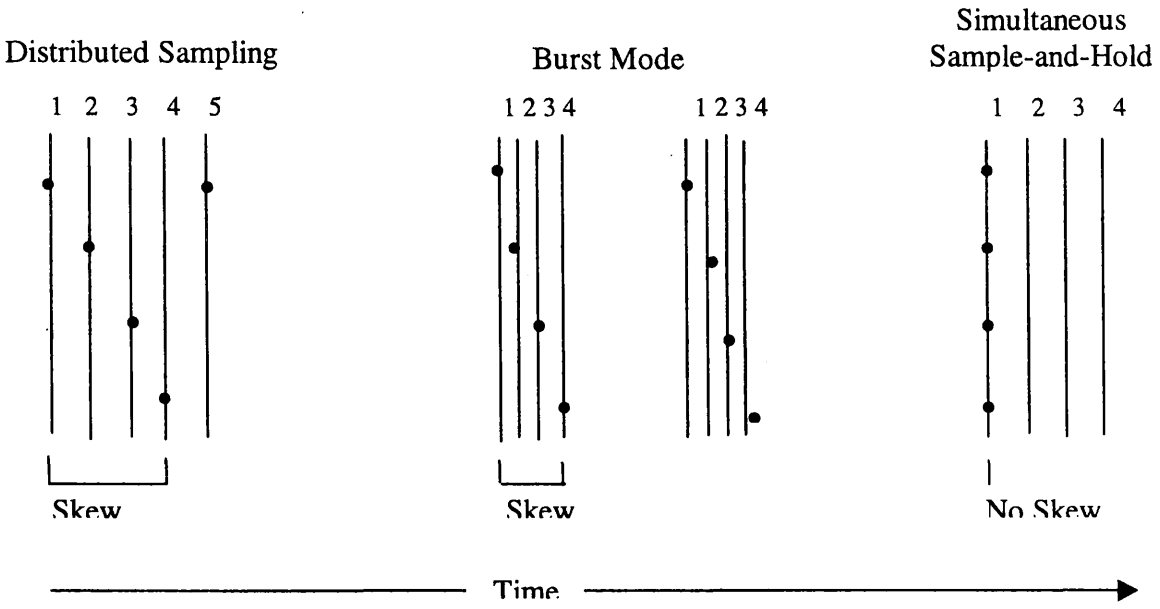

Figure A3.7: Alternative methods for eliminating time skew among multiplexed channels.

True simultaneous sample-and-hold systems can sample all channels within a few nanoseconds of each other, eliminating phase and time discontinuities for all but the fastest processes. Essentially, a switched capacitor on each channel tracks the corresponding input signal. Before starting the A/D conversion process, all switches are opened simultaneously, which leaves the last instantaneous values on the capacitors.

A3.3.3 SIGNAL SCALING

It has been found that A/D converters work best on signals in the 1-10 V dc range, so low voltage signals may require amplification; either individually or after multiplexing on a shared circuit. Conversely, high voltage signals may require attenuation. Additionally, an amplifier can boost very low signals (e.g. microvolt signals from thermocouples). For example, a 12-bit A/D converter with a gain of 4 can digitise a signal with the same resolution as a 14-bit converter with a gain of 1. It is important to note here, however, that fixed-gain amplifiers, which essentially multiply all signals proportionately, increase sensitivity to low voltage signals but do not extend the dynamic range of the converter.

Programmable gain amplifiers (PGA's), on the other hand, can be configured to automatically increase the gain as the signal level drops, which effectively increases the system's dynamic range. For example, a PGA with three gain levels set three orders of magnitude apart can make a 12-bit converter behave more like an 18-bit converter. This function does, however, slow down the sampling rate.

When considering signal scaling from a systems perspective, amplifier performance should be on par with that of the A/D converter itself; i.e. gain accuracy should be specified as a small percentage of the total gain. Also, amplifier noise and offset error should be low.

Further A/D signal conditioning functions utilised will vary according to the application. Among the options, the following should be considered:

i) *Current-to-voltage conversion*: A 4-20 mA dc, current signal can be readily converted to a voltage signal using a resistor (figure A3.8). A resistor value of 250 ohms will yield a 1-5 V dc output.

ii) *Filtering*: A variety of physical devices and circuits are available to help separate desired signals from specified frequencies of undesirable electrical noise, such as ac line pick-up and other electro magnetic (EMI) or radio frequency interference (RFI). If the signal of interest is lower in frequency than the noise, a low-pass filter can be used. High pass and notch-band filters are designed to target low frequency interference and specific frequency bands respectively.

iii) *Excitation*: This is a voltage supplied by the data acquisition card or discrete signal conditioner to certain types of transducers such as strain gauges.

iv) *Isolation*: Isolators are used to protect personnel and equipment from high voltages. Isolators block circuit overloads, while simultaneously passing the signal of interest.

v)

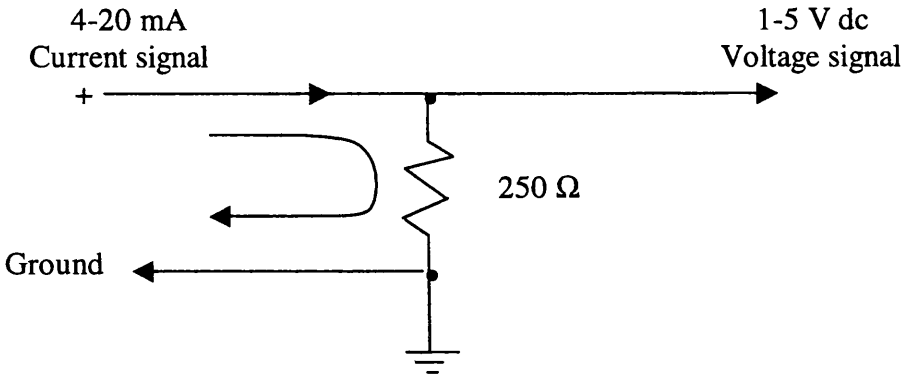

Figure A3.8: Conversion of 4-20mA to 1-5 V dc.

A3.3.4 SINGLE ENDED AND DIFFERENTIAL INPUTS

Another important consideration when specifying analog data acquisition hardware is whether to use single-ended or differential inputs (figure A3.9). In short, single-ended inputs are less expensive but can be problematic if differences in ground potential exist.

In a single-ended configuration, the signal sources and the input to the amplifier are referenced to ground. This is adequate for high level signals when the difference in ground potential is relatively small. However, a difference in ground potentials will create an error causing current flow through the ground conductor (i.e. the ground loop).

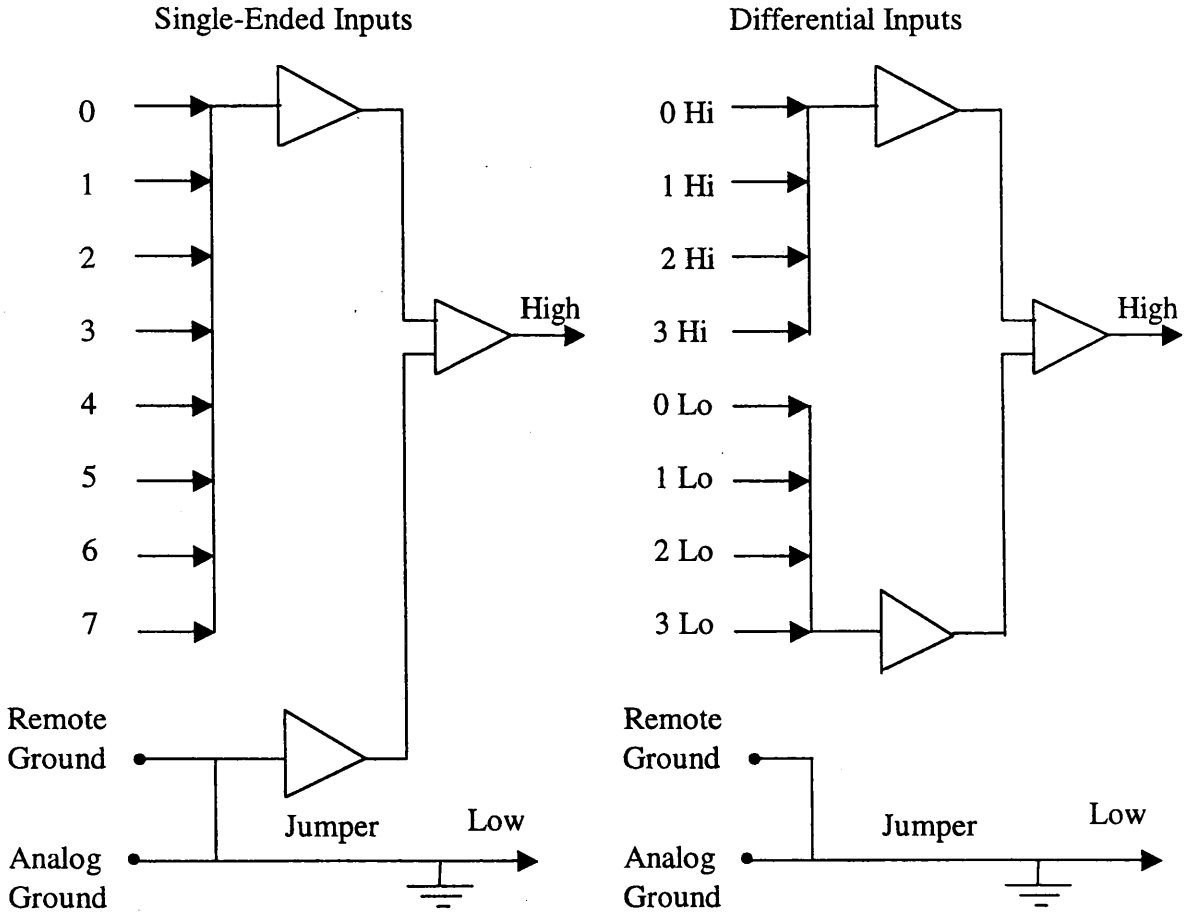

Figure A3.9: Single-ended and differential analog input configurations.

Differential inputs, by contrast, connect both the positive and negative inputs of the amplifier to both ends of the actual signal source. Any ground loop induced voltage appears in both ends and is rejected as a common-mode noise. The downside of differential connections is that they are essentially twice as expensive as single-ended inputs. For example, an eight-channel analog board can handle only four differential inputs.

A3.4 DIGITAL-TO-ANALOG (D/A) CONVERSION

Analog outputs are commonly used to operate valves and motors in industrial and laboratory environments and to generate inputs for electronic devices under test. Digital-to-analog (D/A) conversion is in many ways the converse of A/D conversion, but in practice tends to be more straightforward. Similar to analog input configurations, a common D/A converter can be shared among multiplexed output signals. Standard analog output ranges are essentially the same as analog inputs: ±5 V dc, ±10 V dc, 0-5 V dc, 0-10 V dc and 4-20 mA dc.

Essentially, the logic circuitry for an analog voltage output uses a digital word, or series of bits to drop in (or drop out, depending whether the bit is 1 or 0) a series of resistors from a circuit driven by a reference voltage. This ladder of resistors can be made of either weighted value resistors or an R-2R network using only two resistor values and only one if they are placed in series. While operation of the weighted-value network is more intuitively obvious, the R-2R scheme is more practical because only one resistor value is required. Additionally, it is easier to match the temperature coefficients of an R-2R ladder than a weighted network, resulting in more accurate outputs. Furthermore, for high-resolution outputs, very high resistor values are necessary in the weighted-resistor approach. In short, key specifications of an analog output include:

i) *Settling time*: The period required for a D/A converter to respond to a full-scale setpoint change.

ii) *Linearity*: This refers to the ability of the device to accurately divide the reference voltage into evenly sized increments.

iii) *Range*: The reference voltage sets the limit on the output voltage achievable.

iv) *Full-scale output*: This is the output voltage when the input word is all ones, (i.e. 111111111111 = a 12-bit DAC). For the PCL-818L this is 5.0V DC.

v) *Resolution*: 8-bit to 12-bit DAC's are generally suitable for most microprocessor control. The AD512 is 12-bit.

The input to a digital-to-analog converter (DAC) is via a binary word; the output is an analog signal that represents the weighted sum of the non-zero bits represented by the word. Thus, for example, an input of 0010 must give an analog output that is twice that given by an input of 0001. Figure A3.10 illustrates this for an input to a DAC with a resolution of 1 V for unsigned binary words. Each additional bit increases the output voltage by 1 V.

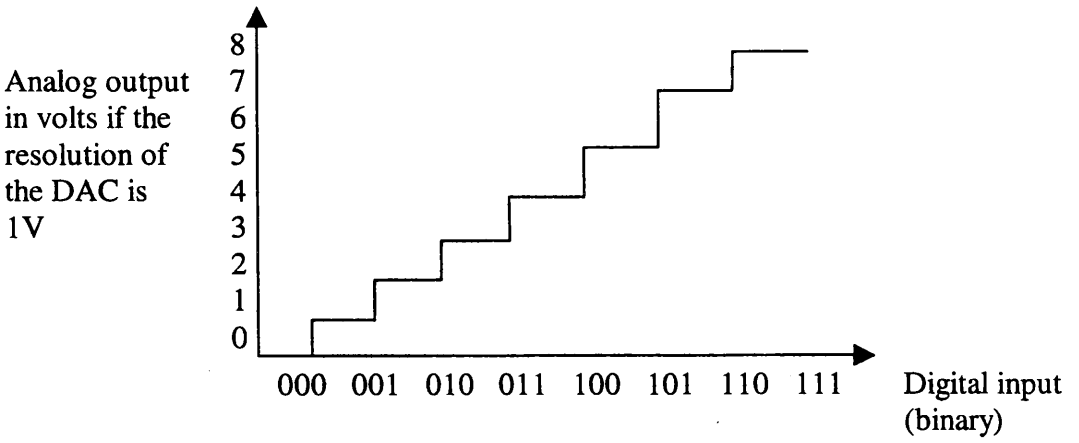

Figure A3.10: Input-output example for a DAC.

The DAC's in Lancaster chamber I/O cards both have 12-bit word outputs. This output is fed through a 12-bit DAC to the control and disturbance fans via the phase angle trigger module and thyristors configuration. The phase angle trigger module requires 5.0 V DC

to allow the AC axial fans to run at their maximum ventilation rate and 0 V DC to halt the fans. If the maximum airflow in the microclimate chamber is represented by 111111111111, then the output to the fan motor for a change of 1 bit will be as follows:

Where, the full scale output voltage is 5.0 V DC using a 12-bit digital-to-analog converter (DAC). A change of 1-bit then gives a change in the output AC voltage of $5.0/2^{12}$ = 1.22×10^{-3} V AC or 0.00122 V AC. If this value is compared to that obtained from a 8-bit or 4-bit DAC (table 5.2) it is obvious how much higher the resolution is with a 12-bit DAC compared to one with less bits.

Table A3.2: Comparison of output AC voltage resolution between 4, 8 and 12-bit DAC's.

No of bits in DAC	DC voltage scale	Conversion	Output voltage (AC)
12-Bit	0-5	$5.0/2^{12}$	0.00122
8-Bit	0-5	$5.0/2^{8}$	0.0195
4-Bit	0-5	$5.0/2^{4}$	0.313

A3.5 DIGITAL INPUT/OUTPUT (I/O) FUNCTIONALITY

In contrast to analog transducers that sense continuous variables such as pressure and temperature, many transducers provide an output that is in one of two states: open or closed, high or low. In this regard, a pressure may be too high or a temperature too low, triggering the closure of a switch. In many cases outputs also are not strictly analog, solenoid valves for example are typically open or closed, many pumps and heating elements are simply turned on or off. Pulse signals are another form of digital I/O, with

one rotation of a turbine flowmeter or tachometer corresponding to a single, countable event. Digital I/O can also be used for parallel communications with pug-in expansion cards, and to generate clock and other timing signals.

Due to the fact these signals are already in the binary language of computers, these kind of digital or discrete, inputs and outputs are much easier for micro-processor-based data acquisition systems to deal with than analog signals. In a similar way to A/D converters used for analog I/O, digital I/O is designed to deal directly with transistor-to-transistor logic (TTL) level voltage changes. TTL typically sets the low voltage level between 0 and 0.8 V dc and the high voltage level between 2.0 and 5.0 V dc. Voltage levels between 0.8 and 2.0 V dc are not used. Thus, a voltage change from the high range to the low range (or vice versa) represents a digital change of state from high to low, on to off etc. Additionally, due to the complexity in acquiring analog signals, analog I/O channels are more expensive than digital. Hence, if digital I/O is adequate for your application it is simpler to ignore analog.

A3.5.1 DIGITAL INPUTS

Digital I/O cards can read directly many types of digital input signals from switch closures, relay contacts to TTL-compatible interfaces (figure A3.11). Some other types of inputs may require some signal conditioning to reduce higher-level voltage changes to TTL levels. The most common type of digital input is the contact closure (figure A3.12). Essentially, a sensor or switch opens a set of contacts in accordance to some process change. An applied electrical signal then

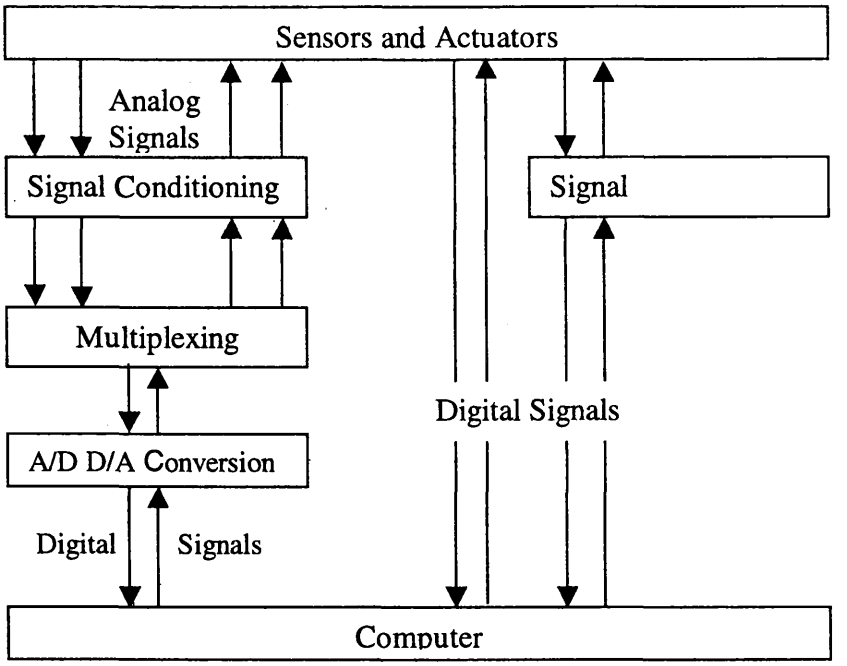

Figure A3.11: Signal processing requirements for digital and analog signals.

determines whether the circuit is open or closed. Current flows if the circuit is closed, registering a "1" in a transistor at the computer interface. While conversely, an open circuit retains a high voltage (and no current), registering a "0" at the transistor.

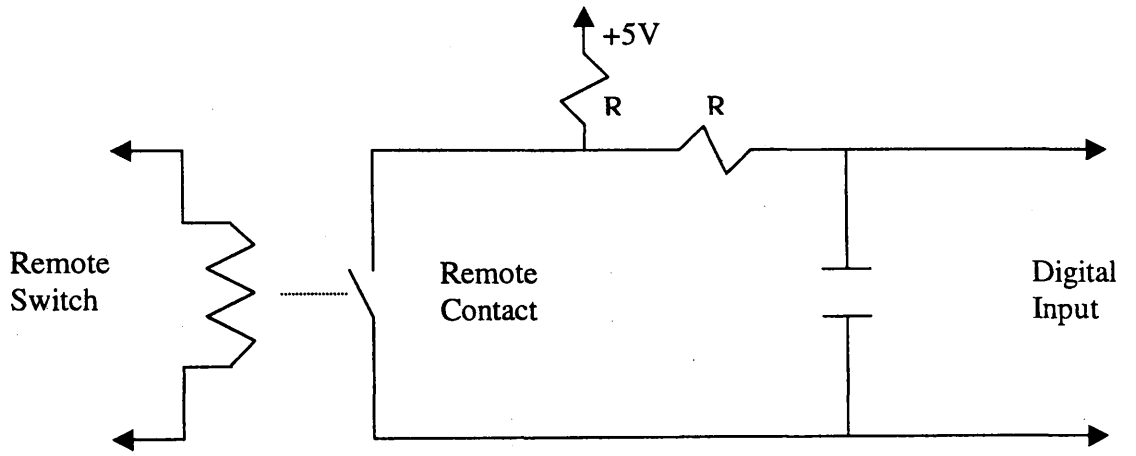

Figure A3.12: Digital input applied to a contact closure.

A3.5.2 DIGITAL OUTPUTS

In its simplest form a digital output provides a means of turning a device on or off. Applications include: turning an indicator lamp on to driving a relay and transmitting data to another computer. For a latching digital output, a "1" typically causes the associated switch or relay to latch and a "0" causes the switch to unlatch. Thus devices can be turned on or off, depending whether the external contacts are normally open or normally closed. A diode is used to protect the digital output circuitry (figure A3.13). It is worth noting that because data acquisition boards typically supply a driving current of only 24 mA, they are intended primarily to drive other logic circuits and not final control elements. In this regard, the digital output from the DAQ boards in the Lancaster chamber is used to switch a phase angle trigger module (section 4.2), that ultimately controls and converts the voltage from DC to AC and controls the speed of the ventilation fans and the temperature of the heating element. If large relays are utilised in the control system design, scaling may be required so that the voltage levels are sufficient to switch them.

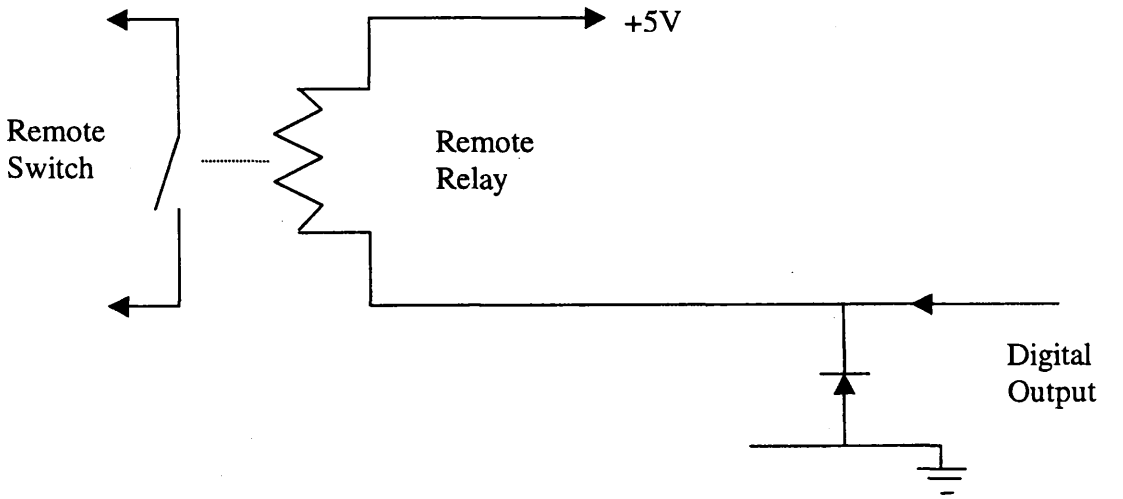

Figure A3.13: A digital output applied to a relay.

A3.6 SOFTWARE FOR REAL-TIME INTERFACE BETWEEN CHAMBER AND PC

An integral part of the design and build process in the Lancaster microclimate chamber is data acquisition in real time. The requirements here are to collect data in planned open loop experiments and visualise the output in real time and to interact 'on the fly' with real time inputs in order to optimise the collected data. In addition, from this collected data, model structures are identified and controllers designed and implemented. This may be carried out in a variety of methods, and there are many companies on the market, which specialise in this field. For the purposes of this chamber the following data acquisition boards and software were chosen.

A3.6.1 EXTENDED REAL TIME TOOLBOX (ERTTB)

Data from the sensors in the Lancaster microclimate chamber are connected to the PC via the real time toolbox and extended real time toolbox software (Humusoft 2001). The real time toolbox (RTTB) is a software package for connecting MATLAB[1] and SIMULINK[1] (Mathworks 1999) to the real world. It has the capacity of acquiring data from sensors in real time via an input/output (I/O) board, processing them on-line through a SIMULINK model and sending the processed signals back to the measured environment. The extended real time toolbox (ERTTB) is as its name implies, an extension of the RTTB. It contains a library of SIMULINK blocks with both real time input and output support. It works on the concept of loadable hardware drivers for all popular I/O boards without the requirement of knowing its hardware details.

[1] SIMULINK® is an iconographic simulation tool which allows for the construction of simulation models in block diagram form. It is an extension to the mathematical computing package MATLAB® (MATLAB, 1999).

A3.6.2 SYSTEM REQUIREMENTS

The real time toolbox 3.0 and extended real time toolbox 3.0 operate under the following specification:

i) MATLAB 5.3 (R11) or higher
ii) SIMULINK version 3.0 or higher
iii) Microsoft Windows 95/98/2000 or NT 4.0
iv) DSP Blockset Toolbox
v) Signal Processing Toolbox
vi) Data Acquisition Board(s) supported with the Real Time Toolbox

A3.6.3 USING EXTENDED REAL TIME TOOLBOX

The Extended Real Time Toolbox (ERTTB) has a library of real time blocks that can be integrated into a SIMULINK block diagram. These are obtained from the real time (RT) library where a selection of RT sinks and sources are accessed. In addition, a hardware adapter block is required. The Hardware Adapter Block (HAB) is a block which represents the I/O board installed in the PC and is used as the real time input and/or output device. The HAB performs the loading of the ERRTB hardware driver and the interfacing of the real time kernel to your data acquisition (DAQ) board. The correct loading and configuring of the HAB is essential for successful communication with the DAQ board. The adapter is a special block that loads the hardware driver, but does not perform any specific actions during the simulation itself. Thus, it has no inputs or outputs but contains the graphical users interface (GUI) for hardware driver definition (i.e. I/O boards). Inside the GUI for the adapter block there are controls for selecting the hardware address of the board and other parameters: bit/byte and gains. The address of the DAQ I/O card must also be specified by switching a bank of eight switches either on or off on

the card itself. This specifies the base address of the I/O ports of the particular card. Switch 8 should always be switched OFF, otherwise the card is disabled (OFF = enable; ON = disable). Once the settings are made on both card and GUI, click ok (see figure A3.14) and this loads and initialises the driver. If multiple I/O DAQ boards are to be used simultaneously as in the Lancaster microclimate chamber, a separate adapter block is required for each I/O board. When using more than one DAQ board it is important to specify different I/O addresses for each card to prevent non-conflicting I/O address space.

A3.7 DATA ACQUISITION CARDS (DAQ's) USED IN LANCASTER CHAMBER

Two data acquisition cards (DAQ's) were utilised for the transfer of data between the Lancaster chamber and the PC and vice-versa. These are the Humusoft AD 512 I/O card and the Advantech PCL-818L I/O card with the PCLD-789D multiplexer board and PCL-8115 screw terminal card. Below, each card is described along with specifications and its function in data acquisition and control within the chamber. The main data acquisition from the 3D array of thermocouples and is carried out through the Advantech PCL-818L and associated multiplexer and screw terminal cards, while the analog (variable 0-5 V dc) output from this card is to the main airflow control fan. The Humusoft AD 512 card is used for additional analog (variable 0-5 V dc) outputs to the disturbance fan and heating element and receives the analog inputs from the air velocity transducers.

Before selecting the afore mentioned DAQ's, a number of criteria had to be considered:

i) What type of computer software system is being used, e.g. Windows, Unix, Mac, etc.

ii) What type of connector is the board to be plugged into, e.g. PCMCIA for laptops, NuBus for Mac, Expansion slot in a PC, etc.

iii) How many analog inputs will be required and what are their ranges?

iv) How many digital inputs will be required?

v) What resolution will be required?

vi) What is the sampling rate?

vii) Are any timing or counting signals required?

Once the above criteria were satisfied the DAQ's could be obtained and installed.

A3.7.1 HUMUSOFT AD 512 CARD

The Humusoft AD 512 card is designed for standard data acquisition and control applications and is optimised for use with the extended real-time toolbox (ERTTB) software for Matlab.

i) 100 kHz 12 bit A/D converter with sample and hold circuit

ii) 8 channel single ended fault protected input multiplexer

iii) Software selectable input ranges ±10V, ±5V, 0-10V, 0-5V

iv) Internal clock and voltage reference

v) 2 double buffered D/A converters with 12 bit resolution and simultaneous update

vi) Output ranges ±10V, ±5V, 0-10V, 0-5V jumper selectable for each analogue output

vii) 8 bit TTL compatible digital input port

viii) 8 bit TTL compatible digital output port

ix) DIP switch selectable I/O port base address

x) Requires one ISA slot

xi) Power consumption 100 mA@+5V, 50mA@+12V, 50mA@-12V

xii) Operating temperature 0°C to +70°C

A3.7.2 ADVANTECH PCL-818L Rev. A2 DATA ACQUISITION CARD

The Advantech PCL-818L is a high specification data acquisition card used for thermocouple measurement and ventilation control in the Lancaster micro environmental chamber (figure A3.14). This card is used in conjunction with the PCLD-789D multiplexer card and PCLD-8115 screw connection card. The PCL-818L has the following specification:

Analogue input (A/D converter)

- Channels: 16 single-ended or 8 differential, switch selectable
- Resolution: 12 bits
- Input ranges (bipolar, V_{DC}): ±0.625, ±1.25, ±2.5, ±5 or ±1.25, ±2.5, ±5, ±10 (all input ranges are software programmable)
- Overvoltage: Continuous ±30V max
- Conversion type: Successive approximation
- Conversion rate: 40 kHz max.
- Accuracy: ±(0.01% of reading), ±1 bit
- Linearity: ±1 bit

Analogue output (D/A converter)

- Channels: 1 channel
- Resolution: 12 bits
- Output range: 0 to +5 (+10) V with on-board –4 (-10) V reference. Max. ±10 V with external DC or AC reference
- Reference: Internal: -5 V or –10 V
  External: DC or AC ±10 V max.
- Conversion type: ±5 mA max.
- Settling time: 5 microseconds

- Trigger mode: software trigger, on board programmable pacer trigger or external trigger
- External trigger: TTL compatible. Load is 0.4 mA max. at 0.5 V and –0.05 mA max. at 2.7 V
- Data transfer: Program, interrupt or DMA

Digital Input

- Channel: 16 bits
- Level: TTL compatible
- Input voltage: Low: 0.8 mA max. at 0.5 V
  High: 2.0 V min.

Digital Output

- Channel: 16 bits
- Level: TTL compatible
- Output voltage:
  Low: Sink 8 mA max. at 0.5 V max.
  High: Source –0.4 mA at 2.4 V min.

- Input load: Low: 0.4 mA max. at 0.5 V
  High: 0.4 mA max. at 0.5 V

Programmable timer/counter

- Device: Intel 8254 or equivalent
- Counters: 3 channels, 16 bit.
  2 channels are permanently configured as programmable pacers
  1 channel is free for your applications
- Time base: Pacer channel 1: 10 MHz or 1 MHz, switch selectable
  Pacer channel 2: Takes input from channel 1
  Pacer channel 3: Internal 100 KHz or external clock (10 MHz max).
  Source selected with Timer/Counter Enable
  Register (BASE+10)
- Pacer output: 0.00023 Hz (71 minutes/pulse) to 2.5 MHz

Interrupt channel

- Level: IRQ 2 to 7, software selectable
- Enable: Via INTE bit of Control Register (BASE+9)

DMA channel

- Level 1: 1 or 3 jumper selectable
- Enable: Via DMAE bit of Control Register (BASE+9)

General

- Power consumption: +5 V: 210 mA typical 500 mA max.
  +12 V: 20 mA typical 100 mA max.
  -12 V: 20 mA typical 40 mA max.

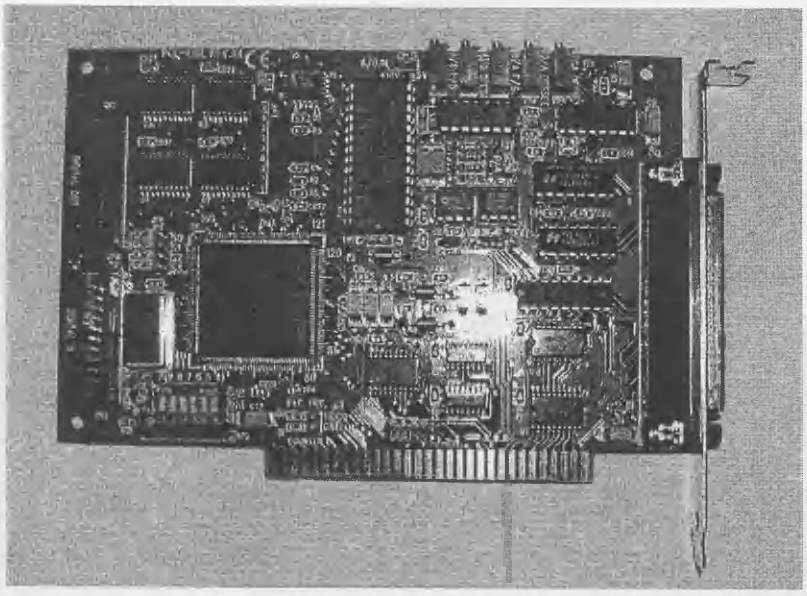

Figure A3.14: Advantech PCL-818L Data Acquisition Board.

- I/O connector: 20 pin post headers for I/O connection. Adapter available to convert to DB-37 connector
- Analogue input/output/counter connector: DB-37
- I/O base: Requires 16 consecutive address locations. Base address definable by the DIP switch SW1 for address line A9-A4. (Factory setting is Hex 300)
- Operating temperature: 0 to +50°C
- Storage temperature: -20 to +65°C

A3.7.3 ADVANTECH PCLD-789D MULTIPLEXING DAUGHTER BOARD AND PCL-8115 SCREW CONNECTION BOARD

These cards are necessary additions to the PCLD-818L I/O card, they are what external devices such as thermocouples and ventilation speed controllers are hard wired to. Some cards, such as the Humusoft AD 512 allow direct connection of certain devices, but a card such as this is not configured for signal processing of temperature transducers such as thermocouples, as used in this application.

A3.7.3.1 ADVANTECH PCLD-789D MULTIPLEXING DAUGHTER BOARD

The PCLD-789D is a powerful front-end signal conditioning and channel multiplexing daughter board. The design allows 16 analog input channels of the PCL-818L Rev. A2 data acquisition card to be multiplexed. This daughter board multiplexes 16 differential input channels into one analog output channel and up to 10 PCLD-789D boards may be cascaded off the PCL-818L to allow expansion of analog inputs to 160 channels. The PCLD-789D daughter board will work with any DAQ that supports both +12 V and +5 V power supplies along with 4-bit programmable TTL digital control and analog input channels.

A special feature of this daughter board is the high grade instrumentation amplifier which provides a range of switch selectable gains of 1, 2, 10, 50, 100, 500, 1000 or a user definable gain. This allows accurate low level analog signal measurement such as that from thermocouple transducers. On board passive circuitry allows signal conditioning functions such as filtering and current shunting. Additionally, the PCLD-789D has a cold junction compensation (CJC) sensing circuit which allows direct measurement of any type of thermocouple. Connection of thermocouple transducers is via screw clamp terminal blocks, which give reliable signal connection.

A3.7.3.2 JUMPER AND GAIN SWITCH SETTINGS

The block diagram for the PCLD-789D multiplexer board is shown in figure 5.15 below. Here, the cold junction compensatory (CJC) sensing circuitry allows direct measurement

of thermocouple transducers. Additionally, the CJC can handle all thermocouple types with software compensation and linearisation. The PCLD-789D has a series of jumpers and gains which all require optimising for individual applications. Here, the settings for the thermocouple signals are as follows:

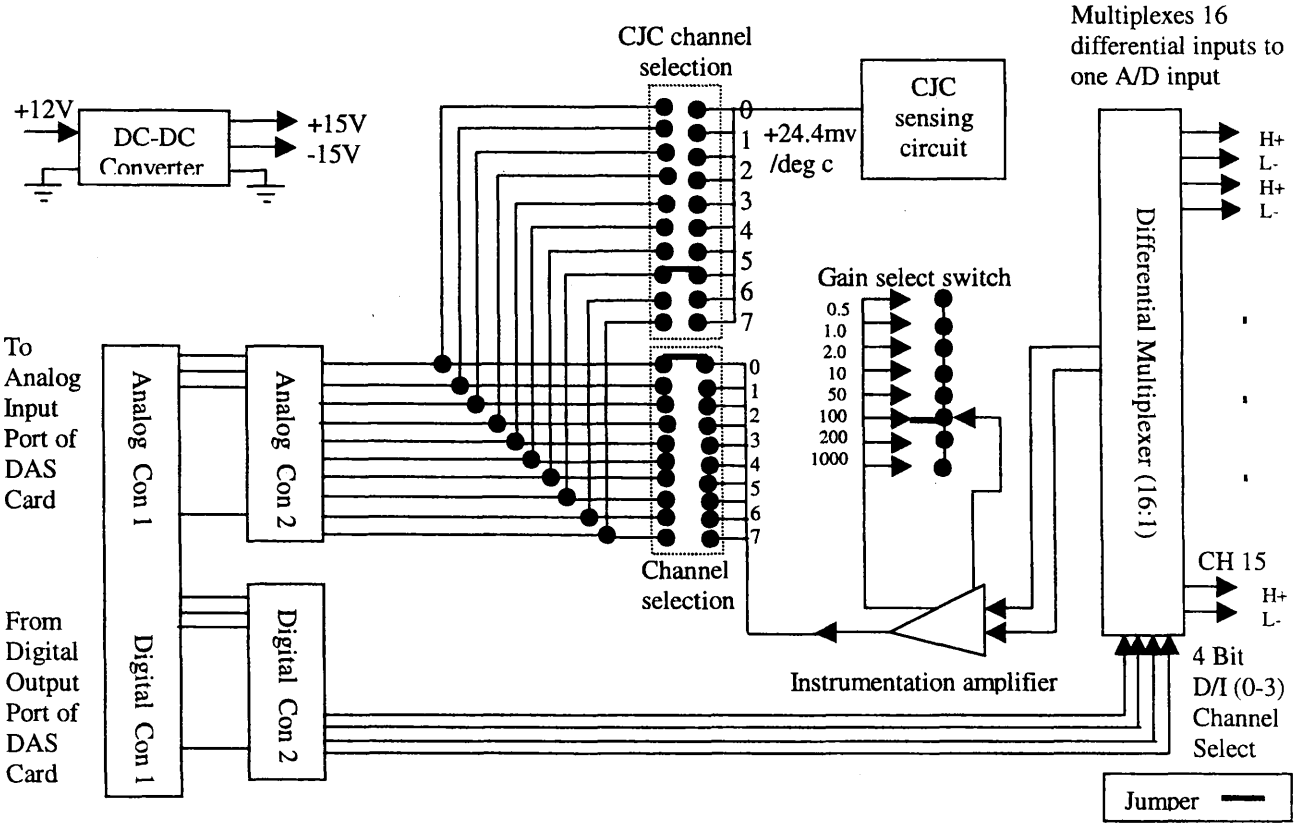

Figure A3.15: Wiring diagram of PCLD-789D multiplexer showing jumpers/gains.

A3.7.3.3 ADVANTECH PCL-8115 SCREW CONNECTION CARD

The Advantech PCL-8115 Screw Connection Card is a further addition to the PCLD-789D multiplexer in that it allows the direct connection of further external devices for control of the Lancaster micro environmental chamber. These include the main ventilation system through the chamber.

Table A3.3: PCLD-789D Daughter Board Test Program.

PCLDTEST VER 1.5 DAUGHTER BOARDS TEST PROGRAM ADVANTECH 1992

DA&C CARD ADDRESS DAUGHTER BOARD A/D CH CJC CH GAIN TC TYPE

DA&C CARD TYPE: PCL818 ADDRESS: 300 A/D CHANNEL: 1
DAUGHTER BOARD: PCLD789D GAIN: 100 CJC CHANNEL: 7
THERMOCOUPLE TYPE: K TEMP RANGE: -269/1232 CJC TEMP: 12.7

CH	TEMPERATURE	VOLTS	MAX	MIN	CH	TEMPERATURE	VOLTS	MAX	MIN
0	14.79°C	0.0061V	2249	2046	8	15.42°C	0.0085V	2052	2050
1	14.16°C	0.0037V	2051	2049	9	**17.31°C**	**0.0159V**	2064	2050
2	15.32°C	0.0085V	2070	2048	10	***12.90°C***	***-0.0012V***	2049	2030
3	14.79°C	0.0061V	3998	2048	11	15.42°C	0.0085V	4095	2049
4	14.79°C	0.0061V	4095	2048	12	15.42°C	0.0085V	2062	2050
5	15.42°C	0.0085V	2052	2050	13	14.79°C	0.0061V	4095	2049
6	15.42°C	0.0085V	3851	2045	14	14.16°C	0.0037V	2073	2049
7	**17.94°C**	**0.0183V**	3593	2037	15	14.79°C	0.0061V	2051	2049

The above table (A3.3) shows the results from running a test program on the thermocouples connected in a 3-D array within the Lancaster micro-environmental chamber. The results show temperature and voltage readings for channels 0-15. If conditions within the chamber are stable all readings at each thermocouple should be similar, i.e. within ~1°C of each other. This program is also an excellent diagnostic tool for broken or disconnected thermocouples. In table A3.3 above it is evident that all the thermocouples are functioning. However, it is clear there are some anomalies in this table, namely channels 7, 9 and 10. The anomalous values have been highlighted in bold type. Two values (7 and 9) are higher than the average of ~15.00°C, while the value for channel 10 is lower. In this case, this is no surprise because heat has been applied to the two readings that are higher than average while the lower reading has been subject to cooling.

This 'treatment' was applied to all channels in turn to test their response to both heat and cold and verified each thermocouple was working and in its correct position in the 3-D array.

A3.8 MAIN CONNECTION LAYOUT BETWEEN PCL-818L, PCLD-789D AND PCLD-8115 BOARDS

The following daisy-chain configuration of the three boards necessary for optimum data collection and external device performance in the Lancaster micro environmental chamber is shown below (figure 5.16).

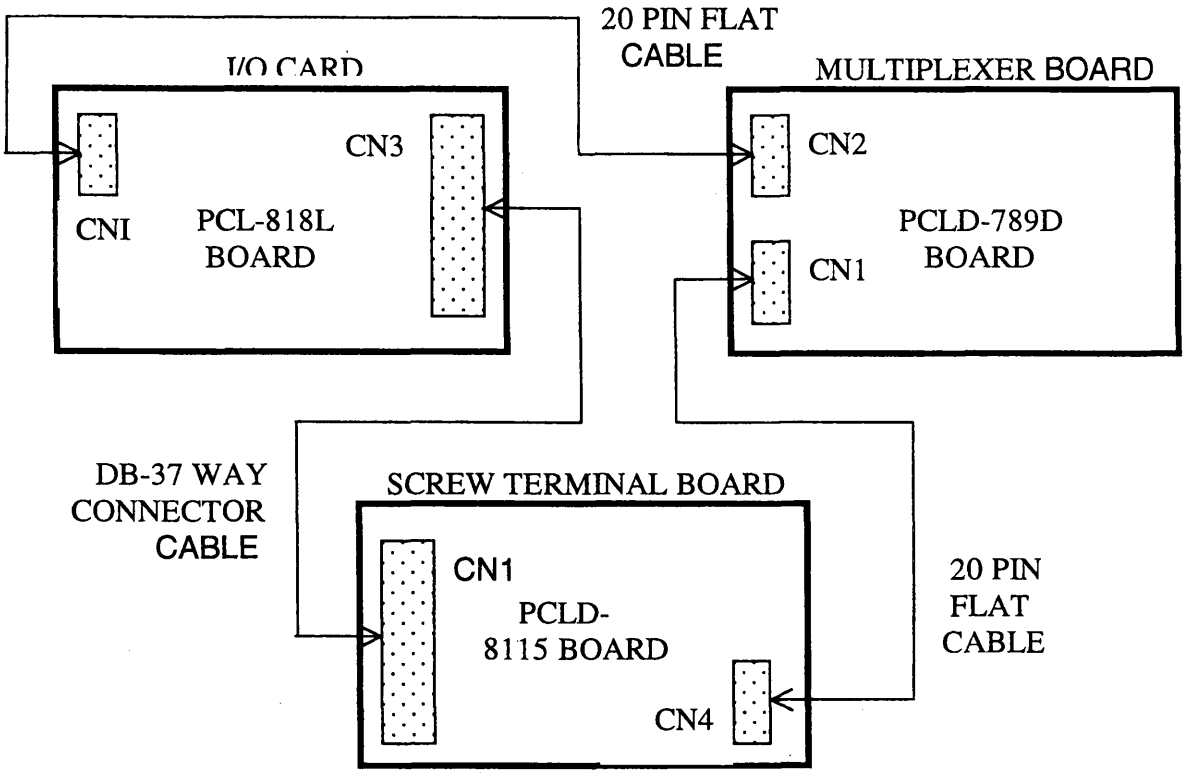

Figure A3.16: Daisy chain configuration for data acquisition boards for Lancaster micro-environment chamber.

5.9 COMPLETE LANCASTER MICRO ENVIRONMENTAL CHAMBER SET-UP

Chapters three and four have concentrated on the design, construction, data acquisition and implementation for the Lancaster micro environmental chamber. This section shows how the external devices and DAQ cards fit together to make a compete system from temperature and airflow measurements via thermocouples and air velocity transducers (AVT's) to computer control of the ventilation system and temperature input. The set-up is shown below in figure A3.16.

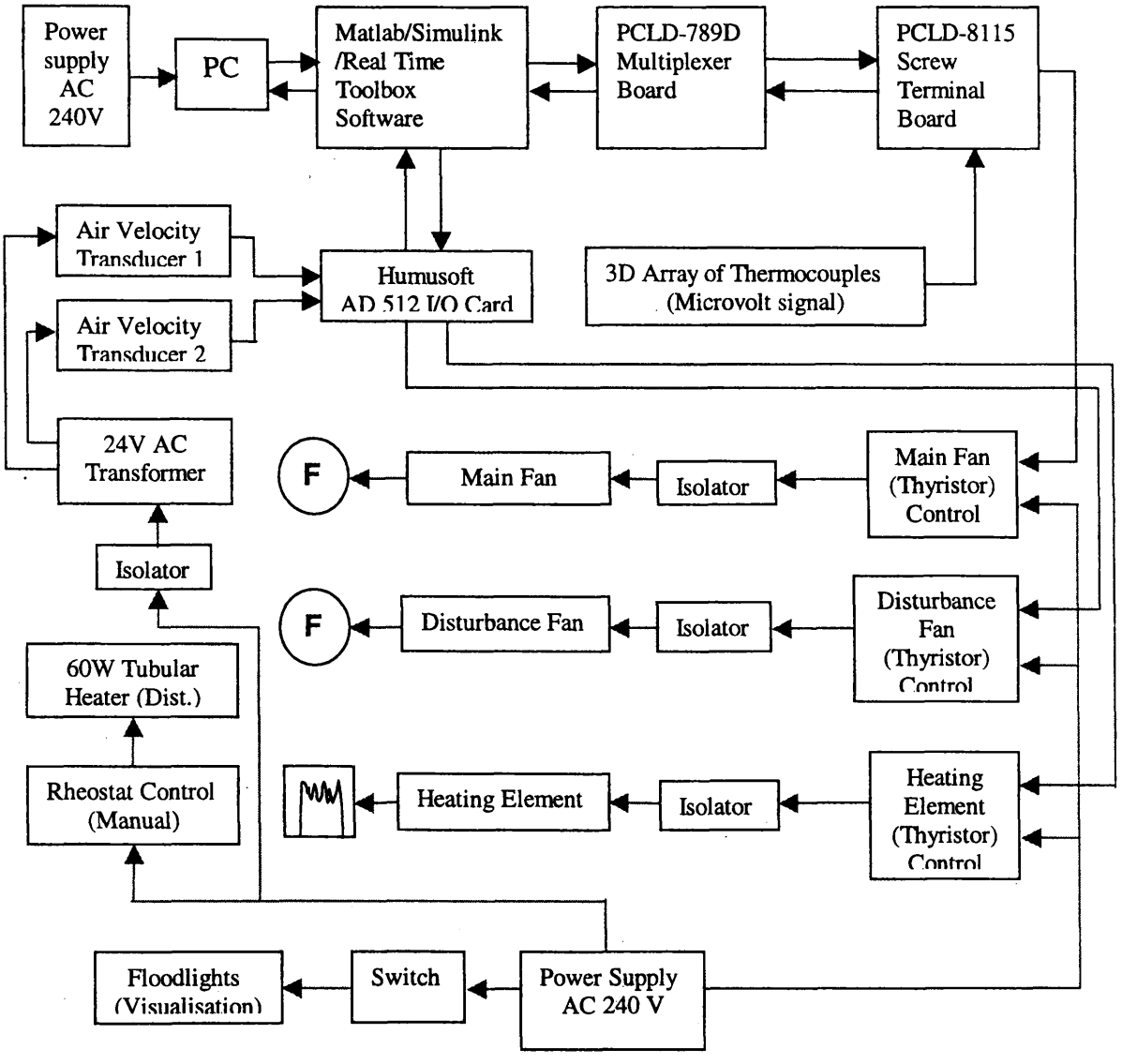

Figure A3.17: Block diagram of Electrical Layout in Lancaster controlled environment chamber, (red lines are 240V AC; blue lines are low voltage signals from sensors or outputs to devices such as fans).

A3.10 CONCLUSIONS

This appendix is the final piece of the jigsaw that makes up the design, construction and finally implementation of the micro environmental chamber in Lancaster. The processes from sampling rate, to data acquisition cards and software selections have been addressed. Chapters 5-8 utilise both the Lancaster and Leuven chambers (chapters 3-4) in demonstrating both modelling and control methodologies that can be applied to micro environmental chambers, such as those described and ultimately scaled up to real livestock housing applications.

Appendix 4

SMOKE EXPERIMENTS IN LANCASTER CONTROLLED ENVIRONMENT CHAMBER

A4.2: EXPERIMENTAL RESULTS

The following figures show further results discussed in chapter 4 (section 4.10).

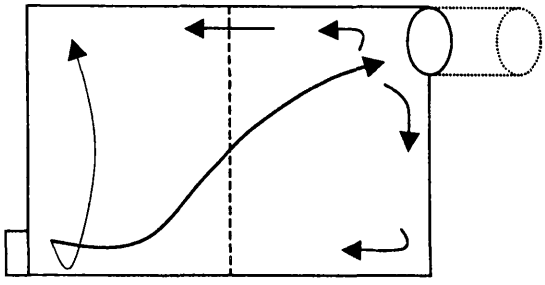

Some circulation: as smoke enters it rises up leading to the fan where a portion is removed and the rest is dispersing. Some anticlockwise motion parallel to the ceiling and free falling. Formation of thermal eddies right to the chamber's edges.

Figure A4.1: Fan 30% Flap fully open, No heater, AVT1=130m^3/hr AVT2=175m^3/hr.

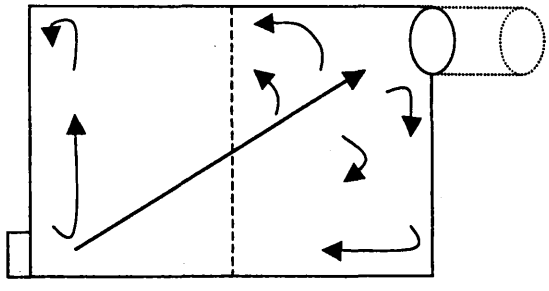

Smoke is directed as a plume towards the ventilator. As the main part moves away there is an occurrence of dispersion becoming more visible as the fan is approached. The remaining part of the smoke splits up it two parts: the first moves anti-clockwise parallel to the ceiling, dispersing in the way. The lower part naturally falls to the ground, dispersing in the way. It should be noted the formation of thermal eddies in the corners.

Figure A4.2: Fan 30% Heat is off, Flap Notch 4, AVT1=70m^3/hr, AVT2=175m^3/hr.

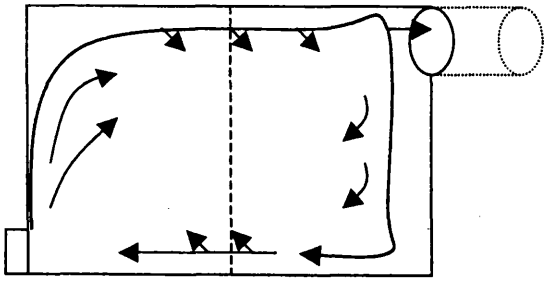

By the time smoke enters the chamber it immediately rises, almost in a vertical fashion, until the ceiling is reached; where small thermal eddies occur. Afterwards the smoke moves in a parallel to the ceiling fashion slowly dispersing in the way, noticeably stronger as the fan is reached. When the fan is reached some smoke is removed, but the main part progressively drops, dispersing in the way, following a clockwise movement, parallel to the floor until the smoke entrance is reached, where it mixes up with the incoming gas. After this stage most of the smoke is well mixed amongst the chamber.

Figure A4.3: Fan 30% Flap Notch 3, Heater is off, AVT1=165m^3/hr, AVT2=6m^3/hr.

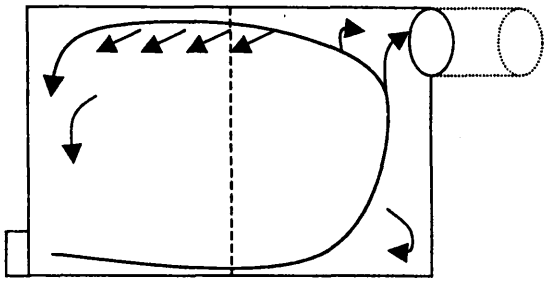

As smoke enters the chamber it moves along the floor with an insignificant dispersion. Once the vertical wall is reached, a small formation of eddies occurs across the adjacent corner. Nevertheless the main part of smoke builds up reaching eventually the fan. Once again a small part is removed where as the rest follows an anticlockwise movement parallel to the ceiling, dispersing in the way.

Figure A4.4: Fan 30% Heater is on working at 0.3 signal, flap is fully open, AVT1=170m^3/hr, AVT2=150m^3/hr, T=34°C.

Same as above:
Figure A4.5: Fan 30%, Full heat, Flap notch 8.

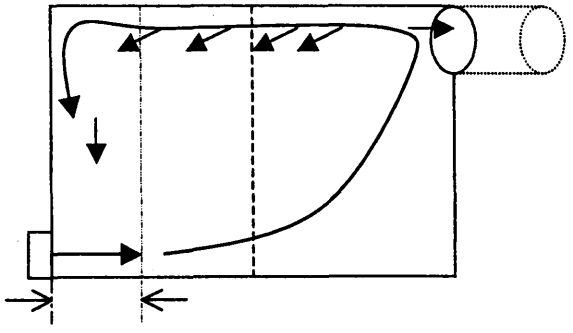

Once smoke enters the chamber it stays horizontal for about 50 cm after which it starts to rise steeply until the fan is reached. Then the majority of the smoke follows a parallel to the ceiling direction, slowly dispersing in the way. Note that until then, the lower part of the chamber beneath the fan remains smoke free.

Figure A4.6: Fan 15%, Flap is horizontal AVT1=50m^3/hr, AVT2=35m^3/hr, T=46C (thermocouple 18).

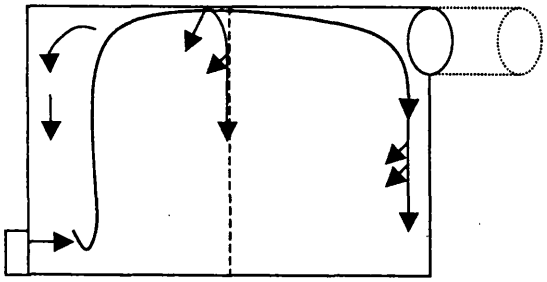

Once smoke enters the chamber it remains in a horizontal level about 30cm away from the entrance. After which it steeply rises until it reaches the ceiling. Minor thermal eddies occur across the edge of the chamber, but the majority of the smoke follows a clock wise path, parallel to the ceiling, towards the fan, with minor dispersions like a noticeable drop of particles halfway to the fan. Once the ventilator is reached, a major part of the original smoke drops towards the floor dispersing in the way.

Figure A4.7: Fan 7.4%, Flap is horizontal, Heat is on, AVT1=30m^3/hr, AVT2=5m^3/hr, T=33°C.

No noticeable difference

Figure A4.8: Same conditions as above, but flap is fully open.

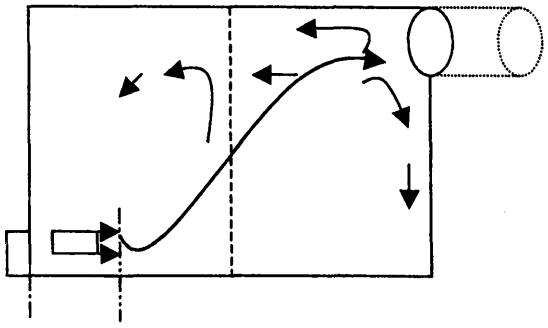

Firstly smoke enters the chamber horizontally to the floor for the first 30cm where it remains static in way, building up for about 10 sec. Then it starts to rise with a noticeable dispersion half way to the fan, where most smoke goes upwards, forming eddies. The rest simply follows the shortest path towards the ventilator. Once it is reached a very small part is removed whereas the rest forms eddies at the corners and simply falls to the floor.

Figure A4.9: Fan 7.5% No heater, T=27.5°C, AVT1=30m^3/hr, AVT2=16m^3/hr.

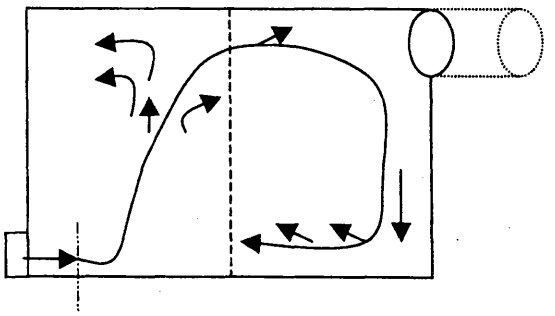

To start with the mobile heater has been placed exactly beneath the inlet. Once smoke enters the chamber it stays horizontal, parallel to the floor. Afterwards it begins to rise until a 30cm horizontal distance is reached where dispersion starts to occur. Nevertheless the main part continuous to rise until it reaches the ceiling where it moves parallel, until the fan is reached. An insignificantly small quantity is removed whereas the rest drops to the floor, dispersing in the way. Once the floor is reached dispersion continuous to occur, now in a rather fuzzy form, following an anticlockwise direction.

Figure A4.10: Fan 7.5%, Mobile heater is on, Main heater is off, Flap fully open, AVT1=30m^3/hr, AVT2=8m^3/hr, T=29-30^{0}C.

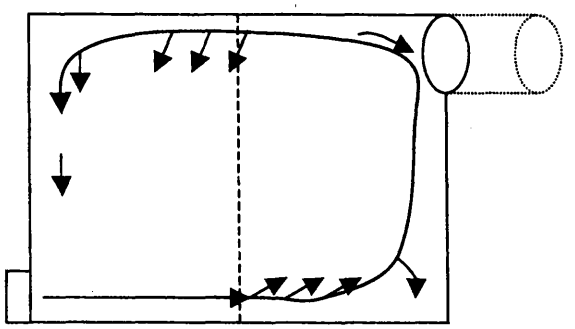

When smoke enters the chamber it stays in a horizontal form until it reaches the middle of the chamber. The it stays for a 8 to 10sec building up, until it eventually starts moving again. This time it follows an anticlockwise direction, dispersing in the way, which becomes more visible as smoke reaches the heater. Once the wall is reached, it progressively builds up towards the ceiling. In height parallel to the fan, there is a minor formation of thermal eddies, with the main gas following an anticlockwise direction parallel to the ceiling, dispersing in the way. This finishes by the time the wall is reached, where it naturally falls, disperses to the floor.

Figure A4.11: Fan 7.5%, Main heater is off, Mobile heater is on (middle), T=24.8-25.6°C, AVT1=24-26m^3/hr, AVT2=30-33m^3/hr.

Appendix 5

THERMOCOUPLES MATERIALS

A5.1 THERMOCOUPLE MATERIALS

The three most common thermocouple alloys for moderate temperatures are Iron-Constantan (Type J), Copper-Constantan (Type T), and Chromega-Alomega (Type K).

1. The first named element of the pair is the positive element.
2. The negative wire is colour coded red.

Three grades of wire are available in each type, based on calibration accuracy: Precision, Standard, and Lead-Wire. The calibration of Precision Grade thermocouple wire is guaranteed within +/- 3.8% or 1°C (2°F), which ever is the larger, while Standard grade is within +/- 3.4% or 2°C (4°F), and Lead-Wire grade within +/- 1%. The accuracy statement can be interpreted as the percent of the difference between the

T_{Jct} and T_{Ref}. Considering the low cost of even the best material, it is hard to justify the purchase of any but Precision Grade material, even for extension wire.

All three types (J, K, and T) are available as insulated duplexed pairs from 0.001-inch diameter on up. For accuracy, and minimum system disturbance, the smaller the wire the better, but wire smaller than 0.003-inch diameter is very fragile.

A5.1.1 IRON-CONSTANTAN

Iron-Constantan (Type J, colour coded white and red) generates about 50 μV/°C (28 μV/°F). The Iron wire is magnetic. Junctions can be made by either welding or soldering, using commonly available solders and fluxes. Iron-Constantan thermocouples can generate a galvanic EMF between the two wires and should not be used in applications where they might get wet.

A5.1.2 CHROMEGA ALOMEGA

Chromega-Alomega (Type K, colour coded yellow and red) generates about 40 μV/°C (22 μV/°F). The Alomega wire is magnetic. Junctions can be made by welding or soldering, but high temperature silver-solders and special fluxes must be used. Chromega - Alomega thermocouples generate electrical signals, while the wires are being bent, and should not be used on vibrating systems, unless strain relief loops can be provided.

Type K Omega thermocouples are the choice for measuring temperature in the Lancaster microenvironment chamber. Here the Chromega-Alomega thermocouples have Teflon-Teflon insulation with a diameter of 0.025 mm (36 gauge), and are in

lengths of two or three meters. The negative leg of the thermocouple is red and is shorter than the positive leg (yellow). The tip of each thermocouple is arranged in a 3D array (figure 3.10) within the chamber, while the negative and positive legs are connected to the PCLD-789D Multiplexer board. The PCLD-789D is in then connected to the PCLD-8115 screw terminal board and the PCL-818L I/O card inside the PC (see section 3.7).

A5.1.3 COPPER-CONSTANTAN

Copper-Constantan (Type T, colour coded blue and red) generates about 40 μV/°C (22 μV/°F). Neither wire is magnetic. Junctions between Copper-Constantan thermocouples can be made by welding or soldering with commonly available solders and fluxes. Copper-Constantan thermocouples are very susceptible to conduction error, due to the high thermal conductivity of the copper, and should not be used unless long runs of wire (100 to 200 wire diameters) can be laid along an isotherm.

Appendix 6

PUBLICATIONS ARISING

Leigh, P., Young, P., Chotai, A., Price, L., Taylor, J., Vranken, E., Berckmans, D., (1999) Modelling and control of forced ventilation in agricultural livestock buildings, *Proc. Int. Conf. On Biometeorology at the turn of the Century.* Sydney, Australia. **1**, 365-370.

Leigh, P., Taylor, C.J., Price, L., Chotai, A., Young, P.C., Vranken, E., Gevers, R. and Berckmans, D., (2000), Modelling and Proportional Integral Plus (PIP) control of ventilation rate in a Fan Test Chamber. *15th International Conference on Systems Engineering*, 12-14 September, Coventry University. 366-371.

Taylor, C.J., Price, L., **Leigh, P.A.,** Young, P.C., Berckmans, D., Janssens, K., Vranken, E and Gevers, R., (2000), PIP Control of Agricultural Buildings. *Proc. Conf. of Control.* Wageningen, Holland.

Vranken, E., Gevers, R., **Leigh, P.A.,** Chotai, A., Berckmans, D. and Young, P.C. (2000) Modelling and control of the ventilation rate in agricultural buildings. *Int. Conf. Eng. Agric.*, Warwick, UK.

Taylor, C.J., **Leigh, P.A.,** Price, L., Young, P.C., Vranken, E., and Berckmans, D. (2001) Proportional-Integral-Plus (PIP) Control of Agricultural Buildings. *International Journal of Control.* In press.